UNIVERSITÀ DEGLI STUDI DI PADOVA

UNIVERSITÀ' DEGLI STUDI DI PADOVA

Dipartimento di Scienze Chimiche

Scuola di Dottorato in Scienze Molecolari
Indirizzo: Scienze Chimiche
XXIX ciclo

Novel mesoporous polymers and their application in heterogeneous catalysis

Direttore della scuola: Ch.mo Prof. Antonino Polimeno

Supervisore: Dott. Paolo Centomo

Dottorando: **Chiara Dalla Valle**

Anno Accademico: 2016/2017

ABSTRACT

The scope of the PhD project is the investigation of acid and Palladium catalysts based on commercially available styrenic resins (both macroreticular and gel type) and a mesoporous poly-divinylbenzene (pDVB) and their application to target technologically relevant reactions, such as the esterification of stearic acid with methanol in sunflower oil and the direct synthesis of H_2O_2. In particular, the acid catalysts where produced by sulfonation with concentrated sulfuric acid, while the metal catalysts were prepared by TCS (Template Controlled Synthesis) approach, using the sulfonic groups to bind a suitable palladium precursor to the polymer matrix and a subsequent reduction step to form the corresponding metal nanoparticles.

Being the sulfonation the main approach for the functionalization of styrenic cross-linked polymers, one of the goals of this project is the in-depth investigation of the effect of this process on the swollen state morphology of the materials. In particular, sulfonic resins prepared with different experimental protocols (i. e. by using concentrated sulfuric acid, chlorosulfonic acid and oleum), were characterized with Inverse Size Exclusion Chromatography (ISEC) to highlight the modification, if any, of pore size and total pore volume, due to the possible additional cross-linking produced by sulfone bridges. The morphological investigation is supported by the chemical analysis of the materials with solid state NMR, elemental analysis and determination of the ion-exchange capacity.

As to the synthetic part of the PhD project, particular attention has been paid to the lipophilization of the cross-linked polymer matrix, in order to obtain promising materials for both the selected target reactions. In particular, an experimental procedure for the Friedel-Crafts acylation with perfluorobutyryl chloride of the aromatic rings of the resin was developed, achieving an appreciable degree of functionalization (12% and 15% of aromatic rings in pDVB and gel-type resins, respectively).

The presence of hydrophobic moieties is expected to facilitate the adsorption of stearic acid inside the catalyst and, at the same time, an efficient expulsion of water, shifting the equilibrium towards the desired product. In the direct synthesis of hydrogen peroxide, the well established affinity of gases like hydrogen and oxygen to fluorinated phases could be the basis forthe enrichment in the reagents around the active Palladium nanoparticles supported by a fluorinated material, with beneficial effects on the catalytic activity. In addition, the highly lipophilic

character of the catalyst should ensure an effective expulsion of the polar product H_2O_2, limiting its further reduction to water.

As an example of acid catalysis, the esterification of stearic acid with methanol in sunflower oil has been chosen as the target reaction. It is a model for the esterification of the free fatty acids (FFA) which can be present in low-grade, cheap raw materials for the biodiesel production and must be abated before the base-catalysed transesterification process. The esterification step not only limits the consumption of the base catalyst , but also prevents the formation of soaps (from the neutralization of FFAs), which make impossible separation and purification processes. In the esterification reaction, the acid catalyst based on mesoporous pDVB showed catalytic performance comparable with those of the catalyst based on gel-type resin: thanks to the presence of an high excess of methanol, the catalysts are completely swollen and the high specific content of acidic groups in the sulfonated gel-type resin ensures conversions similar to those showed by the highly accessible pDVB. The fluorination of pDVB did not improve the catalytic behaviour, differently from related gel-type resins, suggesting that functionalization of this mesoporous material does not affect too much the lipophilic character of the catalyst, at least at the level achieved in this work.

As an example of metal catalysis, the direct synthesis of hydrogen peroxide was investigated under room pressure and at a temperature of 25 °C in a semi-batch reactor, with methanol as the solvent and nano-structured Palladium catalysts based on functional macroreticular resins and macroporous pDVB. Hydrogen peroxide is currently produced by the Riedl-Pfleiderer process that exploits the auto-oxidation of an alkyl–anthrahydroquinone, giving high reaction yields without the direct contact between hydrogen and oxygen. However, this process is profitable only on a large scale, hence H_2O_2 is mainly used only in the bleaching agent of the cellulose pulp and in the preparation of detergents. To expand its rage of application to the production of fine chemicals (hydrogen peroxide is a strong oxidizing agent without polluting reduction by-products) a small scale production process would be highly beneficial. Under this respect, the direct synthesis is currently considered the most promising approach. In direct synthesis of hydrogen peroxide, the 1 %wt Palladium catalyst supported on poly-divinylbenzene shows a higher activity and selectivity towards H_2O_2 with respect to the the catalyst based on a macroreticular resin, as expected on the basis of the mesoporous morphology of the support. Finally, Palladium catalysts based on fluorinated pDVB exhibited higher activity, but smaller selectivity than the pristine

material: the enrichment of the catalyst with gases efficiently promotes the hydrogenation of both oxygen hydrogen peroxide.

RIASSUNTO

Lo scopo di questo progetto di dottorato ha riguardato la sintesi e la caratterizzazione di catalizzatori acidi e di Palladio, basati su resine stireniche commercialmente disponibili (sia macroreticolari che di tipo gel) e su un poli-divinilbenzene mesoporoso (pDVB), e la loro applicazione in reazioni industrialmente interessanti, come l'esterificazione dell'acido stearico in olio di girasole con metanolo e la sintesi diretta dell'acqua ossigenata. In particolare, i catalizzatori acidi sono stati prodotti per solfonazione dei supporti polimerici con acido solforico concentrato, mentre quelli metallici sono stati preparati attraverso approccio TCS (Template Controlled Synthesis), sfruttando i gruppi solfonici per legare alla matrice polimerica un opportuno precursore metallico che, attraverso un processo riducente, permette di ottenere le corrispondenti nanoparticelle metalliche.

Essendo la solfonazione il principale approccio per la funzionalizzazione di resine stireniche, uno degli obbiettivi di questo progetto è stato lo studio approfondito dell'effetto di tale processo sulla morfologia allo stato rigonfiato di tali materiali. Resine solfonate con diversi protocolli sperimentali (acido solforico concentrato, acido clorosolfonico ed oleum come agenti solfonanti) sono state perciò caratterizzate con la tecnica ISEC (Inverse Size Exclusion Chromatography) per mettere in evidenza un'eventuale correlazione tra il diverso processo di solfonazione e variazioni delle dimensioni dei pori e del volume totale del sistema poroso. Lo studio morfologico è stato anche affiancato dall'analisi chimica dei materiali mediante NMR allo stato solido, analisi elementare e determinazione della capacità di scambio ionico.

Per quanto riguarda la parte sintetica del progetto, particolare attenzione è stata rivolta all'ottenimento di matrici polimeriche lipofiliche per ottenere materiali potenzialmente promettenti per entrambe le reazioni studiate. E' stata dunque messa a punto una procedura sperimentale per l'acilazione di Friedel-Crafts con perfluorobutirril cloruro degli anelli aromatici della resina, ottenendo un significativo grado di funzionalizzazione (12% e 15% degli anelli aromatici acilati, rispettivamente, nel pDVB e nella resina di tipo gel).

Nella reazione di esterificazione dell'acido stearico la presenza di gruppi idrofobici dovrebbe favorire l'assorbimento e/o adsorbimento dell'acido stearico all'interno del catalizzatore e, nello stesso tempo, garantire un'efficace espulsione dell'acqua, spostando l'equilibrio di reazione verso il prodotto desiderato. Per

quanto riguarda invece la sintesi diretta dell'acqua ossigenata, un supporto fluorurato dovrebbe promuovere, grazie alla nota affinità dell'idrogeno e dell'ossigeno verso le fasi fluorurate, l'arricchimento del catalizzatore nei reagenti gassosi ed aumentarne dunque l'attività catalitica. Inoltre il carattere lipofilico del catalizzatore dovrebbe assicurare un'efficace espulsione dal catalizzatore dell'H_2O_2 prodotta, limitandone l'ulteriore riduzione ad acqua ed incrementando in questo modo la selettività della reazione.

L'esterificazione dell'acido stearico con metanolo è stata studiata come reazione modello per lo stadio di esterificazione degli acidi grassi liberi, che precede quello base-catalizzato di trans-esterificazione, nell'ambito della produzione di biodiesel da oli e grassi di scarto. La pre-esterificazione acido catalizzata non solo evita il consumo di catalizzatore basico, ma previene anche la formazione di saponi (dalla neutralizzazione dei FFAs) che rendono impossibili i successivi processi di separazione e di purificazione del biodiesel. Nella reazione di esterificazione, il catalizzatore acido basato sul pDVB mesoporoso ha mostrato prestazioni catalitiche confrontabili con quelle del catalizzatore basato sulla resina di tipo gel: grazie alla presenza di un alto eccesso di metanolo nella miscela di reazione, infatti, i catalizzatori sono completamente rigonfiati e l'alto contenuto specifico di gruppi acidi nella resina di tipo gel assicura conversioni simili a quelle osservate con il pDVB. Inoltre, la fluorurazione del pDVB non ne ha migliorato il comportamento catalitico, suggerendo che la funzionalizzazione di un sistema mesoporoso come quello del pDVB non è in grado di influenzare efficacemente il carattere lipofilico del catalizzatore, almeno ai livelli di funzionalizzazione sin qui ottenuti.

Come reazione target per la catalisi metallica, è stata invece studiata la sintesi diretta dell'acqua ossigenata. Il processo è stato condotto a pressione e temperatura ambiente, usando un reattore di tipo semi-batch, metanolo come solvente e catalizzatori nano-strutturati di palladio basati su resine macroreticolari e su pDVB mesoporoso. Attualmente la quasi totalità dell'acqua ossigenata è ottenuta con il processo Riedl-Pfleiderer che sfrutta l'auto-ossidazione di un alchil-antraidrochinone, dando alte rese di reazioni ed evitando il contatto diretto tra idrogeno ed ossigeno. Tuttavia questo processo è economicamente vantaggioso solo su larga scala, il che limita l'utilizzo dell'H_2O_2 principalmente alla preparazione di detergenti e come agente sbiancante per la polpa di cellulosa. Dato che l' H_2O_2 è un forte agente ossidante che dà acqua come unico sottoprodotto, il suo utilizzo per la produzione di fine-chemicals sarebbe potenzialmente molto interessante dal punto di vista ambientale. Pertanto sarebbe auspicabile lo sviluppo di un

processo su piccola scala e la sintesi diretta è attualmente considerata l'approccio più promettente. Nella sintesi diretta dell'acqua ossigenata, un catalizzatore all'1 % in peso di palladio supportato sul pDVB mostra un più alto consumo di idrogeno ed una più alta selettività rispetto al catalizzatore basato sulla resina macroreticolare, come era prevedibile sulla base della morfologia mesoporosa del supporto. Infine, il catalizzatore di Palladio basato sul pDVB fluorurato mostra una più alta attività, ma una più piccola selettività del corrispondente catalizzatore non funzionalizzato: l'arricchimento del catalizzatore con i gas sembra quindi promuovere efficacemente sia la produzione che l'idrogenazione dell'H_2O_2.

CONTENTS

Abbreviations

Chapter 2:

Gel_H_2SO_4	gel-type styrenic resin (2% DVB) sulfonated with concentrated sulfuric acid
Gel_oleum	gel-type styrenic resin (2% DVB) sulfonated with oleum.
Gel_$HClSO_3$	gel-type styrenic resin (2% DVB) sulfonated with chlorosulfonic acid.

Chapter 3:

Gel_acylated	gel-type styrenic resin (2% DVB) acylated with perfluorobutyryl chloride.
pDVB_acylated:	solvothermal poly-divinylbenzene (pDVB1) acylated with perfluorobutyryl chloride.

Chapter 4:

gel_s	gel-type resin (2 %wt of DVB) sulfonated with H_2SO_4.
pDVB_s	poly-divinylbenzene (pDVB1) sulfonated with H_2SO_4.
macro_s_w	macroreticular resin (15 %wt of DVB) sulfonated with H_2SO_4 and washed with methanol.
gel_s_w	gel-type resin (2%wt of DVB) sulfonated with H_2SO_4 and washed with methanol.
pDVB_s_w	poly-divinylbenzene (pDVB1) sulfonated with H_2SO_4 and washed with methanol.
pdvb_c4f7o_s_w	poly-divinylbenzene (pDVB1) acylated with perfluorobutyryl chloride, sulfonated with H_2SO_4 and washed with methanol.
pdvb_c4h7o_s_w	poly-divinylbenzene (pDVB1) acylated with perfluorobutyryl chloride, sulfonated with H_2SO_4 and washed with methanol.
gel_c4f7o_s_w	gel-type styrenic resin (2 %wt of DVB) acylated with perfluorobutyryl chloride, sulfonated with H_2SO_4 and washed with methanol.
pdvb_n	poly-divinylbenzene (pDVB1) sulfonated with H_2SO_4 and neutralized.
pdvb_c4h7o_n	poly-divinylbenzene (pDVB1) acylated with butyryl chloride, sulfonated with H_2SO_4 and neutralized.
pdvb_c4f7o_n	poly-divinylbenzene (pDVB1) acylated with perfluorobutyryl chloride, sulfonated with H_2SO_4 and neutralized.

Chapter 5:

Pd_1%/C commercially available micro-porous active carbon with a Palladium content of 1 %wt.

Pd_1%/macro metal catalyst (Palladium content of 1 %wt) based on a macroreticular resin (15 %wt of DVB) sulfonated with H_2SO_4.

Pd_1%/pDVB metal catalyst (Palladium content of 1 %wt) based on poly-divinylbenzene (pDVB1) sulfonated with H_2SO_4.

Pd_1%/pDVB_C4H metal catalyst (Palladium content of 1 %wt) based on poly-divinylbenzene (pDVB1) acylated with C_4H_7OCl and sulfonated with H_2SO_4.

Pd_1%/pDVB_C4F metal catalyst (Palladium content of 1 %wt) based on poly-divinylbenzene (pDVB1) sulfonated with H_2SO_4 and acylated with C_4F_7OCl.

Pd_1%/pDVB_ATRP metal catalyst (Palladium content of 1 %wt) based on poly-divinylbenzene (pDVB1) sulfonated with H_2SO_4 and functionalized by ATRP.

Pd_3.5%/pDVB metal catalyst (Palladium content of 3.5 %wt) based on poly-divinylbenzene (pDVB1) sulfonated with H_2SO_4.

Pd_3.5%/pDVB_C4F metal catalyst (Palladium content of 3.5 %wt) based on poly-divinylbenzene (pDVB1) sulfonated with H_2SO_4 and acylated with C_4F_7OCl.

Pd_1%/MC metal catalyst (Palladium content of 1 %wt) based on purified mesoporous carbon (MC).

Pd_1%/OMC metal catalyst (Palladium content of 1 %wt) based on mesoporous carbon (MC) functionalized by treating it in 65% HNO_3 solution at 120 °C for 2 hours (OMC).

Pd_1%/NOMC metal catalyst (Palladium content of 1 %wt) based on OMC functionalized by treating it in 100 ppm NH_3 at 400 °C for 6 hours.

Pd_1%/NMC-1 and Pd_1%/NMC-2 metal catalyst (Palladium content of 1 %wt) based on purified N-rich mesoporous carbon (MC) using N-containing precursor for the synthesis. NMC-2 contains a double amount of $CaCl_2$ respect to NMC-1.

Pd_1%/OCNT metal catalyst (Palladium content of 1 %wt) based on carbon nanotubes functionalized by treating them in 65%wt HNO_3 solution at 120 °C for 2 hours.

Chapter 1:
INTRODUCTION

1.1: Morphology of cross-linked polymers

Styrenic resins are prepared by free radical polymerization of styrene in the presence of DVB as the cross-linking agent [1]. Generally, they are produced in the form of beads with a diameter of 0.5-1 mm by suspension polymerization. The first report about their preparation dates back to 1935, when Staudinger and Huseman [2] described the co-polymerization of styrene and divinylbenzene, leading to a material able to swell in suitable solvents without dissolution. The liquid phase, in fact, solvates the polymer chains and enters the polymer network, increasing the volume of the resin, with the formation of a nanometer scale porous system (*Figure 1*). Consequently, the whole volume of the resin becomes accessible at molecular scale. It is important to underline that a good affinity between the liquid medium and the polymer matrix is required: in fact, a lipophilic resin (like polystyrene resins) can swell in lipophilic solvents, whereas in hydrophilic solvents the swelling is absent.

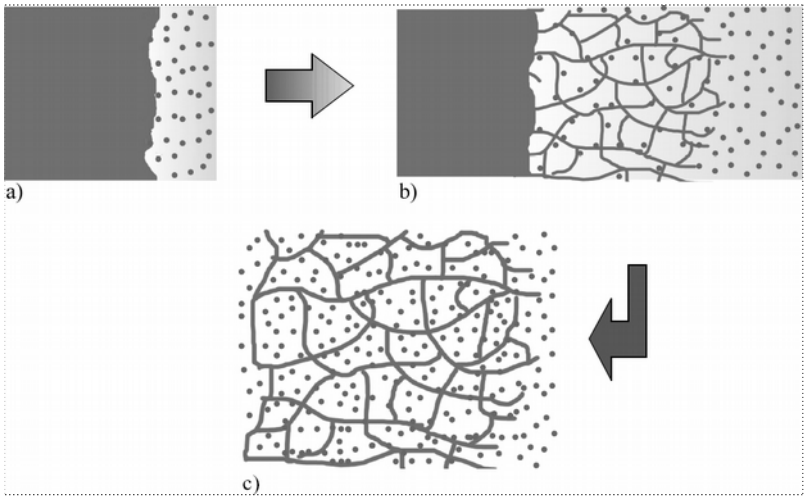

Figure 1: *swelling of a resin. a) the liquid phase solvates the polymeric chains of the external part of the resin; b) the osmotic pressure favours the enter of solvent molecules; c) the solvation is complete: the resin is fully swollen.*

The interest towards styrenic resins started at the beginning of 1940 with the sulfonation of natural powders (like for example coal) and later with the exploitation of sulfonated phenol-formaldehyde resins as ion-exchangers. However, the presence, beside the sulfonic groups, of weak acidic groups (phenolic hydroxyls) makes the exchange capacity of phenol-formaldehyde resins dependent on the pH of the solvent [3]. Therefore, the subsequent literature investigations were mainly focused on resins with a single type of ionisable groups such as cross-linked polymethacrylic acid [4] (with weakly carboxylic acid groups) and styrene based sulfonic resins [5] (with strongly acid sulfonic groups). In particular, the possibility to adjust the degree of swelling (and simultaneously the pores size) and the flexibility of the network by modifying the content of DVB in the polymerization mixture, made styrenic resins one of the most important ion-exchange materials. Nevertheless, the lack of porosity at the dry state and its dependence on the degree of the swelling was considered as a limit for gel-type resins in some applications. Thus, at the end of 1950 was developed a new type of styrenic resin, called “macroreticular resin”, featured by the presence of porosity also at the dry state. The morphology and swelling behaviour of gel-type and macroreticular resins is highlighted in *Figure 2*.

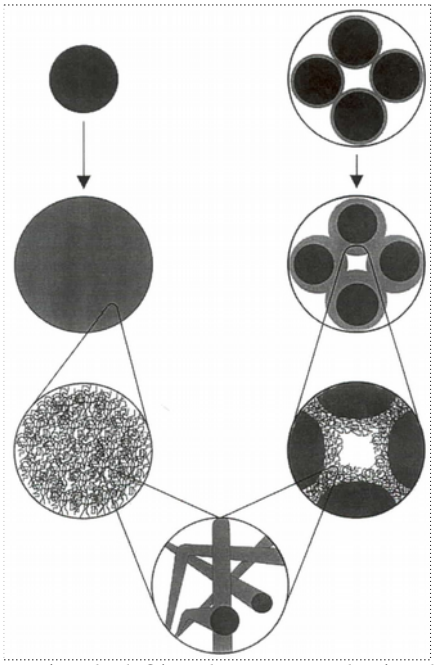

Figure 2: *morphology of gel-type (on the left) and macroreticular (on the right) resins , at the dry (top illustrations) and swollen (bottom illustrations) state.*

At the dry state, gel type cross-linked polymers have no porosity, whereas macroreticular resins show permanent pores, mainly mesopores (up to 50 nm) and some macropores, providing a limited surface area (a few tens of m^2/g). After suspension in suitable solvents, gel-type resins develop a nanometer scale porous system, that encompasses the whole volume of the polymer beads. Similarly, the swelling of macroreticular resins produces an extended porous system, that is only limited to a thin layer close to the surface of mesopores. The surface area of the resulting porous framework is similar for the two different polymer systems (800-1000 m^2/g) and comparable to that of the conventional porous materials.

After the introduction on the market of ion-exchange materials, by the mid of seventies, many industrial applications were explored. Chloromethylated polystyrene resins were successfully employed by Merrifield, who was awarded with the Nobel Prize in Chemistry in 1984 for the solid state synthesis of peptides [6]. In addition, sulfonic resins began to be used as solid acidic catalysts in the addition of alcohols to olefins [7,8] and the industrial production of methyltert-butyl ether (MTBE), an anti-knocking fuel additive, still involves styrene based sulfonic resins as catalysts. In the same period, styrenic resins were also exploited for the first time as solid supports for the synthesis of heterogeneous metal catalysts [9–11]. At the present, sulfonic resins are widely used as ion-exchange materials, selective absorbers, acid catalysts and catalytic supports in metal catalysis.

1.2: Synthesis of macroreticular and gel-type resins

The morphology of the cross-linked polymers strongly depends on the evolution of the polymer framework during the polymerization (*Figure 3*) [12,13].

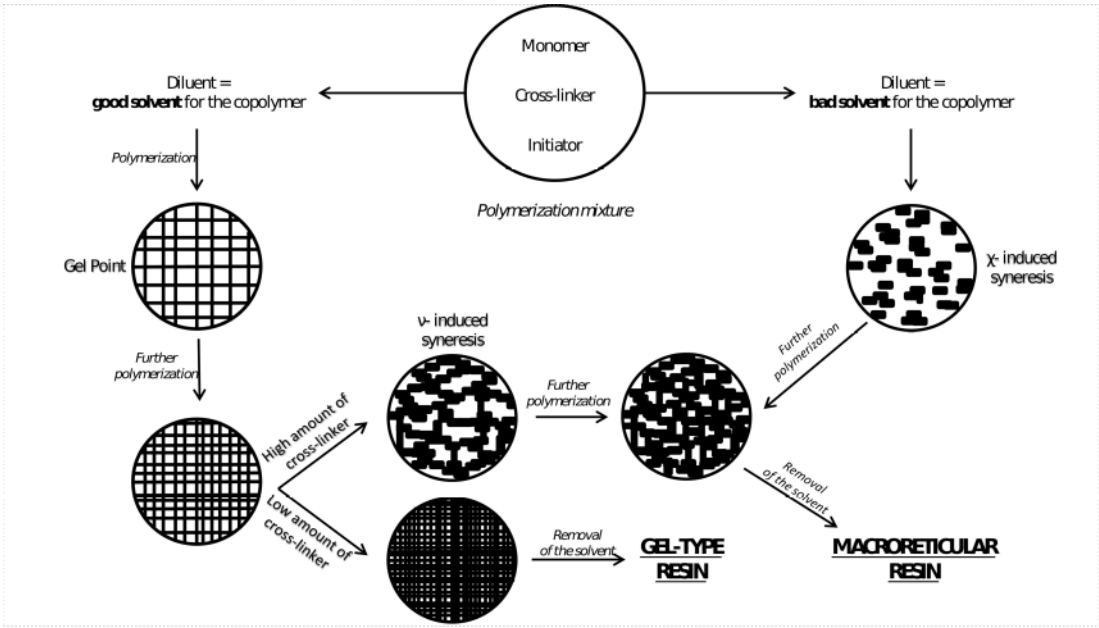

Figure 3: *evolution of the polymer framework during the polymerization.*

The polymerization mixture is composed by the monomer (styrene, S), the cross-linking agent (divinylbenzene, DVB), a radical initiator and a solvent. The radical polymerization starts with the decomposition of the initiator. The polymerization of S and DVB takes place until a continuous polymer network, completely filling the reaction vessel, is formed.

With the progress of the polymerization, the cross-linking degree of the polymer increases and monomers are consumed. Depending on the content of DVB and the nature of the solvent, different pathways are possible:

a. *Presence of a good solvent for the copolymer and a low amount of DVB (1-5%)*. The polymerization proceeds until the complete consumption of the monomer and a continuous gel is produced. After the removal of the solvent, the network collapses and a non-porous material (a gel type resin) is formed.
b. *Presence of a good solvent for the copolymer and an high amount of DVB (5-60%)*. The cross-linking of the polymer network, and consequently its rigidity, is higher than the previous case. Thus, the polymer gel is not able to absorb all the solvent molecules and a separation of phase occurs (“macrosyneresis”).

The gel collapses forming small nuclei surrounded by a continuous phase of liquid. The polymerization continues generating new nuclei reacting each other through their dangling vinyl groups to form a continuous polymer phase. After the removal of the solvent, empty spaces remain among the nuclei, generating the mesoporous morphology typical of a macroreticular resin. This mechanism is called v-induced syneresis, where v is the cross-link density of the network [14].

c. *Presence of a precipitating solvent for the copolymer*. A phase separation occurs before the gel point, forming a discontinuous polymer phase surrounded by a continuous phase, formed by a solution of the remaining monomers in the selected solvent. With the progress of the polymerization, new nuclei are formed, the agglomeration of which gives rise to larger clusters called microspheres. Finally, a continuous polymer phase is formed and also in this case a macroreticular resin is obtained. This alternative mechanism is named χ-induced syneresis, where χ is a polymer-solvent interaction parameter and is equal to the squared of the difference between the solubility parameter of the diluent and the solubility parameter of the polymer [14].

Although both b and c processes lead to the formation of macroreticular resins, some morphological differences are present. When a solvating liquid phase is used (path b), permanent pores develop a limited pore volume (about 0.3 ml/g), whereas the surface area (500 m^2/g) is quite high, due to smaller pores with a narrow size distribution (around 10 nm). On the contrary, macroreticular resins obtained in the presence of a non-solvating diluent (path c) show a “cauliflower” morphology where bigger agglomerates (100-200 nm) consist of smaller microspheres (10-30 nm), formed by the fusion of the nuclei produced during the phase separation. Pores with size between 5 and 15 nm are present among these nuclei, whereas bigger pores (20-50 nm) are generated by the spaces between microspheres.

Independently on the mechanism that origins macroreticular resins, permanent mesopores are generated by the syneresis, the process of expulsion of a liquid from a gel, and they derive from spaces between polymeric nuclei. The density of cross-linking is not uniform in the whole volume of these nuclei and, in particular, it decreases from the centre to the surface. At the beginning of the polymerization, in fact, DVB tends to polymerize more readily with respect the styrene, due to its higher reactivity. Thus the inner part of each nucleus, formed at

the earlier stage of the polymerization, contains an higher amount of DVB respect to the external part and this is the reason for the peculiar swelling behaviour of macroreticular resins (*Figure 2*): the higher the cross-linking degree of the polymer network, the lower the swell-ability, because the rigidity of the polymer matrix prevents the complete solvation of the polymer chains. As the matter of fact, the very high cross-linking degree of the inner part of the nuclei makes its swelling completely impossible.

1.3: Characterization of the porous system of resins

According to Chapter 1.1, the structural morphology of resins remarkably changes after swelling. To study the dry state morphology of resins, conventional characterization methods based on physisorption of nitrogen can be used. Generally, in adsorption experiments the variation in the amount of adsorbed gas with pressure is measured, under constant temperature conditions. The obtained adsorption isotherms provide information about the surface area, the pore volume and the pore size distribution. Similar information on the total pore volume of a porous material can be provided by the mercury porosimetry. In this case a non-wetting liquid (mercury) is employed to fill the pores and the volume of the mercury forced to enter the porous system is plotted versus the applied pressure. This technique is suitable for the investigation of porous materials with size in the 3.5 - 7500 nm range.

Differently from common inorganic materials (zeolites, for example), the porous systems of resins, especially in the case of gel-type polymers, is completely developed only after swelling in a suitable solvent. Therefore, it is of paramount importance the availability of techniques for the swollen state investigation of the resins: in fact, the characterization of the materials in their working state makes possible the rationalization of their reactivity.

To this regard, ESR spectroscopy of paramagnetic probes (usually nitroxide radicals, such as TEMPO, TEMPOL and TEMPONE) absorbed in the porous system of resins, by swelling the material in a solution of such a probe, provides useful information about the pore size through the rotational correlation time, depending on the mobility of the paramagnetic molecules [15,16]. This technique

provides an averaged description of the mobility of the radical probe within the different porous domains of the material and can be used to study the morphology of the resins in any solvent.
In addition, a very detailed description of the swollen state morphology of cross-linked polymers, although limited to a restricted number of solvent commonly used for these materials, is obtained with Inverse Steric Exclusion Chromatography (ISEC, Chapter 1.4) [17,18]. in fact, this technique provides the pore size distribution of the swollen polymer, making possible the evaluation of the reactivity of the material on the basis of its morphology.

1.4: ISEC (Inverse Steric Exclusion Chromatography)

Generally, Steric Exclusion Chromatography (SEC) is a chromatographic technique in which a mixture of solutes is separated by elution through a chromatographic column containing a stationary phase with well-known porosity. Conversely, with *Inverse* Steric Exclusion Chromatography, a stationary phase with unknown porosity is investigated by eluting solutes with known hydrodynamic sizes.
For the exploitation of ISEC (and, more in general, of steric exclusion chromatography) it is mandatory to minimize the enthalpic interactions between the stationary phase and the solutes, so that the elution volume of each solute is only determined by steric interactions with the stationary phase. In the case of resins, the solvent must be able to swell the polymer matrix and has to be carefully selected according to the chemical structure of the polymer material: THF, 1,2-dicloroethane and toluene are usually used for the characterization of lipophilic materials, whereas an aqueous solution of sodium sulfate (with a suitable concentration, in order to suppress the enthalpic interactions between probes and pores surface) is the best choice for hydrophilic resins. The solutes, that must be soluble in the selected solvent, are sugars and dextrans for the Na_2SO_4 solution and alkanes and polystyrenes for organic solvents.
From a theoretical point of view, the mathematical relationship between the elution volume of a solute (V_e) and its size is expressed according Freeman's equation (*Equation 2*):

$$V_e = \sum_{i=1}^{i=n} K^i V_p^i + V_0$$

***Equation 1**: Freeman's equation*

where

- V_0 is the so-called "dead volume", the sum of the instrumental volume and the volume of interstitial spaces among the particles of the resin. It does not depend on the nature of the standard and can be easily determined experimentally;
- K^i is the partition coefficient of each solute in the i^{th} pore fraction and represents the ratio between the concentration of the solute inside the pores and in the mobile phase;
- V^i_p is the volume of the i^{th} pore fraction. Usually, the number of pore fractions is equal to (or sometimes smaller than) the number of solute (*n* in the equation).

The aim of the mathematical treatment is the achievement of the volume of each pore fraction, V_p, through the resolution of a system of linear equations. Although the analytical solution could be obtained, usually a numeric approach is preferred: in fact, due to the error in the estimation of the elution volumes, the analytical result could contain negative values of some roots (i. e. V^i_p), which is inconsistent with the their physical meaning. Therefore, the pore volumes (V^i_p) are numerically determined by minimizing the sum of the squares of the differences between the experimental elution volumes and those obtained with Equation 2, binding the solutions to positive (or zero) values.

The partition coefficients are defined on the base of the model used to describe the porous system. The most common model, used also for the computation of BET data, is the cylindrical pores model, in which pores are depicted as spaces of cylindrical shape and are characterized by their diameter. The partition constants for a solute "*s*" in a fraction of pores "*p*" can be calculated with Equation 3, where d_s is the diameter of the solute molecule and d_p the diameter of the cylindrical pores in that fraction.

$$K_s^p = \left[1 - \left(\frac{d_s}{d_p}\right)\right]^2$$

***Equation 2**: partition coefficient in the cylindrical pores model*

If d_s is larger than d_p, the partition coefficient is imposed to zero because the solute cannot enter the pore. When d_s is smaller than d_p, the partition constant decreases with the size of the solute, corresponding to a decrease of the solute concentration in the pore fraction. Although far from the actual geometry of the pores of a swollen polymer gel, the cylindrical pores model allows a reliable description of the porous system of swollen resins.

In the case of gel-type resins, in which pores are formed only after a swelling process and are spaces between solvated polymer chains, the Ogston model, depicting the pores as spaces among randomly oriented rigid rods, is generally preferred. Differently from the cylindrical pores model, each pore fraction is featured by its *polymer chain concentration*, expressed in nm/nm^3, representing the total length of polymer chains present within a unit volume of polymer. This definition implies that fractions with smaller chain concentrations are characterized, on average, by bigger pores. The partition coefficient can be calculated with Equation 4, where C is the chain concentration and d_c is the polymer chain diameter (usually 0.4 nm).

$$K_s^p = \exp\left[-\pi C \left(d_s + d_c\right)^2 / 4\right]$$

Equation 3: *partition coefficient in the Ogston model*

The choice of the proper geometrical model for the pore system depends on the structural features of the resin. A particular case is represented by macroreticular resins, showing both macro- and mesoporosity: these can be conveniently described by using the cylindrical pores model for pores larger than 10 nm and the Ogston model for the gel-type porosity.

1.5: Mesoporous pDVB

In 2009 Zhang at al. reported about the synthesis of a novel kind of porous resin obtained by the homo-polymerization of DVB under solvothermal conditions [19]. The polymerization of a highly diluted monomer solution (2 g of DVB in 20 ml of solvent) occurs at 100 °C, by using a H_2O : THF mixture (10% vol) as the solvent.

The preparation leads to a cross-linked polymer material with a high pore volume (1.35 cm^3/g), high surface area (702 m^2/g) and pore size of about 22 nm. Noticeably, these pores are permanent also at the dry state. Its lipophilic nature and its remarkable porous system makes pDVB an efficient absorbent for organic compounds, like, for example, volatile organic compounds (VOC).

The experimental conditions to be carefully controlled in order to obtain a such type of porous system are the temperature (a porous system is formed only at temperature higher than 60 °C), the nature of liquid phase and the duration of the polymerization (at least 24 hours). On the one hand, precipitating solvents for polystyrene (such as ethanol and n-hexane) only produce non-porous materials. On the other hand, a liquid phase able to solubilize polystyrene (for example acetone, benzene, THF, DMF, ethyl acetate) produces highly porous materials. The highest specific pore volume is obtained when the solvent is a mixture of THF and water (H_2O/THF = 0.1). The presence of water seems to be beneficial for the formation of an highly porous material: changing the volumetric ratio of water to THF between 0 to 0.1, the pore volume increases from 0.51 cm^3/g to 1.35 cm^3/g and the pore diameter from 3.9 to 22 nm.

The same authors, later, reported also the functionalization of this material with sulfonic acid groups, yielding materials with a cation exchange capacity (4.1 mmol H^+/g) comparable to commercial sulfonated macroporous styrenic resins (between 4 and 5 mmol H^+/g) [20]. The obtained acid solid materials were tested as catalysts in the esterification of hexanoic acid, acetic acid and lauric acid. They showed higher conversions respect to Amberlyst 15, a commercial sulfonated macroreticular resin, especially in the esterification of bulky lauric acid, thanks the enhanced accessibility of the reagent toward catalytic sites in pDVB.

Whereas in gel-type and macroreticular resins high pore volumes are generated, after their swelling, by micropores, pDVB presents a high surface area generated by permanent mesopores at the dry state. This peculiar property cannot be explained by the conventional description of the porous system of macroreticular resins, in which mesopores are depicted as spaces between polymeric nodules (*Paragraph 1.1*). The surface area of conventional cross-linked polymers, in fact, is only few tens of m^2/g, whereas larger values (around 800 m^2/g) are reached only after swelling. Conversely, pDVB can rather be described as a solid foam, in which pores are cavities in a continuous polymer phase. The polymerization mechanism

includes a stage of *"microsyneresis"* in which, differently from "*macrosyneresis"*, the solid forms a continuous phase surrounding droplets of liquid (*Figure 4*).

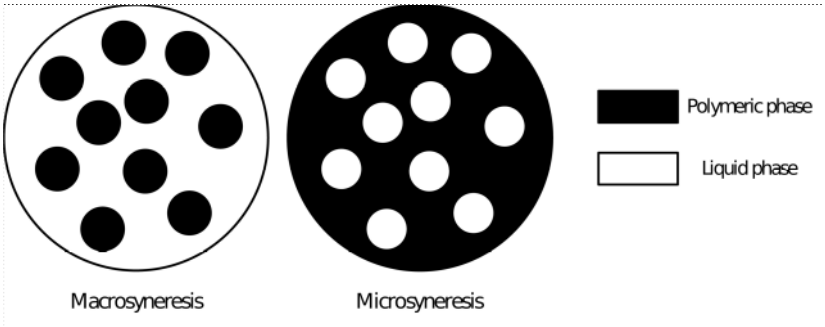

Figure 4: *representation of macro- and microsyneresis.*

After removing the solvent, pores with size comparable with those of the solvent droplets are formed. Usually microsyneresis is considered possible only in a polymerization mixture with very low degree of cross-linking [21]. On the contrary, in this case, microsyneresis seems to occur although DVB is the only monomer. In a recent article[22], Jerabek et al. investigated the porosity of solvothermal pDVB both at the dry and swollen state with BET and ISEC, respectively. The subject of the investigation were two kinds of pDVB, prepared with different content of DVB (solvent:monomer volume ratio 5:1 for pDVB2, 10:1 for pDVB1).
The results of nitrogen adsorption and desorption measurements are reported in Table 1.

Table 1: *dry-state porosity of pDVB1 and pDVB2.*

Sample	**BET surface area (m^2/g)**	**Cumulative surface area in pores bigger than 4 nm (m^2/g)**	**Total pore volume (cm^3/g)**
pDVB1	1096	436	2.07
pDVB2	899	392	1.89

The results of nitrogen adsorption measurements were also analysed by the t-plot analysis (*Figure 5)*.

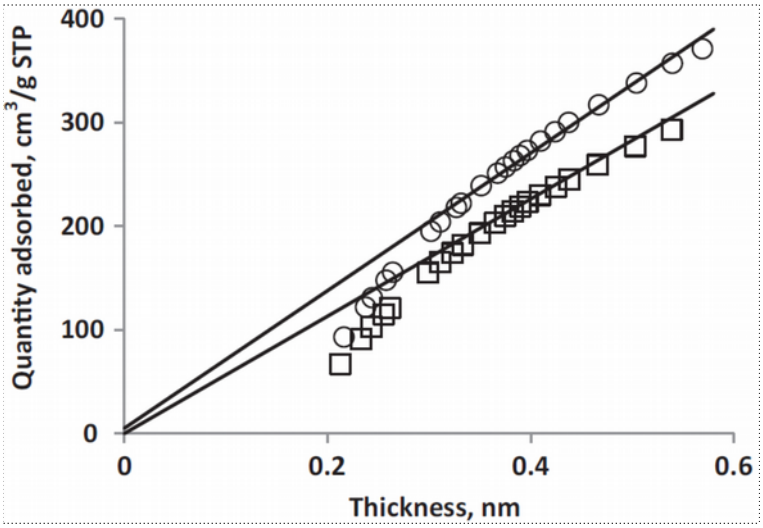

Figure 5: *adsorbed nitrogen as a function of the statistical thickness of the adsorbed layer*

BET surface area is remarkably high for both the materials and appears slightly higher for pDVB1, reasonably due to the lower content of monomer. Exceptionally, t-curve shows a negligible presence of microporosity. Consequently the particularly high pore volume of pDVB is not due to the presence of micropores.

The pore size distribution for pDVB1 and pDVB2 resins is reported in *Figure 6*.

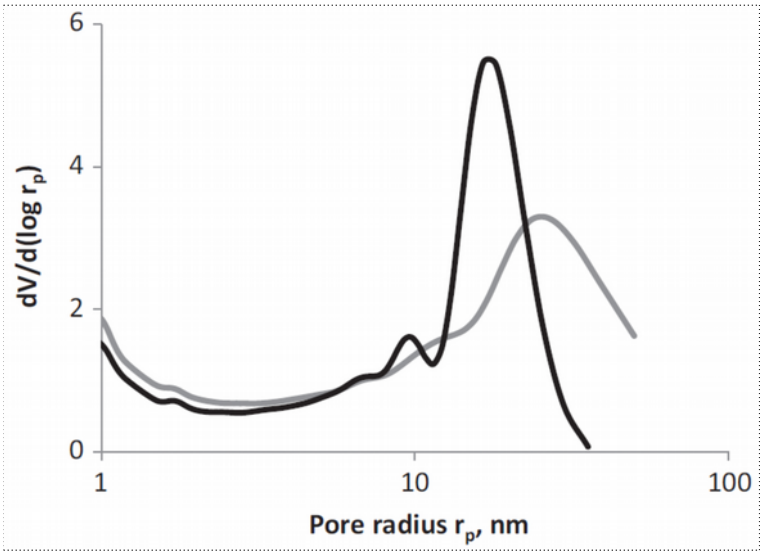

Figure 6: *pore size distribution in dried pDVB materials. Black line: pDVB2; grey line: pDVB1.*

Bigger pores have been detected for pDVB1: the maximum of the distribution can be observed at 50 nm, whereas for pDVB2 it is found at 33 nm. For both types of pDVB the least pore diameter is at 4 nm. The cumulative surface area developed by pores with diameters higher than 4 nm (436 m^2/g for pDVB1 and 392 m^2/g for pDVB2) is approximately the half of the total BET surface area. Since micropores

are not present, pores of about 4 nm are accountable for the remaining surface area. As a matter of facts, mesopores larger than 4 nm noticeably contribute to the extended surface area of pDVB, making realistic the description of its porous system as a nano-foam.

The results of ISEC characterization of pDVB1 and pDVB2 for pores bigger and smaller than 10 nm are separately reported in Table 2 and Table 3, respectively.

Table 2: *ISEC characterization of pores bigger than 10 nm of pDVB1 and pDVB2 (cylindrical pores model).*

Pore diameter (nm)	**pDVB1**		**pDVB2**	
	Pore volume (cm^3/g)	*Pore wall surface area (m^2/g)*	*Pore volume (cm^3/g)*	*Pore wall surface area (m^2/g)*
600	0.62	4	0.00	0
300	0.00	0	0.00	0
150	0.00	0	0.00	0
80	6.78	339	0.00	0
40	0.70	70	4.42	442
20	0.00	0	0.11	22
10	0.00	0	0.00	0
Total	**8.10**	**413**	**4.53**	**464**

Table 3: *ISEC characterization of pores smaller than 10 nm of pDVB1 and pDVB2 (Ogston model).*

Polymer chain concentration (nm/nm^3)	*Polymer fraction volume (cm^3/g)*	
	pDVB1	***pDVB2***
0.1	0.00	0.06
0.2	0.60	0.00
0.4	0.18	0.00
0.8	0.20	0.30
1.5	0.54	0.51

The combined characterization of the dry- and swollen state morphology of pDVBs materials provides important information:

- the pore volume *at the swollen state* is remarkably higher than the pore volume at the dry state (*Tables 1 and 2*). Therefore, pDVB is featured by a permanent pore system able to swell in the presence of a suitable solvent, like THF used for ISEC measurements;

- for dry pDVBs, the surface area of pores bigger than 10 nm is comparable to that generated by pores bigger than 4 nm. It can be deduced that pores smaller than 4 nm collapse during the drying of the material and can be restored by the swelling. Thus, in spite of the rigidity of the polymer matrix, pDVB is able to swell and produces a visible volume increase during swelling process;
- for pDVB1 and pDVB2 the distribution of pores smaller than 4 nm, collapsed after drying, appears similar (*Table 3*). Probably, the swelling of these pores, that reasonably can be described as nano-bubbles like the bigger pores, is a sort of restoration of wrinkled cavities, instead of a real process of solvation.

Further details on the mechanism of formation of the porosity of pDVB by microsyneresis has been reported later by the same research group [23]. As previously pointed out, under conditions of high dilution of monomers and in the presence of a good solvent for the polymer, microsyneresis is favoured. When gel density is sufficiently high to promote the syneresis, the polymer network is too extended to be broken into nuclei (macrosyneresis) and therefore microsyneresis occurs.

According to SEM characterization, the pores of pDVB materials prepared by using good solvents, such as THF, toluene and 1,2-dichloroethane, are hollows in a continuous polymer phase, whereas the porosity of similar material synthesised in the presence of less compatible solvents, such as acetone, n-propanol and n-heptane,. is the result of spaces between loosely packed micro-globules (*Figure 7*).

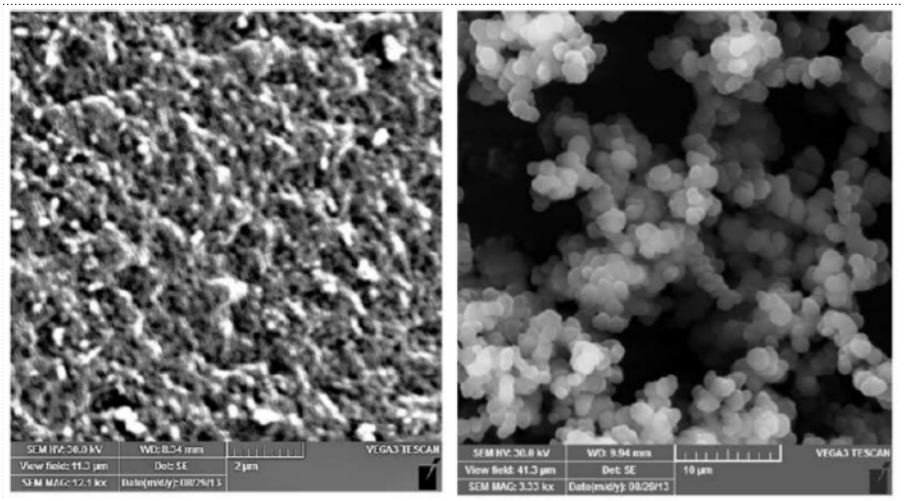

Figure 7: *SEM micrographs of pDVB obtained in THF (left) and in n-propanol (right).*

This outcome clearly shows that the employment of a good solvent for the growing polymer is mandatory to promote microsyneresis; on the contrary, the conventional macrosyneresis mechanism occurs and the foam morphology is not obtained.

In addition to the role of the solvent, the role of the temperature on the swollen state morphology of pDVB can be evaluated by comparing the total pore volume of the material after the synthesis (without drying) with that of the same sample after drying and re-swelling at various reaction temperatures. As an example, the results for pDVB synthesised in toluene are reported (*Table 4*).

Table 4: *swollen-state pore volume, determined by ISEC, in polymers prepared at various temperatures determined just after the polymer preparation ad after drying and re-swelling.*

Reaction Temperature (°C)	**Total pore volume (cm^3/g)**	
	As prepared	**Re-swollen**
100	9.08	8.24
80	10.14	8.99
70	9.57	8.23
60	9.88	8.11
50	10.08	5.18

According to Table 4, the pore volume does not significantly change by modifying the reaction temperature. With the exception of the material prepared at 50 °C, any sample is able to restore the porous system after the drying, in spite of a slight decrease of the total pore volume. Concluding, these outcomes show that the reaction temperature is not a critical parameter for the morphology of the mesoporous system.

On the contrary, the degree of dilution of the monomer in the polymerization mixture is a key factor. ISEC characterization confirms that the mesoporous system typical of pDVB materials can be obtained only at high dilution ratio, supporting the main role of microsyneresis in the formation of the polymer framework.

Similar to the effect of the temperature, the role of the non-solvent in the reaction mixture, considered mandatory in an earlier report for the formation of mesoporosity [20], can be evaluated from the comparison of the pore volume and diameter of the as prepared material and that of the sample after drying and re-swelling. As an example, the results of ISEC characterization of pDVB materials,

prepared by the addition of increasing amounts of n-heptane (0-25 vol. %) to the toluene solution of monomers, are summarized in *Table 5*.

Table 5: *total pore volume and volume-averaged diameter of pores greater than 10 nm for pDVB prepared in toluene (DVB-monomer 1:10 v/v) with different amount of n-heptane.*

Vol % of n-heptane in toluene	As prepared		Re-swollen	
	Total pore volume (cm^3/g)	Mesopores diameter (nm)	Total pore volume (cm^3/g)	Mesopores diameter (nm)
0	10.80	65	7.50	45
6	10.10	68	3.60	23
12	10.00	68	7.50	44
19	10.00	119	8.90	70
25	10.90	83	8.90	74

The total pore volume of the as-prepared materials does not significantly change with the content of n-heptane, mainly affecting, on the contrary, the diameter of mesopores. Moreover, with a high fraction of non-solvent (19 and 25% of heptane), both the total pore volume and mesopores diameter of the re-swollen material are more similar to those of the as-prepared ones: this suggests that the resulting polymer is less sensible to the drying process.

Chapter 2:

EFFECT OF THE SULFONATION ON THE CHEMICAL STRUCTURE AND MORPHOLOGY OF RESINS

Chemical structure and morphology of a set of sulfonated gel-type poly(styrene-divinylbenzene) resins (2 %mol DVB), prepared with different synthetic approaches (sulfonation with concentrated sulfuric acid, oleum and chlorosulfonic acid), were investigated by solid state NMR and Inverse Size Exclusion Chromatography (ISEC). The aim of the investigation is to point out possible modifications in the polymer structure, induced by the different protocols of sulfonation, with particular attention to the formation of sulfone bridges between aromatic rings and its effect on the porosity of the swollen polymer framework. In view of the extensive exploitation of sulfonic resins based on polystyrene-divinylbenzene in the frame of acid catalysis and ion exchange, this issue is particularly relevant for both technological and research purposes. At the present, the issue of the presence of sulfone bridges has been reported in an early study of Goldstein and co-workers [24] and more recently by Sherrington [25], in the frame of the solid state NMR investigation of the mechanism of cross-linking of polymer hypercrosslinked polymers. This investigation is focused on the morphological features of polymer materials obtained by different methodologies of sulfonation and also proposes a relatively simple approach, based on solid state NMR, for the qualitative evaluation of the content of sulfone bridges.

2.1: Proton-exchange capacity

The proton exchanges capacity of the polymer materials, determined by back-titration, is reported in Table 6.

***Table 6**: Proton exchange capacity determined by back-titration and the fraction of sulfonated aromatic rings.*

Sample	Acid content	% of sulfonated rings
Gel_H_2SO_4	5.20 mmol H^+/g	96 %
Gel_oleum	5.51mol H^+/g	100 %
Gel_$HClSO_3$	4.16 mmol H^+/g	77 %

The maximum exchange capacity achievable in a gel-type styrenic resin is 5.4 mmol H^+/g, corresponding to one sulfonic group for each aromatic ring. Therefore, only the resins sulfonated with oleum (*Gel_oleum*) and, to a lesser extent, with concentrated H_2SO_4 (*Gel_H_2SO_4*) can be considered fully sulfonated. On the contrary, the sulfonation with chlorosulfonic acid appears incomplete. This outcome is unexpected on the basis of the known mechanism of the process of sulfonation with these reagents. In fact, sulfuric acid (and oleum) is not able to swell the lipophilic poly(styrene-divinylbenzene) resin and the sulfonation starts from the surface of resin beads: consequently, the sulfonated hydrophilic layer becomes increasingly thicker with the progress of the reaction, up to the complete sulfonation. Thus, in partially sulfonated materials obtained with concentrated sulfuric acid, the distribution of the sulfonic groups within the resin beads is egg-shell [26]. On the contrary, chlorosulfonic acid is soluble in the solvent of the reaction, 1,2-dichloroethane, which is also a swelling solvent for an unfunctionalized poly(styrene-divinylbenzene) resin: therefore, a more homogeneous distribution of the sulfonic groups is expected within the resin particles.

2.2: Total content of sulphur and evidence of sulfone bridges

The results of the CHNS elemental analysis are reported in Table 7. In Table 8 the proton-exchange capacities determined by elemental analysis are compared with those obtained by titration. The ion exchange capacity of Gel_$HClSO_3$ has been calculated by taking into the account the amount of chlorine determined by elemental chlorine analysis (0.11 mmol/g). This residual chlorine comes from an incomplete basic hydrolysis of -SO_2Cl groups in the second stage of sulfonation reaction (*Paragraph 6.6*).

***Table 7**: results of elemental analysis.*

% C	%S	(mmol of benzene rings)/ (gram of resin)	(mmol of sulphur)/ (gram of resin)	Proton exchange capacity determined by elemental analysis	Proton exchange capacity determined by titration
Gel_oleum					
44.96	19.99	4.68	6.24	6.24 mmol H^+/g	5.51 mmol H^+/g
Gel_H_2SO_4					
50.64	17.31	5.27	5.40	5.40 mmol H^+/g	5.20 mmol H^+/g
Gel_$HClSO_3$					
50.40	17.33	5.25	5.40	5.40 mmol H^+/g	4.16 mmol H^+/g

***Table 8:** Comparison between proton exchange capacities determined by elemental analysis and by back titration.*

Sample	Proton exchange capacity determined by elemental analysis	Proton exchange capacity determined by titration
Gel_oleum	6.24 mmol H^+/g	5.51 mmol H^+/g
Gel_H_2SO_4	5.40 mmol H^+/g	5.20 mmol H^+/g
Gel_$HClSO_3$	5.40 mmol H^+/g	4.16 mmol H^+/g

Only for the resin prepared by treatment with sulfuric acid (*Gel_H_2SO_4*) the proton exchange capacity determined by titration is quite in agreement with that obtained by elemental analysis.

The apparent underestimation of the ion exchange capacity in the case of *Gel_$HClSO_3$* and *Gel_oleum* can be reasonably explained with the formation of sulfonic bridges (*Figure 8*), a well known side reaction of the sulfonation with these sulfonating agent [24,27–29].

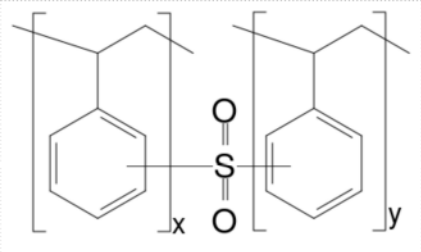

***Figure 8:** sulfone bridge between two monomers of the resin.*

Interestingly, both *Gel_$HClSO_3$* and *Gel_H_2SO_4* show very similar specific amounts of benzene rings (ca. 5.25 mmol/g, Table 7) and sulfur containing groups (5.40 mmol/g, Table 7). This means that, from the statistical point of view, either a

sulfonic group or a sulfone bridge is present on each aromatic ring, but not both of them.

On the contrary, in the case of "Gel_oleum" resin the specific content of sulphur is significantly higher (6.24 mmol/g) than the benzene rings (4.68 mmol/g), suggesting the considerable presence of aromatic rings bearing more than one functional group (sulfonic groups or sulfone bridges). This evidence is consistent with the remarkable sulfonating power of oleum, possibly leading to the oversulfonation of poly(styrene-divinylbenzene) materials and to the obtainment of a resin with an ion exchange capacity higher than the specific content of aromatic rings [30]. Since the formation of sulfone bridges is the product of the condensation reaction between two sulfonic groups, the presence of doubly functionalized aromatic rings, according to Table 8, is also in agreement with a possible over-sulfonation of the material.

Finally, the sulfonation with concentrated H_2SO_4 produces a negligible amount of sulfone bridges with respect to the other sulfonating agents. In fact, according to literature [31], the proposed mechanism involves the protonation of a sulfonic group followed by the condensation with a further sulfonic group. Accordingly, the employment of a very strong acid and dehydrating agent as oleum is expect to promote the formation of bridges in a greater extent compared to sulfuric acid. Moreover, in case of doubly sulfonated rings, the acidity of the sulfonic groups is significantly enhanced [32], due to the deactivation of the aromatic unit, and the protonation step is expected to be more effective.

2.3: ISEC characterization

ISEC is a chromatographic technique aimed to the investigation of the swollen state morphology of cross-linked polymers [17,18,33]. Although the surface area of these polymer materials (a few m^2/g and few tens of m^2/g for gel-type and macroreticular resins, respectively) is almost negligible for their exploitation for chemical purposes, they develop an extended porous system (800-1000 m^2/g of specific surface area) after swelling in a suitable liquid medium, due to the solvation of the polymer chains. Therefore, the utilization of cross-linked polymers

in catalysis is possible only in liquid phase and the investigation of their swollen state morphology is essential to rationalize their chemical behaviour.

The resin morphology is described with ISEC as a set of discrete pore fractions, each one featured by a definite size and a pore volume. The determination of the latter from the elution volumes requires a suitable geometrical description of the porous system. In the cylindrical pores model, usually employed also in the conventional porosimetric techniques (BET and Hg porosimetry), the pores are depicted as cylinders with a specific pore diameter. Alternatively, the porosity of a swollen polymer gel can be also described with the Ogston model, depicting the pores as free spaces between randomly oriented rigid polymer chains. In this case, each pore fraction is featured by a chain concentration, expressed in units of length of polymer chain per unit of volume (i.e. nm/nm^3). It is worthwhile to remark that polymer domains with higher polymer chain concentrations are featured by smaller porosity and vice versa (*Paragraph 1.4*).

The sulfonated resins prepared in the frame of this investigation were characterized by ISEC to assess the role of the sulfonation strategy on their nanometer scale morphology. To obtain a reliable description of the swollen gels, the evaluation of the elution volumes has been performed by using the Ogston model. The selected polymer chain concentrations ranges from 0.1 to 2 nm/nm^3, approximately corresponding to pore diameters from 6 to 1 nm, respectively. The results of ISEC characterization are summarized in Table 9 and in Figure 9.

Table 9: *ISEC characterization of Gel_H_2SO_4, Gel_oleum, Gel_$HClSO_3$*

polymer chain concentration (nm/nm^3)	**Gel_H_2SO_4**	**Gel_oleum**	**Gel_$HClSO_3$**
	Volume of pore fraction (mL/g)		
0.1	0.44	0.10	0.27
0.2	1.30	0.68	0.37
0.4	1.41	2.13	1.92
0.8	0.00	0.00	0.00
1.5	0.00	0.00	0.00
2	0.00	0.00	0.00
Total pore volume (ml/g)	***3.15***	***2.91***	***2.56***

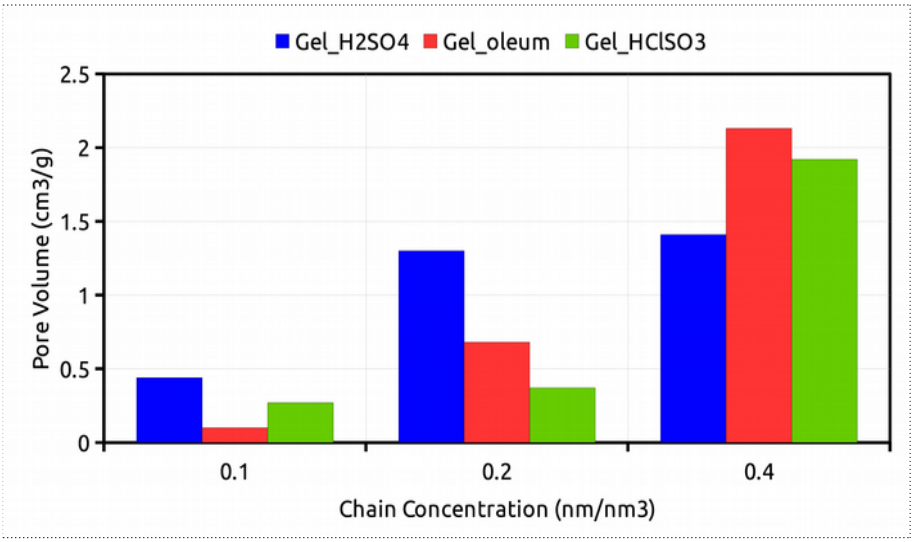

Figure 9: *pore size distribution from ISEC of Gel_H_2SO_4, Gel_oleum and Gel_$HClSO_3$.*

According to ISEC, the main pore fractions for all the investigated materials are 0.2 and 0.4 nm/nm^3. Nevertheless, the values of pore volumes are different among the three investigated resins. Whereas in *Gel_H_2SO_4* the pore fractions with chain concentration of 0.2 and 0.4 nm/nm^3 have practically the same pore volumes, in *Gel_oleum* and *Gel_$HClSO_3$* the fraction at 0.4 nm/nm^3 has remarkably greater pore volume. Also the fraction at 0.1 nm/nm^3 is more significant for *Gel_H_2SO_4* than for other materials, especially for *Gel_oleum*.

This outcome clearly shows a similar morphology for *Gel_oleum* and *Gel_$HClSO_3$*, featured by a pore size significantly smaller of that of *Gel_H_2SO_4*. For materials prepared from the same starting cross-linked polymer, the different swollen state morphology can be directly related to the sulfonation process. This is particularly straightforward for materials with similar ion exchange capacity like *Gel_oleum* and *Gel_H_2SO_4* (5.42 and 5.20 mmol H^+/g, respectively): the smaller pore size obtained with oleum clearly suggests the formation of an additional cross-linking, due to the formation of sulfone bridges, as confirmed by the significant lack of agreement between the total content of sulphur (elemental analysis) and the ion exchange capacity (titration) (*Table 8*). Similarly, the outcomes of ISEC characterization point out the presence of sulfone bridges also for *Gel_$HClSO_3$*, as expected from the results of elemental analysis and titration of the sulfonic groups (*Table 8*).

Complementary information can be also obtained from the overall pore volume of the swollen materials (*Table 9*). The cumulative swollen polymer volume depends on the interactions between solvent molecules and the polymer chains and on the

rigidity of the polymer matrix. The former, for sulfonated poly(styrene-divinylbenzene) materials, are related to the sulfonation degree: the higher the proton-exchange capacity, the higher the ability to swell in polar solvent, such as the aqueous solution of sodium sulfate used during ISEC characterization. Conversely, the rigidity of the polymer matrix is related to cross-linking degree. According to ISEC (*Table 9*) the higher the ion-exchange capacity (*Gel_oleum* and *Gel_H_2SO_4*), the higher the cumulative swollen polymer volume, due to the more efficient solvation of the polymer chains . The significant difference between the cumulative swollen polymer volume of *Gel_oleum* and *Gel_H_2SO_4* results from the additional cross-linking exerted by the sulfone bridges on the polymer framework of *Gel_oleum.*

2.4: FT-IR characterization

The sulfonated materials have been characterized with FT-IR spectroscopy to identify the diagnostic signals of the expected functional groups. The spectra, collected in attenuated total reflectance (ATR) geometry, are reported in Figures 10, 11 and 12.

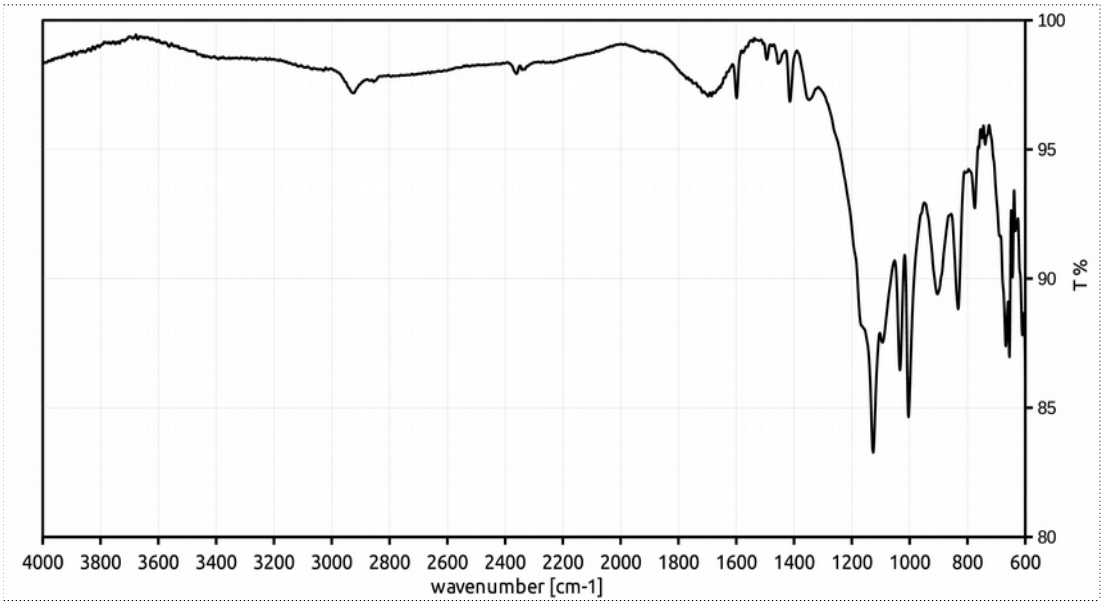

Figure 10: *IR spectrum of Gel_H_2SO_4.*

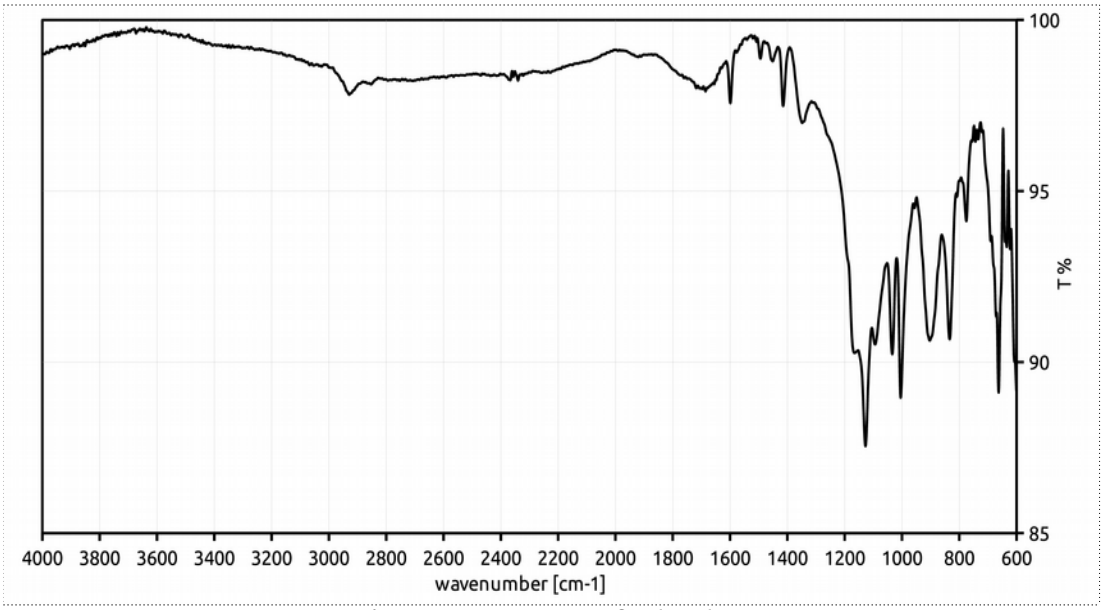

***Figure 11**: IR spectrum of Gel_HClSO₃*

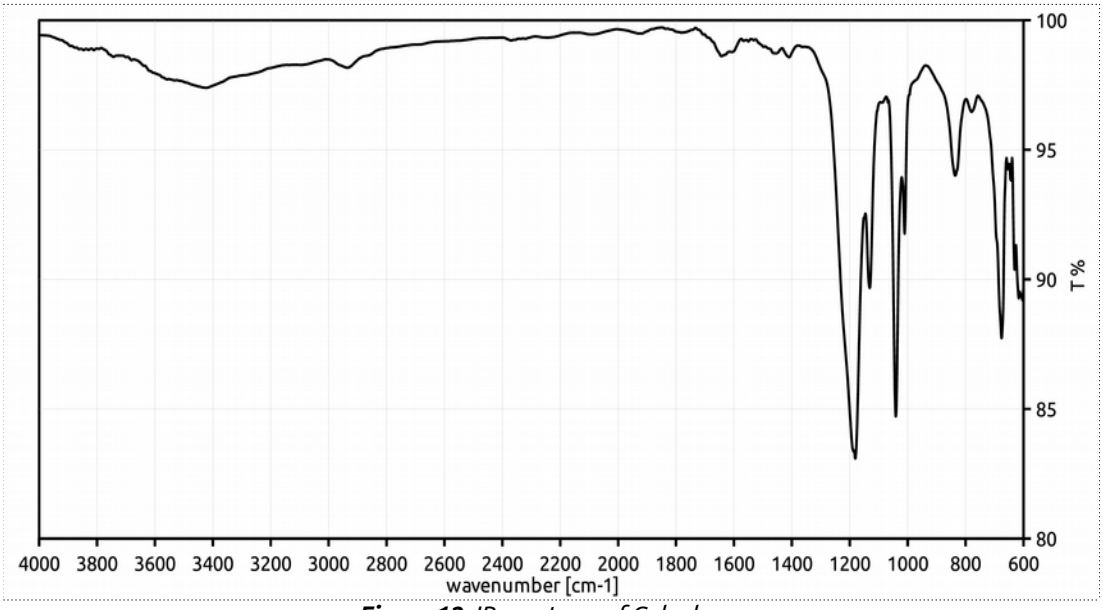

***Figure 12:** IR spectrum of Gel_oleum*

The position of the diagnostic signals of sulfonated poly(styrene-divinylbenzene) materials, with the pertinent assignments, are summarized in Table 10 [34].

***Table 10**: diagnostic signals of sulfonated poly(styrene-divinylbenzene) materials, with the pertinent assignments*

Peak/Band (cm^{-1})	**Assignment**
1599, 1495, 1413	Skeleton stretching vibrations of the benzene ring
1451	scissor vibration of CH_2 group
1348	antisymmetric stretching vibration of the S=O bonds
1033	symmetric stretching vibration of the $-SO_3^-$ ion
1126, 1097	in-plane skeleton vibration of the benzene ring. Bands characteristic of disubstituted benzene rings
1004	in-plane bending vibrations of the CH groups for benzene ring
836 or 831	out-of-plane vibration of the pairs of CH groups in the p-substituted benzene ring (in comparison with p-toluensulfonic acid, 817 cm^{-1})
772	out-of-plane vibration of four CH groups in the o-substituted benzene ring (as the term of comparison, 765 cm^{-1} for o-toluensulfonic acid)

Interestingly, the presence of the signals at 836 and 772 cm^{-1} suggests that reaction of sulfonation could involve either ortho or para positions of the benzene rings. However para position appears the most probable position for the sulfonic group, due to the lower steric hindrance exerted by the alkyl chain of the polymer framework.

Moreover, in the IR characterization of *Gel_HClSO*$_3$ the SO_2-antisymmetric stretching of the $-SO_2Cl$ group is not recognized. Accordingly, the chlorine content is very low (0.11 mmol/g) and the conversion of the sulfonyl chloride units into sulfonic groups in the second stage of sulfonation process can be considered almost complete.

The signal at 907 cm^{-1} can be reasonably assigned to the stretching vibration of the S-O bond of the SO_3H group, in spite of a significant shift from the literature (897 cm^{-1}).

The signal at 1166 cm^{-1} (present as a shoulder in the spectra of Gel_oleum and Gel_$HClSO_3$ materials) has been considered by some authors as diagnostic for the sulfone bridges. In fact, the diphenyl sulfones shows the symmetric stretching vibration of two S-O bonds between 1160 and 1164 cm^{-1} [35,36]. Conversely, a signal at 1172 cm^{-1}, due to the symmetric stretching vibration of the S=O bonds of the SO_3H group, is also reported for sulfonated polystyrene materials [34]. Therefore, the signal at 1166 cm^{-1} cannot unambiguously support the presence of sulfone bridge in the sulfonated resins.

2.5: Solid state MAS ^{13}C NMR characterization

The solid state CP-MAS spectra of the sulfonated resins are reported in Figures 13, 14 and 15. For sake of comparison, the NMR spectrum of the starting cross-linked polymer has also been collected (*Figure 16*). The position of spectral lines at the isotropic chemical shifts has been checked by comparing spectra registered at different MAS speeds. Deconvolution of the observed signals has been carried out taking into account the chemical non-equivalence of the different carbon atoms.

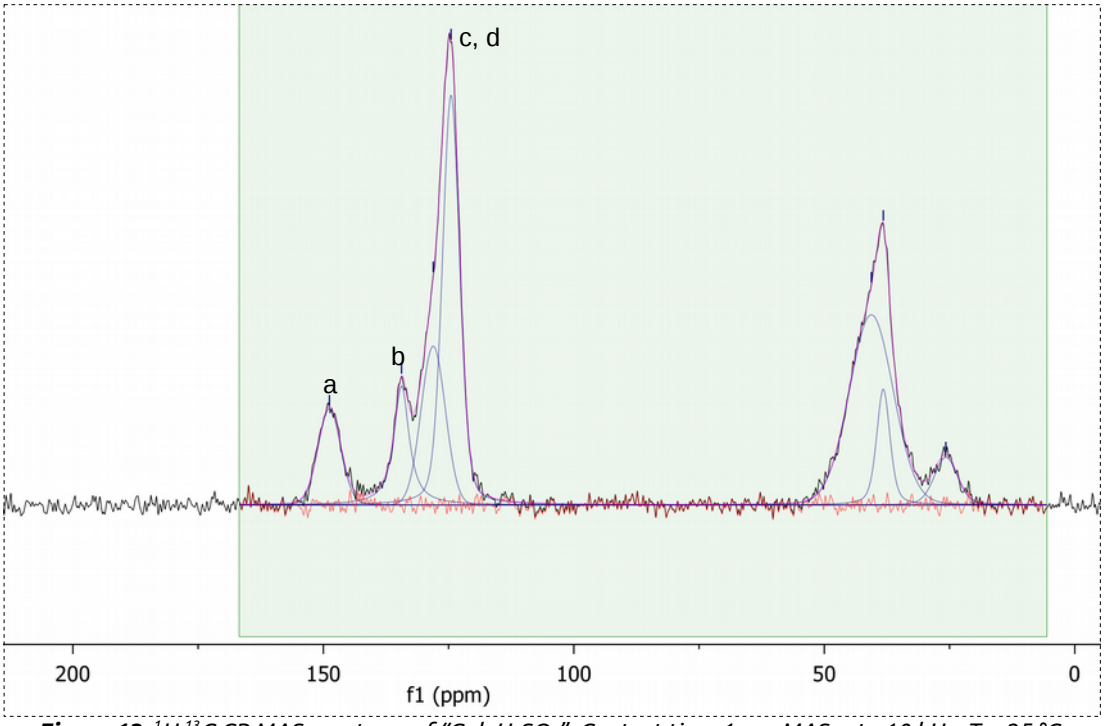

Figure 13: *^{1}H-^{13}C CP MAS spectrum of "Gel_H_2SO_4". Contact time 1 ms, MAS rate 10 kHz, T = 25 °C.*

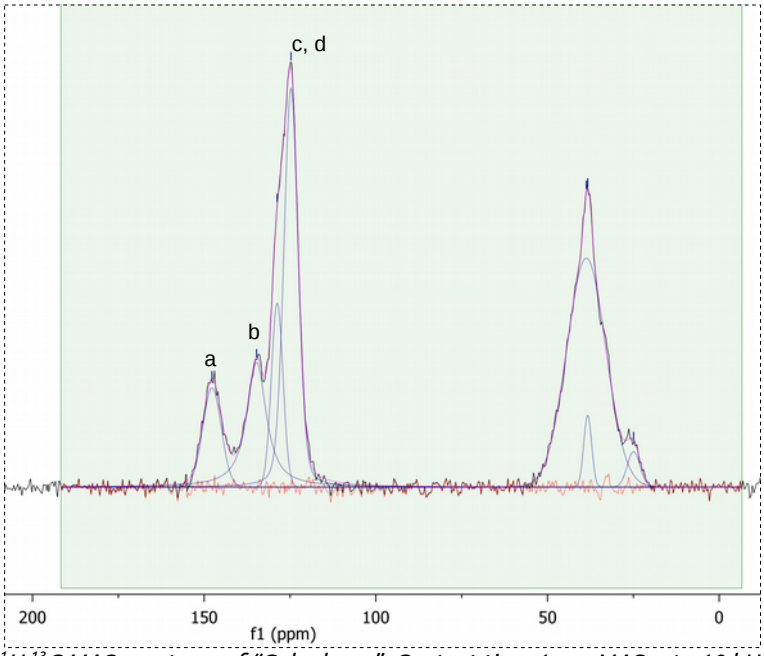

Figure 14: *^{1}H-^{13}C MAS spectrum of "Gel_oleum". Contact time 1 ms, MAS rate 10 kHz, T = 25 °C.*

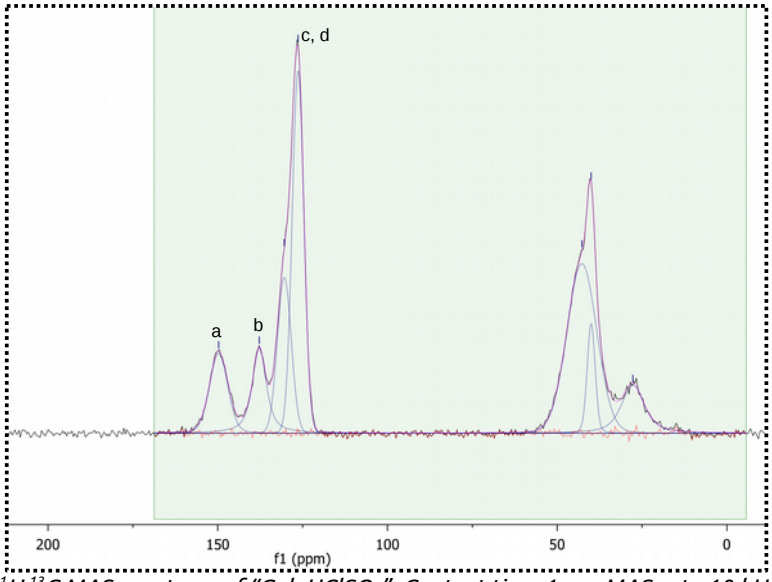

Figure 15: *^{1}H ^{13}C MAS spectrum of "Gel_$HClSO_3$". Contact time 1 ms, MAS rate 10 kHz, T = 25 °C.*

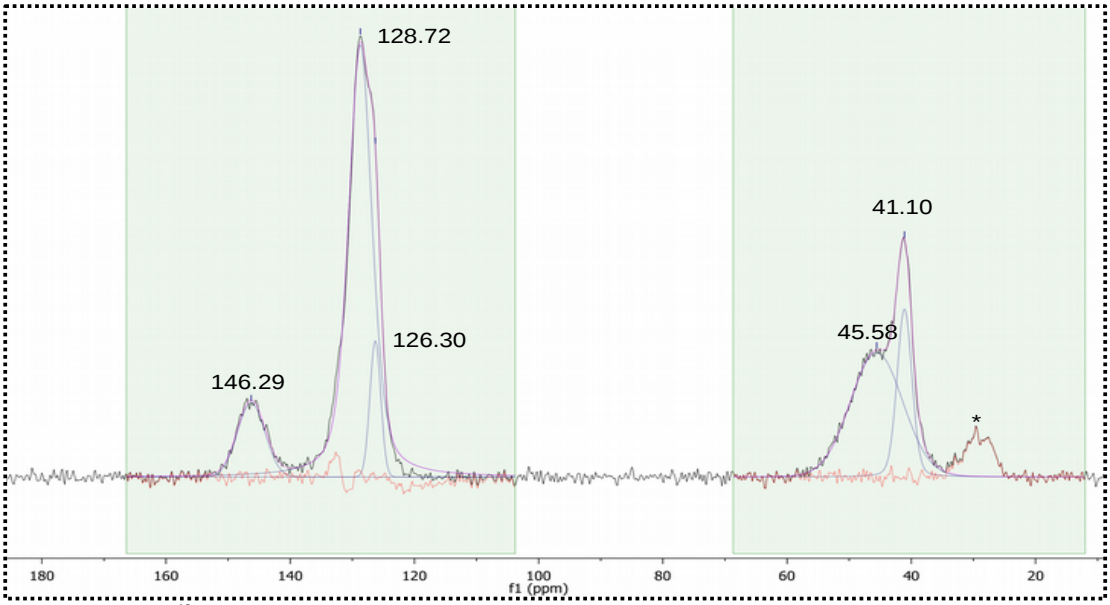

Figure 16: *H ^{13}C MAS spectrum of the starting gel-type poly(styrene-divinylbenzene) (2% mol DVB). Contact time 1 ms, MAS rate = 10kHz, T = 25 °C.*

The signals at 41.10 ppm and 45.58 ppm in the the spectrum of the starting material (*Figure 16*) can be assigned to the backbone carbons. The signal at 146.29 ppm is due to the quaternary carbon of the aromatic rings, whereas the signals at 128.72 and 126.30 ppm have been attributed to non-functionalized aromatic carbons [25].

In polymer samples, broader signals are generally observed for matrices with a low stereo-regularity [37], whereas sharp signals are observed in the presence of regular internal patterns (e.g. isotactic or syndiotactic polystyrene). To this respect, the quite narrow peaks in the spectrum of the non-functionalized gel-type resin (*Figure 16*) suggest a certain amount of order in the polymer matrix.

The signals of sulfonated resins, summarized in Table 11, have been assigned according to the literature [38–40].

Table 11: *signal attribution of H ^{13}C MAS spectra of the sulfonated samples.*

	Chemical Shift (ppm)					
	C $_{ipso}$ (a)	**C $_{para}$ (b)**	**C $_{ortho, meta}$ (c,d)**		**C $_{aliphatic}$**	
Gel_oleum	147.7	134.7	128.7	124.7	38.7	38.3
Gel_H_2SO_4	148.8	134.4	128.1	124.5	40.6	38.2
Gel_$HClSO_3$	149.7	137.8	130.4	126.3	42.7	40.0

In particular, the signal at ca. 135 ppm is due to the carbon atom of the aromatic ring bearing the sulfonic group, when it is in para position respect to the aliphatic chain. This suggests that the sulfonation process mainly involves the para- position of the aromatic ring, in agreement to the literature on the sulfonation of polystyrene [38–41]. Consequently, the extent of the sulfonation in *ortho*- position is negligible, in agreement to the presence of the signal at 836 cm^{-1} in the IR spectra. Although the intensity of cross-polarized signals cannot be directly related to the number of resonating spins, the ratio between the areas of selected signals can be compared among similar samples. The results of this elaboration are collected in Tables 12 and 13**.**

Table 12: *Integrated signal intensities of aromatic carbon atoms*

	Peak area		
	Gel_H_2SO_4	**Gel_oleum**	**Gel_$HClSO_3$**
C_{ipso} (a)	723.8	1476.1	3467.2
C_{para} (b)	834.5	2831.2	3574.5
$C_{ortho,\ meta}$ (c)	1229.3	1716.8	4811.8
$C_{ortho,\ meta}$ (d)	2542.3	5038.1	9517.5

Table 13*: ratio between the integrated signal intensities of selected aromatic carbon atoms*

	Gel_H_2SO_4	**Gel_oleum**	**Gel_$HClSO_3$**
$A(C_{ipso})/A(C_{para})$ [a/b]	0.87	0.52	0.97
$A(C_{ortho,meta})/A(C_{meta/orto,meta})$ [c/d]	0.48	0.34	0.51
$A(C_{ipso})/A(C_{orto,meta})$ [a/c]	0.59	0.86	0.72
$A(C_{ipso})/A(C_{orto,meta})$ [a/d]	0.28	0.29	0.36

The ratios between the integrated NMR signal intensities further supports a possible variation of the composition of the three samples. Notably, according to the results of the elemental analysis and ion exchange capacity (*Tables 7 and 8*), Gel_H_2SO_4 mainly contains aromatic rings with sulfonic groups and only a negligible fraction of sulfone bridges. Similarly, Gel_oleum should not contain unfunctionalized aromatic rings, but, with respect to Gel_H_2SO_4, the fraction of benzene rings bearing two sulfonic groups or, possibly, one sulfonic groups and a sulfone bridge, is significant. Finally, Gel_$HClSO_3$ is featured by mono-functionalized aromatic rings, with either a sulfonic group or a sulfone bridge, and an appreciable amount of unfunctionalized benzene rings. The composition of the

sulfonated gel-type resins, determined on the basis of elemental analysis, ion exchange capacity and ISEC, is summarized in Table 14.

Table 14: *Chemical structures of the samples, expected on the basis of comparison between elemental analysis and ion exchange capacities. The aromatic carbon atoms with similar chemical shifts are labelled with the same letters. The R group can be –OH (in the case of sulfonic group) or the aromatic ring of the polymeric framework (in the case of sulfone bridge)*

Gel_H_2SO_4	Gel_oleum	Gel_$HClSO_3$
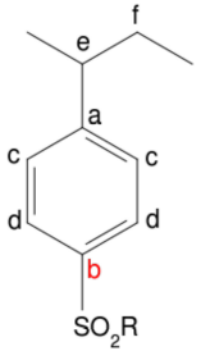	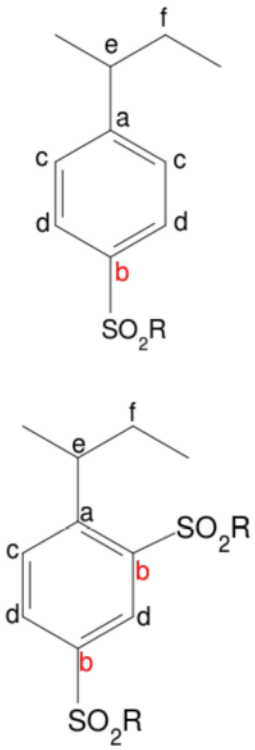	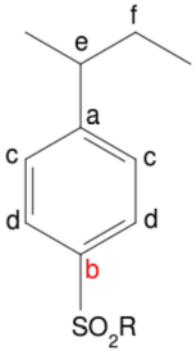

In this discussion, it has been assumed that the chemical shifts of carbon atoms bearing $–SO_3H$ and $–SO_2$- groups are very similar and cannot be resolved in the solid state NMR spectrum. In addition, by comparison with the NMR characterization of the starting material (*Figure 16*), the chemical shift of the carbon atom of the benzene ring bearing the aliphatic chain is not affected by the functionalization of the aromatic ring.

According to the above assumptions, the evaluation of the area ratio among magnetically inequivalent carbon atoms of the benzene rings provides valuable information about the functionalization of the resin materials.

As expected, the ratio [a/d] is similar for any sample, because the number of [d] carbon atoms is not expected to change with the considered functionalization of the aromatic ring (*Table 14*). However, the expected presence in Gel_oleum of a

substantial fraction of aromatic rings bearing two sulphur containing groups (signal at 135 ppm, b) is confirmed by the ratio [a/b], being the smallest among the three samples. This evidence is also indirectly supported by the lowest value of [c/d] and the highest value of [a/c] ratio among the selected materials.

In the case of Gel_$HClSO_3$, the ratio [a/c] is close to that found in Gel_oleum and points out the presence of aromatic rings bearing two sulphur containing groups. In addition, according to elemental analysis and ISEC, in this sample, beside sulfonic groups, also sulfone bridges are present.

Chapter 3:
FUNCTIONALIZATION OF RESINS WITH FLUORINATED MOIETIES

3.1: Fluorinated resins for catalytic applications

The functionalization of aromatic compounds is extensively reported and makes styrenic resins versatile materials for catalytic purposes [42]. Beside the introduction of catalytically active chemical groups, like sulfonic groups for acid catalysis, they can be properly functionalized to tune their chemical and/or physical properties, determining the overall behaviour of the catalysts [42–45].

In this work, the introduction of highly lipophilic fluorinated moieties was investigated since this type of functionalization can lead to promising supports for both acid and metal catalysis. Two new approaches were developed: the first one is based on the Friedel Crafts acylation with perfluoroacylic chains, whereas the second concerns the grafting of a fluorinated polymer inside pDVB by ATRP (Atom Transfer Radical Polymerization) of a fluorinated monomer.

Previously, it was observed that the introduction of lipophilic domains inside acidic hydrophilic catalysts could be useful to promote reactions between reagents with very different polarity, fostering the diffusion of the lipophilic component towards the hydrophilic sulfonic groups[46]. As to the sulfonated styrenic resins, widely used in acid catalysis [42,47], a gel-type resin (2% of DVB) was successfully acylated with linear acyl chlorides with two (acetyl chloride), four (butyryl chloride) or eight (octanoyl chloride) carbon atoms, reaching an acylation degree of 50-80% of aromatic rings. Subsequently, the acylated resins were sulfonated and tested in the esterification reaction of an oil solution of free fatty acids with methanol in the frame of biodiesel production. When the amount of methanol in the reaction mixture is low (5%wt), sulfonated resins give a conversion of about 5% due to its low swelling degree. On the contrary, acylated catalysts show greater conversions due to the assisted absorption of the lipophilic reagent inside the polymer framework[48]. On the basis of these results, the introduction of perfluoro-acylic chains could be potentially interesting thanks to their higher lipophilic character respect to the analogous non fluorinated acylic chains.

Moreover, it is well known that the solubility of gases like hydrogen and oxygen in fluorinated solvents is remarkably higher than in organic solvents[49]. The use of fluorinated supports could therefore be useful to enhance the activity of metal catalysts in the direct synthesis of hydrogen peroxide thanks to the assisted absorption of the gaseous reagents close to the active metal nanoparticles.

3.2: Acylation with perfluoroacylic chlorides

To develop the synthetic procedure for the acylation with perfluoroacylic chains, a gel-type resin (with a 2%wt of DVB) was employed because of the well-known and quite easy morphology of its porous system [17]. First, the established experimental procedure for the acylation of styrenic resins [48] was employed, using perfluorobutyryl chloride as the acylating agent. On the one hand, a short acylic chain is expected to exert a limited effect on the lipophilicity of the resin respect to longer acylic chains. On the other hand, using acylating agents with a greater steric hindrance would probably bring diffusive limitations with a consequent lower degree of acylation. In this preliminary work, aimed to the development of a suitable synthetic protocol, a perfluoro - acylating agent with a relatively small steric hindrance has been therefore selected. However, the literature procedure [48] was completely unsuccessfully, due to the insolubility of the acylating agent in the reaction solvent (carbon disulfide). The synthesis, using a liquid medium (chloroform) in which the solubility of perfluorobutyryl chloride was verified, was successful, leading to a material subsequently named *Gel_acylated*. Subsequently, the same approach was applied to the solvothermal pDVB (*pDVB_acylated*).
In Tables 15 the acylation degree determined from the results of the elemental analysis and by gravimetric approach is reported.

Table 15: *acylation degrees, expressed as the fraction of acylated aromatic rings, determined by elemental analysis and by gravimetric approach*

	%C	%H	% of acylated rings	
			By elemental analysis	**By gravimetric approach**
Gel_acylated	76.36	6.05	21	19
pDVB_acylated	78.69%	7.05%	13	10

The degrees of acylation determined by gravimetric approach are slightly lower than the ones determined by elemental analysis, probably due to the inevitable loss of material during the different stages of the synthesis of the material, leading to an underestimation of the yield.

For each material a characterization of the starting cross-linked polymer by solid state NMR spectroscopy has been performed (*Figures 17 and 18*).

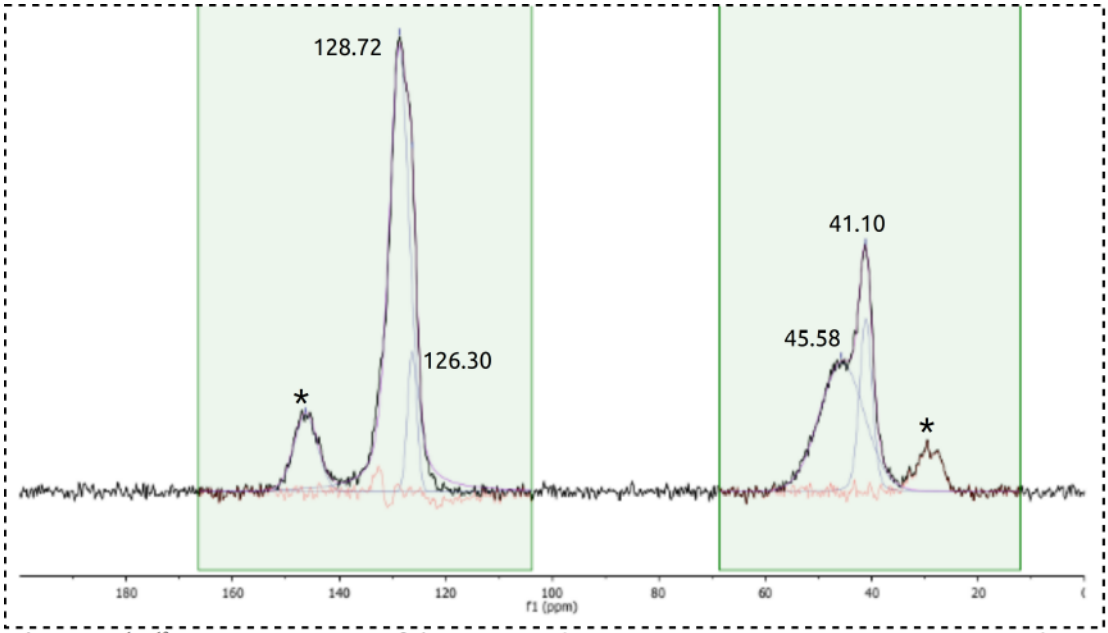

Figure 17: *^{1}H ^{13}C CP MAS spectrum of the pristine gel-type resin. Contact time 1 ms, MAS rate = 10kHz, T = 25 °C.*

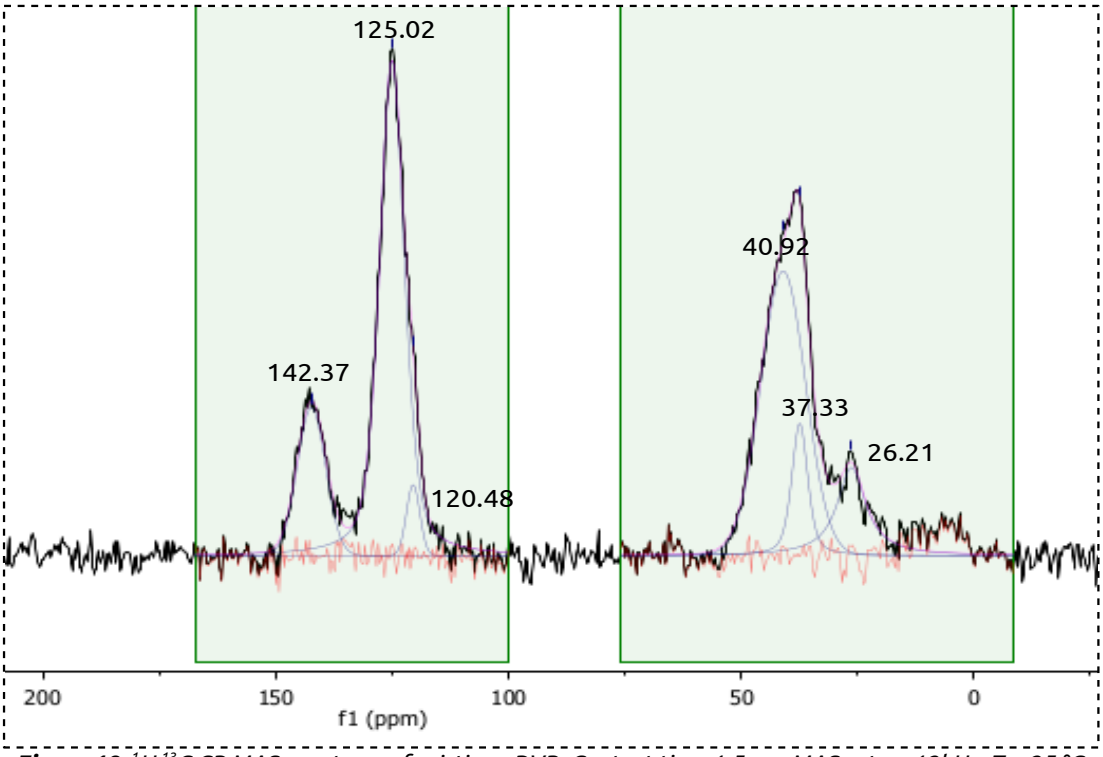

Figure 18: *^{1}H ^{13}C CP MAS spectrum of pristine pDVB. Contact time 1.5 ms, MAS rate = 12kHz, T = 25 °C.*

The spinning side-bands have been recognised by comparison among spectra registered at different spinning speeds. The resonances of each magnetically inequivalent carbon atoms have been analysed by signal deconvolution.

The signals at 41.10 ppm and 45.58 ppm in the the spectrum of gel type un-functionalyzed resin (*Figure 17*) can be assigned to the backbone carbons. The signal at 146.29 ppm is due to the quaternary carbon of the aromatic rings, whereas the signals at 128.72 and 126.30 ppm have been attributed to non-functionalized aromatic carbon atoms [50].

Similarly, in the spectrum of un-functionalyzed pDVB (*Figure 18*) the signals of the backbone carbons lie at 40.92 and 37.33 ppm. The signal at 142.37 ppm is due to the quaternary carbon of the aromatic rings, whereas the signals at 125.02 and 120.48 ppm have been attributed to non-functionalized aromatic carbons [51,52]. In the literature spectrum [53] there are also signals due to carbon atoms of vinyl groups (111.4 and 137.5 ppm) that did not react during polymerization reaction. In Figure 18 such signals are absent, so we can deduce a complete polymerization of divinylbenzene monomers.

In Figures 19 and 20 ^{19}F spectra of the acylated resins are reported.

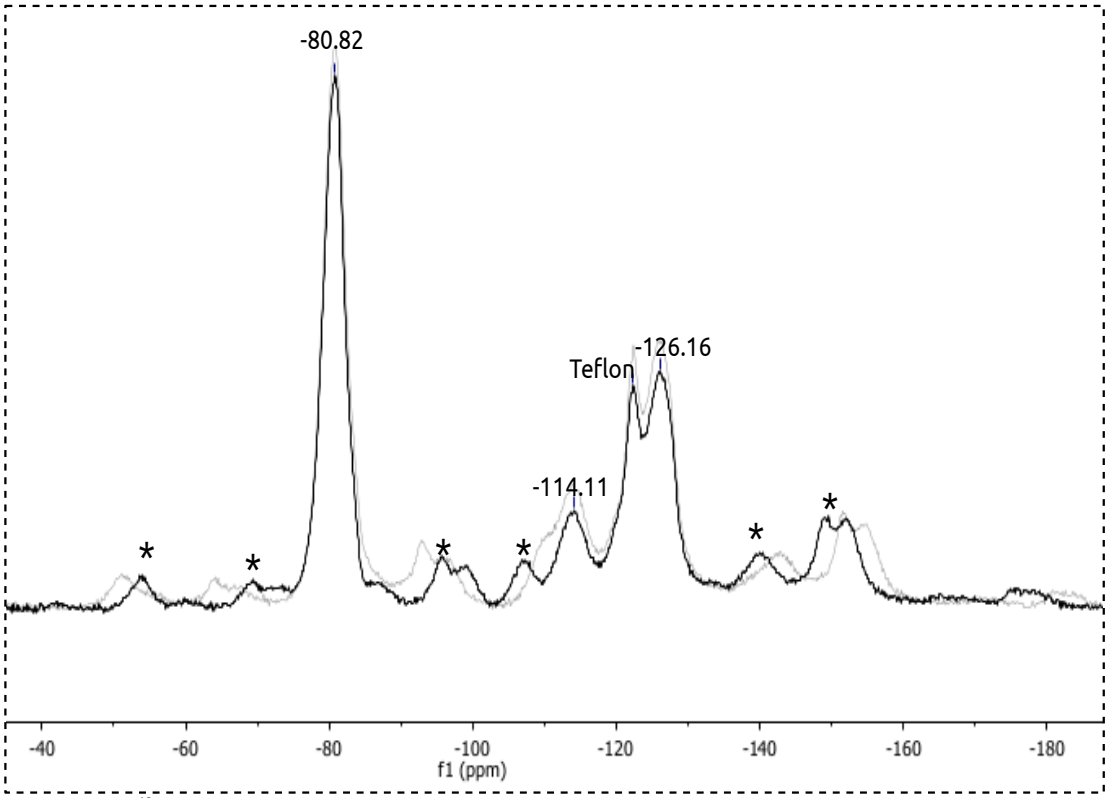

Figure 19: *^{19}F MAS spectrum of acylated gel-type resin (Gel_acylated). Black trace: MAS rate = 10 kHz. Gray trace: MAS rate = 11 kHz. The spinning side bands are marked with an asterisk.*

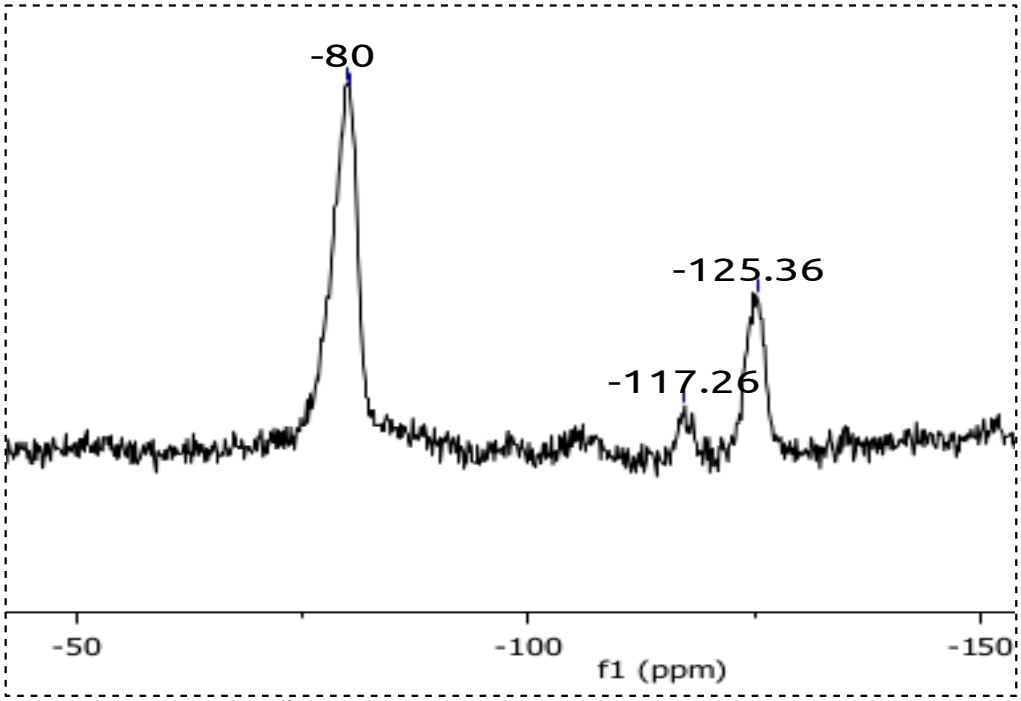

Figure 20: *^{19}F MAS spectrum of pDVB (pDVB_acylated). MAS rate = 10 kHz.*

The signals (*Table 16*) present in ^{19}F spectrum can be ascribed on the basis of the spectrum of perfluorobutyril chloride reported in literature [54]. In addition, DFT calculations on a model molecule (*Figure 21 and Table 16*) further support the attribution of the ^{19}F MAS signals. For a reliable comparison, the differences between the DFT values and the experimental ones (reported as "delta" in Table 16) must be considered. These differences are very similar for each type of magnetically equivalent fluorine atoms in both the acylated resins, therefore indicating a systematic offset between the data.

***Table 16**: signals present in ^{19}F spectra for the samples Gel_acylated and pDVB_acylated. The reported DFT values are the average values calculated for each fluorine atom.*

	Resin-CO-C**F2**-CF2-CF3	Resin-CO-CF2-C**F2**-CF3	Resin-CO-CF2-CF2-C**F3**
DFT	-130.42	-139.54	-93.94
Gel_acylated	-114.11	-126.16	-80.82
pDVB_acylated	-117.26	-125.36	-80
Δ (Gel_acylated)	16.31	13.38	13.12
Δ (pDVB_acylated)	13.16	14.18	13.94

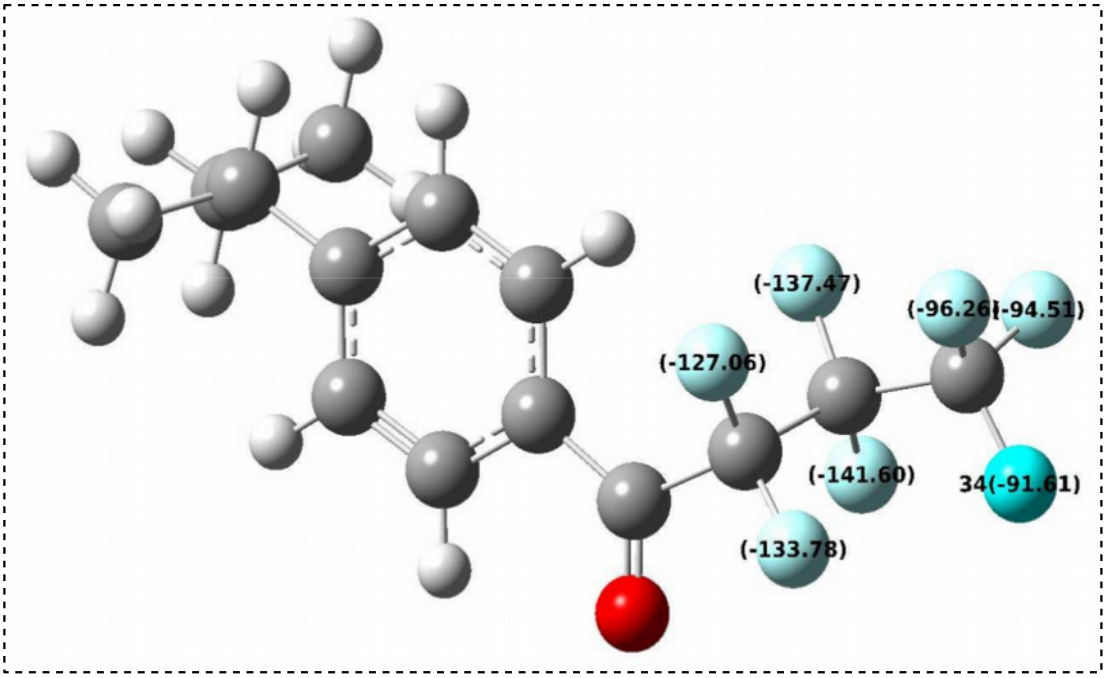

***Figure 21:** DFT calculations on the model molecule 1-(4-(sec-butyl)phenyl). Geometry optimization was performed at the B3LYP-6-31G(d, p) level of theory. Chemical shifts were calculated at the B3LYP-CC-pVTZ level of theory.*

The ^{13}C spectra, obtained by cross-polarization from protons, are reported in Figures 22 and 23 and the signals are summarized in Table 17 and in Figure 24.

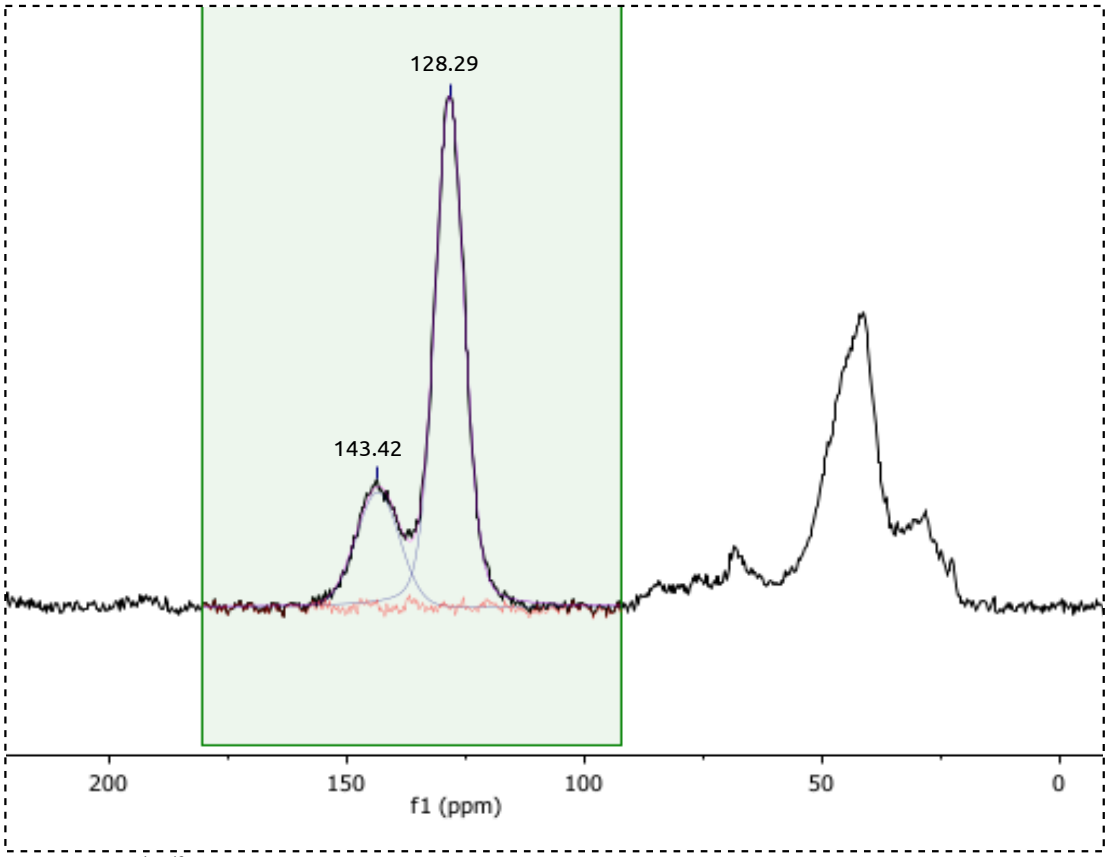

Figure 22: *^{1}H ^{13}C MAS spectrum of the acylated gel-type resin (Gel_acylated). Contact time 1 ms, MAS rate = 10kHz, T = 25 °C.*

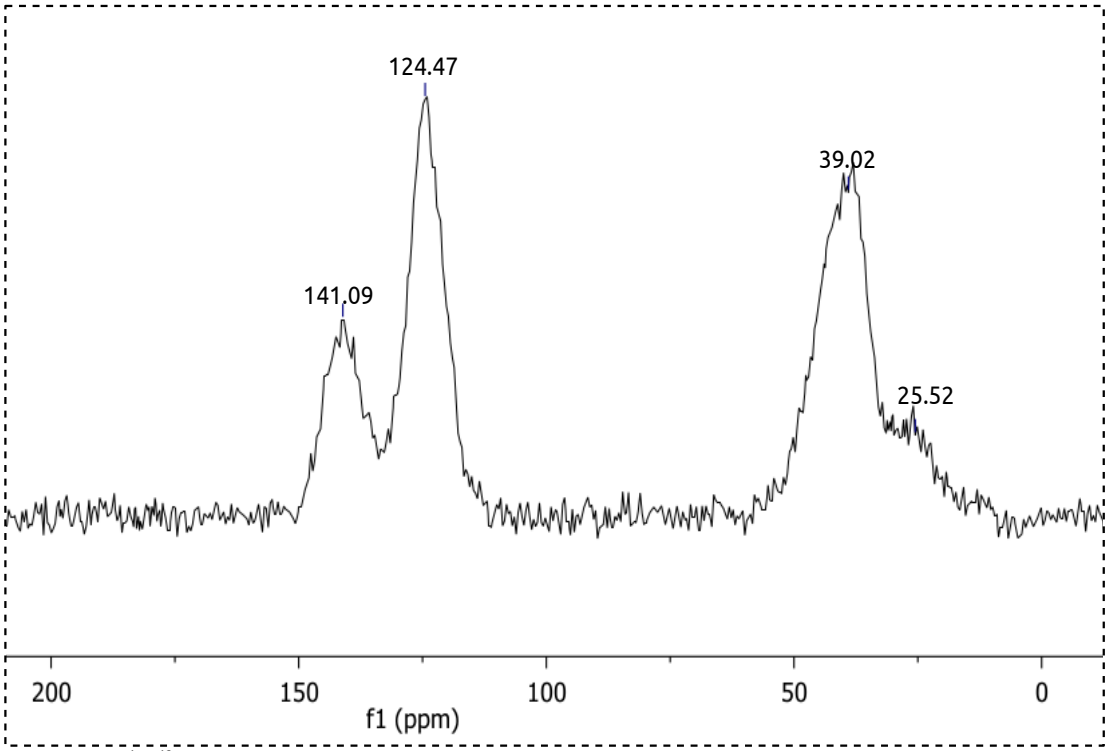

Figure 23: *^{1}H ^{13}C CP MAS spectrum of the acylated pDVB (pDVB_acylated). Contact time 1 ms, MAS rate = 10kHz, T = 25 °C.*

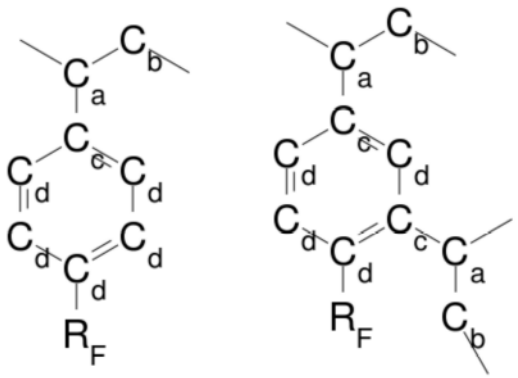

Figure 24: *schematic representation of acylated monomers of a gel-type resin, on the left, and of pDVB, on the right. For simplicity, in the case of pDVB only para- isomer is represented.*

Table 17: *attribution of the signals in the ^{1}H ^{13}C MAS spectra (Figures 22 and 23) of acylated resins (Figure 24).*

	C_a	**C_b**	**C_c**	**C_d**
Gel_acylated	43.03 ppm	28.33 ppm	143.42 ppm	128.29 ppm
pDVB_acylated	39.02 ppm	25.52 ppm	141.09 ppm	124.47 ppm

Interestingly, this kind of pattern for the aromatic signals suggests a para-acylation of the aromatic rings. Although this is expected on the basis of electronic and steric features of electrophile aromatic substitutions, in the case of resins, steric hindrance exerted by the polymer chains could severely affect the substituent orientation. In the case of pDVB, this pattern is interesting, because technical DVB is a mixture of para- and meta- isomers and therefore para- position is partially occupied. The fraction of each geometrical isomer has not been provided by the supplier and, therefore, it was determined from the ^{1}H NMR spectrum of technical DVB (*Figure 25*). Upon comparing the area of the signals of the geminal cis $=CH_2$ protons of divinylbenzene (5.70-5.55 ppm) and the methylene group of the ethyl moiety of ethylvinylbenzene, the nominal content of divinylbenzene (80%wt) is confirmed. More interestingly, on the basis of the ratio between the areas of the geminal cis $=CH_2$ protons of the para- (5.64 ppm) and of the meta- (5.66 ppm) isomers, the molar fraction of the meta- isomer turns out to be prevalent (65 %) [55]. According to the lower steric hindrance of para- position, the significantly higher abundance of m-divinylbenzene in the monomer mixture and the relatively low acylation degree (12%), para- position appears the most probable site for the functionalization of the aromatic rings, in agreement with the ^{1}H ^{13}C MAS pattern of pDVB (Figures 23 and 24).

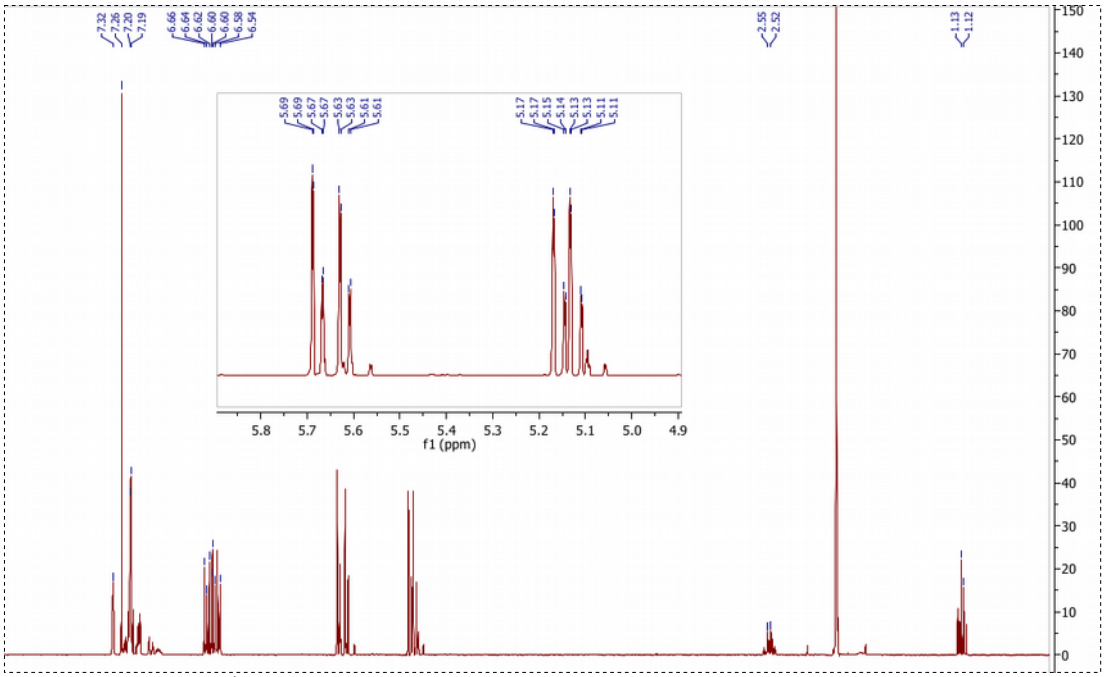

Figure 25: *^{1}H NMR spectrum of technical DVB (80%) used for the synthesis of pDVB.*

Interestingly, the spectra of pristine resins show a significantly smaller signal line-width then the acylated materials. A broadening of the signals is generally due to a decrease of the order of the matrix. In fact, a micro-crystalline material should provide ^{13}C MAS spectra with defined peaks in both the solid- and the solution-state. Therefore, the chemical modification of the polymer matrix obtained by acylation reaction changes the crystal structure of the resin, reducing the local order.

Finally, ^{19}F ^{13}C MAS spectrum cross-polarized from the fluorine of acylated gel-type resin is reported in Figure 26 and the signal attributions are collected in Table 18.

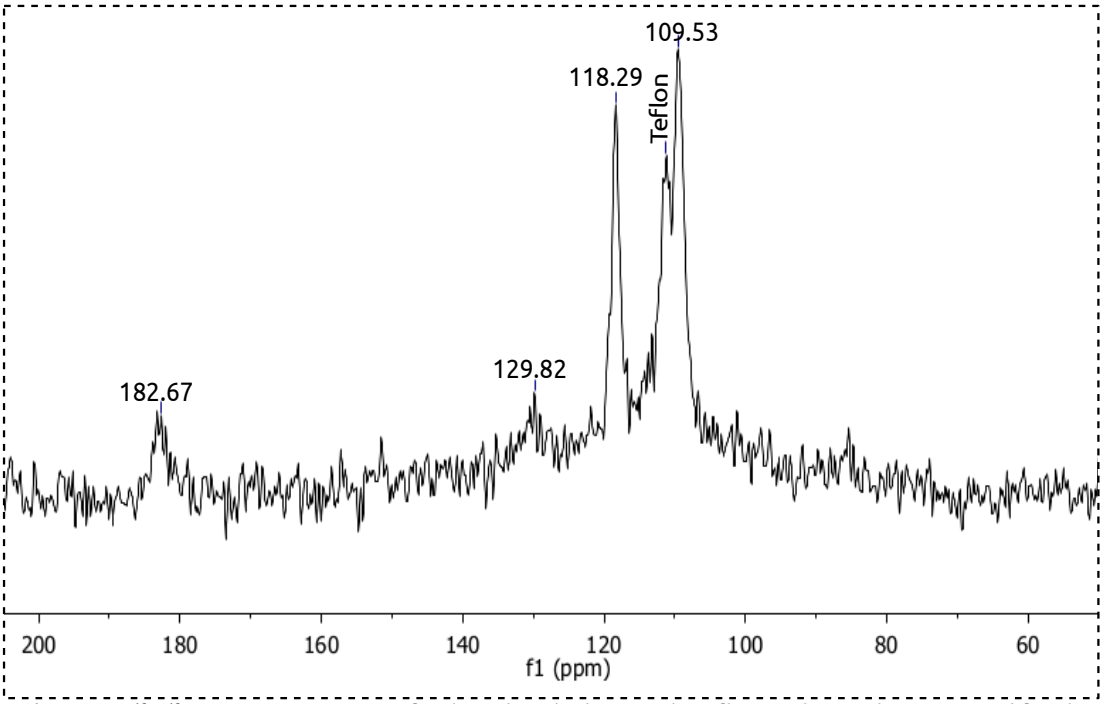

Figure 26: *^{19}F ^{13}C CP MAS spectrum of Gel_acylated. The signal "Teflon" is due to the rotor used for the collection of the spectrum. Contact time 2 ms, MAS rate = 10kHz, T = 25 °C.*

Table 18: *Signals of acylated resins in the ^{19}F ^{13}C MAS spectra.*

	Resin-**C**O-CF2-CF2-CF3	Resin-CO-**C**F2-**C**F2-CF3	Resin-CO-CF2-CF2-**C**F3
Gel_acylated	182.67 ppm	109.82 ppm	118.47 ppm
pDVB_acylated	n. d.		

Interestingly, the signal at 129 ppm 8 (*Figure 26*) is too weak to be attributed to the acylic chain. Probably, it is due to an aromatic carbon atom of the resin receiving polarization from the acylic chain. Because cross-polarization is transferred through neighbouring atoms, this circumstance confirms that acylation reaction effectively occurred on the polymer matrix and the observed pattern is not due to the inclusion of butyric acid inside the porous system of the resin.

The spectrum for acylated pDVB is not reported because the signals are too weak to be properly determined. Compared to gel-type resin, the low density of pDVB, as expected from its extensive porous system (*Paragraph 1.5*), significantly limits the mass of sample introduced in the rotor, with the consequent reduction of the signal-to noise ratio.

3.3: ATRP

ATRP (Atom Transfer Radical Polymerization) is a kind of living radical polymerization, proceeding without irreversible chain transfer and termination reactions. The general mechanism of ATRP is shown in Figure 27 [56].

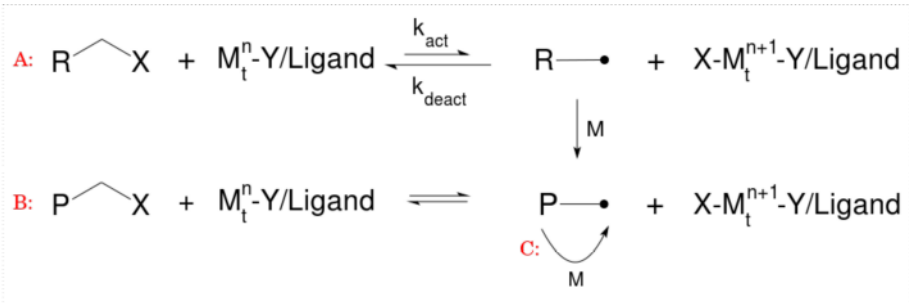

Figure 27: *mechanism of ATRP.* ***A****: initiation.* ***B****: equilibrium with dormant specie.* ***C****: propagation.*

First, the active radical specie (*R·)* is generated thanks to a redox process, catalysed by a transition metal complex (*M_t^n-Y/Ligand*, where Y is a counter-ion) that abstracts an halogen atom from the "dormant specie" *RX* undergoing to one-electron oxidation step (step A in Figure 27). Once *R·* is formed, a common radical polymerization of a monomer *M* starts, giving the growth of the polymeric chains (step C in Figure 27). Each growing chain is in equilibrium with the corresponding dormant specie (step B in Figure 27), thanks to the reversibility of the redox reaction. These new chains can continue their growth as long as new monomers are available in the polymerization mixture.

ATRP is a powerful polymerization technique. In fact, beside its living character that permits to obtain block copolymers, it provides a final product with a very low polydispersity index, thanks to the uniform growth of the polymeric chains. The proper selection of the experimental parameters, in fact, makes possible to adjust the equilibrium constant of the initiation process ($K_{eq} = k_{act}/k_{deact}$). In particular, the deactivation process must be faster than the activation one ($k_{act} >> k_{deact}$) because, otherwise, the amount of radical species in solution would be too high and the termination reactions would occur easily, cancelling the living character of the polymerization and preventing the uniform growth of the polymer chains. Generally, the equilibrium involving dormant species (step B in Figure 27) is also shifted toward the dormant species and this further contributes to maintain low the concentrations of radical species in solution.

With ATRP, it is possible to polymerize a great variety of monomers (styrenes, (meth)acrylates, (meth)acrylamides, and acrylonitrile for examples), as long as they contain substituents able to stabilize the propagating radicals. As to the catalysts, the most commonly used are based on Copper, thanks to the presence of two readily accessible oxidation states separated by one electron and its affinity with halogens.

In this work, the ATRP of a fluorinated monomer was employed as the synthetic approach, alternative to Friedel-Crafts acylation, for the introduction of fluorinated moieties in poly-divinylbenzene. First the bromination of the benzyl carbon group of the resin has been obtained by reaction with NBS (N-Bromosuccinimide) to create, on the resin, a number of "dormant species", necessary to the initiation step of the polymerization (*Figure 28*) [57]. The results of the elemental analysis of the pristine and functionalized resins show a bromination degree of 25% respect to the total amount of aromatic units.

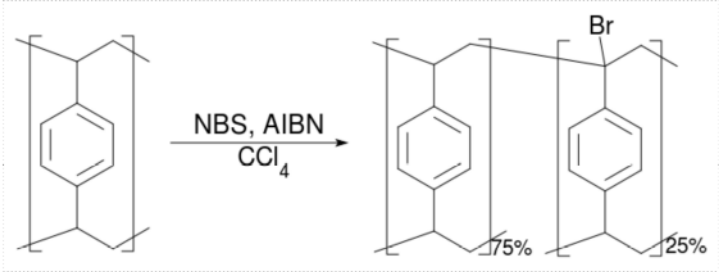

Figure 28: *bromination of the polymer framework in the benzylic position.*

After the generation of alkyl bromide moieties inside the resin, ATRP (*Figure 29*) can be carried out. The selected monomer for the present investigation is 1H,1H, 2H, 2H-perfluorodecylacrylate (*PFDA*).

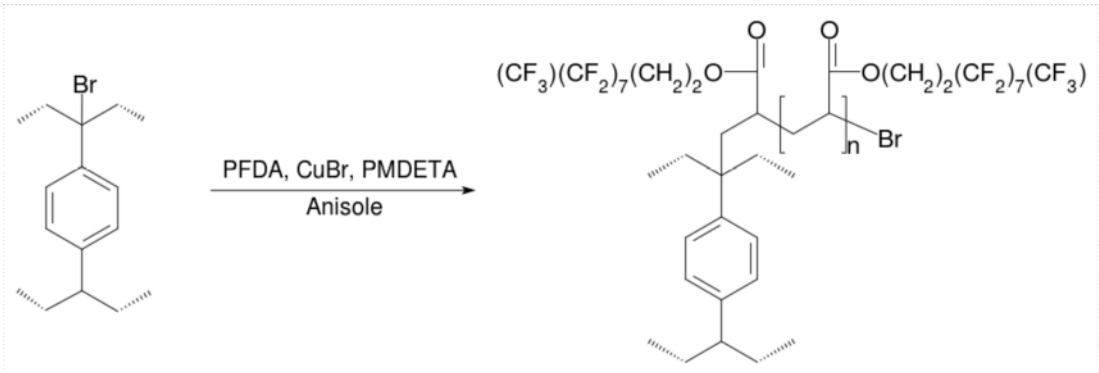

Figure 29: *ATRP of PFDA inside the pDVB resin. PMDETA (pentamethyl-diethylenetriamine) is used as ligand for CuBr. The solvent of reaction is anisole and the reaction temperature is 80 °C.*

After functionalization, the resin sample showed an increased of weight of 14%, respect to the brominated resin and, according to the results of the elemental analysis, the moles fraction of introduced fluorinated monomers is 8%, respect to those of the aromatic units of the resin. The obtained degree of functionalization is rather low with respect that reached by acylation with perfluorobutyryl chloride (ca. 12% of acylated aromatic rings). However, the remarkably high steric hindrance of both PFDA and the resulting polymer, respect to perfluorobutyryl chloride, has to be taken into the account and therefore the lower degree of functionalization is likely connected to the higher diffusion limitations of the perfluorinated monomer.

To generate Palladium nanoparticles inside the fluorinated material obtained with ATRP exploiting the TCS approach (*Paragraph 5.5*), the introduction of suitable functional groups (such as sulfonic groups), aimed to bind the metal precursor, is necessary. However, the treatment of the fluorinated resin with concentrated sulfuric acid (*Paragraph 6.5*) leads to the hydrolysis of the ester bonds of fluorinated chains. Similarly, the sulfonation process with chlorosulfonic acid (*Paragraph 6.6*) is not suitable: in fact, the grafted polymer, although not damaged by the introduction of chlorosulfonic groups, is unfortunately hydrolysed during the subsequent basic treatment (*Figure 30*).

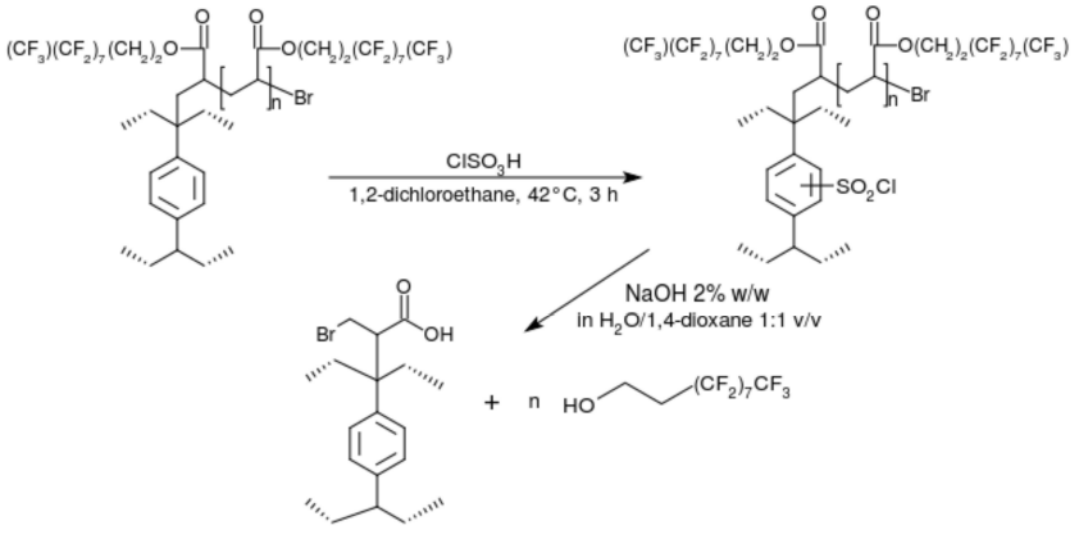

Figure 30: sulfonation of pDVB_ATRP by chlorosulfonic acid ($ClSO_3H$). During the step of basic hydrolysis of cholosulfonic groups ($-SO_2Cl$) to chlorosulfate groups ($-SO_3Na$), the grafted polymer is also hydrolysed 1*H*,1*H*,2*H*,2*H*-Perfluoro-1-decanol.

Consequently, because the sulfonated resin is not swellable in CCl_4, the solvent for bromination reaction, the sulfonation must be carried out on the brominated resin before the functionalization by ATRP. The new synthetic approach, exploited for the preparation of the fluorinated support, is summarized in Figure 31.

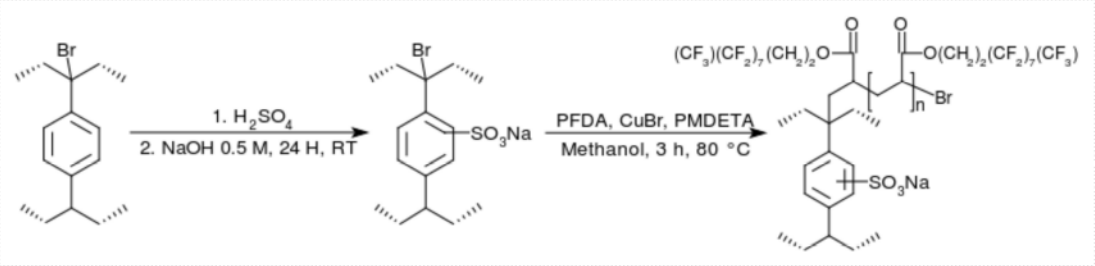

Figure 31: *strategy for grafting pPFDA on sulfonated pDVB with ATRP. The sulfonation is performed on the brominated pDVB by using concentrated sulfuric acid. After the neutralization of the resin with an aqueous solution of NaOH, ATRP of PFDA can be performed.*

Before ATRP, the brominated and sulfonated resin is neutralized with an aqueous solution of NaOH, to avoid the presence of heterogeneous acid during the subsequent ATRP. Moreover, in this case case methanol is used as solvent instead of anisole, being methanol a better swelling solvent for sulfonated resins. Generally protic solvents are not the first choice as the solvent for ATRP, because they can coordinate the Cu^{II} centre and the halide ions, thus suppressing the equilibrium with dormant species (step B in Figure 27). Consequently, the living character of the polymerization is partially lost with a poor control on the polydispersity of the resulting polymer. Although in literature strategies to overcome this drawback are reported [58–60], for the sake of the preparation of a fluorinated support for Pd nanoparticles, the accurate control of polydispersity has been neglected.

On the basis of the results of elemental analysis, the molar fraction of introduced fluorinated monomers respect to the aromatic rings of resin is about 7%. This outcome is very similar to the degree of functionalization obtained by ATRP using CCl_4 as the solvent (8%).

Although the degree of functionalization is not particularly high, probably due to diffusion limitation connected to the steric hindrance of the PFDA and the resulting grafted polymer, the lipophilic effect exerted by the long C_{10} alkyl chains could be relevant for the catalytic property of the material.

Chapter 4:
Sulfonic resins as solid acid catalysts for the esterification of stearic acid

4.1: Brief overview of worldwide energy consumption

The worldwide energy demand is continuously increasing, mainly as the result of the economic growth of developing countries, like China and India [61]. This trend is clearly documented by BP in the statistical review of 2016 [62], reporting an almost linear increase of world energy consumption, allegedly still increasing in the next years (*Figure 32*).

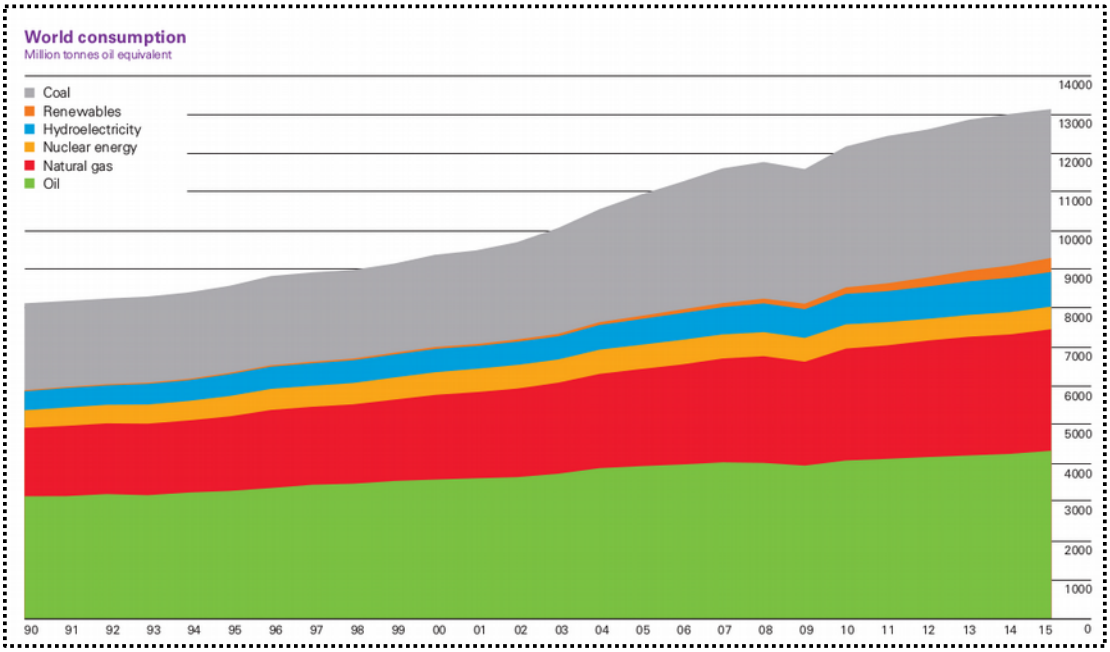

Figure 32: *world energy consumption from 1990 to 2015. The negative peak between 2008 and 2009 is due to the financial crisis. To allow a comparison, all the data are expressed in term of tonnes of oil equivalent (toe).*

According to Figure 32, both the production and the consumption of traditional fossil resources (oil, natural gas and coal) remarkably increased from 2004 to 2015. On the contrary, over the same period of time, the production of nuclear and hydroelectric energy remains practically unchanged. Similarly, the utilization of renewable resources, beside hydroelectric ones, is constantly growing, although

they represent only a small fraction of the total energy consumption. Although oil is still the main source of energy, the increase of consumption and production is sensibly smaller than natural gas and coal and this can be explained considering the distribution of fossil resources over the world (*Figure 33*).

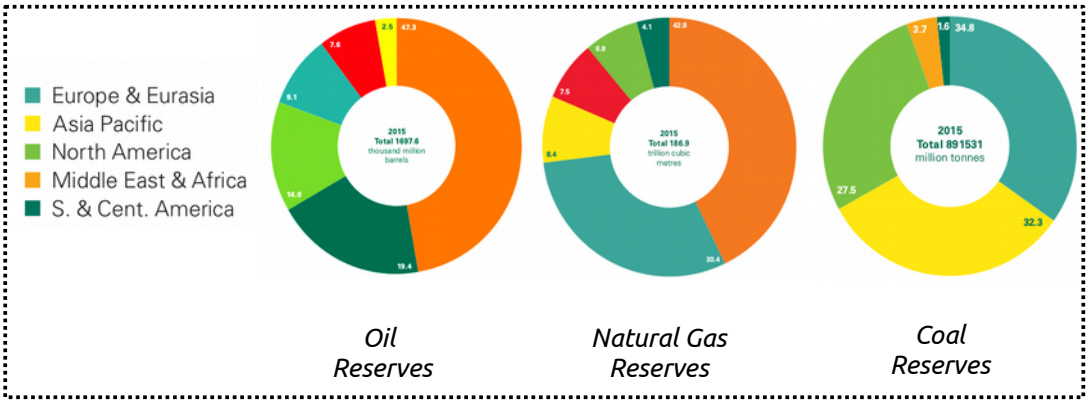

Figure 33: *distribution of proved reserves of oil, natural gas and coal.*

The most abundant fossil feedstocks in Asia-Pacific are coal and natural gas, respectively: it is therefore expected that the developing countries China and India are mainly exploiting these local resources to promote their economic growth. Similarly, coal is also abundant in Eurasia and its consumption in the Eastern Europe is, in fact, larger than in the Western Europe (*Figure 34*).

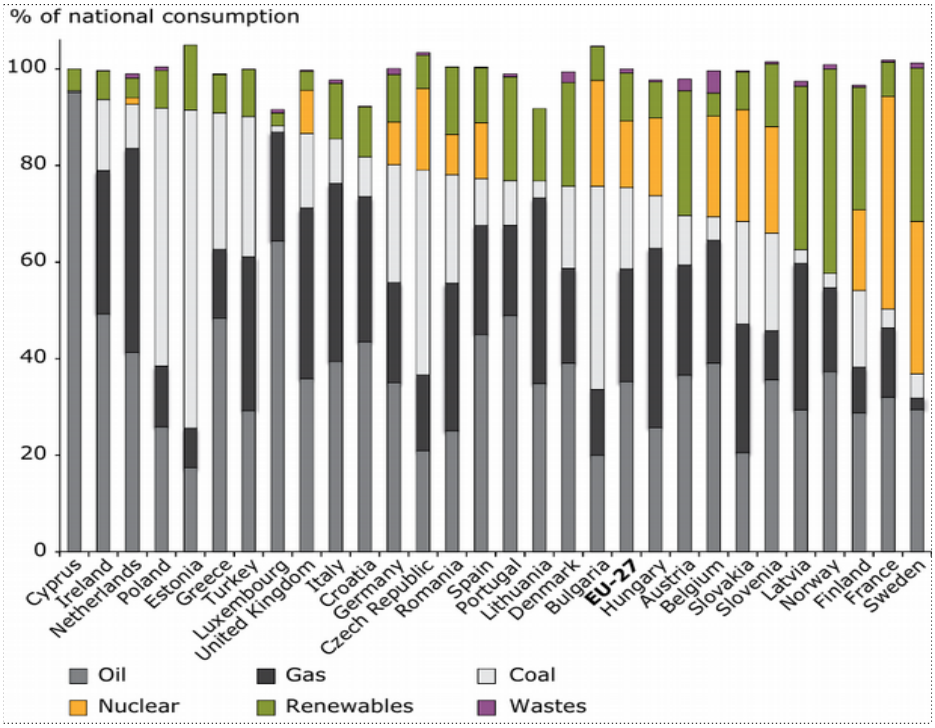

Figure 34: *national consumption of energy in 2011 (Source: European Environment Agency)*

In these countries, therefore, the production of energy is essentially based on oil and natural gas. The production of renewables is not negligible, in particular in countries where hydroelectric power can be extensively generated. The increasing demand of energy is also demonstrated by the steady increase in the period 1995-2015 of the proved reserves of oil and natural gas (52% and 57%, respectively [62]): in fact, to satisfy the growing request of fossil sources, the mining companies focus a significant part of their activity to discover new potential points of extraction.

As mentioned, the renewable energy, only marginally contributes to the total world energy consumption (*Figure 32*). However, its consumption tripled from 2004 (75.7 million tonnes oil equivalent) to 2014 (316.9 million tonnes oil equivalent) and this shows the increasing interest for the renewable sources. A major boost to their development was the introduction of laws to prompt their exploitation, as the consequence of evident environmental issues related to the utilization of fossil sources. In particular, the emission a noteworthy amount of carbon dioxide and other greenhouse gases (CH_4 and N_2O, for example), mainly produced by the combustion of fossil fuels, is considered the main reason of the global warming [63].

Nowadays, the need for reduction of greenhouse gases emission to contain the negative effects of global warming is world-wide recognised by practically all the countries in the world. This common feeling led 192 countries to sign, in 1997, "Kyoto Protocol" that entered into force in 2005. According to this agreement, the signatory countries undertake to reduce the emissions of greenhouse gases [64].

Ten years after, the European Union issued the "Strategy 20-20-20" [65] that establishes three goals to be achieved by 2020:

- Reduction by 20% of the greenhouse emissions, respect to the emissions in 1990;
- Increasing the renewable energy consumption to 20%, respect to the total consumed energy;
- Increasing the energy efficiency to 20%.

In Italy, in 2008, was approved the "Pacchetto Clima ed Energia" introducing six directives with the aim of realizing the goals defined by the European Union with "Strategy 20-20-20". Subsequently, further directives completed the Italian regulatory framework in the field of energetic politics.

Finally, the Paris Agreement on climate, stipulated in 2015 by 195 countries, [66–69] with the main aim of keeping the increase of the global average temperature below 2 °C respect to the pre-industrial levels (with a target value of 1.5 °C). After ratification by 125 countries (also including Italy), the Paris Agreement entered into force on 4th November 2016 and the first session of the Conference of the Parties, serving as the Meeting of the Parties (CMA 1), took place in Marrakech, Morocco in 15-18th November 2016.

Then the need of increasing the ability to adapt to the adverse impacts of climate change and lowering greenhouse gas emissions, without threatening food production, is declared. To achieve these goals, a suitable financial support must be allocated.

4.2: Global warming: reasons and consequences

The term *global warming* describes the trend of increasing surface temperature that scientists are observing in the last decades.

The "NASA Goddard Institute for Space Studies" studied the changes in surface temperature from 1880 to the present. The results clearly show that surface temperature of the Earth is continuously raising over the investigated period of time (*Figure 35*).

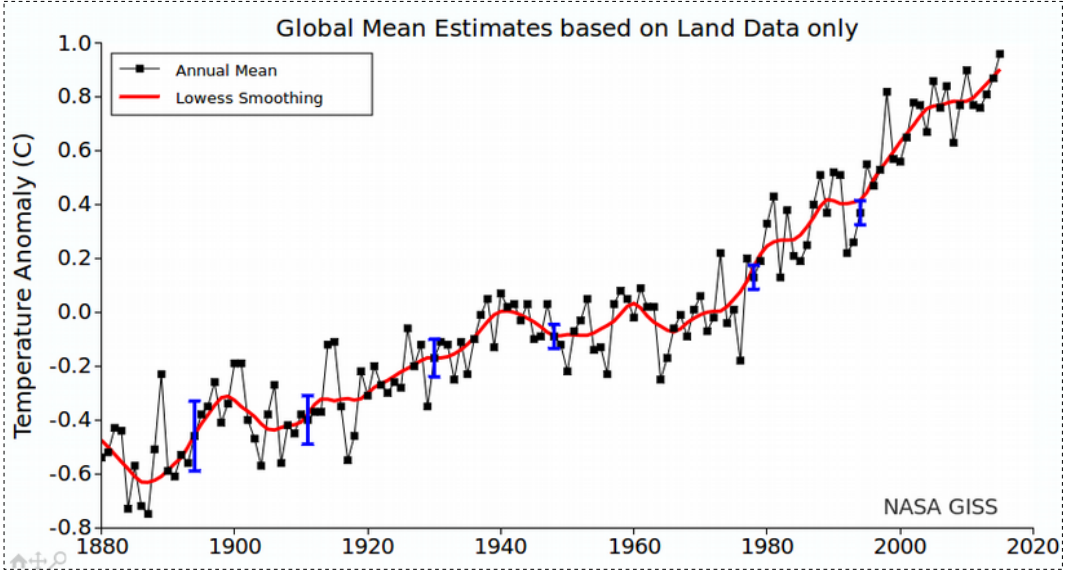

Figure 35: *trend in surface air temperature based on land data. Data before 1880 are not reliable.*

Moreover, the linear trend, particularly after 1940, suggests that this trend is not ending.

The United Nations Intergovernmental Panel on Climate Change (IPCC) [70] estimates that 1983-2012 was probably the warmest 30-year period of the last 1400 years in the Northern Hemisphere. In the same period, the globally averaged surface and ocean temperature showed an increment of the temperature between 0.65 and 1.06 °C. The effects of the global temperature increase are already clear. Since the beginning of the industrial era, the pH of ocean decreased of 0.1 units. Between 1992 to 2011 the Greenland and Antarctic ice lost mass, because of ice thaw, and permafrost temperature decreased in many regions. Thus, the annual mean sea-ice extent decreased in the period from 1979 to 2012 with a rate of 3.5 % per decade and the global mean sea level is growing over the period 1901 to 2010 (0.17-0.21 m).

At the present, nearly all scientists agree on a strong connection between human activity, in particular the high emissions levels of greenhouse gases, and the observed temperature growth during the last decades. Greenhouse gases tend to rise the temperature of atmosphere [71]. In fact, they are able to absorb infrared radiation emitted from the terrestrial surface, as the result of the warming by the solar radiation. Greenhouse gases (that are aqueous vapour, carbon dioxide, nitrous oxide and methane) are naturally present in the atmosphere, mitigating the temperature and making possible the life on Earth. However, during the last decades, anthropogenic activity increased their concentration, leading to the observed significant global growth of the temperature. The continuous increase of the greenhouses gases emissions during the last decades is reported in Figure 36.

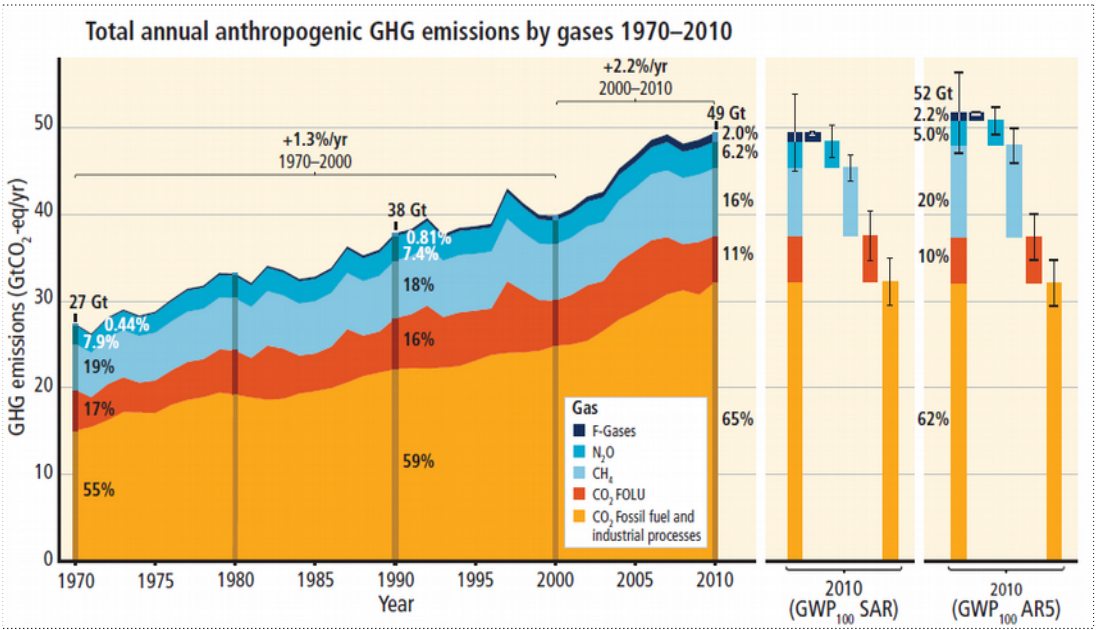

Figure 36: *total annual anthropogenic greenhouses gases emissions over the period 1970-2010. The acronym FOLU stands for Forestry and Other Lands Uses. The data are expressed in terms of equivalent gigatonnes of CO_2 per year* [70].

A further increase in the terrestrial temperature could create significant risks for natural systems and the mankind. In particular, the most relevant problem could be the supply of food and drinking water. Climate changes, in fact, irremediably modify the distribution and the availability of fertile lands and freshwater reserves. Also extreme climate events, like hurricanes or long period of drought, are expected to be more frequent and severe.

At the time, the effects of the global warming are still reversible but, if the emission of greenhouses gases is stopped today, the global warming will be present in the future for many decades. On the contrary, if the emission continues with the current trend, the climatic and ambient changes, resulting from the global warming, will be irreversible [70].

4.3: Biofuels: from first to fourth generation

Petroleum, also known “black gold” since long, is at present the most important source for the production of fuels and almost the only raw material for the manufacturing of organic substances and chemicals that we daily use [72,73].

The current level of oil reserves is continuously debated by the supporters of "peak oil theory" [74], expecting a quick decline of the extraction of oil, and oil companies, claiming that the discovery of new reserves will allow the extraction for many decades. Even according to this optimistic scenario, the oil shortage is a middle-term perspective, hence, because of its non-renewable nature, the future replacement of petroleum as the main source of fuels and chemicals has to be necessarily considered. The worldwide increase of the energy demand could accelerate this process unless enduring global economic crisis and/or catastrophic events produce a drop of fuel consumption (*Paragraphs 4.1 and 4.2*).

In addition, global warming and pollution are steady increasing environmental concerns and the exploitation of renewable sources appears the best solution under many points of view to cope with these problems. In particular, biomasses are currently considered the best candidates as possible sources of sustainable fuels and, above all, chemicals [75–77]. The directive 2009/28/CE defines the term "biomass" as "the biodegradable fraction of organic products, waste and residues made by the agriculture (including vegetal and animal substances), forestry and related industries including fishing and aquaculture, as well as the biodegradable fraction of industrial and municipal waste". Finally, due to the highly inhomogeneous geographic distribution of fossil resources , biofuels are considered as an opportunity, especially for developing countries, to reduce the economical dependence on oil-producers.

Nowadays, in the field of traction, bioethanol and biodiesel, that have similar (or, in some cases, better) physical and chemical properties of traditional fuels, have been considered as the most promising substitutes for gasoline and diesel, respectively [78,79].

The direct utilization of both bioethanol and biodiesel needs suitable engine modifications, whereas no modifications are required if they are used as blends with fossil fuels [80]. Moreover, the addition of biofuels to the traditional fuels has a positive influence on the engine performance and reduce exhaust emissions, mainly carbon monoxide and hydrocarbons [81]. The most relevant difference between biofuels and conventional fuels is, in fact, the content of oxygen which is remarkably higher for the first ones [82], making their combustion more efficient. In addition, the emissions of carbon dioxide, the main greenhouse gas responsible for the world warming, is almost negligible because a consistent part of emitted CO_2 will be used by the plant to regrow [83].

Bioethanol is obtained by fermentation of sugars contained in plants, mainly sugar canes, sugar beet and cereals, with about 60% of bioethanol produced from sugar crops. Respect to gasoline, the production of bioethanol is currently more expensive in all regions. Only in Brazil and India, due to the availability of lands and the warm climate, the cost of bioethanol is becoming competitive with that of gasoline. However, the use of edible products and the exploitation of high-quality agricultural lands for the production of fuels raised ethical issues on the interference of this activity with the human food chain. Therefore, the attention moved towards non-edible materials ("lignocellulosic biomass"), like agricultural and urban wastes and forest residues, that are abundant and low cost raw materials. Moreover, the use of waste materials is also expected to decrease the production cost of bioethanol, mainly depending on the price of the crop feedstock. The possible large scale exploitation of these materials is limited by the low yield and the high cost of the hydrolysis process, necessary to obtain fermentable sugars from cellulose. Thus, at the present, the industrial production of bioethanol from lignocellulosic wastes (the so called "second generation bioethanol") is not yet implemented [84–86].

In recent years "third generation biofuels", that are biofuels produced from algal biomass, were also studied [87–91]. The exploitation of algae as the feedstock for the production of biofuels shows many advantages. First, respect to terrestrial plants, algae have higher photon conversion efficiency and they can store large quantities of carbohydrates or/and lipids (their ratio depends on the type of algae). Moreover, algae are generally buoyant plants, therefore they do not need structural biopolymers, such as lignin or hemicellulose, and the hydrolytic pre-treatment is easier and faster. In addition, algae have a short period of growth compared to other feedstock: for example, selected strains of algae can produce oil within 3-5 days, thus the harvesting can be completed on daily basis. Finally, they can be harvested in marginal lands and in saline or sewage water, avoiding the competition with the agriculture for the exploitation of lands and water.

There are two main categories of algae, both exploitable for fuels synthesis: macro-algae and micro-algae. While macro-algae are the marine plants usually found on the sea bottom, micro-algae are microscopic photosynthetic organisms, mainly unicellular. Obviously, a great variety of algal species are present, therefore the selection of species able to produce the highest amounts of oils or starch in the shortest time is an important task.

The most actively investigated production systems are open ponds and enclosed photobioreactors. Open ponds are cheaper to build, but usually the productivity is lower and the harvesting cost higher. To optimize the growth of algae and the yield in biofuels, they can be cultured in controlled environments (photobioreactors) in which the conditions affecting the productivity of the culture are strictly maintained. For example, artificial sources of light guarantee a continue and suitable illumination, also under conditions of inadequate exposition, whereas a continuous flow of water containing nutrients, air and CO_2 (in a controlled and optimized ratio) can be used. Respect to open ponds, in photobioreactors the harvesting cost is reduced because, as soon the algae grows, the excess culture overflows and can be harvested. Conversely, an expensive task is the separation of algal cells from the culture environment, because of their low density. Mechanical and/or chemical methods have to be used: membrane filtration, chemical flocculation and ultrasound waves are some examples.

To build a photoreceptor plant, a high capital cost is required and also an intensive maintenance is necessary [88]. Furthermore algae need 55-111 times more nitrogen fertilizer respect to, for example, a rapeseed cultivation [89]. Therefore, producing microalgal biomass is generally more expensive than growing crops.

Once algae have been collected, their treatment depends on the desired type of biofuel, bioethanol or biodiesel.

In the case of bioethanol, first it is necessary to extract starch form the algal cells by mechanical methods (mechanical shear for example) or by using specific enzymes. The starch is subsequently extracted with water and treated to produce bioethanol. This involves two steps: *saccharification* in which starch is hydrolysed to sugars (acidic or enzymatic hydrolysis) and *fermentation* to ethanol by adding a suitable yeast. By using suitable enzymatic strains, these two processes can be carried out in a single step, reducing the production costs of bioethanol. Finally, ethanol is purified by distillation to remove water and further impurities. Generally, the yield in ethanol ranges from 3.8 g/L to 10 g/L of substrate. Similarly, the residual cellulosic biomass remained after the extraction of starch can also be treated to obtain bioethanol. Furthermore, it is worthwhile to remark that the hydrolysis of algal cellulose is easier than that of plant cellulose, thanks to the absence of the lignin.

Currently, the third generation bioethanol cannot not be technological implemented, although it is the subject of many research projects supported also by important companies, like Shell [91].

For the biodiesel production, algal species with a high lipid content (up to 70% on a dry weight basis) have been selected. In addition, suitable processes for the extraction of oil from algae have been developed [88,89]. To this respect, the most convenient approaches are: the exploitation of a mechanical expeller/press and the solvent extraction, with hexane or supercritical fluid (mainly carbon dioxide). The latter is the most efficient method (making possible to extract up to 100% of the oil) and ensures the highest purity of the extracted oil. After oil extraction, the residual biomass can be used for the production of methane by anaerobic digestion, making more profitable the entire process. The production of biodiesel from the extracted oil can be carried out through the conventional process for the biodiesel production from traditional feedstock (transesterification reaction, possibly after the esterification of free fatty acids) [87].

As a future development of the biofuels production, the possible genetic engineerization of micro-algae, to directly convert CO_2 into biofuels ("fourth generation biodiesel"), is currently under investigation. Accordingly, only the steps of extraction and purification of biofuels would be necessary, hence considerably lowering the overall cost of production. However, this field of research, although potentially promising, is still in an early stage.

4.4: Second Generation Biodiesel

From the chemical point of view, biodiesel is a mixture of alkyl esters of fatty acids. It is produced by transesterification of triglycerides, coming from vegetable oils or animal fats, with an alcohol (*Figure 37*).

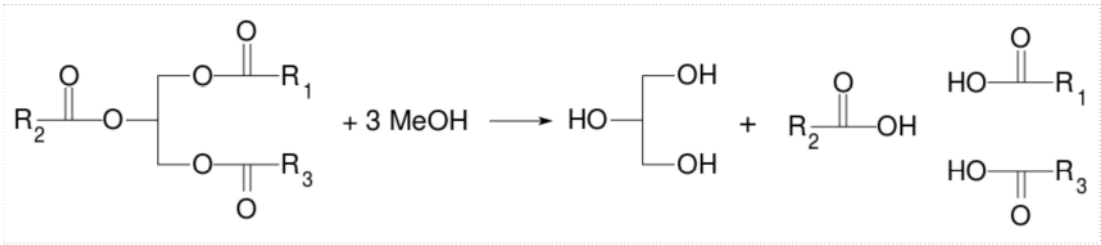

Figure 37: *transesterification reaction of a triglyceride with methanol. Methyl esters are the biodiesel product, whereas glycerol is the main by-product.*

Although the use ethanol obtained from renewable biomass is sometimes preferred, methanol is principally employed because of its lower cost [92]. The name "Biodiesel" was introduced in 1992 in the United States by the National Soy Diesel Development Board, the first company commercializing biodiesel in the United States. The exploitation of vegetable oils as fuels dates back to 1893, when Rudolf Diesel tested for the first time peanut oil as the fuel [93]. Later, during world wars, vegetable oils were used as fuels in case of emergency. However, their high viscosity, low volatility and poor cold flow property lead to the incomplete combustion with the consequent formation of solid deposits in the fuel injector of diesel engines. On the contrary, fatty acids methyl esters, having properties close to those of traditional diesel, can be considered a promising replacement [92,94,95].

In the last decades the research on biofuels and, particularly for transportation purposes, on biodiesel was boosted by environmental concerns and the attempt, due to developing countries, to reduce the dependence from oil [95]. Thus, the industrial production of biodiesel steadily increased in the last years (*Figure 38*) and 70792 thousand tonnes oil equivalent were produced in 2014.

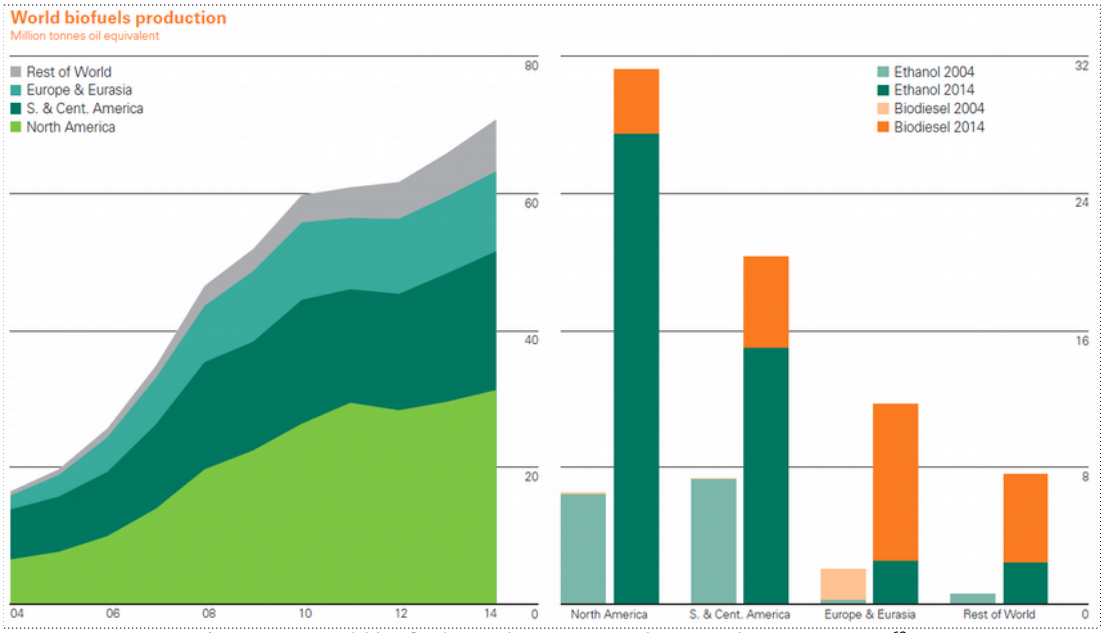

Figure 38: *world biofuels production over the period 2004 to 2014* [62].

With respect the geographic area, the production of biofuels is growing worldwide and in North America the higher rate of increase is observed. In both North and South America, the production of bioethanol remarkably exceeds biodiesel, whereas the opposite occurs in Europe and Eurasia.

As to the biodiesel production, an excess of alcohol is generally employed to shift the transesterification equilibrium towards the products. Transesterification process needs to be catalysed either with basic or acid catalysts [92]. In particular, the acid catalyst (normally inorganic acids) protonates the carbonyl oxygen of the ester substrate making it more susceptible to the electrophilic attack of the alcohol molecule. On the contrary, the basic catalyst enhance the nucleophilicity of the alcohol molecule producing, by deprotonation, the alkoxide ion that is the actual active specie.

In the industrial practice, alkaline conditions are generally preferred for the transesterification reaction, because basic catalysis is remarkably faster than acid one [96]. Sodium and potassium hydroxides are usually employed due their low cost [92], but, from the chemical point of view, sodium methoxide is far more effective. In fact, water obtained by deprotonation of alcohol can hydrolyse both the produced alkyl esters or triglycerides, generating soaps. The formation of soaps not only lowers the yield in esters, but also makes more difficult the separation of esters and glycerol, because of the formation of emulsions during the water washing. Accordingly, glycerides and alcohol must be anhydrous. The formation of soaps,

with consumption of base catalyst, can be observed also in case free fatty acids (FFAs) are present in the oil feed. As the matter of fact, It is possible to use an alkali catalyst with a concentration of FFAs lower than 0.5% respect to oil weight. [92,94,95,97]

Glycerol represents the main sub-product of the process and its commercialization is not currently feasible, because its price is out of market, due the cost of purification. Consequently, to make profitable the biodiesel production, the economical valorisation of glycerol, though its conversion into valuable products, received particular attention [98].

At the present, biodiesel is not competitive, from the economical point of view, with the traditional fossil fuels and the its final price is mainly determined (60-75%) by the cost of the feedstock [92]. To make the price of biodiesel more competitive, a possible strategy is the exploitation of very low cost raw materials, such as waste greases, instead highly refined vegetable oils. Waste greases includes yellow grease, i. e. animal fats and restaurant waste oils, and brown grease, obtained from traps installed in sewage sludge [95].

As expected, waste greases must be pre-treated to be used as the feedstock for the production of biodiesel. Possible particulate matter (for example food residuals) is removed by filtration, water is removed by gravity, proteins are degraded by steam distillation and bleaching removes spoiled proteins.

A further issue connected to the use of waste oils is their high content of free fatty acids that can represent a consistent fraction (up to 15% wt) of the feedstock. FFAs are mainly produced during the frying process, due to the partial hydrolysis of triglycerides, promoted by high temperature and the presence of water, released by food (*Figure 39*) [99].

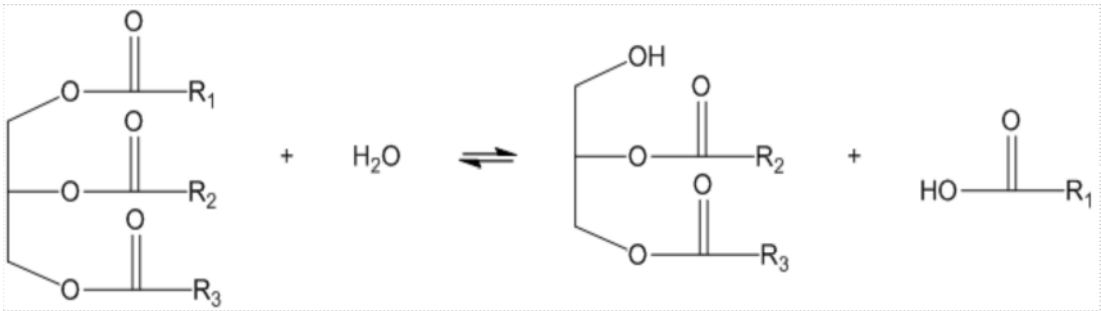

Figure 39: *partial hydrolysis of a triglyceride with the production of a diglyceride and a long-chain carboxylic acid*

The presence of FFAs is unwanted because of the formation of soaps in the presence of alkali, making difficult the technological exploitation of the transesterification process. There exist two possible strategies to overcome the problem: performing the transesterification process under acid catalysis conditions and removing FFAs from the feedstock before the transesterification reaction with a suitable pre-treatment. The former approach represents a one-pot process for the preparation of biodiesel, because both esterification of FFAs and transesterification of triglycerides are promoted by the same catalyst. However, acid catalysed transesterification reaction is about 4000 times slower than the corresponding basic process and, therefore, requires a greater amount of methanol to achieve more favourable conditions. As a matter of fact, nowadays in the industrial practice a two-step approach is preferred. First, waste grease is treated with methanol and an acid catalyst to convert FFAs to the corresponding methylesters and finally the basic catalysed transesterification of triglycerides can be performed.

4.5: Experimental procedure for the esterification of stearic acid

In this work the pre-esterification step, catalysed by sulfonated resins, of the process of biodiesel production was investigated. In particular, to simulate a real waste oil a mixture of sunflower oil and stearic acid was employed and the esterification reaction with methanol was studied.

The experimental conditions of catalytic tests were chosen according to Hoelderich et al.[100]

A stearic acid (*SA*) solution in sunflower oil is prepared in a glass bottle under mechanical mixing and mild heating. After cooling the solution at room temperature, a homogeneous, pale yellow and gelatinous solid is obtained. The concentration of SA (10% wt) is close to that of fatty acids in exhausted oils (up to 15% wt [92]) as to mimic a real industrial situation. Methanol (25% wt respect to the oil mixture) is added in remarkably larger amount than required by stoichiometry in order to shift the equilibrium towards the products.

The reaction mixture is thus formed by a lipophilic phase of oil and stearic acid and an hydrophilic phase of methanol (*Figure 40*). The solid acid catalyst is a hydrophilic sulfonated resin, hence it remains suspended in the alcoholic phase.

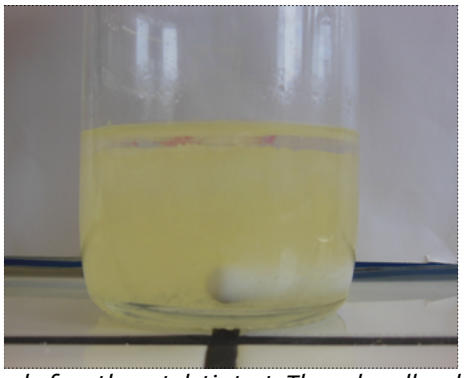

***Figure 40**: reaction mixture before the catalytic test. The pale yellow lipophilic (bottom) and the colourless hydrophilic (top) phases are clearly separated.*

Mixing is a crucial parameter: it must be efficient to maximise the contact area between the two phases and allow the exchange of SA and methyl stearate between them. Moreover, its rate must be the same in all the catalytic tests to make the results comparable.

SA is only slightly soluble in methanol (ca 48 g per litre of alcohol, at room temperature), but this is enough to ensure its presence in the hydrophilic phase and its contact with the catalyst. Methyl stearate is mainly soluble in the lipophilic phase, where it is readily extracted after its production. The consumption of SA is appreciable at a glance from the aspect of reaction mixture. At the end of the test (*Figure 41*) the lipophilic phase is almost as clear and of the same colour of the sunflower oil; the methanol phase is no longer completely transparent and presents a pale brown colour due to the presence of the catalyst, ground by the mechanical stirring.

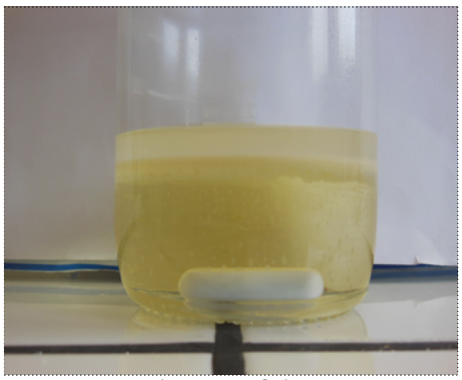

***Figure 41**: typical aspect of the reaction mixture at the end of a catalytic test.*

The catalytic test is carried out at about 65 °C under refluxing methanol. The glass reactor is closed with a home-made Teflon head (*Figure 42*), providing three connections for an Allihn condenser, a thermocouple and a sampling line. The latter is protected by a sintered steel filter to prevent the removal of the catalyst upon sampling. After each sampling the line and the filter are cleared with a manual blower to prevent the clogging of the latter.

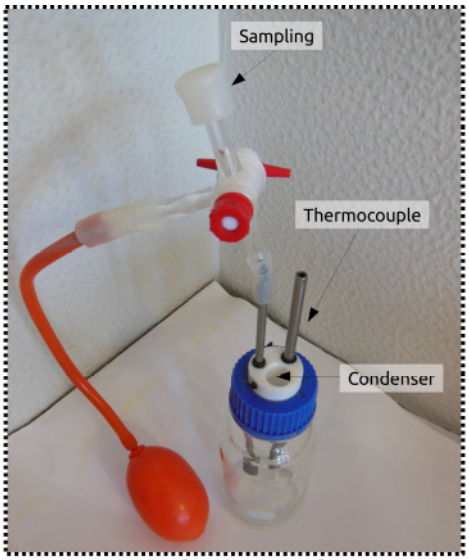

Figure 42: *reactor for the esterification reaction.*

The sealed reactor is warmed with an oil bath (about 150 °C). The test begins when the temperature of the reaction mixture reaches the reflux temperature. Exactly measured amounts of the reaction mixture are periodically withdrawn and titrated with a standard aqueous solution of NaOH to assess the conversion over time.
A few samples of SA has also been titrated with NaOH to assess the actual content of acid (*Table 19*). This appears to be smaller than expected from the nominal purity of SA (95 %) and has been used as the reference for the evaluation of the catalytic results.

Table 19: results of the titration of three samples of commercial stearic acid (second column), compared with the content of stearic acid expected on the basis of its nominal purity (third column).

m_{SA} (g)	mmoles H^+	Expected mmoles SA
0.0826	0.286	0.316
0.0820	0.285	0.314
0.0808	0.283	0.309

The acidity of oil phase has been determined for any oil batch used in the present investigation (ca. 1-2 μmoles H^+/g) and has been considered for the evaluation of the catalysts.

4.6: Preliminary tests of esterification

To properly compare the catalytic results, especially at higher reaction times, it is convenient to interpolate the experimental values of conversions according to a suitable a suitable kinetic model. To this regard, diffusive and adsorption phenomena were neglected and only the esterification equilibrium has been considered, where A states for stearic acid, B for methanol, C for methyl stearate and D for water (*Equation 4*).

$$[A]+[B]\rightleftarrows[C]+[D]$$

Equation 4: *equilibrium of esterification reaction.*

Considering as bimolecular the mechanism of the acid catalysed esterification (i.e. bimolecular nucleophilic substitution reaction, S_N2) [101], the kinetic law is:

$$r=\frac{d[A]}{dt}=-k_1[A][B]+k_2[C][D]$$

Equation 5: *kinetic law of esterification reaction*

According to literature [102,103], Equation 4 can be conveniently rearranged to express the stearic acid conversion versus time:

$$C_{\%}=100\cdot\left(1-\frac{1}{[A]_0}\cdot\left([A]_e+\frac{cde^{at}}{1+(1-K)(de^{at})}\right)\right)$$

Equation 6: *percentage conversion of stearic acid*

where $[A]_0$ is the concentration of stearic acid at the beginning of the catalytic test, $[A]_e$ is the concentration of stearic acid when the equilibrium is reached, K is the equilibrium constant and c,d,a are parameters related to the regression.
The equilibrium constant of esterification reactions is generally close to unity. To experimentally estimate the equilibrium constant under the test conditions, the

equilibrium concentration of stearic acid has been determined with a two days test, using *gel_s* as the catalyst (Figure 43).

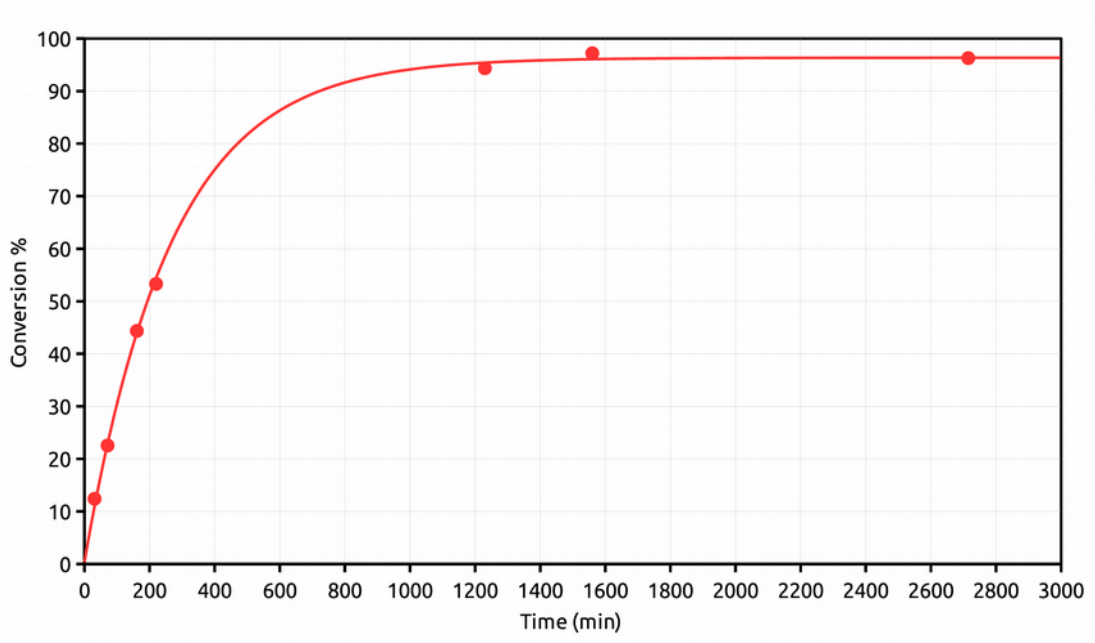

Figure 43: *conversion of stearic acid obtained using a sulfonated gel-type resin as catalyst (72 g of oil, 8 g of stearic acid, 20 g of methanol; 0.5 g of catalyst; T = 65 °C).*

By assuming that the equilibrium has been reached, on the basis the final values of conversion and the composition of the reaction mixture at the beginning of the test, the equilibrium constant results 1.2. In case the equilibrium constant is close to unity, equation 6 can be remarkably simplified:

$$C\% = 100 \cdot b\left(1 - e^{at}\right)$$

Equation 7: *percentage conversion of stearic acid (simplified equation)*

The fitting of the experimental values of conversion reported in Chapter 4 has been performed according to equation 7.

A library of catalysts was initially tested to investigate the effect of the morphology of the porous system in the esterification of SA. Table 20 illustrates the catalysts, their structural morphology and their proton exchange capacity determined by titration.

Table 20: *acid catalysts employed for the preliminary screening.*

Catalyst	Description	Proton Exchange Capacity (mmol H^+/g)
K2621	Commercially available sulfonated macroreticular resin	4.69
macro_s	Macroreticular resin (16%wt of DVB) sulfonated with H_2SO_4	4.40
gel_s	Gel-type resin (2%wt of DVB) sulfonated with H_2SO_4	5.27
pDVB_s	Poly-divinylbenzene (pDVB1[a]) sulfonated with H_2SO_4	3.32

[a]: prepared with a solvent:monomer volume ratio 10:1 (Paragraph 1.5)

The catalytic results, reported in Figure 43, can be compared in terms of catalytic activity (i.e. the slope of the initial linear part of the curve of conversion in time) and maximum value of conversion reached after 24 hours of reaction.

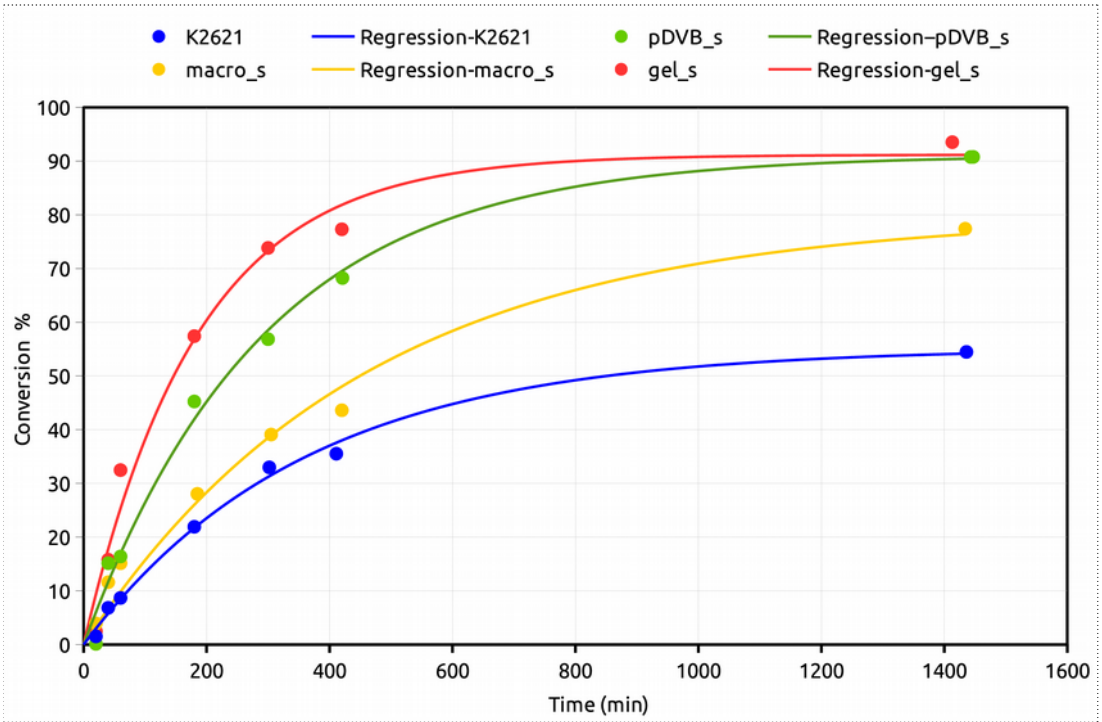

Figure 44*: conversion of stearic acid over sulfonated resins with different structural morphology. (r72 g of oil, 8 g of stearic acid, 20 g of methanol; 0.5 g of catalyst; T = 65 °C)*

With the sulfonated poly-divinylbenzene (*pDVB_s*) and the sulfonated gel-type resin (*gel_s*) the conversion after 24 h is close to quantitative. Lower conversions are obtained with the sulfonated macroreticular resins.

Sulfonated resins show different contents of acidic groups that are the catalytically active sites (*Table 20*). To take this into account it is convenient to

normalize the conversion of SA to the acidic content and obtain the turn-over number (TON) (*Figure 45*).

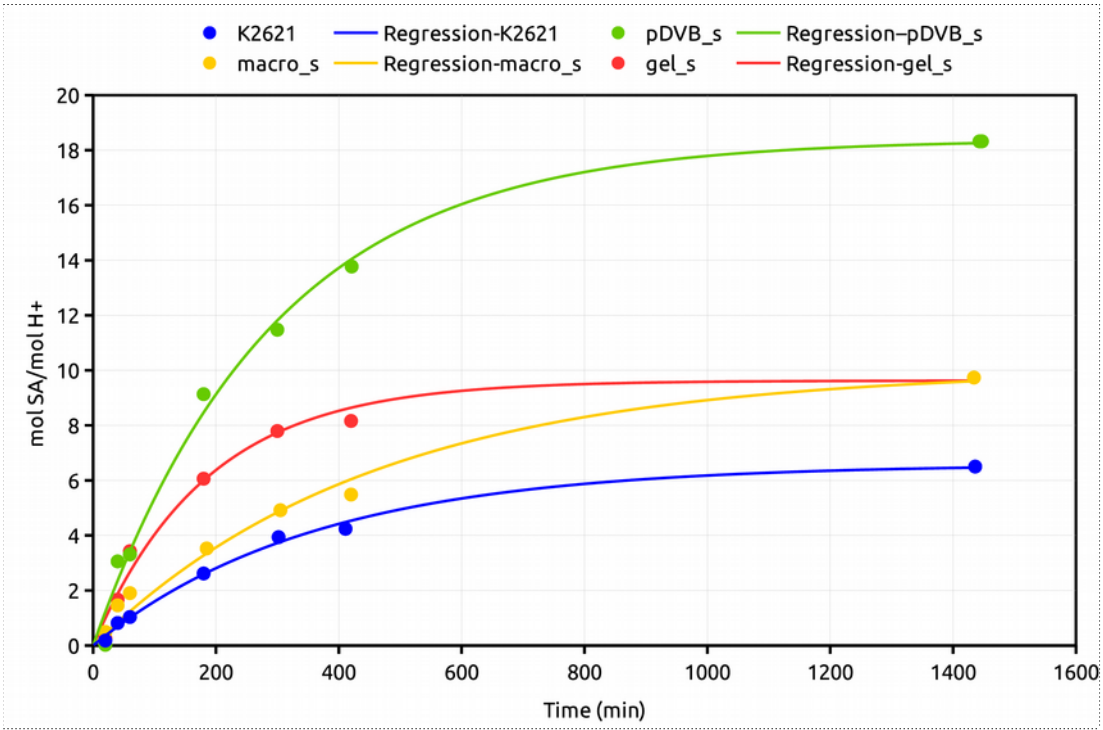

Figure 45: *TON of sulfonated resins with different structural morphology. (reaction mixture: 72 g of oil, 8 g of stearic acid, 20 g of methanol; 0.5 g of catalyst; T = 65 °C)*

If TONs are compared at the same time, *pDVB_s* shows generally the best performance ans *gel_s* is the second best. The ratio of their TONs when the reaction is not too close to the final plateau (equilibrium; t<400 min) is ca 1.5 and more or less independent of time. If we assume that the nature of the active site is the same for both these catalysts and their TOFs as well, this suggests that the number of the accessible sites in gel_s is about two thirds of the accessible sites in *pDVB_s*. As the catalysts are wet by the alcoholic phase, the gel type catalyst should be swollen to the maximum possible extent, and under these conditions it is more active than macroporous resins [48]. This is fully confirmed by the results of the preliminary tests reported here. The macroporous catalysts K2621 (commercial) and *macro_s* are much less active than *gel_s* even when TONs are taken into account. On the other hand, this is not true for *pDVB_s*, which ensures an exceptionally high fraction of accessible sites owing to its very open porous system (*Paragraph 1.5*). By contrast, in *gel_s* only 40% of the sulfonic groups are employed at best, in spite of the favourable conditions for the diffusion of the reagents in the expectedly fully swollen polymer framework. It could be argued

that rather than by limited mass transport rate (or in addition to it) the concentration of SA in the catalyst is limited by a small partition constant between the liquid phase and the swollen gel. In fact, according to the literature [44,104,105], when a liquid mixture is used to swell cross-linked polymers, the component showing the strongest interactions with the polymer framework (i. e. able to swell the material to a high extent) is preferentially absorbed. During an esterification experiment, the only components of the reaction mixture expected to swell a sulfonated polystyrene-divinylbenzene matrix are methanol and, at higher degree of conversion, water: to this respect, a gel-type catalyst, such as *gel_s*, is expected to be mainly swollen by methanol, whereas the concentration of stearic acid inside the material should be significantly lower than the nominal content of the bulk solution. In a broader sense, the behaviour of the cross-linked polymers in the presence of a liquid mixture resembles a chromatographic process, in which the solutes with the highest the affinity towards the solid material are preferentially retained. Accordingly, in spite of the high degree of swelling, the concentration of stearic acid inside the polymer framework can be low enough to actually involve only a fraction (ca. 40% in the case of *gel_s*) of the total amount sulfonic groups as the catalytic sites.

This preliminary screening also includes a *blank test* performed in order to evaluate the progress of the uncatalyzed reaction (*Figure 46*), if any.

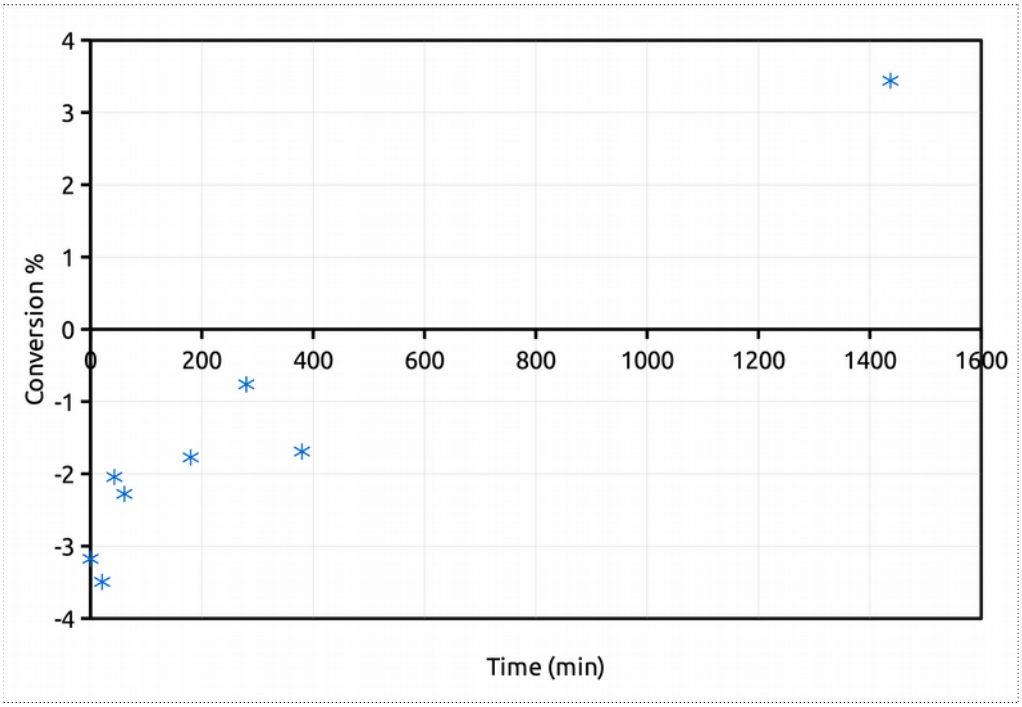

***Figure 46**: uncatalyzed esterification of stearic acid with methanol (reaction mixture: 72 g of oil, 8 g of stearic acid, 20 g of methanol; 0.5 g of catalyst; T = 65 °C).*

After 24 hours the conversion is only about 3.5%, showing that the uncatalysed esterification of stearic acid is slow and gives a negligible contribution to the overall process. The most interesting result of the blank test is the negative conversion observed at the beginning. The most reliable reason is some evaporative loss of methanol during the withdrawal of the samples for the titration of the residual SA. As the amount of each sample is measured by its weight, this implies the overestimation of the SA and an underestimation of the conversion. When it is close to 0, the result is that nominal negative values. The relevant systematic error can be reasonably estimated in about -3%, the value obtained at the smallest sampling time.

Sulfonated resins are hydrophilic materials and absorb water from the atmosphere. Therefore we dried them prior use in a oven at 110°C in order to achieve a better reproducibility of their weight in the catalytic tests. However, drying produces a strong osmotic stress of the resin and the polymer framework can break when shrinking takes place. As the consequence, short segments of polymer chains can be released in solution. The decrease of the pH of methanol, used for their swelling, is a clear evidence that acidic species are released in methanol from our catalysts. We rule out the leaching of residues of sulfuric acid from the sulfonation in view of the thorough washing of the materials after this step. Rather, the presence of soluble fragments of resin in the solvent (also suggested by its pale yellow or brown colour) seems the most reliable explanation. This suggested to prepare a library of sulfonated catalysts (*Table 21*) free of acidic species which could be released in solution and act as a homogeneous catalyst.

***Table 21**: catalysts washed with methanol after the first drying at 110 °C.*

Catalyst	**Proton Exchange Capacity**	
	mmol H^+/g	*relative to the catalyst before washing*
macro_s_w	3.43	78 %
gel_s_w	4.93	93.5 %
pDVB_s_w	1.83	55 %

For this purpose a known amount of the dried catalyst was carefully washed upon suspending it in methanol and separating by decantation. The cycle was repeated until neutral pH of the liquor. Finally, the washed catalyst was mildly dried (under vacuum at 40 °C) to remove the excess of solvent without promoting the polymer decomposition and titrated to assess the actual proton exchange capacity after the treatment (*Table 21*).

Figure 47 illustrates the change of conversion with time for the washed and not washed catalysts.

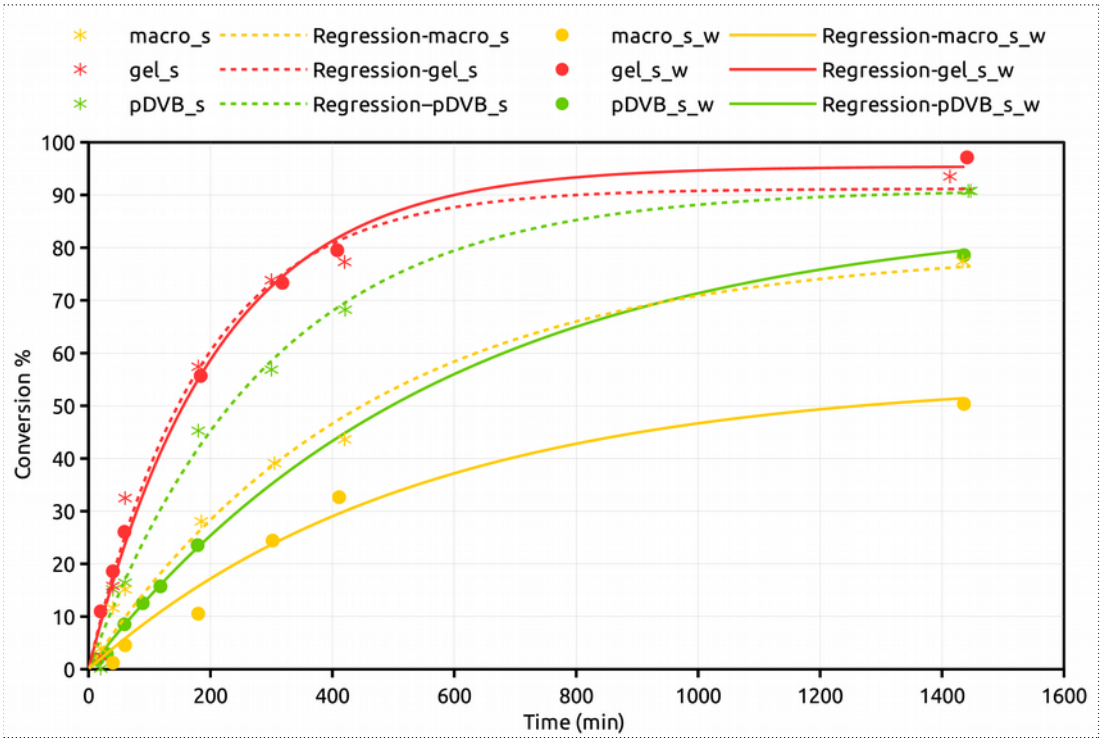

Figure 47: *conversion of washed and non washed catalysts (reaction mixture: 72 g of oil, 8 g of stearic acid, 20 g of methanol; 0.5 g of catalyst; T = 65 °C).*

In the case of gel-type sulfonated resin the washing treatment apparently does not change the catalytic behaviour. This is in agreement with the small decrease of the proton exchange capacity in gel_s_w with respect to gel_s. The TON values, too, are practically the same at any time for both the gel-type catalyst (*Figure 48*).

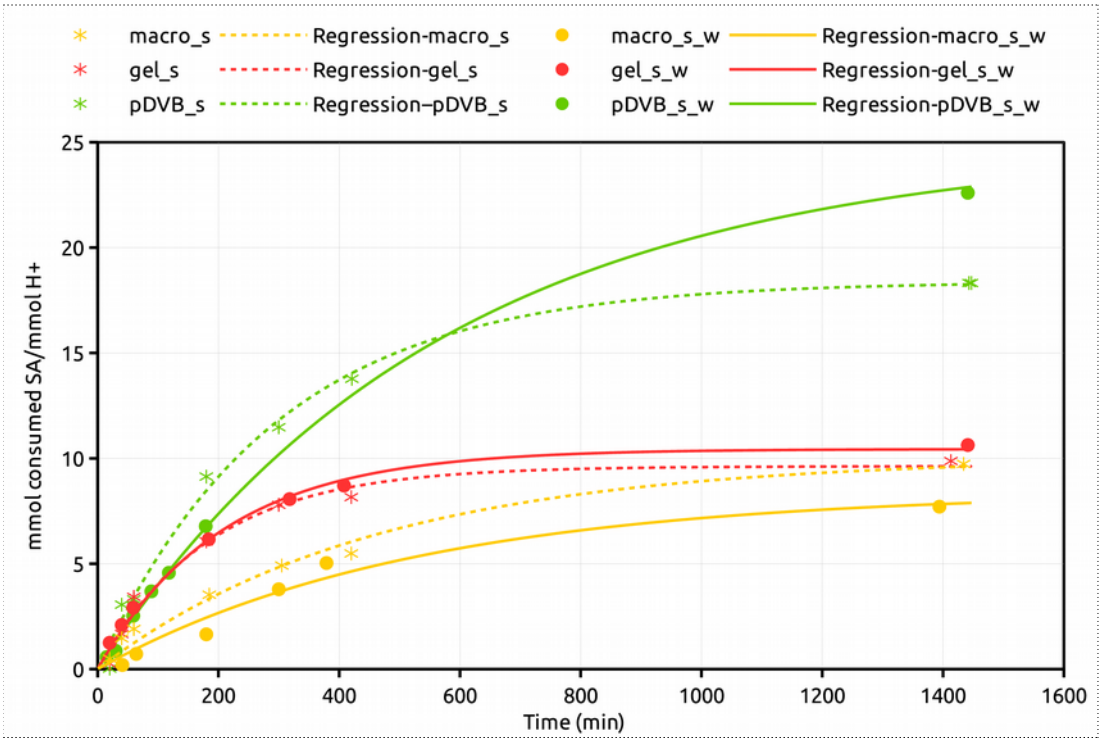

Figure 48:*TON of washed and non washed catalysts (reaction mixture: 72 g of oil, 8 g of stearic acid, 20 g of methanol; 0.5 g of catalyst; T = 65 °C).*

On the contrary *pdvb_s_w* and *macro_s_w* show a remarkably lower conversion over the time and a significant reduction of the proton exchange capacity in comparison with their parent catalysts. p*dvb_s_w,* in particular, shows by far the largest loss of proton exchange capacity, in agreement with the osmotic stress as the cause of the breakdown of the polymer framework. During the polymerization of DVB to prepare the kind of pdvb employed here, in fact, microsyneresis rather than macrosyneresis takes place (*Paragraph 1.5*), as the consequence of the peculiar polymerization conditions which favour the growth of chain length rather than cross-linking. This leads to pore volume of the resin so high that polymeric chains must have been fixed by cross-linking, which eventually prevails, in very extended conformations which likely set up a large tension over the polymer framework of pdvb. As the consequence it is more easily damaged by the osmotic stress.

Macro_s_w and *pdvb_s_w* have generally lower TONs than the parent catalysts (*Figure 48*). This suggests that, for the latter ones, not only the contribution of homogeneous catalysis from the released species was not negligible, but also that the released species are more active than the truly heterogeneous catalyst. It could also imply that the loss of sulfonic groups involves mainly the most

accessible ones, hence the fraction of them available in the polymer for heterogeneous catalysis gets lower in the washed materials. However, at least for *pdvb_s_w,* the TON data are not conclusive, since the difference of TON in comparison with *pdvb_s* is generally lower than the difference of the respective proton exchange capacities and the final TON is even higher for *pdvb_s_w*.

4.7: Role of the morphology of the catalytic support

The catalytic behaviour of sulfonated and washed resins with different morphology is illustrated in Figures 49 and 50.

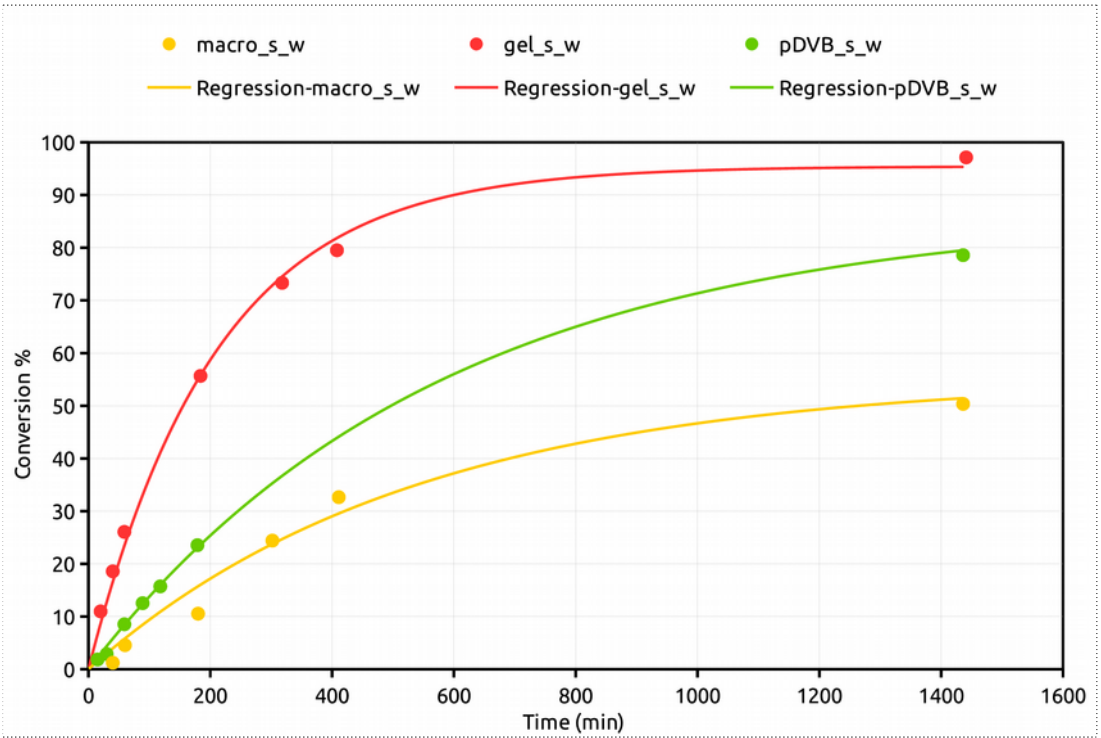

Figure 49: *conversion over time for catalysts with different morphology (reaction mixture: 72 g of oil, 8 g of stearic acid, 20 g of methanol; 0.5 g of catalyst; T = 65 °C).*

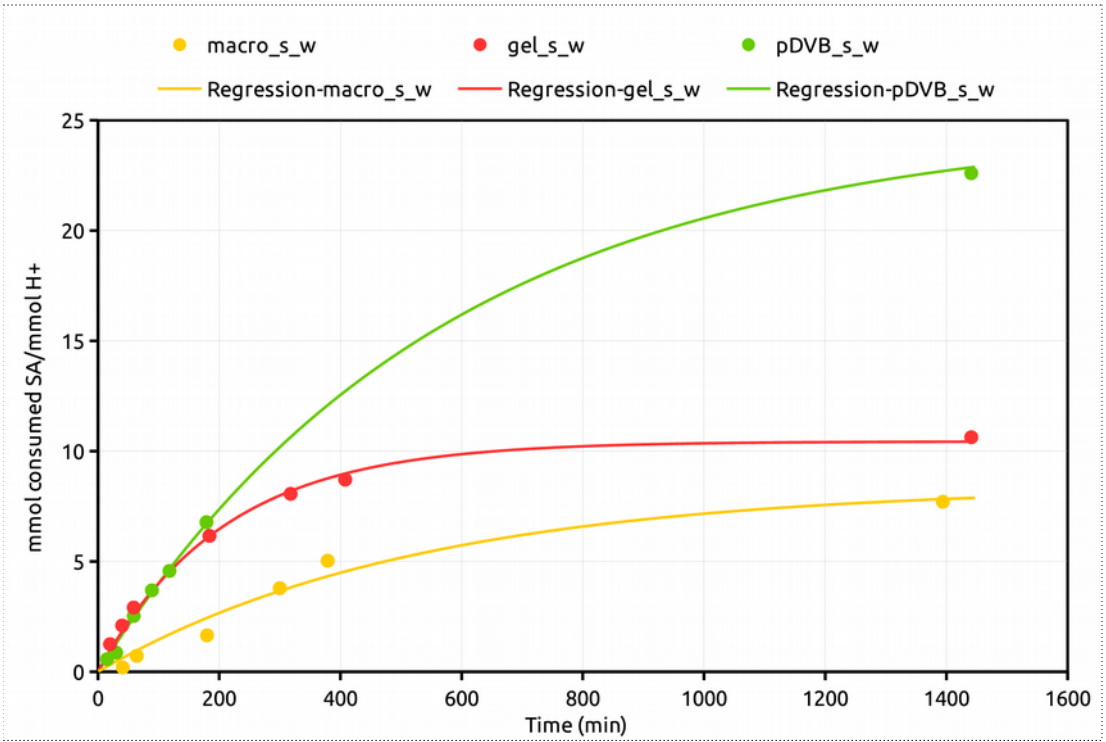

Figure 50: *TON for catalysts with different morphology (reaction mixture: 72 g of oil, 8 g of stearic acid, 20 g of methanol; 0.5 g of catalyst; T = 65 °C).*

Gel_s_w shows the highest conversion at any time. However, if TON values are taken into account, *pdvb_s_w* is closely comparable to the gel-type catalyst at the beginning of the catalytic run. *Macro_s_w* shows both the lowest conversions and TONs.

The relatively high conversion achieved with the sulfonated gel-type catalyst is therefore simply explained by its high acidic content. In presence of an high excess of methanol (20% wt in the reaction mixture) the gel-type catalyst should be fully swollen and its acidic sites completely accessible. Also the sulfonic groups of *pdvb_s_w* seem to be completely accessible (or to the same extent of *gel_s_w*), but, due to the lower proton exchange capacity, the observed conversion is lower. Interestingly, the final TON at ca 1400 min is much higher for *pdvb_s_w* in comparison with *gel_s_w*, which suggests that the catalysts is not likely affected by early deactivation caused by an accumulation of species of high molecular weight within its pores. This result is again in agreement with the expectedly good accessibility of the catalytic sites ensured by the extended pore volume, the wide pore size and the foam-like structure of poly-divinylbenzene.

Although it has been reported that the total conversion of stearic acid can be obtained within 24 hours with the sulfonated macroreticular resin Amberlyst 15,

the sulfonated macroreticular resin included in the present investigation reaches only a conversion of about 50%. We cannot say whether this is the result of a low apparent catalytic activity or of relatively fast de-activation. In any case, the behaviour of *macro_s_w,* again, suggests that it must have the lowest fraction of accessible sulfonic groups, due to its limited ability to swell in comparison with *gel_s_w* and its relatively little open porous structure in comparison with *pdvb_s_w.*

Finally, a catalytic test with para-toluenesulfonic acid (ptsa) as the homogeneous catalyst was performed for comparison (*Figures 51 and 52*), with an amount of sulfonic groups not too far (ca 0.9-2.5) with that of the resin-based catalysts.

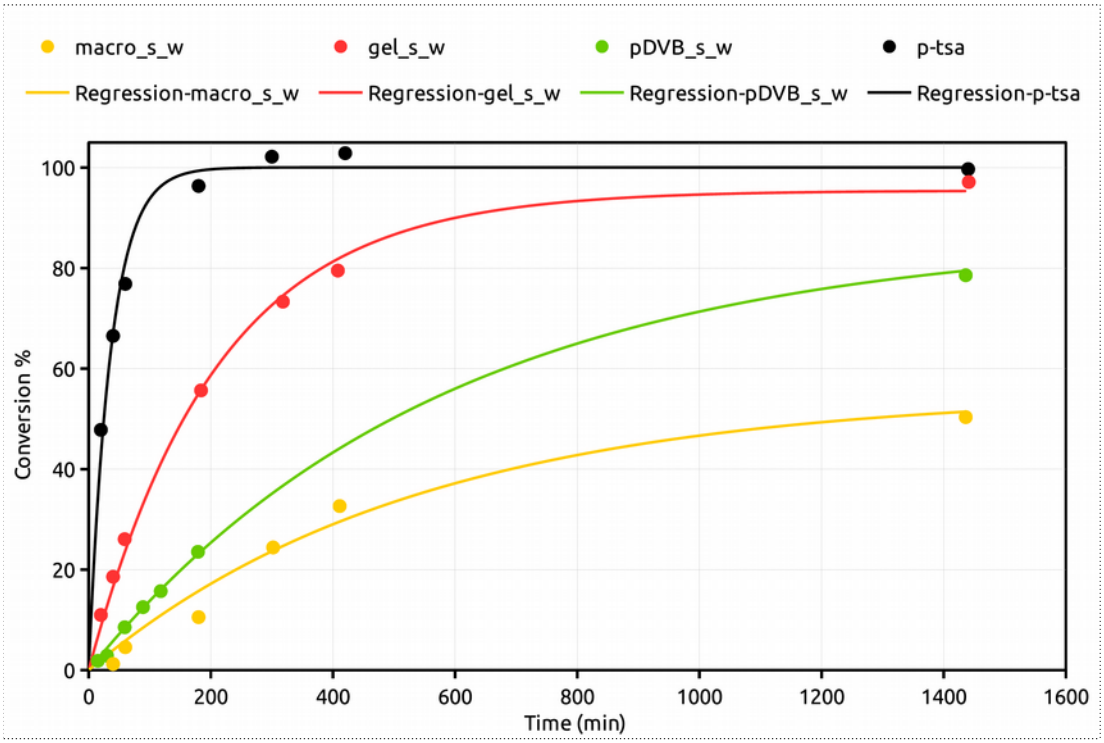

Figure 51: *conversion over time for catalysts with different morphology and for p-toluenesulfonic acid (reaction mixture: 72 g of oil, 8 g of stearic acid, 20 g of methanol; 0.5 g of heterogeneous catalyst and 0.25 g of the homogeneous one; T = 65 °C)*

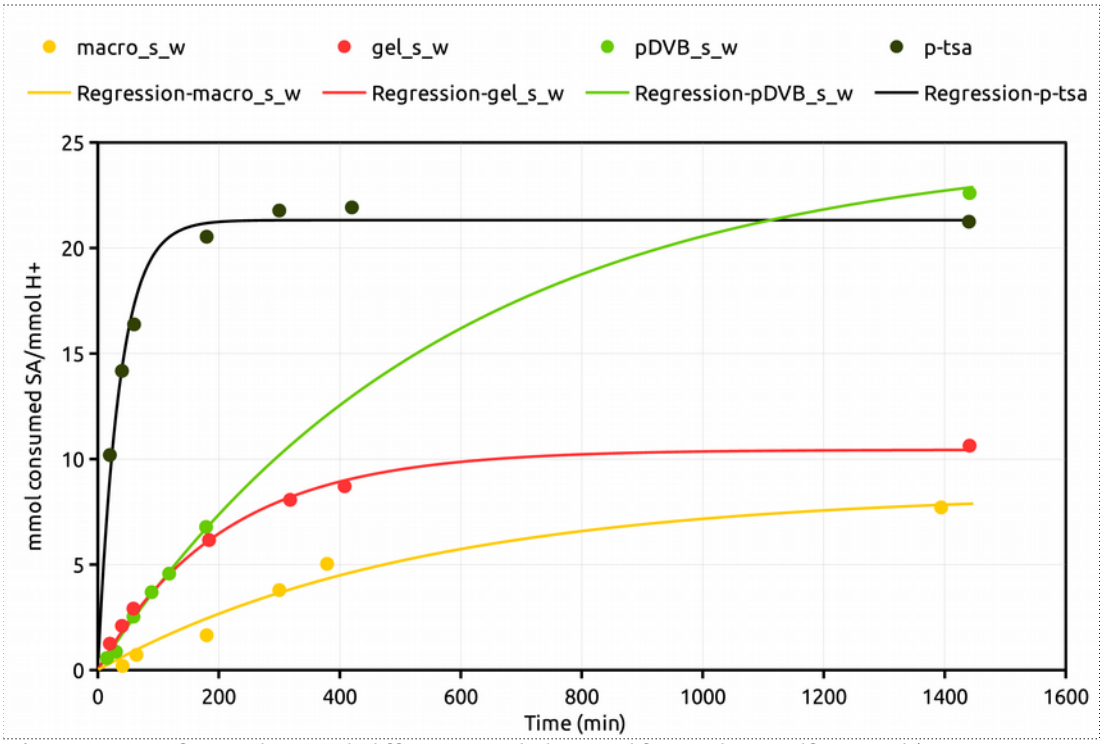

Figure 52: *TON for catalysts with different morphology and for p-toluenesulfonic acid (reaction mixture: 72 g of oil, 8 g of stearic acid, 20 g of methanol; 0.5 g of heterogeneous catalyst and 0.25 g of the homogeneous one; T = 65 °C).*

Thanks its homogeneous nature, p-toluenesulfonic acid shows the best performance. Its TON values are generally higher (*Figure 52*) and the complete conversion of SA is achieved in only 300 minutes of reaction, while the second best, *gel_s_w*, takes 24 hours. The other catalysts are not able to fully convert all the reagents into methyl stearate. However, it can be appreciated that the final TON for *pdvb_s_w* is as high as the highest TON achieved with *ptsa*. This indicates that the sulfonic groups of *pdvb_s_w* are as effective as those of *ptsa* and this again highlights the excellent properties of this catalyst arising from its accessible porous system.

4.8: Effect of acylation of the polymer matrix

4.8.1 Effect of acylation on the catalytic performance

Sulfonated resins are very hydrophilic materials and not suitable catalysts in reactions involving reagents with very different polarity. The concentration of a

lipophilic reagent inside the hydrophilic resin could be limited by thermodynamics (a low partition constant, due to a poor compatibility) or by mass transport restrictions, with the result of an unsatisfactory catalytic performance. The acylation of the aromatic rings of gel-type and macroreticular styrenic sulfonated resins proved successful to overcome this problem in the esterification of SA with methanol[48].

However, neither sulfonated poly-divinylbenzene nor the functionalization of the catalysts with perfluoroacyls were taken into account. We have now extended the investigation to these cases too and Table 22 illustrates the catalysts employed for this study.

***Table 22**: acylated and non acylated catalysts employed in the catalytic tests.*

Catalyst	Fraction of acylated rings [a]	Acyl group loading [b]	Proton exchange capacity [b]	Acyd/sulfonic group ratio [a]
pdvb_s_w	///	///	1,83	///
pdvb_c4f7o_s_w	10 [c]	0.5	2.33	21.5
pdvb_c4h7o_s_w	40 [c]	1.5	2.91	51.5
gel_s_w	///	///	4,93	///
gel_c4f7o_s_w	19 [d]	0.9	3.04	29.6

a: mmol/g; b: percent; c: from gravimetric analysis; d: from elemental analysis.

The acylation of the cross-linked polymers, which is expected to increase their lipophilicity, was performed with acylating agents with four carbon atoms. Although longer chains would be preferable to enhance the effect, the introduction of fluoroacyls with more than four C atoms proved unsuccessful so far. For this reason and for sake of comparison, the functionalization was carried out only with butyryl and perfluorobutyryl chlorides.

The acylated and sulfonated resins contain both lipophilic and hydrophilic groups and their overall nature should depend on the balance between the degree of acylation and of sulfonation. In this sense, the ratio between the content of the acyl groups and the proton exchange capacity can be used as a first approximation indicator of lipophilicity of the catalysts (*Table 22*, rightmost column). Under this respect, *gel_c4f7o_s_w* and *pdvb_c4f7o_s_w* should have comparable lipophilicity, and *pdvb_c4h7o_s_w* should be the most lipophilic. However, this analysis does not take into account the possibly different effects produced by the same relative amount of acyl and perfluoroacyl groups. Moreover, in resins with the same molar

ratio between the acyl and sulfonic groups, but with much higher absolute values, more severe steric congestion in proximity of the acidic active sites should be present.

The catalytic results for poly-divinylbenzene based materials are reported in Figures 53 and 54.

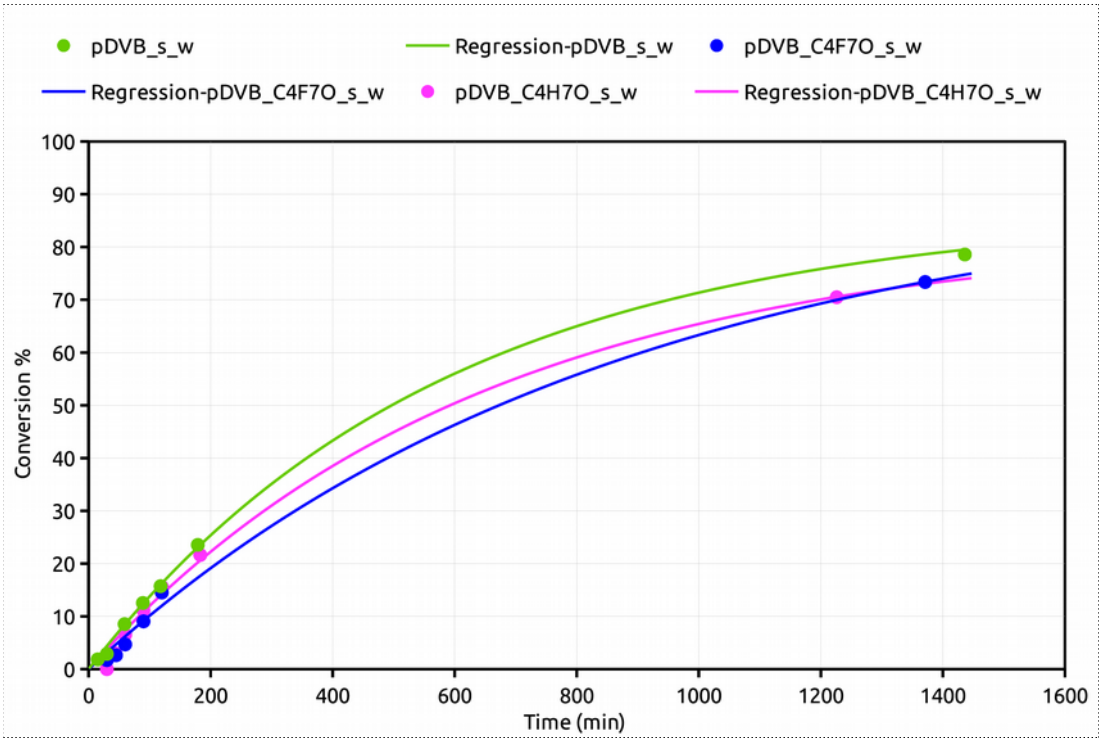

***Figure 53**: conversion of stearic acid over poly-divinylbenzene based catalysts (reaction mixture: 72 g of oil, 8 g of stearic acid, 20 g of methanol; 0.5 g of catalyst; T = 65 °C).*

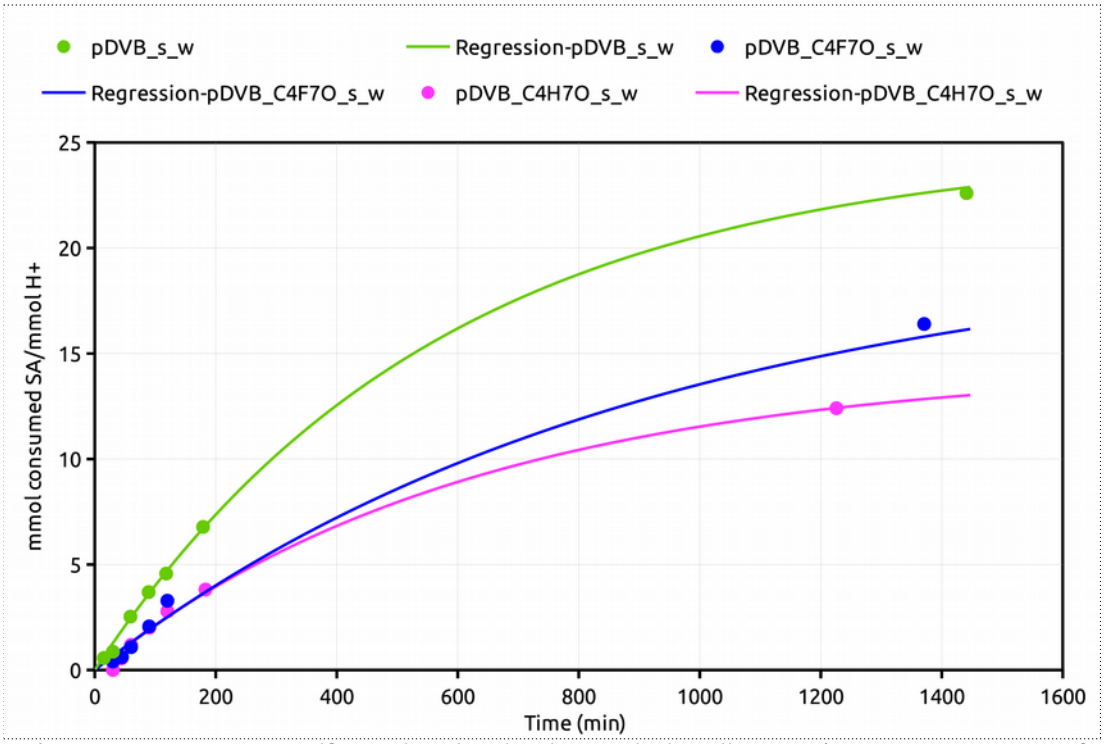

***Figure 54**: TON over time sulfonated, acylated and not, poly-divinylbenzene (reaction mixture: 72 g of oil, 8 g of stearic acid, 20 g of methanol; 0.5 g of catalyst; T = 65 °C).*

All the catalysts reach, at any time, almost the same conversion (*Figure 53*). If the TON are taken into account instead of the conversion (*Figure 54*), *pdvb_s_w* seems to be slightly more active, with both a higher TOF at the beginning of the reaction (calculated from the slope of the initial linear portion of the curve, *Table 23*) and a final TON value.

Table 23: TOF of poly-divinylbenzene based catalysts (reaction mixture: 72 g of oil, 8 g of stearic acid, 20 g of methanol; 0.5 g of catalyst; T = 25 °C).

Catalyst	**TOF (mol converted SA / mol H^+h)**
pdvb_s_w	2.10
pdvb_c4h7o_s_w	1.99
pdvb_c4f7o_s_w	1.90

However, the difference with the acylated catalyst is small and the effect of acylation almost negligible. The performance of the acylated catalysts are so close to each other that the effect of acylation with butyryl or perfluorobutyryl groups, if any, must be practically the same or so small, at these level of functionalization, that differences cannot be appreciated. The apparent ineffectiveness of the acylation of poly-divinylbenzene based catalysts can be explained by its

morphology. In pores as large as 30 nm (the average diameter of the permanent pores of pDVB) we can suppose that the acylic chains will only decorate the surface of the pores, with no appreciable reduction of their volume and occupation of their inner space. Accordingly, the diffusion of SA in these pores will be not significantly affected by the presence of the acyl groups and the effect of "assisted adsorption" observed in other cases [48] is not achieved. Also the mass transport from the mesopore space to their walls seems to be unaffected, possibly because the acylic chains are too short in comparison with the distance between the sulfonic and the acylic groups in a material with very high specific surface area as pDVB.

Also the performance of the gel-type acylated catalyst and non-acylated catalysts are not very different from each other (*Figure 55*). In this case we have not been able yet to produce an optimized catalyst acylated with butyryl chloride.

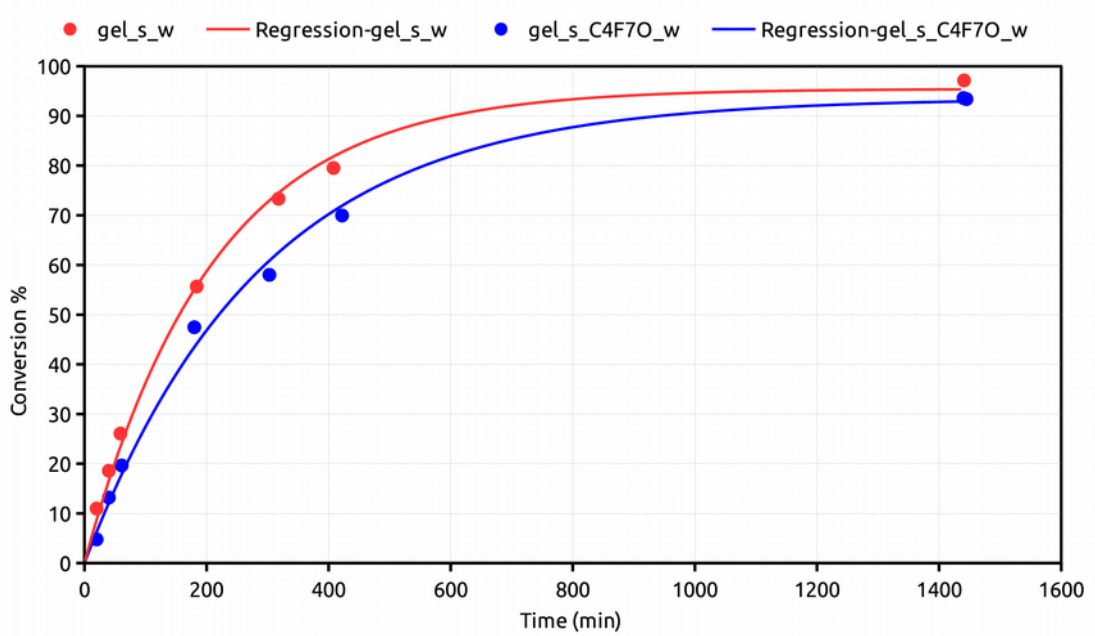

***Figure 55**: conversion of stearic acid with sulfonated gel-type resins (reaction mixture: 72 g of oil, 8 g of stearic acid, 20 g of methanol; 0.5 g of catalyst; T = 65 °C).*

However when TON (*Figure 56*) and TOF (*Table 24*) are compared for *gel_s_w* and *gel_c4f7o_s_w* the acylated catalyst proves to be better.

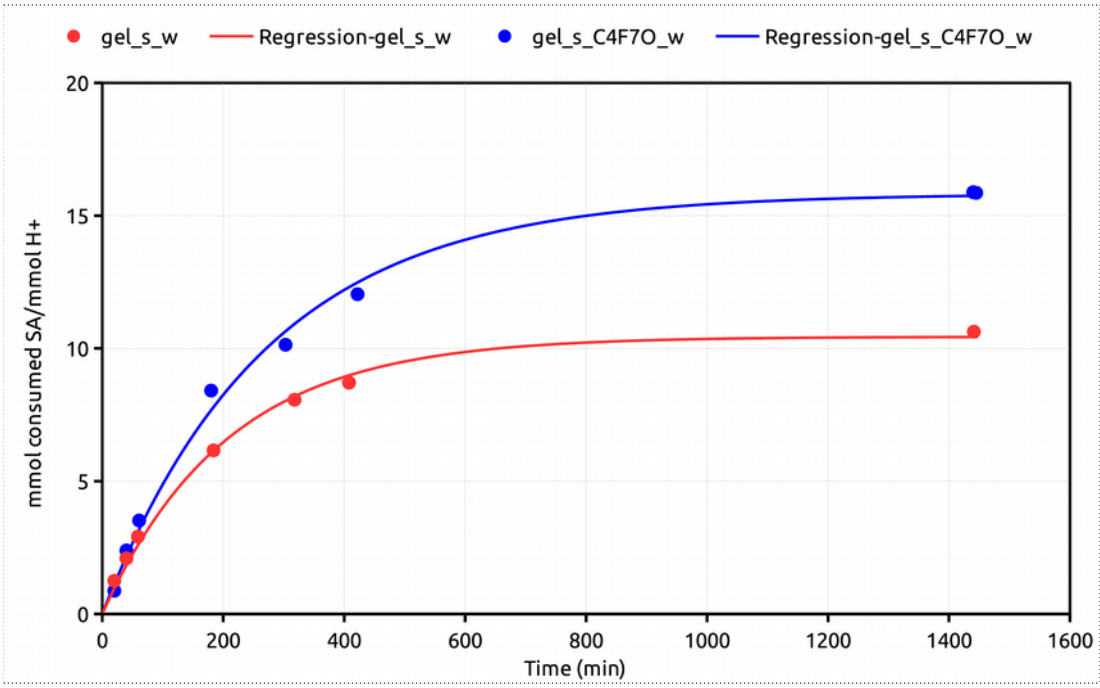

Figure 56: *TON of sulfonated gel-type resins in the esterification of stearic acid with methanol (reaction mixture: 72 g of oil, 8 g of stearic acid, 20 g of methanol; 0.5 g of catalyst; T = 65 °C).*

Table 24*: TOF values for sulfonated gel-type resins*

Catalyst	**TOF (mol consumed SA / mol H^+h)**
gel_s_w	3.06
gel_c4f7o_s_w	3.42

Its initial activity is higher by ca 15% and the final TON (which corresponds in both cases to practically quantitative reaction) higher by more than 50%. This indicates that acylation in this case has a positive effect on the absorption or adsorption of SA, in particular when its concentration is low (i.e high conversion). In addition, the lipophilic environment promotes the expulsion of the water, that is produced by the reaction and accumulates close to the catalytic sites, with detrimental effects on the catalytic activity.

These results indicate that gel-type catalysts are positively affected by the acylation, differently from those based on pDVB. As the acyl/sulfonic groups molar ratios are similar for both types of catalysts, the difference must arise from their different morphology. In gel-type resins the pores are formed when the polymer swells in the reaction medium and they are in the range of micropores or small mesopores. In a such confined space the relatively short acyl groups are

more effective in interfering with the diffusion of the SA molecules and a measurable, albeit small, effect of assisted adsorption is achieved.
To summarize, the acylation with butyryl and perfluorobutyryl chloride produces a negligible effect on the catalytic performance of sulfonated pDVB. Some effects could be possibly achieved with longer acylating agents, which should impart a stronger lipophilic character to the catalyst. Unfortunately, the acylation protocol developed in this work proved unsuitable and new procedures are needed for this purpose. New procedures could be useful also for the gel-type catalyst, because some effect of the acylation with perfluorobutyryl chloride can be observed, but is pretty small.

4.8.2 Behaviour of neutralized (deactivated) catalysts

Although in the standard reaction conditions employed in this work there is no appreciable effect of the acylation of the catalysts based on the pDVB matrix, the enhanced lipophilic character of these materials is not only suggested by the increased lipophilicity already observed in other acylated gel-type and macroreticular ion-exchange catalysts, but is also supported by the impossibility to characterize them with ISEC with polar mobile phase and probes (sugars and dextrans, *Paragraph 1.4*). In fact, the probes were completely retained by the acylated and sulfonated catalysts obtained from pDVB used as the stationary phase in the ISEC experiments. By contrast, standard ion-exchange sulfonated catalysts can be usually subjected to this kind of analysis. This indicates that the interaction between the acylated catalysts and alkanes and linear polystyrenes is much stronger in comparison with non acylated materials.
Therefore we tried a different approach to find hints of assisted absorption of SA in the acylated catalysts, based on pseudo-catalytic runs of SA esterification with catalysts neutralized with an aqueous solution of sodium hydroxide (*Table 25*).

Table 25 residual acidity of sulfonated poly-divinylbenzene, acylated and not, after their neutralization

Catalyst	Proton exchange capacity (mmol H^+/g)
pdvb_n	0.19
pdvb_c4h7o_n	0.65
pdvb_c4f7o_n	1.84

These materials are of course expected to be inactive, but in the case of enhanced absorption of the substrate, SA concentration in the liquid phase could be lowered to some extent even in the absence of any reaction.

After the neutralization, the materials (*pdvb_n*, *pdvb_c4h7o_n*, *pdvb_c4f7o_n*) were titrated, showing a residual proton exchange capacity, which is appreciably higher in the acylated resins (in *pdvb_c4f7o_n* it is likely overestimated because, due to shortage of the catalyst amount, we were forced to neutralize a sample recovered from a catalytic test which could also contain residues of SA).

This result could be connected with the different conditions employed in the sulfonation of the acylated pDVB matrices, in their neutralization and in the final titration. We speculate that a number of aromatic rings within the polymer framework are made accessible to the sulfonating agent by the presence of the acylic chains, but a fraction of them is no longer accessible during the neutralization in water-dioxane. Some internal sulfonic groups would retain the acidic form and would be detected upon the titration, which is carried out in a different medium (isopropanol) which is seemingly able to make them accessible again.

The results of the pseudo-catalytic experiments are illustrated in Figure 57.

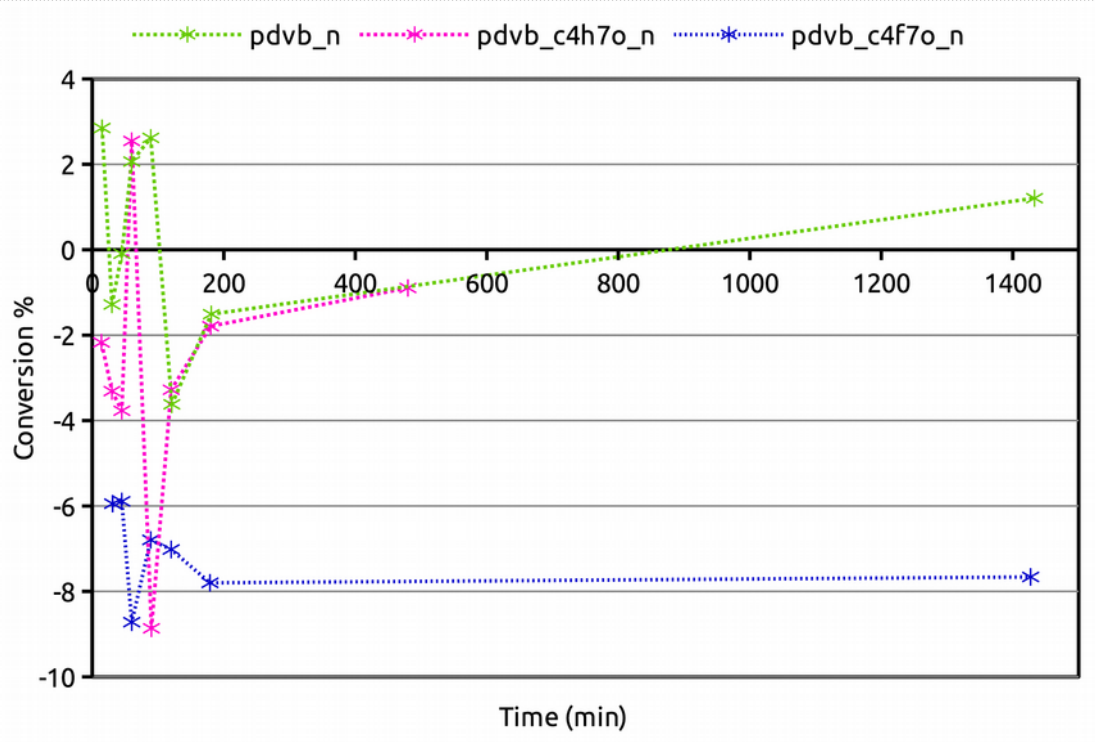

Figure 57: *conversion of stearic acid with the neutralized catalyst based on sulfonated pDVB (reaction mixture: 72 g of oil, 8 g of stearic acid, 20 g of methanol; 0.5 g of catalyst; T = 65 °C).*

No apparent decrease of SA concentration ("conversion") is detected, but rather an oscillation of its value around 0 by a few percent units.
As mentioned above, small negative conversion values were systematically observed under non-catalytic conditions at short reaction times (*Figure 46*). However, even taking into account a positive offset of the data of *Figure 57,* for this effect the erratic "conversion" data are most likely the consequence of the experimental error in the sampling and the determination of SA concentration. In conclusion, these experiments too do not provide evidence of any assisted absorption or adsorption brought about by the acylation of the catalysts. Moreover, in spite of their residual proton exchange capacity, the neutralized catalysts are completely inactive, which confirms that the small amount of acid sulfonic groups still present are located in the least accessible domains of the catalysts.

4.8.3: Effect of the addition of water on the catalytic performance

In addition to the assisted absorption or adsorption of SA, more lipophilic catalysts could take benefit from the assisted expulsion of the water produced in the esterification reaction. The development of water inside the catalysts close to the sulfonic groups could shift the reaction equilibrium toward stearic acid or could produce an increase of the polarity of the environment just close to the active sites, preventing the approach of the molecules of SA (and also of methylstearate for the back-reaction, by the way) [106–108]. In both cases, the presence of water would have a detrimental effect on the catalytic performance.
In the catalytic tests with added water its amount is 10% wt with respect to methanol (2% wt to the reaction mixture). For a careful control of the concentration of water, methanol is dried on molecular sieves prior to use and the reactor is protected with a calcium chloride tube. The reaction is still carried out at 65 °C, but with no reflux of the liquid phase, due to the increase of its boiling point in the presence of water.
As expected, the catalytic activity was strongly quenched by the presence of water (*Figure 58*): both the initial reaction rate and the final conversion are considerably lowered.

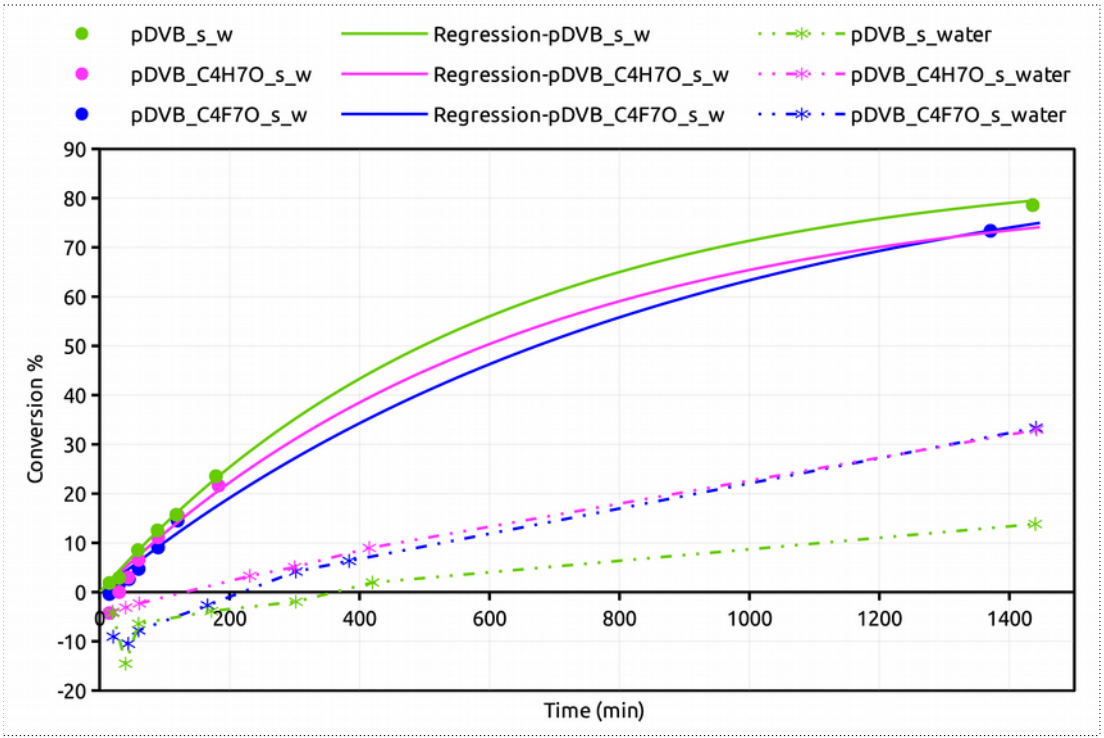

***Figure 58**: comparison of conversion of stearic acid for sulfonated pDVB (reaction mixture: 72 g of oil, 8 g of stearic acid, 20 g of methanol; 0.5 g of catalyst; T = 65 °C), including the tests performed with the addition of water to the reaction mixture (reaction mixture: 72 g of oil, 8 g of stearic acid, 18 g of methanol, 2 g of water; 0.5 g of catalyst; T = 65 °C). The tests performed in the presence of added water are indicated with the suffix "water".*

Remarkably, the strongest effect is obtained for the *pdvb_s_w*, the non acylated catalyst (*Figure 58*).

In view of their different proton exchange capacities the TONs are a better basis for the comparison of the catalysts (*Figure 59*).

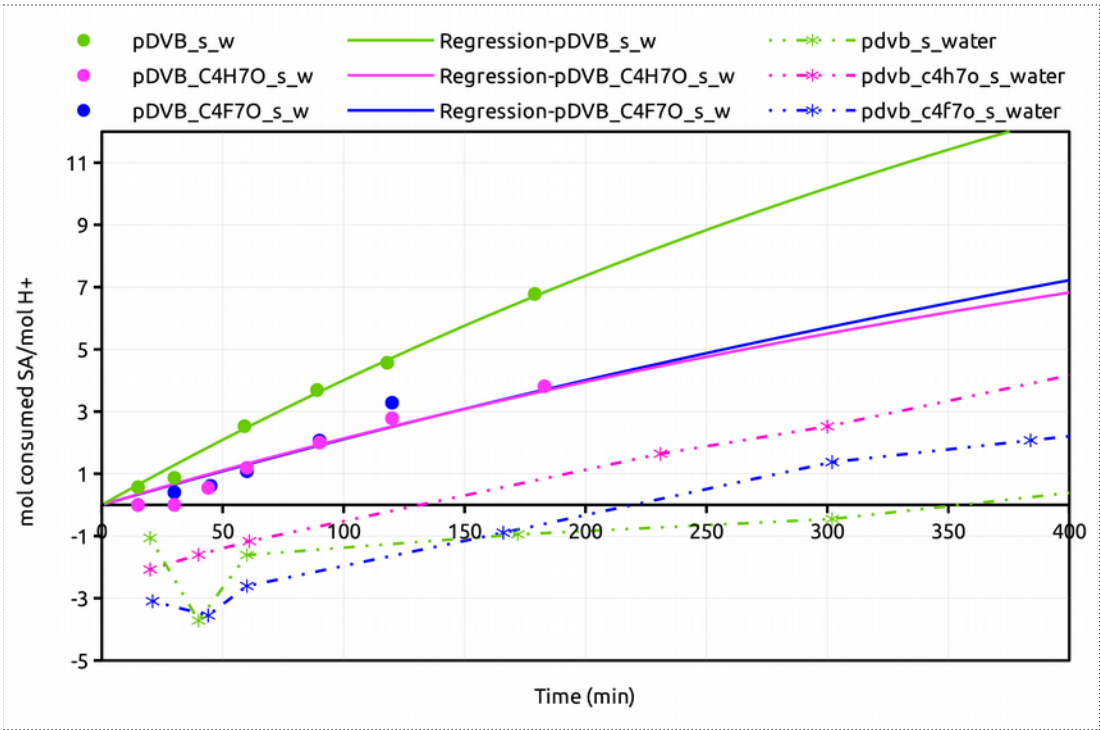

Figure 59:*comparison of TON for sulfonated pDVB (reaction mixture: 72 g of oil, 8 g of stearic acid, 20 g of methanol; 0.5 g of catalyst; T = 65 °C), including the tests performed with the addition of water to the reaction mixture (reaction mixture: 72 g of oil, 8 g of stearic acid, 18 g of methanol, 2 g of water; 0.5 g of catalyst; T = 65 °C). The tests performed in the presence of added water are indicated with the suffix "water".*

In this case the difference between the activity of *pdvb_s_w* and of the acylated catalysts are smaller, but still appreciable, especially at relatively high conversions, when the concentration of SA is lower and that of water is higher. At low conversion the slope of the TON vs time curve for *pdvb_c4f7o_s_w* is apparently higher than for *pdvb_s_w*. To summarize, these results show that acylation does not fully protect *pdvb_c4h7o_s_w* and *pdvb_c4f7o_s_w* from the action of water, but that, to some extent, it limits their deactivation. This is in line with the higher lipophilic character of the acylated materials.

Moreover, for the tests in the presence of water, the initial values of conversions (up to 200 minutes) are clearly negative. The highly negative initial conversion (ca. -15% for unfunctionalized pDVB and pDVB_C4F7O_s) cannot be explained only by the experimental error. In fact, on the one hand, according to the experimental procedure (Chapter 6), an estimation of the experimental error of the conversion is not obvious, on the other hand, it can be roughly evaluated from the catalytic experiments performed with the catalysts in the neutralized form, for which no reactivity is expected to be observed (*Figure 57*). In this case, the highest variability is observed for the catalyst pdvb_c4f7o_n (in the range -8÷3%), whereas

a significantly lower scattering of the conversion values is observed for pdvb_n and pdvb_c4h7o_n catalysts. In the case of the catalytic tests in the presence of water, the initial conversion values, especially for pdvb_c4f7o_s_w and pdvb_s_w, appear beyond the variability observed for the catalysts in the neutralized form. In addition, it can be clearly observed that the experimental error generally leads to a slight underestimation of the conversion, as suggested by the evident increasing trend of the values (*Figure 59*), rather than a random dispersion (*Figure 57*). In the presence of water the triglycerides of the sunflower oil could be effectively hydrolysed to their fatty acids. The conversion of SA is measured by means of its acid-base titration; however this method is not selective and any increase of the overall fatty acid concentration in the reaction mixture would give a decrease of the apparent conversion.

To test this hypothesis selected reaction mixtures collected during the early stages of the catalytic test were characterized by ^{1}H NMR. The ^{1}H NMR spectra of sunflower oil and SA are shown in Figures 60 and 61 and the relevant attributions are reported in Table 26.

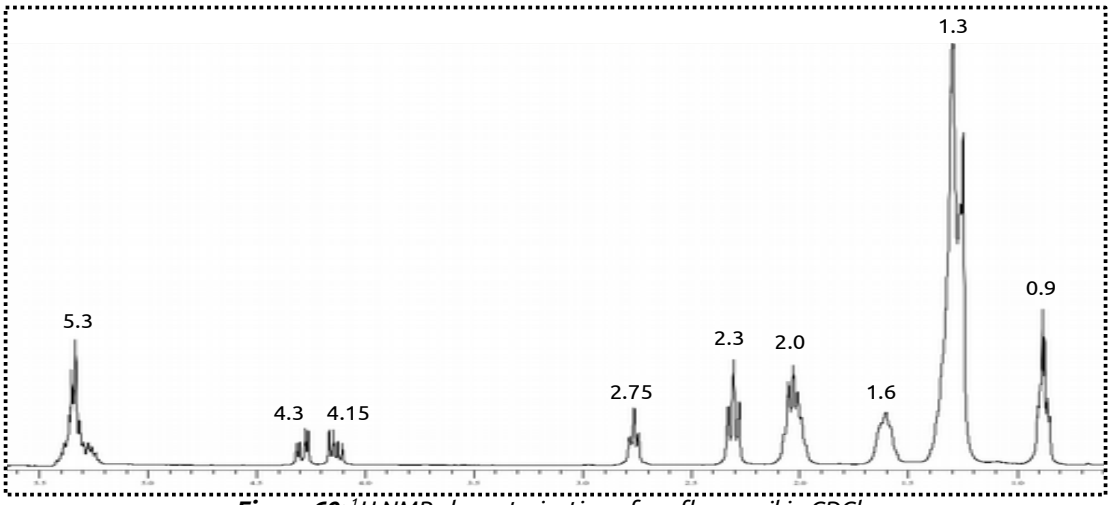

***Figure 60**: ^{1}H NMR characterization of sunflower oil in $CDCl_3$.*

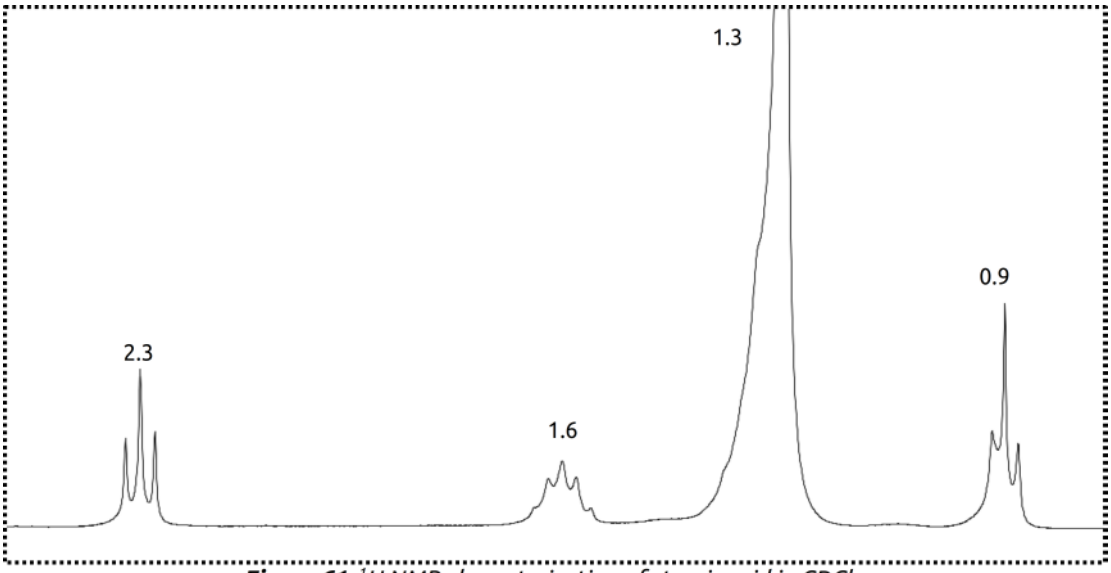

***Figure 61**: ^{1}H NMR characterization of stearic acid in $CDCl_3$.*

***Table 26**:attribution of signals of NMR spectra reported in Figures 60 and 61.*

δ (ppm)	**Sunflower oil**	
5.3 (m)	CH of the glyceryl and vinyl groups (a)	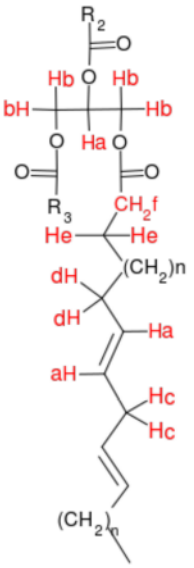
4.3 (m), 4.15 (m)	CH_2 of the glyceryl group (b)	
2.75 (t)	internal allylic CH_2 (c)	
2.3 (t)	CH_2 α to the carbonyl group (f)	
2.0 (m)	external allylic CH_2 (d)	
1.6 (m)	CH_2 β to the carbonyl group (e)	
1.3 (m)	Other CH_2 of the aliphatic chain	
0.9 (m)	CH_3	
	Stearic Acid	
2.3	CH_2 α to the carbonyl group (b)	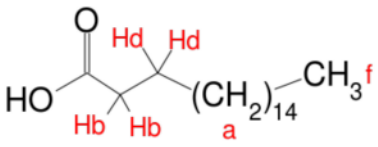
.6	CH_2 β to the carbonyl group (d)	
1.3	Other CH_2 of the aliphatic chain(a)	
0.9	CH_3 (f)	

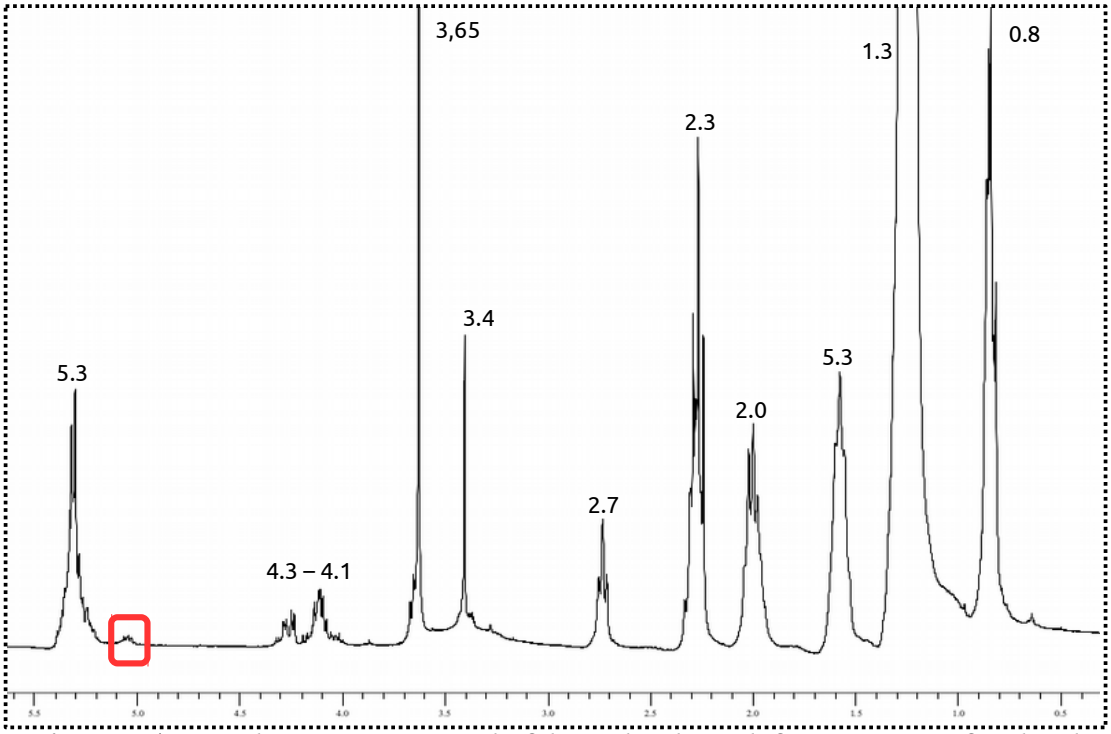

Figure 62: *^{1}H NMR characterization in $CDCl_3$ of the residue obtained after evaporation of methanol (reaction mixture: 72 g of oil, 8 g of stearic acid, 20 g of methanol; 0.5 g of pDVB catalyst; T = 25 °C).*

The NMR characterization of the residue obtained after evaporation of the methanol of the hydrophilic phase of a catalytic test with a catalyst based on sulfonated pDVB is reported in Figure 62.

In addition to the signals of SA and of the sunflower oil a multiplet at about 5 ppm (highlighted in the red rectangle in Figure 62) is detected. It is observed in the spectra of residues obtained from the hydrophilic phase of different reaction mixtures, which rules out an accidental contamination and supports the presence of a new substance formed during the catalytic reaction. The most likely attribution is to the methine and methylene in the glyceryl group of mono- and/or diglycerides, formed upon hydrolysis of trigylcerides. As this must also produce an equivalent amount of free fatty acids, this further supports the presence of an extra amount of the latter which contributes to the apparently negative conversions at the beginning of the reaction. However, even in the case that this is entirely due to the hydrolysis of triglycerides, the final conversion of SA in the presence of water would be relatively low. Therefore, the deactivation of the catalyst by water is confirmed and the previous discussion on its effect can be considered valid in any case.

Chapter 5:
DIRECT SYNTHESIS OF HYDROGEN PEROXIDE

5.1: Brief overview on direct synthesis of hydrogen peroxide

Hydrogen peroxide is a strong oxidant agent over a wide range of pH (E_0 = 1.763 V at pH 0; E_0 = 0.878 V at pH 14) and the residue of its reduction is only water, so that it is considered one of the greenest oxidant agent (*Equation 8)* [109].

$$H_2O_2 + Substrate \rightarrow Oxidized\ Substrate + H_2O$$

Equation 8: *oxidation of a substrate S to SO by H_2O_2*

Currently main uses of hydrogen peroxide include bleaching in the paper and textile industry, where it replaces the chlorine-based bleaches and leaves waste streams free of halogenated residues. It is also widely employed in the treatment of municipal wastes and in chemical manufacturing (extraction and purification of metals, oxidation, epoxidation and hydroxylation reactions, etc.) [110,111].
Hydrogen peroxide is produced by the "Riedl-Pfleiderer process", introduced by IG Farben in Germany in the 1940s, and based on the auto-oxidation of anthraquinone (*Figure 63*).

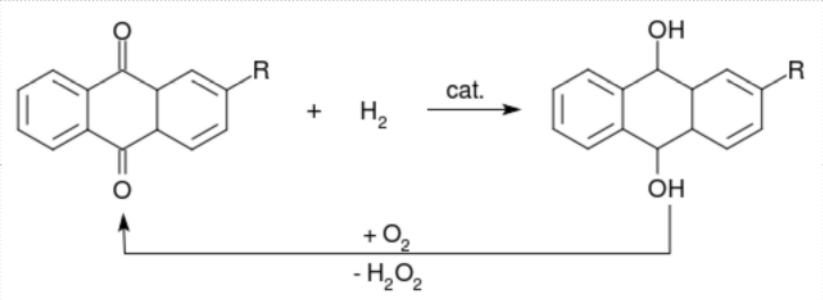

Figure 63: *auto-oxidation of 2-alkylanthraquinone involved in the Riedl-Pfleiderer process for the synthesis of hydrogen peroxide.*

A 2-alkylanthraquinone (AQ) is first catalytically hydrogenated to the corresponding 2-alkylanthrahydroquinone (AHQ) at 40-50 °C and at a partial pressure up to 4 bar. The solution, is separated from the catalyst and oxidized with

air in a second reactor. This non-catalytic oxidation gives back the AQ and produces an equimolar amount of H_2O_2, which is extracted in water in a counter-current column. The 30% wt aqueous solution of H_2O_2, is finally purified and concentrated to 70% wt upon distillation and the organic solution from the extraction step is recycled back to the hydrogenation reactor. This process currently accounts for more than 95% of the world-wide production of H_2O_2, thanks to its high yields and the avoided contact between hydrogen and oxygen. However, because of its high capital and operating costs, it is economically viable only for a large-scale production. As the consequence, the production of very concentrated solutions, which is energy-intensive, is necessary for the storage and the transportation, even though they are potentially explosive and that H_2O_2 is most often used at much lower concentrations.

To widen the scope of this environmentally friendly oxidizing agent, a new cost-effective and clean production process for the in-situ production of hydrogen peroxide could be very useful. Among the many proposed approaches (oxidation of alcohols and electrochemical synthesis for example), the metal catalysed direct synthesis (CDS) of H_2O_2 from its elements (H_2 and O_2) seems to be the most promising [110,111]. However, this reaction is only apparently simple: not only water is the thermodynamically favourite product of the reaction between hydrogen and oxygen, but hydrogen peroxide is an intermediate that can be easily converted into water upon decomposition (dismutation) or hydrogenation (*Figure 64*).

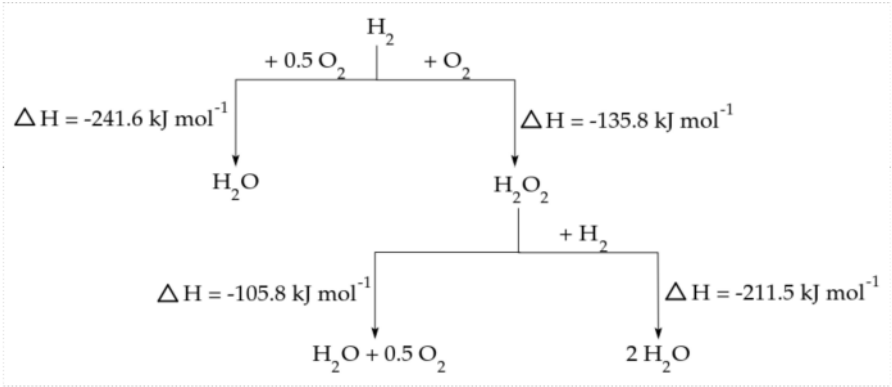

Figure 64: *reactions involved in the direct synthesis of hydrogen peroxide.*

Although CDS of hydrogen peroxide has been known since 1914 [112] and in spite of occasional claims, its industrial application has not yet be implemented and the challenge of the research is the development of a catalyst able to guarantee an high selectivity of the process and, possibly, also a satisfactory activity.

The catalysts reported in the literature are generally based on nanostructured noble metals, in particular on Palladium. Bi-functional catalysts , especially Pd-Au[113–115] and Pd-Pt [116] have also been proposed for this reaction, because the presence of small amounts of gold or platinum seems to be beneficial for the selectivity of the reaction. Different types of supports have been studied, ranging from the inorganic (alumina [113,117–119], titania [120] , iron oxide [121] and, the most promising, carbon [122–126]) to the organic materials, like polymer resins.

To improve the selectivity, mineral acids are added to the reaction mixture to prevent the dismutation of hydrogen peroxide that is favoured in basic conditions. Moreover, the addition of halide ions (in particular bromides and chlorides) increases the selectivity of the reaction, limiting the combustion of hydrogen to water [127–131]. Thus, often hydrogen halides are the preferred choice as selectivity enhancers, because they combine the effect of both acids and halides [132–135]. The drawback of this approach is the consequent corrosion of the equipment due to the use of hydrogen halides and the reactivity of these specie with most of the organic substrates hydrogen peroxide is expected to be used with [110,111].

Furthermore, the exploitation of hydrophobic supports seems to increase the selectivity of the reaction, making easier the diffusion of the produced H_2O_2 from the catalyst towards the bulk solution, limiting, consequently, its further reduction to water. With this purpose carbon treated with fluorine [131], inorganic supports coated with a thin layer of hydrophobic material were proposed [136].

As to the choice of the solvent, the most important feature to be considered is the solubility of the gases. Water would be the most suitable choice from the environmental point of view, but the solubility of gases is very low [137], giving therefore low rates of H_2O_2 production. Thus, organic solvent are preferred [138] and, in particular, alcohols (the solubility of H_2 in alcohol is 4-5 times higher than in water, whereas that of O_2 may be increased up to eightfold) are widely used, because they are generally used for oxidation reactions and consequently interesting from the point of view of the potential exploitation of H_2O_2 solutions.

The exploitation of supercritical CO_2 has also been proposed in literature, [139] since H_2 and O_2 are soluble in any proportion above 31°C and their solubility is higher than in organic solvents and in water. Moreover, the solubility of hydrogen peroxide in supercritical CO_2 is low and therefore it can be expelled from the solvent after its production, decreasing the time of contact with the catalyst and consequently the rate of its hydrogenation. The produced H_2O_2, moreover, does

not need to be distilled to remove traces of organic solvent. However, it was observed that a working temperature higher than 31°C increases the rate of decomposition of H_2O_2, limiting the beneficial effects resulting from the use of this medium [140].

5.2: Effect of the oxidation state of Palladium

The effect of the oxidation state of Palladium is widely debated in literature.
Choudary et al. [133] studied the rate of decomposition of H_2O_2 with a PdO catalyst supported on zeolites, under the same experimental conditions used to perform the catalytic tests, without reactive gases. They observed an increase of the decomposition rate when the catalyst is reduced with hydrazine and stated that non-reduced catalysts are more selective than the reduced ones.
Melada et al. claimed that the selectivity of catalysts based on PdO and supported on anion doped-zirconia is lowered after a reducing treatment [141]. They explained the outcome on the basis of the formation of beta-hydride during reduction and the consequent formation of surface defects, making less selective the catalysts. At the same time, they observed that, during the catalytic test, also PdO is reduced to Pd, according to literature [142].
Burch and Ellis [143] studied Palladium catalysts supported on different inorganic oxides (TiO_2, Al_2O_3, Fe_2O_3, etc.) and reported a remarkable increase of activity and selectivity when the catalysts are reduced before the catalytic test. The only exception was observed for 1% Pd/TiO_2, probably because, according to TPR characterization, the low reduction temperature of the catalysts (12 °C) makes possible the reduction of PdO also during the catalytic test.
Thomson and coworkers [134] pre-reduced all the catalysts (Palladium on Phosphate Viologen Phosphonate) before performing the catalytic tests to avoid the presence of surface PdO, the formation of which occurs when nanoparticles are stored in air.
Finally, Lunsford and coworkers [144] compared the catalytic performance of Pd^0/SiO_2 and PdO/SiO_2 and observed a complete inactivity for the oxidized

catalyst. Only after the in situ reduction with hydrogen, the catalysts became active, showing a consumption of hydrogen and a production of H_2O_2.

5.3: Selectivity enhancers

The main issue of the liquid-phase process of direct synthesis of H_2O_2 is the low selectivity of the reaction. Therefore, it is of essential importance to optimize the reaction conditions to maximize the selectivity of the reaction, with particular attention to [110,111]:

- temperature: low temperatures avoid the decomposition of the produced H_2O_2;
- solvent: alcohols, for example, seem to favour a more selective production of H_2O_2 respect to other organic solvents;
- oxidation state of the Palladium catalyst;
- chemical and morphology features of catalytic supports;
- reaction time: it is important to stop the reaction before a drop in selectivity or, alternatively, choosing the most suitable contact time in a continuous process.

Besides the experimental parameters, a crucial role is played by the presence of selectivity enhancers that, in the direct synthesis of hydrogen peroxide, are known to be protons and halides. The role of protons as enhancers in the direct synthesis of H_2O_2 was first explained by Pospelova et al [145] in their early works, pointing out the inhibition effect of protons on the dissociation equilibrium of H_2O_2, forming the hydroperoxide anion, HO_2^-, and H^+.

Burch and Ellis [143] and Landon et al. [113] claimed that an acid reaction medium simply prevents the basic-promoted decomposition of hydrogen peroxide. Ishihara et al. [120] observed no formation of H_2O_2 when basic oxides are employed as catalytic supports (MgO or Al_2O_3), whereas production is present when acidic oxides are used (SiO_2 or ZrO_2). They ascribed this finding to the high stability of hydrogen peroxide in acid media.

On the contrary, Chinta and Lunsford [135] stated that protons, in the presence also of chloride ions, take part to the catalytic system, in which Pd^0 colloids react with oxygen to form a dichloroperoxopalladium(II) complex which subsequently reacts

with H^+ to yield H_2O_2 and $PdCl_4^{2-}$. In the catalytic cycle, Pd^0 is finally regenerated by reaction of $PdCl_4^{2-}$ with Hydrogen, releasing protons and the chloride ligands. The role of protons in favouring hydrogen peroxide production, rather than its decomposition, is reported also by Lunsford in a further investigation[146].

Abate et al. [147] also proposed that protons are involved in the mechanism of formation of hydrogen peroxide. Accordingly, oxygen is first adsorb on Palladium without dissociation, then protonation from an external H^+ takes place and, finally, the reaction with H_2 forms H_2O_2 and regenerates the proton.

Finally, Choudary and Samantha [148] supposed that protons are involved in a complicate reaction mechanism, including free radical and ionic reactions, in which the substrates also is involved.

Halogen ions are known to be selectivity enhancers since the first work of Pospelova [149] who early reported the beneficial effect of the addition of a mineral acid, as HCl, on the selectivity of the direct synthesis of H_2O_2.

There is a general agreement the literature on the fundamental mechanism with which halogens act as selectivity enhancers. Their main role is the inhibition of the combustion of H_2 to water, blocking the most active sites on the surface of the Palladium nanoparticles, where the dissociative chemisorption of O_2 is believed to occur. After the dissociation of the oxygen atoms, in fact, only water can be produced by reaction with hydrogen [113]. This hypothesis is experimentally supported by the investigation of Dissanayake and Lunsoford [150]. The authors analysed by Raman Spectroscopy the reaction mixture after a catalytic test performed with Pd/SiO_2 as the catalyst and in presence of a mixture of $^{16}O_2$ and $^{18}O_2$. Since signals ascribable to $H_2{}^{16}O^{18}O$ were not observed, it is possible to conclude that hydrogen peroxide is produced only if oxygen is diatomically adsorbed on the catalyst. Consequently, water is formed when a dissociative pathway is followed.

According to Burch et al, [143] the presence of halogen ions decreases also the consumption of hydrogen, because a fraction of active sites is involved in the adsorption of halide ions. However, since the selectivity remarkably increased, this is of limited importance.

Among halide ions, only chlorides and bromides behave as selectivity enhancers for the direct synthesis [148]. The addition of fluorine ions, in fact, does not improve the selectivity of the reaction. On the contrary, the addition of iodide ions poisons the metal catalyst, completely suppressing the consumption of hydrogen.

Moreover, also the concentration of enhancers must be optimized. For example, Ntainjua et al. [151] reported that the pre-treatment with bromides deactivates an Au–Pd bimetallic catalyst based on carbon or MgO respect to production of H_2O_2, when high concentrations are used.

Choudhary and Samantha [152] studied the hydrogenation of hydrogen peroxide over Pd(5%wt)/carbon in aqueous medium both under batch and semi-batch conditions. The consumption of H_2O_2 is observed in the presence of Br^- and Cl^-, but, without the addition of mineral acid, the disproportionation of hydrogen peroxide initially prevails on the hydrogenation reaction. Therefore, they recommend the combined use of halides and acids. These results support previous findings of the same authors[148] in which reduced Palladium catalysts supported on inorganic oxides showed a limited increase of selectivity when alternatively acid or halide ions were added.

5.4: Cross-linked polymers as supports for metal nanoparticles

According to Paragraph 1.1, cross-linked polymers are able to develop an extended porous system when swollen in a suitable solvent. The sizes of the pores depend on the chemical nature of both resin and the swelling solvent. In gel-type resins, mesopores with diameter up to 10 nm are generated by swelling. Conversely, in macroreticular ones, in addition to this type of porosity, bigger permanent mesopores are also present (10-30 nm). A particular case is pDVB that has permanent mesopores up to 50 nm (*Paragraph 1.5*)

When the synthesis of metal nanoparticles takes place inside the swollen polymer network, the polymer chains exert a steric control on their growth. Consequently, the final size of the metal nanoparticles is determined by those of the porous system in which they are generated and are in the range of few nanometers[153].

The resin does not only support metal nanoparticles, but it can also play a catalytic role as enhancer. For example, it can exert a size exclusion effect on a reagent with beneficial effects on chemoselectivity [154,155]. Also the lipo- or hydrophilic nature of the support can remarkably influence the catalytic performance. For example, if the product of the reaction has a lesser affinity with the support than the reagent,

its expulsion from the catalyst bead is favoured, with beneficial effects on the selectivity of the reaction [156,157].

Moreover, the introduction of catalytically active groups inside the resin framework can be exploited for the creation of a multifunctional catalyst. This approach was used to develop the catalyst for the industrial synthesis of MIBK (Methyl Isobutyl Ketone) from acetone and H_2, over a nanostructured Palladium catalyst supported on a sulfonated resin. The sulfonic groups catalyse the condensation of two acetone molecules to produce mesytylene oxide, further reduced to MIBK over the Pd^0 nanoparticles [158].

5.5: Synthesis of metal catalysts supported on cross-linked functional polymers

A possible strategy to obtain metal catalysts supported on polymeric resin is the Incorporation of Metal Precursors during polymerization and its subsequent Reduction (IMPR) [159–163]. Another approach consists in the Immobilization of pre-formed Metal Nano-clusters (IMN) [157,164,165]. Both these method, however, are not widely used.

The simplest and most widely used method is RIMP (Reduction of Immobilized Metal Precursor). First the resin is swollen in a suitable solvent and the desired metal precursor is anchored to the functional groups of the polymer framework by ion exchange or metal coordination. Finally, the metal centres are reduced to generate the metal nanoparticles. If functional groups suitable to grafting the metal precursor are not present within the polymer matrix, the metal uptake is driven only by diffusion and this can lead to a metal catalyst with an eggshell radial distribution. On the contrary, if functional groups are present, a quantitative uptake even of small amounts of metal precursor can be obtained [44].

In this work, the metal catalysts were synthesized by a RIMP approach, using sulfonic resins as catalytic supports. When polymeric resins are used as support, this synthetic approach is named TCS (Template Controlled Synthesis) to highlight the role of the resin as template for the growth of nanoparticles [153,166].

According to the procedures employed in the frame of the Thesis, the synthesis of metal catalysts consists of some essential steps (*Figure 65*):

1) *Sulfonation of the resin*: sulfonic groups are introduced by treating a styrenic resin with concentrated sulfuric acid.
2) *Metallation:* introduction of $[Pd(NH_4)_4]^{2+}$ by ion-exchange with protons of sulfonic groups of the resin, after swelling of the resin in water.
3) *Reduction of the metal precursor*: metal atoms are generated by reduction of the precursor with hydrogen in THF (step b in Figure 65).
4) *Generation of metal nanoparticles:* metal atoms aggregate until metal nanoparticles with sizes comparable with those of pores are formed (steps c and d in Figure 65).

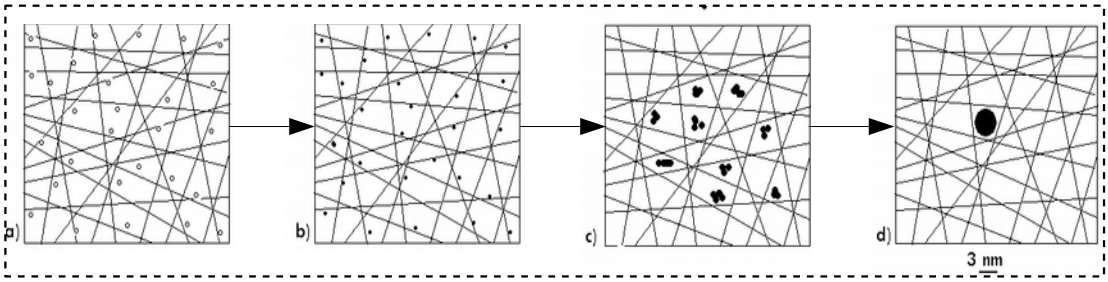

Figure 65: *representation of TCS synthesis of metal nanoparticles. a) a precursor is anchored to the resin by ion-exchange or metal coordination. b) the precursor is reduced to metal atoms. c) metal atoms aggregate and d) the growth of metal nanoparticles stops when their size are comparable with those of pores.*

The same procedure is applied also in case of acylated resins: the only difference is the presence of an acylation step, before the sulfonation one. In fact, Friedel-Crafts acylation does not occur on aromatic groups more deactivated than halo-benzene [101]. The sulfonation and metallation steps are summarized in Figure 66 for acylated pDVB.

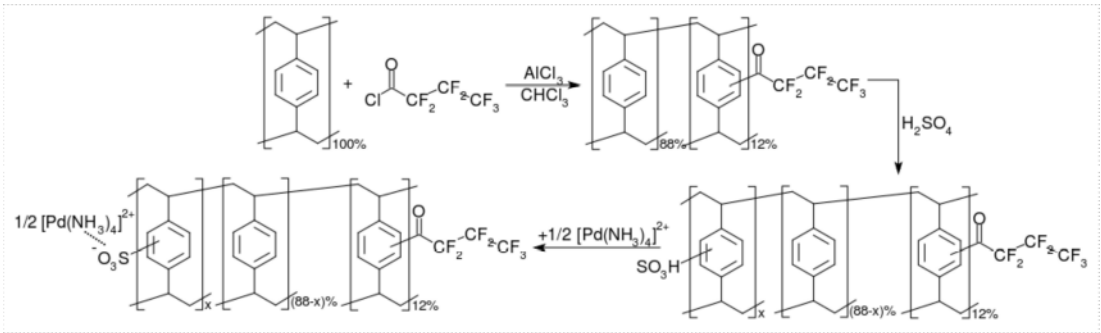

Figure 66: *metallation of an acylated (with perfluorobutyryl chloride) and sulfonated pDVB. Each mole of $[Pd(NH_3)_4]^{2+}$ as the precursor needs two moles of sulfonic groups for its uptake.*

5.6: Experimental setup and conditions of the catalytic tests

To perform the catalytic tests of direct synthesis of hydrogen peroxide, a semi-batch reactor was first developed.

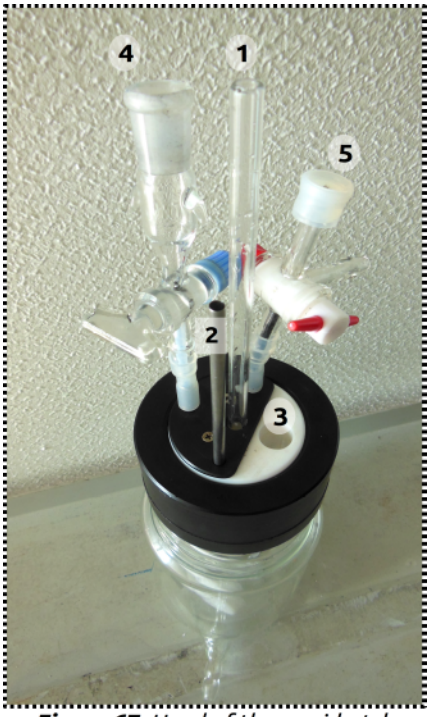

Figure 67: *Head of the semi-batch reactor for the direct synthesis of H_2O_2*

The reaction takes place in a jacketed-glass vessel with a capacity of about 500 ml (*Figures 67 and 68*). The jacket of the reactor is connected with an external thermal bath to maintain constant the reaction temperature at 25 °C during the catalytic test. The vessel is closed with a suitable teflon cap (*Figure 67*) bearing five entries:

1. glass tube ending with a porous sintered glass septum (*Figure 68*) aimed at the feeding of the gaseous reagents, maximizing the surface of contact between liquid and gas phases;
2. housing for a thermocouple to check the temperature of the reaction mixture;
3. connection for a coiled condenser aimed to the recovery of traces of methanol present in the outgoing gas flow;
4. line for the introduction of the solid catalyst;
5. line for the extraction of samples of the reaction mixture.

Figure 68: *structure of the inner part of the reactor*

The gaseous reagents (hydrogen and oxygen) are fed into the reactor with constant and precise flow rates with two mass-flow controllers. The chosen flow rates are 1 and 24 ml/min for hydrogen and oxygen respectively, producing a gaseous mixture with 96% mol oxygen content (4% mol hydrogen). A mixture of hydrogen and oxygen, with the concentration of one of the

components below 4% is, in fact, not explosive at ambient pressure [167]. In this case hydrogen is the minor component: in fact, in the direct synthesis of H_2O_2 it is usually the limiting reagent because its cost determines the overall cost of the process [168]. Alternatively, the risks connected to the handling of hydrogen-oxygen mixtures can also be minimized by also feeding an inert diluent gas, like, for example, carbon dioxide [110].

The unreacted gaseous reagents exit the reactor through the condenser and are disposed under a fume hood, therefore the tests are performed at ambient pressure.

During the test the products (hydrogen peroxide and water) are formed and accumulate in the liquid phase inside the vessel, while the reagents are continuously fed at constant flow rate . The reactor is therefore semi-continuous.

The evaluation of the performance of the catalysts is based on the concentration of produced H_2O_2 and on the consumption of hydrogen, being this the limiting reagent under these experimental conditions. Consequently, it is possible to determine the yield of H_2O_2, the conversion of H_2 and the selectivity.

The concentration of H_2O_2 is obtained by titration of samples of the reaction mixture, collected every twenty minutes (*Paragraph 6.11*). In the sampling system, at the end of the steel tube is present a sintered steel filter to prevent the removal of small amounts of catalyst during the collection of portions of the reaction mixture. At the other side, a three way glass valve makes possible the insertion of a needle for the sampling with a syringe and connection of the tube with the mass-flow controllers. The sampling procedure consists of three steps:

1. the sampling line is flushed with the reagents flow for about 30 seconds to clean the filter from stagnant solution. In this period, the reagents are fed through the sampling line;
2. the three way valve is switched in order to feed the reagent gases through the main feeding line and to insert into the sampling line a needle connected to a glass syringe. About 1 ml of solution is taken out;
3. The sampling line is isolated, by switching the three way tap, to prevent any leak and air contamination.

The quantitative analysis of the hydrogen content of the outgoing gas mixture is performed with a micro-GC, connected to the condenser line. The analysis is automatically performed every 3 minutes. The hydrogen content is determined

from the area of the chromatographic peak of hydrogen, after calibration of the TCD detector.

The condenser is needed for the abatement of the vapour of methanol, which otherwise would affect the reproducibility of the chromatographic measures. The condenser is cooled at -9 °C with an ethanol bath to ensure the complete condensation of the vapour of methanol.

An overall view of the semi batch reactor for the direct synthesis of H_2O_2 is reported in Figure 69.

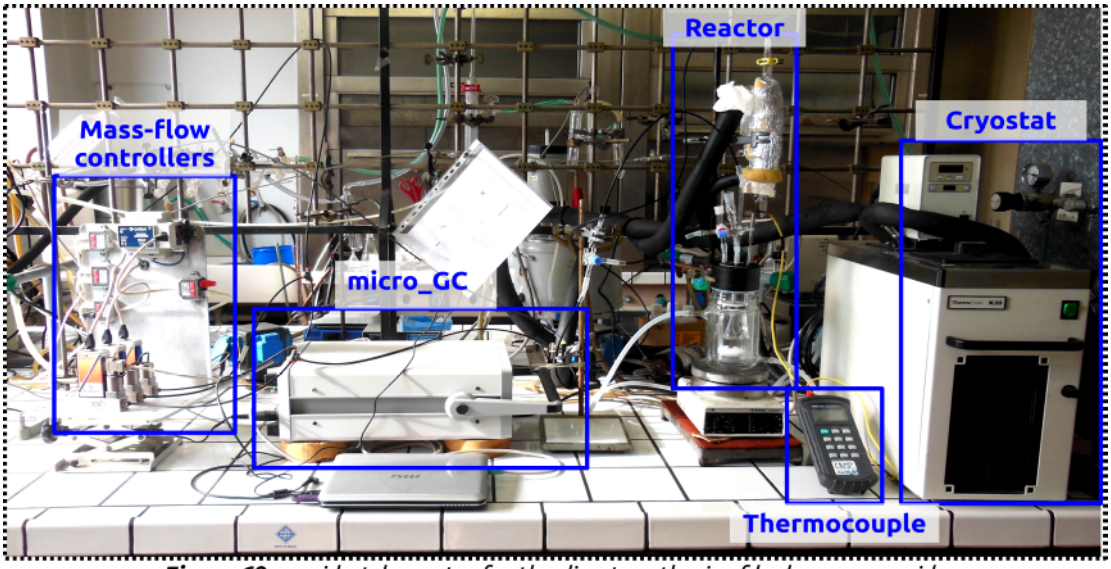

Figure 69: *semi-batch reactor for the direct synthesis of hydrogen peroxide*

In liquid phase reactions involving gaseous reagents, the dissolution of the gaseous reactants has to be carefully considered. To this regard, an efficient mixing is of primary importance. Therefore, a neodymium stirring bar, making possible to reach high stirring rate (ca. 1250 ppm), and steel baffles, avoiding the formation of a vortex, are employed (*Figure 68*).

Finally, the chosen solvent for the reaction is methanol. In fact, the solubility of hydrogen and oxygen in methanol are comparable with common organic solvents (*Table 27*) [169]. Moreover, the selectivity enhancers are soluble in alcohols that is able to swell the hydrophilic catalysts.

Table 27: solubility data for hydrogen and oxygen in various organic solvents.

Solvent	Solubility of H_2 (mmol/L)	Solubility of O_2 (mmol/L)
water	0.81	1.25
methanol	3.96	10.12
ethanol	3.75	10.0
isopropanol	3.46	10.1
Acetone	4.08	11.38
1,4-dioxane	2.06	7.22

5.7: STEM and TEM characterization

Three of the most important palladium catalysts used for the direct synthesis of H_2O_2 were characterized by Transmission Electron Microscopy (*TEM*) and Scanning Transmission Electron Microscopy (STEM):

- *Pd_1%/C*: commercially available Palladium (1 %wt) on activated carbon with an eggshell distribution of metal nanoparticles. It was employed for the investigation of the role of bromide ions as selectivity enhancers (*Paragraph 5.3*) and, generally, as the reference for the resin based catalysts.
- *Pd_1%/pDVB*: Pd nanoparticles (1 %wt) supported on sulfonated poly-divinylbenzene.
- *Pd_1%/pDVB_C4F7O*: Pd nanoparticles (1 %wt) supported on acylated (with perfluorobutyryl chloride) and sulfonated poly-divinylbenzene.

In Figures 70, 71 and 72 the STEM images of the selected catalysts are reported.

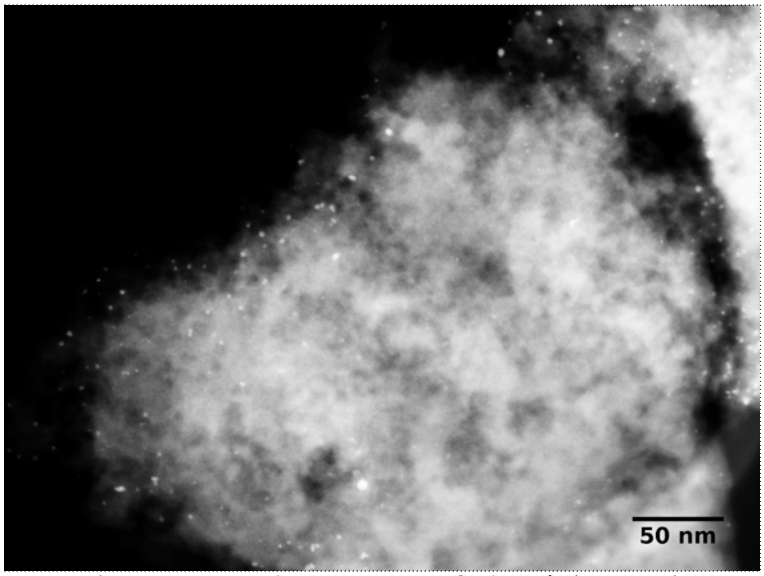

Figure 70: *STEM characterization of Pd_1%/C (283061X).*

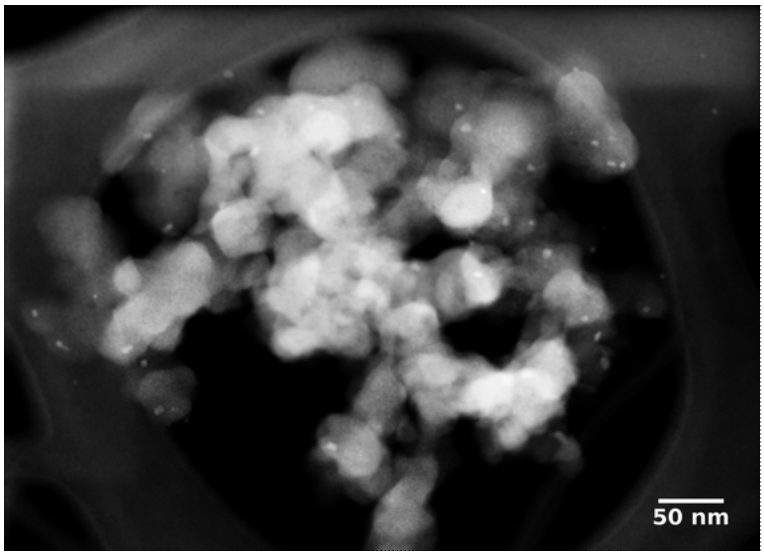

Figure 71: *STEM characterization of Pd_1%/pDVB (203657X)*

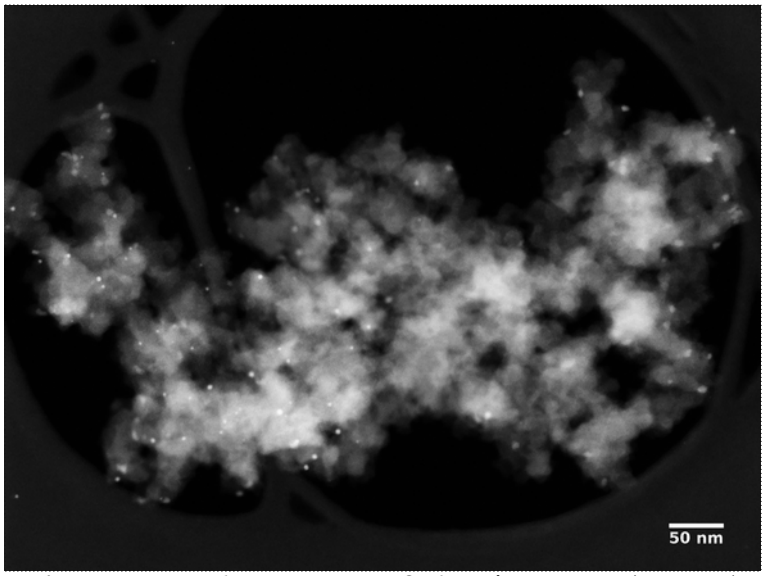

Figure 72: *STEM characterization of Pd_1%/pDVB_C4F7 (170662X)*

As to *Pd_1%/C* (*Figure 70*), the metal nanoparticles are particularly visible on the external layer of the selected grain, according to the eggshell distribution declared by the supplier. On the contrary, a homogeneous distribution of metal nanoparticles inside the catalytic support is present in the catalysts based on pDVB (*Figures 71 and 72*). Moreover, in this case, pores smaller than 50 nm, as expected from the mesoporous nature of the polymer (*Paragraph 1.5*), can be recognized inside the polymer framework as black holes.

The TEM characterization of the materials (*Figures 73, 74 and 75*) confirms the homogeneous distribution of metal nanoparticles observed in the STEM images of Pd_1%/pDVB and Pd_1%/pDVB_C4F7.

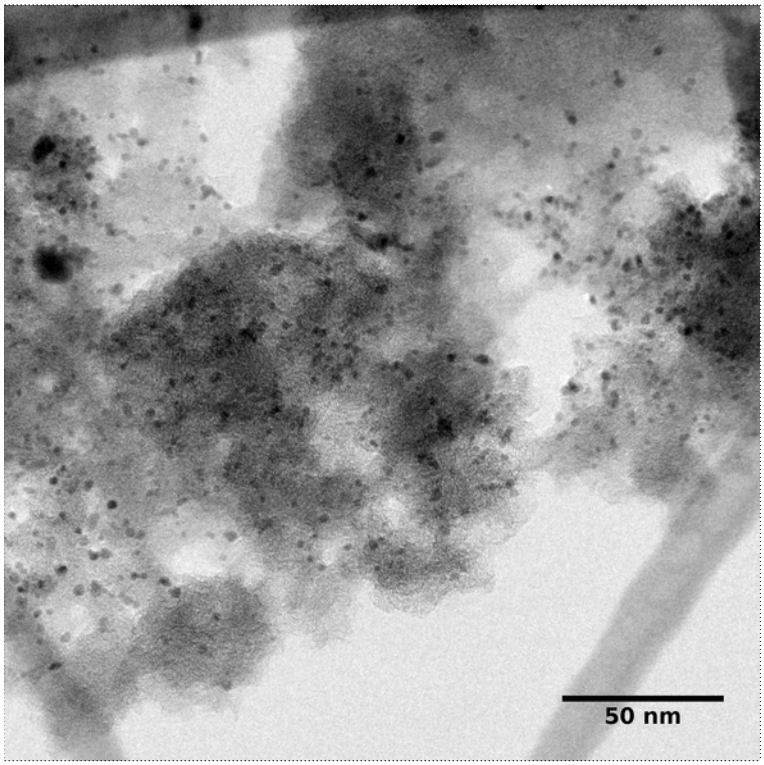

Figure 73: *Representative TEM image of Pd_1%/C (125000X)*

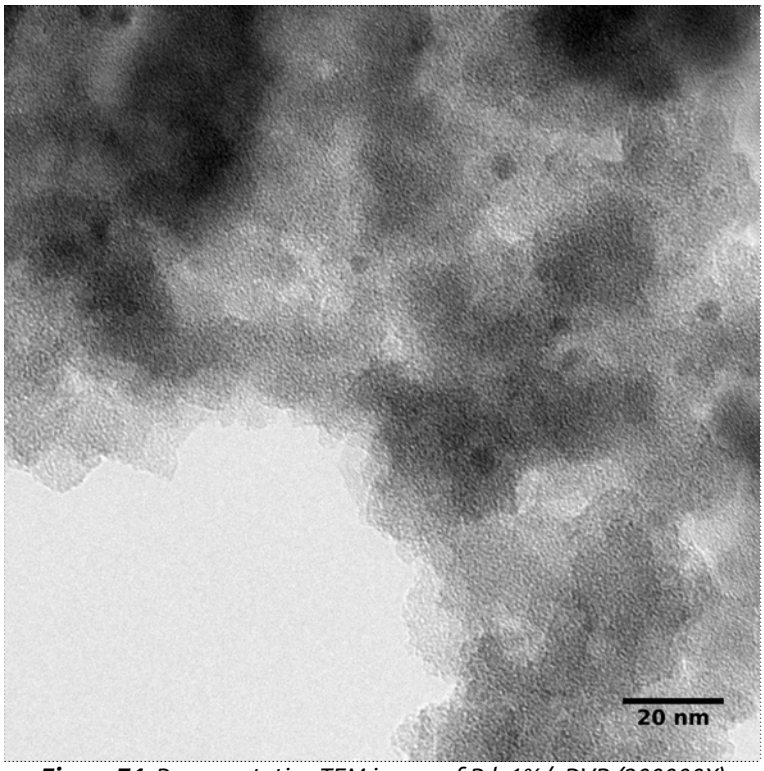

Figure 74: *Representative TEM image of Pd_1%/pDVB (200000X)*

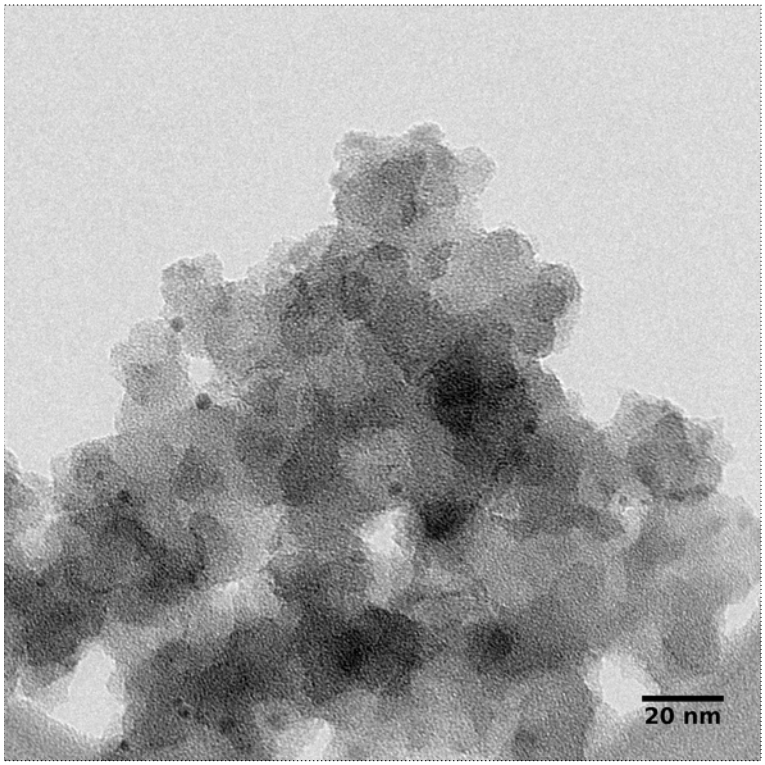

Figure 75: *Representative TEM image of Pd_1%/pDVB_C4F7O (160000X)*

The broad log-normal particle size distribution of the selected catalysts is presented in Figure 76.

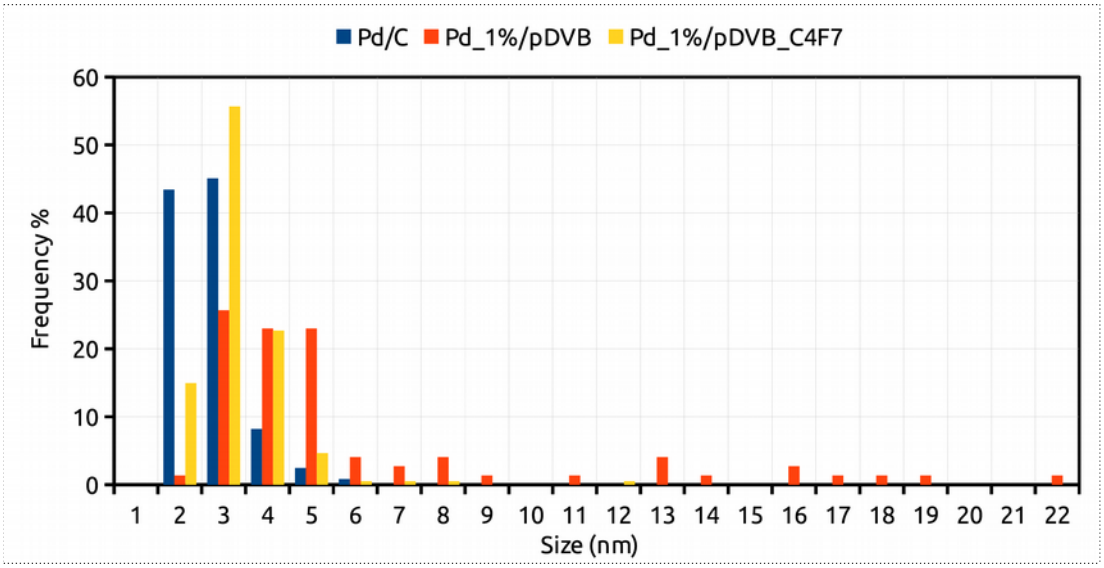

Figure 76: *particle size distribution for Pd/C (122 nanoparticles), Pd_1%/pDVB (74 nanoparticles) and Pd_1%/pDVB_C4F7 (194 nanoparticles).*

As to the catalysts based on pDVB, the presence of a small number of particles larger than 5 nm is observed only in *Pd_1%/pDVB*. This is reasonably due to the

higher ageing of *Pd_1%/pDVB* catalysts (prepared some months before the analysis), possibly susceptible to a more extended coalescence phenomena. However, for Pd_1%/pDVB and Pd_1%/pDVB_C4F7 the particle size distribution below 5 nm is similar.

The catalyst *Pd_1%/C* is featured by the presence of small nano-clusters, with a narrow particle size distribution centred in the range 1-3 nm. Nevertheless, the average diameter of nanoparticles (2.3 nm) is comparable with that of *Pd_1%/pDVB_C4F7O* (2.8 nm) (*Table 28*).

Table 28: *Highest, smallest and average size of metal nanoparticles for Pd/C Pd,_ 1%/pDVB and Pd_1%/pDVB_C4F7 catalysts.*

	Pd/C	**Pd_1%/pDVB**	**Pd_1%/pDVB_C4F7**
Max. size (nm)	5.4	21.0	11.6
Min. size (nm)	1.2	1.7	1.3
Average size (nm)	2.3	5.5	2.8

Finally, the catalysts were also characterized with HRTEM (*High Resolution Transmission Electron Microscopy*, Figures 77, 78 and 79) to a better insight on the structure of the nanoparticles. According to literature, the inter-planar distances measured for Pd/C, Pd_1%/pDVB and Pd_1%/pDVB_C4F7 catalysts. (*Table 29*) can be ascribed to fcc crystal structure of metal Palladium[170–172]. This outcome confirms that nanoparticles are formed by zerovalent Palladium. The possible presence of superficial PdO is not verifiable by HRTEM.

Table 29: Inter-planar distance (nm) and related attribution.

Catalyst	**Inter-planar distance (nm)**	**Attribution (Phase, plane)**
Pd_1%/C	0.216 [a]	Pd^0, {111}
	0.220 [a]	Pd^0, {111}
Pd_1%/pDVB	0.185	Pd^0, {200}
	0.230	Pd^0, {111}
Pd_1%/pDVB_C4F7O	0.224 [a]	Pd^0, {111}
	0.200 [a]	Pd^0, {200}
	0.199 [b]	Pd^0, {200}

[a]: determined by FT analysis of HRTEM lattice

[b]: determined by directly measuring the inter-planar distance in an HRTEM lattice image

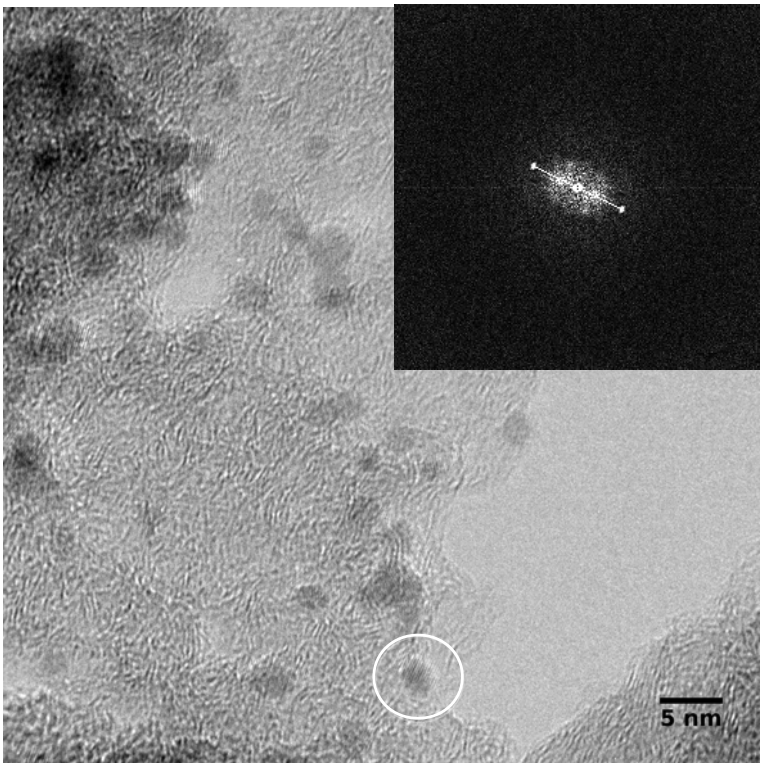

***Figure 77**: HRTEM characterization of Pd_1%/C (500000X) and inverted FTT pattern related to circled particle.*

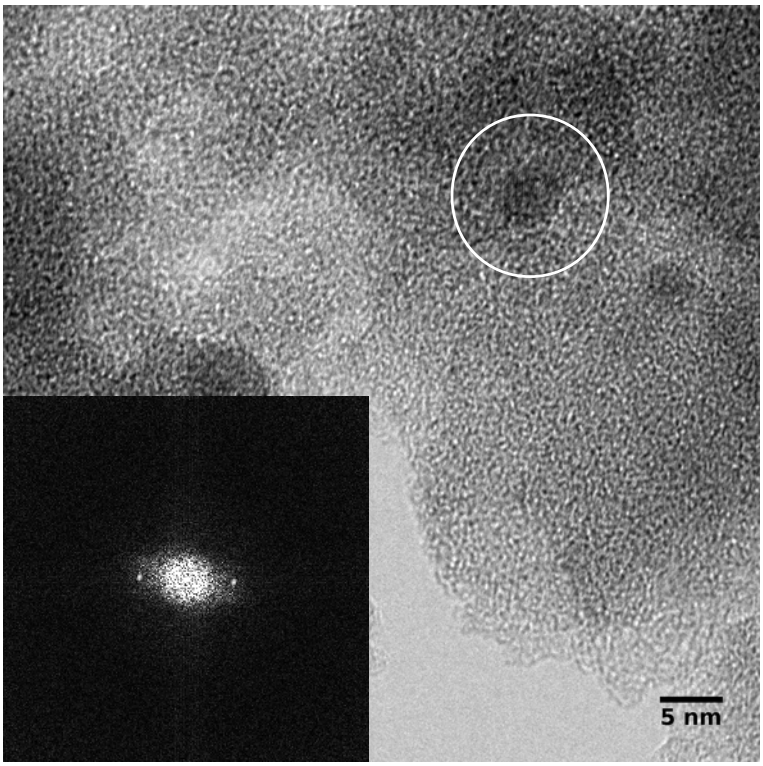

***Figure 78:** HRTEM characterization of Pd_1%/pDVB (500000X) and FTT pattern related to circled particle.*

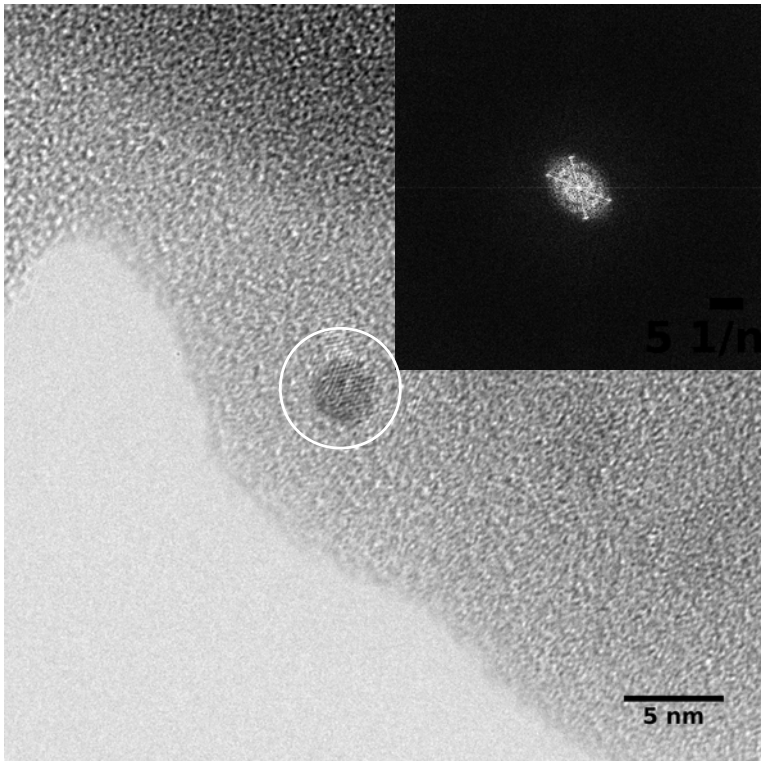

***Figure 79**: HRTEM characterization of Pd_1%/pDVB_C4F7O (800000X) and pertinent FTT pattern. particle.*

Concluding, these results show that, although based on different supports, the investigated catalysts have comparable size distributions of metal nanoparticles. This suggests that the catalytic performance observed in the direct synthesis of hydrogen peroxide is mainly influenced by the morphological characteristics of the support, rather than by differences in nanoparticles sizes.

5.8: Role of the catalytic support

The morphology of the catalytic support strongly affects the performance of a heterogeneous catalyst [173]. In fact, it influences not only the diffusion of the reagents towards the catalytic sites, but could also affects, in the case of cross-linked polymers, the shape and the sizes of metal nanoparticles [153].

As a preliminary investigation on the direct synthesis of hydrogen peroxide, the performance of poly-divinylbenzene based metal catalysts was initially compared with those of a catalyst based on a conventional macroreticular resin (15 %wt of DVB). The effect of functionalization of poly-divinylbenzene was also investigated

by using poly-divinylbenzene materials, acylated with C_4H_7OCl or C_4F_7OCl, as catalytic supports. The introduction of lipophilic chains should, in fact, make the expulsion of hydrogen peroxide from the catalyst beads easier, preventing its hydrogenation to water and therefore enhancing the selectivity of the process. In addition, the presence of fluorinated moieties, thanks to the affinity of fluorinated phases for gases, is expected to increase the solubility of gaseous reagents inside the catalyst and close to the nanoparticles, with beneficial consequences on the activity.

The features of the polymer supports and the cumulative H_2 consumption of the palladium catalysts based on sulfonated pDVB and on a macroreticular resin are reported in Table 30 and Figure 80, respectively.

Table 30 *functionalized pDVB catalysts for the DS of H_2O_2*

Catalyst	Description of the support	Proton exchange capacity (mmol H^+/g)	% of acylated rings
Pd_1%/macro	Sulfonated macroreticular resin	5.0	//
Pd_1%/pDVB[a]	Sulfonated pDVB	2.0	//
Pd_1%/pDVB_C4H	Sulfonated pDVB, acylated with C_4H_7OCl	1.6	24.9 %
Pd_1%/pDVB_C4F	Sulfonated pDVB, acylated with C_4F_7OCl	1.9	11 %
Pd_1%/pDVB_ATRP	Sulfonated pDVB, functionalized by ATRP	1.7	//

[a:] prepared with a solvent:monomer volume ratio 10:1 (Paragraph 1.5)

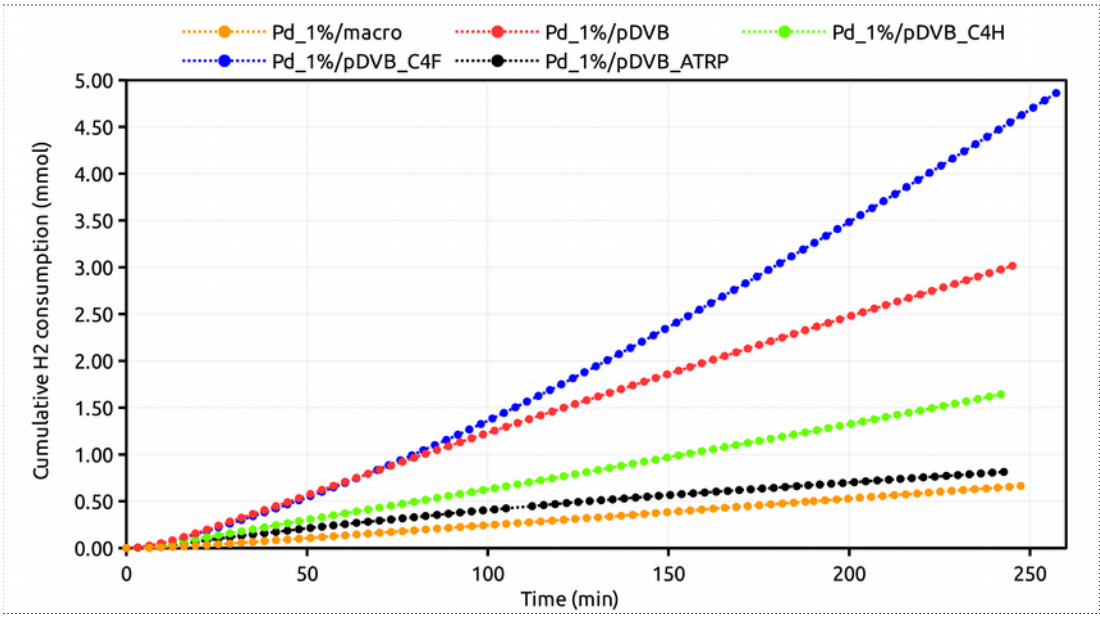

Figure 80: *cumulative consumption of hydrogen for metal catalysts supported on pDVB and macroreticular resins. (flow-rates: O_2 = 24 ml/min, H_2 = 1 ml/min; solvent = methanol; volume = 300 ml; T = 25 °C, catalyst: 100 mg, 1% w/w Pd)*

As to the non-acylated catalysts, the activity (i.e the slope of the curve of conversion in time) of the catalyst based on macroreticular resin is remarkably lower than that of the catalyst based on poly-divinylbenzene (*Figure 80*). The different morphology of the polymer materials could determine the formation of nanoparticles with different shapes and catalytic behaviour. The TCS approach used for the synthesis of the metal catalysts (Paragraph 4.7) is based on the growth of the nanoparticles generated by reduction of a suitable metal precursor bound to the sulfonic groups. The extent of the thermodynamically favoured aggregation is controlled by the size of the pores, acting as templates for the growing nanoparticles that assume sizes comparable with those of pores. This is particularly true for gel-type resins that only present a mesoporosity of few nm [43,153,166]. On the contrary, in macroreticular resins nanoparticles with a broader size distribution are obtained because of the presence in the swollen polymer matrix also of macropores, limiting the steric control during their growth [142,174–176]. In the case of poly-divinylbenzene, featured by the presence of mesopores up to 50 nm, the dimensional control is expected to be further weaker.

The functionalization of poly-divinylbenzene with non-fluorinated acylic chains (*Pd_1%/pDVB_C4H*) decreases the activity of the catalyst with respect to the non acylated one (*Pd_1%/pDVB*). The behaviour of the fluorinated catalyst (*Pd_1%/pDVB_C4F*), instead, is remarkably different: at the beginning of the

reaction it is as active as *Pd_1%/pDVB* and the activity of both increases, but after ca. 120 minutes *Pd_1%/pDVB_C4F* becomes distinctly more active (*Figure 80*).

The presence of acylic chains should make the sulfonated poly-divinylbenzene more lipophilic, but could also create a steric hindrance around nanoparticles and, although hydrogen and oxygen are small molecules, this could limit their diffusion towards the active metal phase. The high acylation degree of *Pd_1%/pDVB_C4H* could therefore explain its smaller activity with respect *Pd_1%/pDVB* (*Table 30*). On the other hand, the good performance showed by *Pd_1%/pDVB_C4F*, which has a small acylation degree, could be the result of the combination of a good lipophilicity of the support and and relatively high affinity towards the gases with a limited steric hindrance.

The presence of fluorinated acylic chains could also, in principle, lead to metal nanoparticles with different sizes with respect to the non acylated catalyst (*Pd_1%/pDVB*). However, the results of TEM (*Paragraph 4.7*) showed that the size distributions of *Pd_1%/pDVB_C4F* and *Pd_1%/pDVB,* except for the presence of a small number of particles bigger than 5 nm for the acylated catalyst, are very similar. This suggests that the observed catalytic performances are mainly influenced by the morphological features of the support, rather than by differences in nanoparticles sizes.

Finally, the activity of the catalyst based on poly-divinylbenzene functionalized with per-fluorinated chains by ATRP (*Pd_1%/pDVB_ATRP)* is comparable with that of *Pd_1%/*macro. This low activity can be explained, as in the case of acylated poly-divinylbenzene, by the steric hindrance. For this catalyst the hypothesis of steric hindrance appears to be particularly reliable, because the monomer used for the ATRP (1*H*,1*H*,2*H*,2*H*-Perfluorodecyl acrylate) has a bulky alkyl chain of ten carbon atoms. Therefore, although the functionalization degree (the moles of introduced fluorinated monomers are 8% of the DVB monomers of the resin) is similar to that of *Pd_1%/pDVB_C4F,* the hindrance created by the functionalization is higher.

The differences in activity is highlighted by the TOF values (*Table 31* and *Figure 81*).

Table 31: *TOF values (min^{-1}) for Pd/pDVBs and Pd/macro catalysts. (flow-rates: O_2 = 24 ml/min, H_2 = 1 ml/min; solvent = methanol; volume = 300 ml; T = 25 °C; catalyst: 100 mg, 1% w/w Pd)*

Catalyst	Slope of H_2 consumption (mmol/min)	mmol of palladium	TOF (min^{-1})
Pd_1%/macro	$2.81 \cdot 10^{-3}$	$9.98 \cdot 10^{-3}$	0.28
Pd_1%/pDVB	$1.27 \cdot 10^{-2}$	$9.92 \cdot 10^{-3}$	1.28
Pd_1%/pDVB_C4H	$6.84 \cdot 10^{-3}$	$9.87 \cdot 10^{-3}$	0.69
Pd_1%/pDVB_C4F	$2.29 \cdot 10^{-2}$	$1.02 \cdot 10^{-2}$	2.25
Pd_1%/pDVB_ATRP	$2.84 \cdot 10^{-3}$	$9.70 \cdot 10^{-3}$	0.29

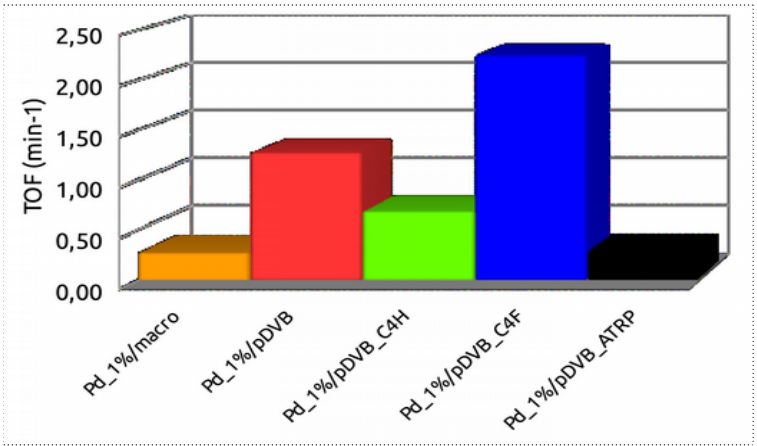

Figure 81: *TOF values (min^{-1}) for Pd/pDVBs and Pd/macro (flow-rates: O_2 = 24 ml/min, H_2 = 1 ml/min; solvent = methanol; volume = 300 ml; T = 25 °C, catalyst: 100 mg, 1% w/w Pd).*

For an heterogeneous metal catalyst the number of catalytic sites corresponds to the number of metal atoms on the surface of the nanoparticles. However, this value can be obtained only experimentally (by, for example, reaction of active sites with CO, that requires gas-solid conditions and cannot be employed for resin based catalysts) and usually any metal atom of the catalyst is considered catalytically active. This approximation leads to an underestimation of the effective catalytic activity, but it is generally considered acceptable for sake of comparison. TOF values were calculated from the slopes of the consumption curves (*Figure 80*). In the case of *Pd_1%/pDVB_C4F* TOF the value is referred to the time range (120-250 minutes) where the cumulative consumption of hydrogen shows a linear dependence with the time and the slope is at its relative maximum.
The productivity and the selectivity of Pd/pDVBs and Pd/macro catalysts are reported in Figures 82 and 83, respectively.

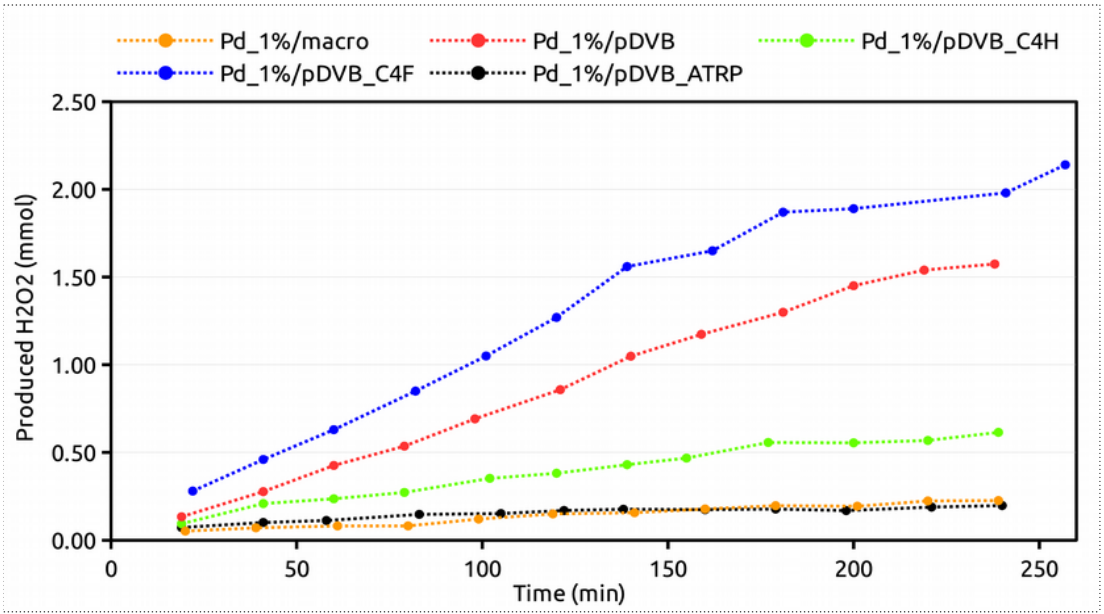

Figure 82: *cumulative production of hydrogen peroxide for metal catalysts supported on pDVB and macroreticular resins. (flow-rates: O_2 = 24 ml/min, H_2 = 1 ml/min; solvent = methanol; volume = 300 ml; T = 25 °C, catalyst: 100 mg, 1% w/w Pd)*

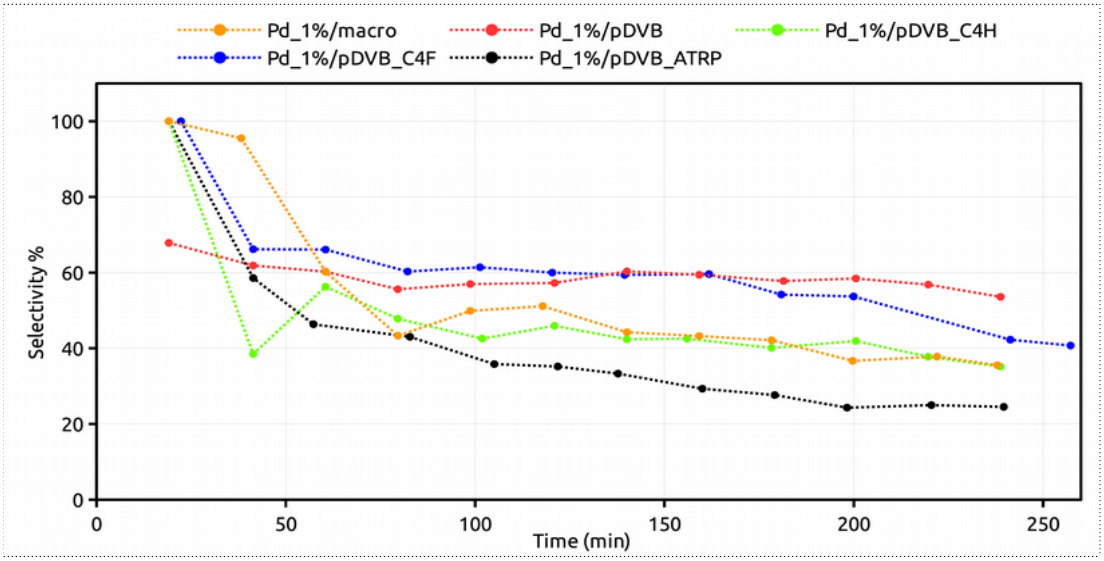

Figure 83: *selectivity toward hydrogen peroxide for metal catalysts supported on pDVB and macroreticular resins. (flow-rates: O_2 = 24 ml/min, H_2 = 1 ml/min; solvent = methanol; volume = 300 ml; T = 25 °C, Pd content = 1% wt; 0.100 g of catalyst)*

The selectivity towards H_2O_2 of *Pd_1%/macro* and *Pd_1%/pDVB_ATRP* is comparable to that of *Pd_1%pDVB*, but their activity is so low that the productivity is practically negligible. The trend in productivity of poly-divinylbenzene based catalysts reflects the trend in activity (*Pd_1%/pDVB_C4F* > *Pd_1%/pDVB* > *Pd_1%/pDVB_C4H).* According to Figures 82-84, it appears that the low productivity of *Pd_1%/pDVB_C4H* is due not only to the low activity (*Figure 80*),

but also to the low selectivity (*Figure 83*). On the contrary, *Pd_1%/pDVB_C4F* shows the highest activity, but its selectivity is only comparable with that of *Pd_1%/pDVB*. The functionalization with fluorinated acylic chains (*Pd_1%/pDVB_C4F*), therefore, determines an improvement in activity respect to the unfunctionalized catalyst (*Pd_1%/pDVB*), but does not affect significantly the selectivity. This suggests that fluorinated moieties are effectively able to increase the concentration of gases close to the palladium nanoparticles. Probably, this affects to comparable extent the rates of the direct synthesis of hydrogen peroxide and of its hydrogenation and/or combustion of hydrogen.

Concluding (*Figure 84*), from this investigation pDVB appears a more effective catalytic support for palladium catalysts for the direct synthesis of H_2O_2 than the largely employed macroreticular resins.

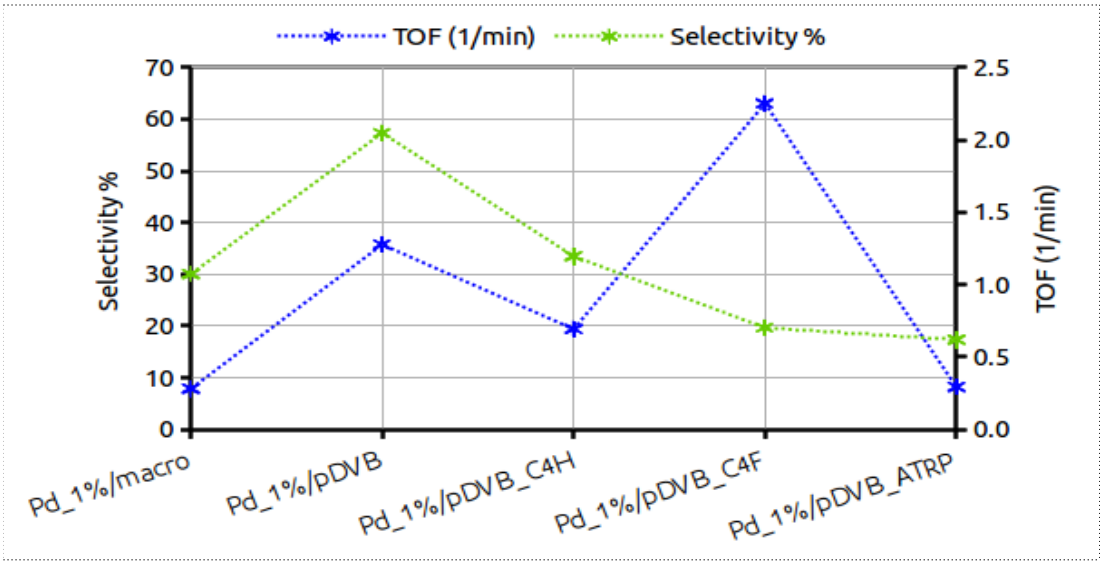

***Figure 84**: comparison between TOF and selectivity values from the ratio between the slopes of H_2O_2 production and H_2 consumption curves over 120-240 minutes (flow-rates: O_2 = 24 ml/min, H_2 = 1 ml/min; solvent = methanol; volume = 300 ml; T = 25 °C; catalyst: 100 mg, 1% w/w Pd)*

The functionalization of poly-divinylbenzene by acylation or by ATRP worsens the catalytic performance. In fact, in the case of *Pd_1%/pDVB_C4H* and *Pd_1%/pDVB_ATRP* the lower activity and selectivity respect to the unfunctionalized *Pd_1%/pDVB* are the result of the steric hindrance around palladium nanoparticles, which offset the potentially positive effect of the increased lipophilic character of their polymer matrix. Conversely, in the case of *Pd_1%/pDVB_C4F* catalyst, thanks to its smaller degree of functionalization respect to *Pd_1%/pDVB_C4H*, the accessibility of the metal phase is not

significantly reduced and the effect of the increased concentration of gases inside the catalyst leads to a higher activity. The performance of the catalyst is therefore improved and the productivity of Pd_1%/pDVB_CF4 is ca 25% higher than that of Pd_1%/pDVB.

5.9: Effect of ageing of the catalyst on the catalytic performance

The effect of the oxidation state of Palladium on the catalytic activity of the catalysts for the direct synthesis of H_2O_2 is widely debated in literature. Choudhary *et al.* [1] studied palladium catalysts based on inorganic oxides (Al_2O_3, ZrO_2, CeO_2, ThO_2, Y_2O_3 and Ga_2O_3) and claimed lower activity and selectivity for the pre-reduced materials, with respect unreduced ones. However, in their more recent works, [178] [179] they investigated the process of formation of H_2O_2 with Pd^0 catalysts, implicitly suggesting the better performance of the pre-reduced catalysts with respect the corresponding materials only containing Pd(II) species. Strukul *et al.* [141] investigated the catalytic performances of zirconia supported catalysts containing PdO. They observed a decreased selectivity when the catalyst is reduced during the catalytic test. On the contrary, Burch *et al.* [117] recommended a pre-reduction step when catalysts based on inorganic oxides are employed. Also Thompson *et al.* [180] stated that Palladium supported on phosphate viologen phosphonate catalysts must be pre-reduced if stored for a long time after the synthesis, to avoid the presence of PdO. Similarly, Pd^0 is considered the real active phase also by Lunsford e*t al.* [181] in their study using Pd/SiO_2 catalyst.

In our experience we observed that some catalysts became inactive (no consumption of hydrogen) if tested some weeks after their preparation and we ascribed this outcome to the surface oxidation of metal nanoparticles. To experimentally support this consideration, four catalytic tests were performed for the same batch of metal catalyst (*Pd_1%/macro*, *Pd_1%/pDVB_C4H* and *Pd_1%/pDVB_C4F*):

- a test the day after the synthesis of the catalyst (coded as *pristine*);
- a test two weeks after the synthesis, with the catalyst stored in a desiccator with $CaCl_2$ (coded as *aged*);

- a test three weeks after the synthesis , with the catalyst stored in dry-box under N_2 (coded as *nitrogen*);
- a test four weeks after the synthesis with a reducing treatment (5 bar of H_2, 60 °C, 5 hours) before the reaction (coded as *restored*).

The results obtained for the catalysts based on macroreticular resin (*Pd_1%/macro*) are reported in Figures 85 and 86.

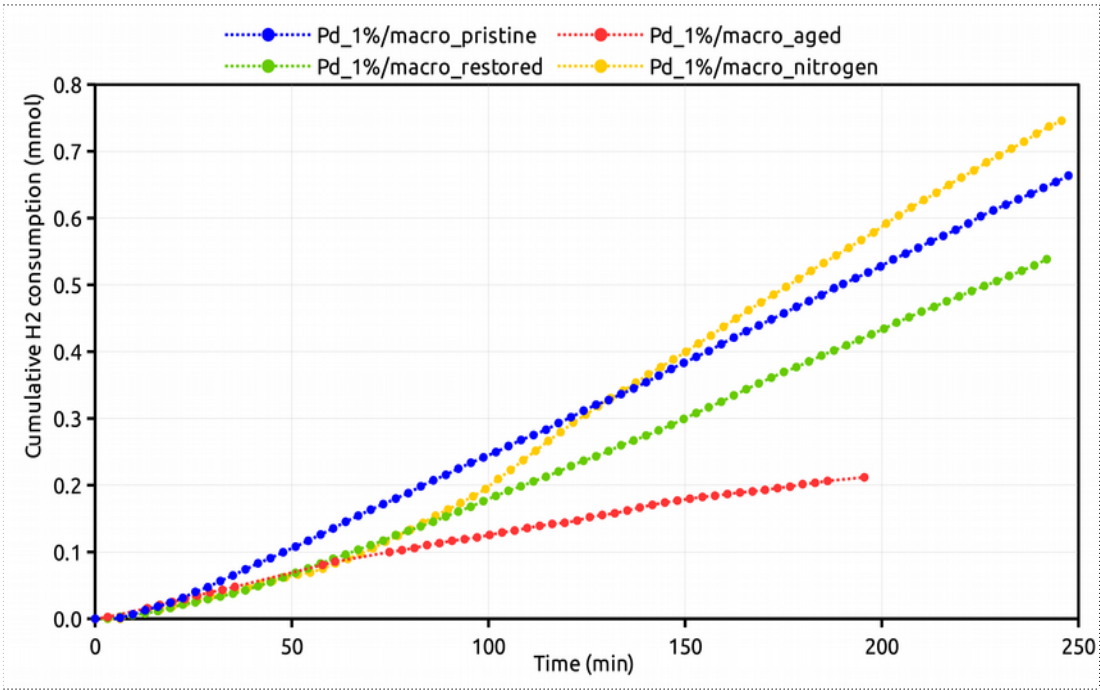

Figure 85: *Cumulative consumption of hydrogen for Pd_1%/macro as prepared, aged in air or nitrogen and restored by reduction. (flow-rates: O_2 = 24 ml/min, H_2 = 1 ml/min; solvent = methanol; volume = 300 ml; T = 25 °C; catalyst: 100 mg, 1% w/w Pd)*

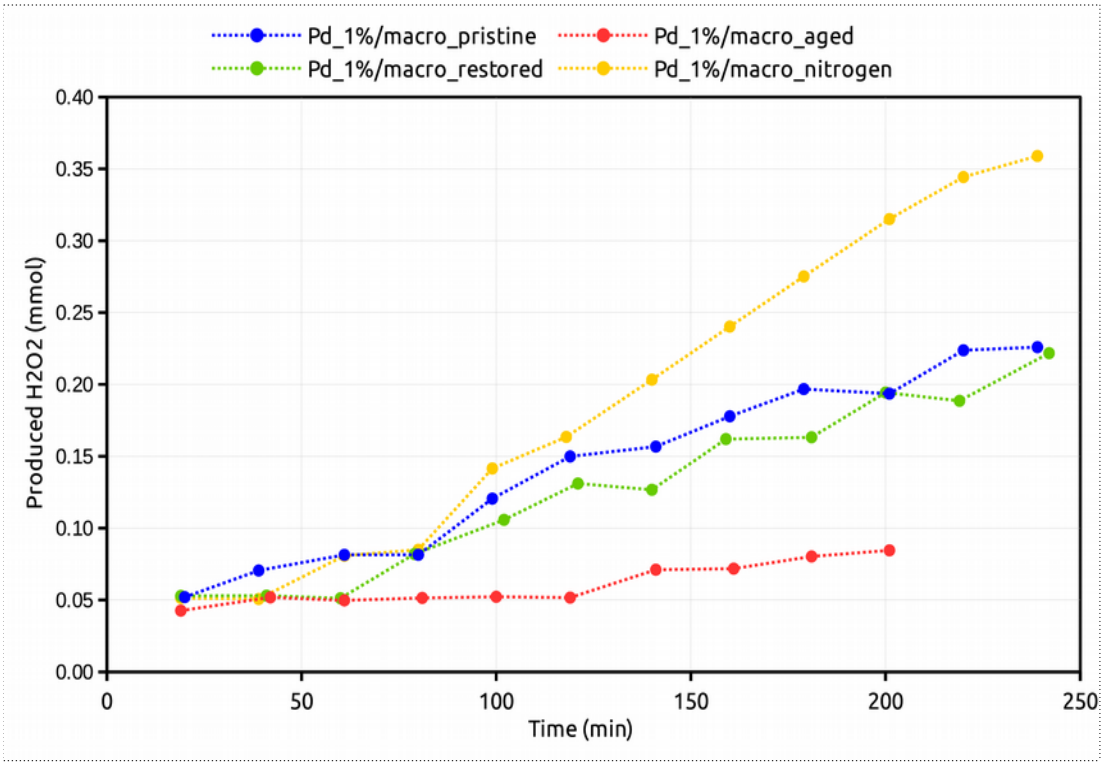

Figure 86: *Cumulative production of hydrogen peroxide for Pd_1%/macro as prepared, aged in air or nitrogen and restored by reduction. (flow-rates: O_2 = 24 ml/min, H_2 = 1 ml/min; solvent = methanol; volume = 300 ml; T = 25 °C; catalyst: 100 mg, 1% w/w Pd)*

The values of TOF, calculated after 120 minutes from the beginning of the reaction, and selectivity, calculated from the ratio between the slopes of the interpolation curves of consumption and production (after 120 minutes), are compared in Figure 87.

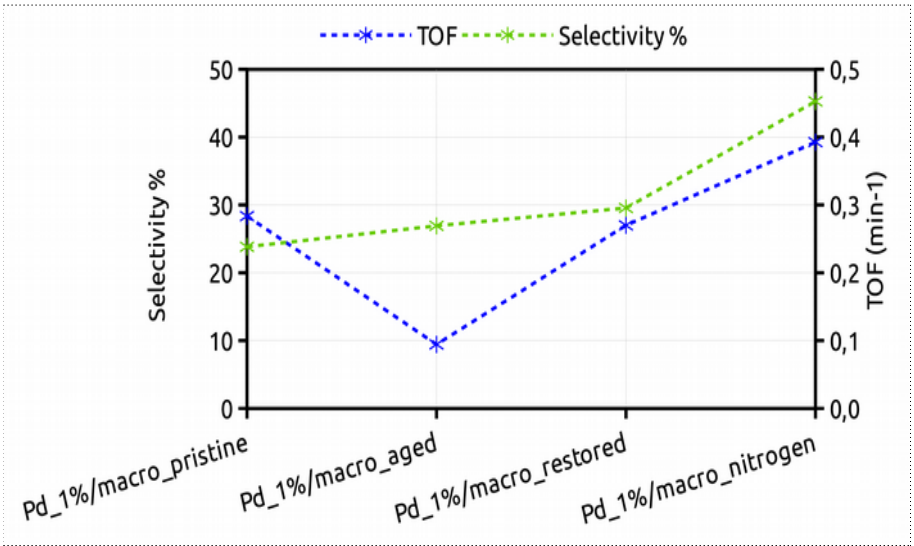

Figure 87: *comparison between TOF and selectivity values for Pd_1%/macro as prepared, aged in air or nitrogen and restored by reduction. (flow-rates: O_2 = 24 ml/min, H_2 = 1 ml/min; solvent = methanol; volume = 300 ml; T = 25 °C; catalyst: 100 mg, 1% w/w Pd)*

As expected, the aged catalyst (*Pd_1%/macro_aged*) shows a remarkable reduction of activity, according to TOF values (*Figure 87*). The increase of the selectivity is not particularly significant because the conversion is very low. After the reducing treatment, the catalyst (*Pd_1%/macro_restored*) recovers both its initial activity and selectivity. The catalyst stored in dry-box under N_2 atmosphere (*Pd_1%/macro_nitrogen*) has the relatively best performance. This behaviour was not expected and could be attributed to a some modification of the metal phase. Since in the dry state the gel-type portion of macroreticular resins is collapsed, the aggregation of nanoparticles is strongly hindered because of their limited mobility. Conversely, when the catalyst is restored with a reducing treatment, the swelling in THF (although limited for a sulfonated pS-DVB resin) enhances the mobility of the metal nanoparticles, making possible their aggregation.

The catalytic performance of the catalysts based on poly-divinylbenzene (*Pd_1%/pDVB_C4H* and *Pd_1%/pDVB_C4F*) are remarkably different from that ones of *Pd_1%/macro* and cannot be directly ascribed to the possible oxidation of the metal phase.

The catalyst based on acylated pDVB (*Pd_1%/pDVB_C4H*) shows an activity lower than the pristine catalyst, regardless of the type of storage (*Figure 88*).

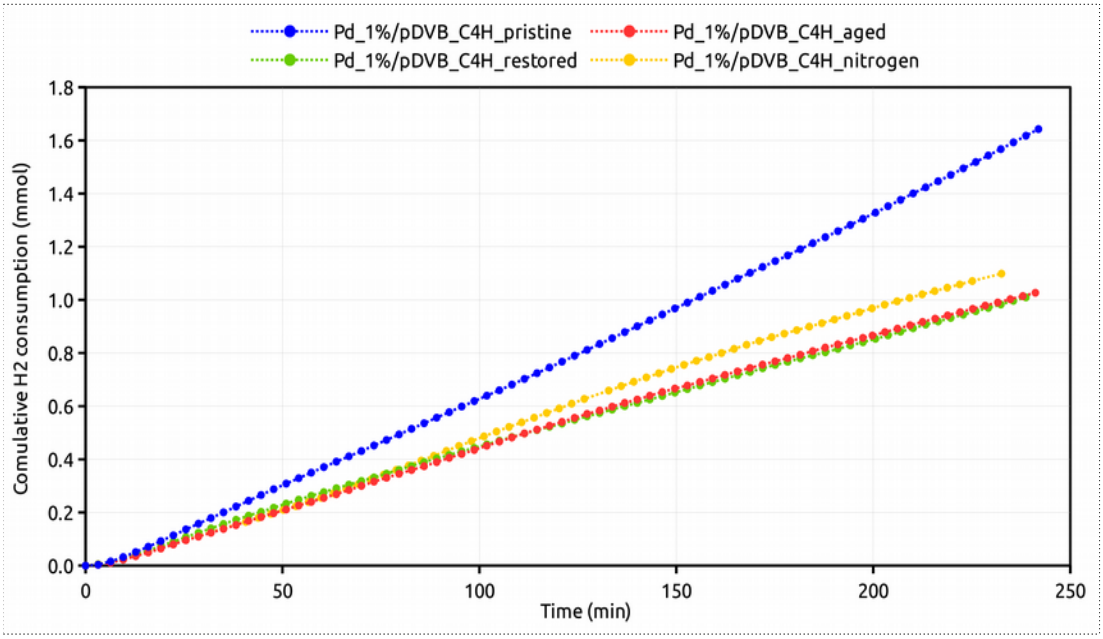

Figure 88: *Cumulative consumption of hydrogen for Pd_1%/pDVB_C4H as prepared, aged in air or nitrogen and restored by reduction. (flow-rates: O_2 = 24 ml/min, H_2 = 1 ml/min; solvent = methanol; volume = 300 ml; T = 25 °C; catalyst: 100 mg, 1% w/w Pd)*

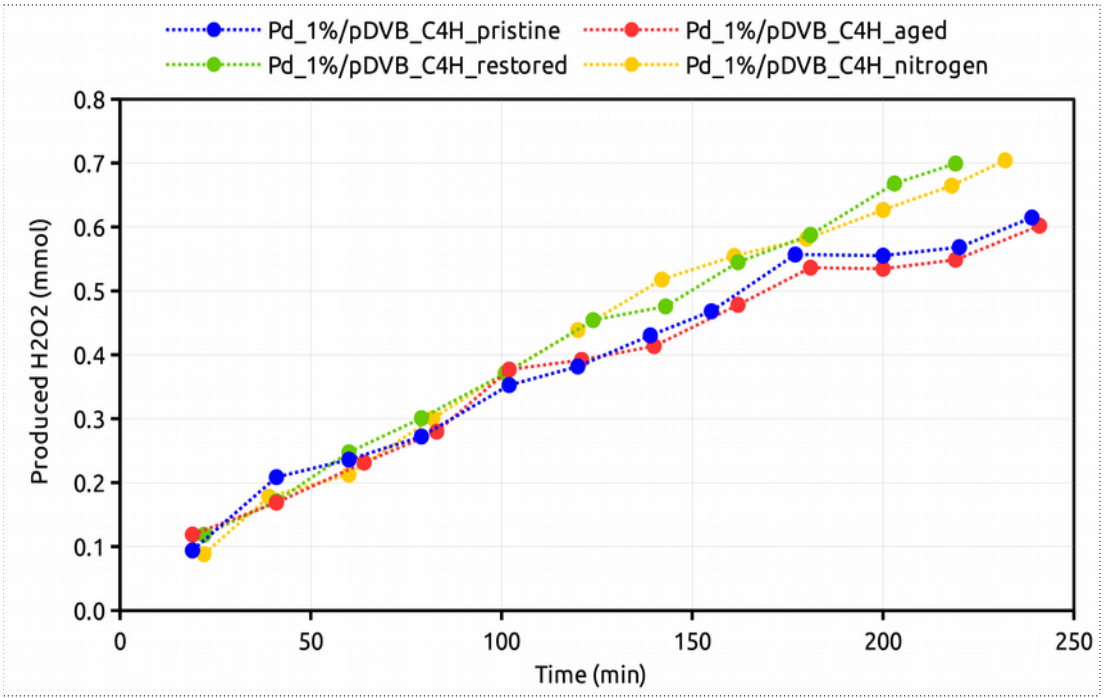

Figure 89: *cumulative production of hydrogen peroxide for Pd_1%/pDVB_C4H as prepared, aged in air or nitrogen and restored by reduction. (flow-rates: O_2 = 24 ml/min, H_2 = 1 ml/min; solvent = methanol; volume = 300 ml; T = 25 °C; catalyst: 100 mg, 1% w/w Pd)*

However, the productivity is similar (*Figure 89*), which implies that, in spite of lower TOF values, all the aged catalysts are more selective and in particular the restored catalyst (*Figure 90*).

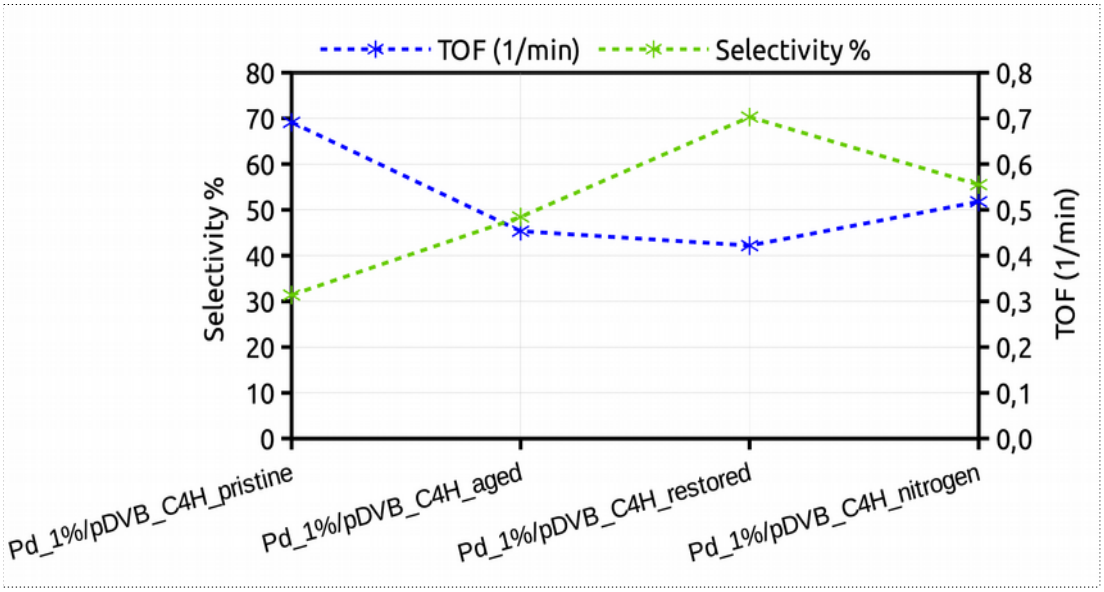

Figure 90: *comparison between TOF and selectivity values for Pd_1%/pDVB_C4H as prepared, aged in air or nitrogen and restored by reduction. (flow-rates: O_2 = 24 ml/min, H_2 = 1 ml/min; solvent = methanol; volume = 300 ml; T = 25 °C; catalyst: 100 mg, 1% w/w Pd)*

Interestingly, the values of TOF and selectivity for the aged catalyst and for the one stored under N_2 are comparable. Taking into the account that *Pd_1%/pDVB_CH4_nitrogen* was protected against oxidation, we can speculate that its ageing is mainly due to aggregation of metal nanoparticles, changing the structural features of the active metal phase. This tentative explanation is suggested by the morphology of the porous system of poly-divinylbenzene. In fact, the aggregation is expected to play a more important role in the permanent porous system of pDVB, than in the collapsed porous system of a dry macroreticular resin, where the mobility of metal nanoparticles is remarkably hindered. For *Pd_1%/pDVB_CH4_aged* oxidation (at least partial) of the metal phase is possible, but its performance close to that of *Pd_1%/pDVB_CH4*_nitrogen suggests that it underwent the same ageing process with no appreciable oxidation of the metal. Somehow, therefore, the acylic chains are able to prevent it, forming a sort of protective film at the surface of the permanent mesopores and around the metal nanoparticles.

Finally, in this case the reduction of the catalyst stored for four weeks under air has the most positive effect on the selectivity, but not on the activity.

The behaviour of the *Pd_1%/pDVB_C4F* family is pretty different (*Figures 91, 92 and 93*).

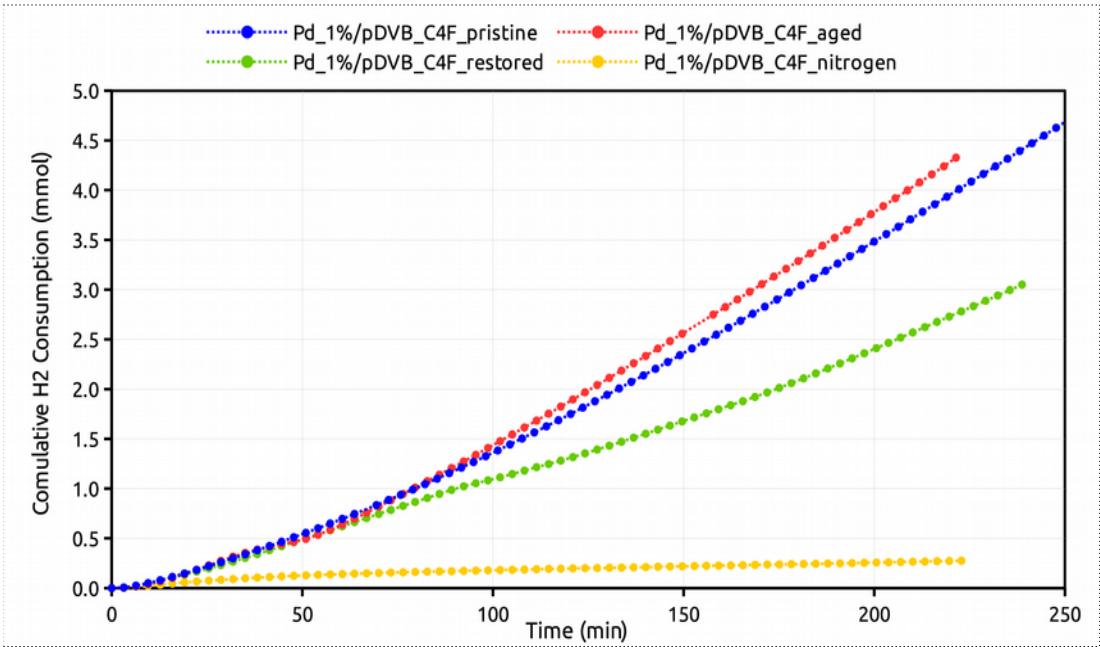

Figure 91: *cumulative consumption of hydrogen for Pd_1%/pDVB_C4F as prepared, aged in air or nitrogen and restored by reduction. (flow-rates: O_2 = 24 ml/min, H_2 = 1 ml/min; solvent = methanol; volume = 300 ml; T = 25 °C; catalyst: 100 mg, 1% w/w Pd)*

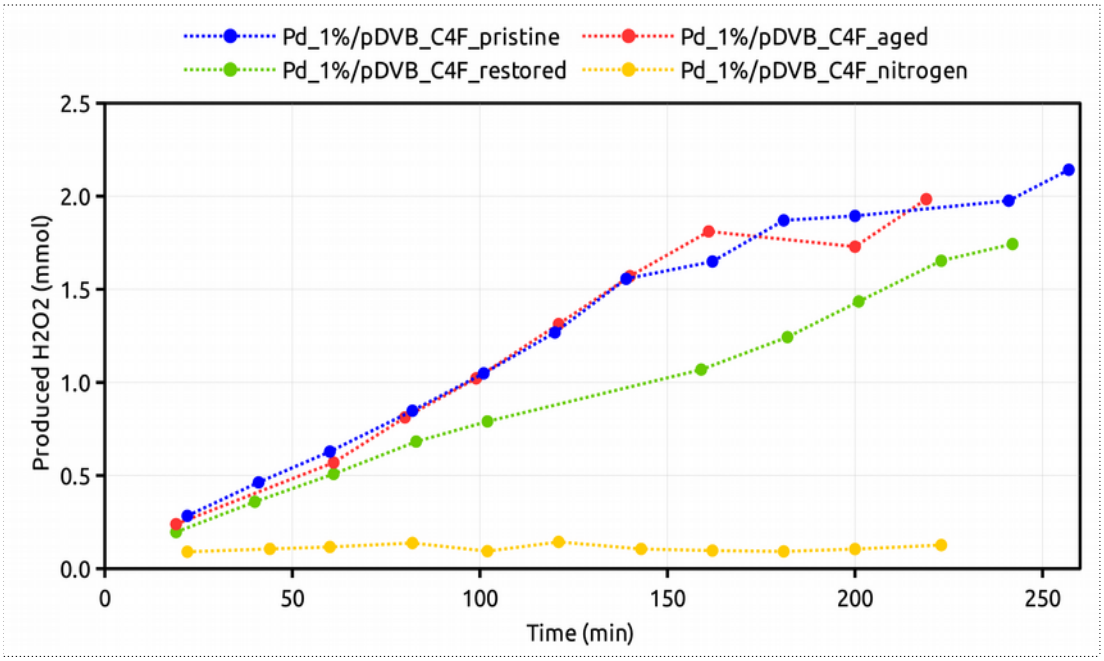

Figure 92: *cumulative production of hydrogen peroxide for Pd_1%/pDVB_C4F as prepared, aged in air or nitrogen and restored by reduction. (flow-rates: O_2 = 24 ml/min, H_2 = 1 ml/min; solvent = methanol; volume = 300 ml; T = 25 °C; catalyst: 100 mg, 1% w/w Pd)*

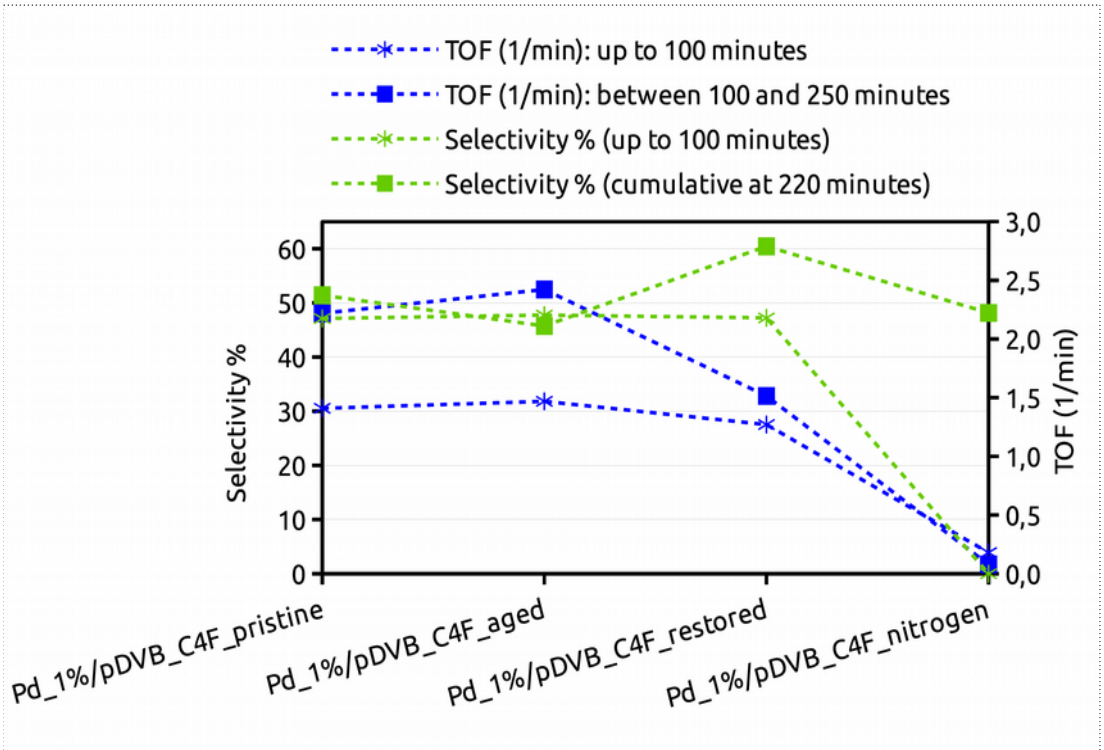

Figure 93: *comparison between TOF and selectivity values for Pd_1%/pDVB_C4F as prepared, aged in air or nitrogen and restored by reduction. (flow-rates: O_2 = 24 ml/min, H_2 = 1 ml/min; solvent = methanol; volume = 300 ml; T = 25 °C; catalyst: 100 mg, 1% w/w Pd)*

Whereas neither the consumption rate of H_2 or the production of H_2O_2 substantially change upon the ageing under air in the desiccator, the catalyst

stored under inert atmosphere is almost completely inactive. Only the reduction of the catalyst after four weeks under air leads to similar result as illustrated above.

This preliminary investigation shows that the storage of catalysts based on functional resins has a remarkable influence on their catalytic activity and selectivity. Therefore, this issue must be carefully taken into account to evaluate the reproducibility of the performances of the catalysts and to compare the catalytic results obtained with different catalysts. It is therefore unfortunate that, as far as we know, this issue has not yet been paid proper attention in the pertinent literature.

5.10: 3.5 %wt Palladium Catalysts

Two metal catalysts with a content of Palladium of 3.5 %wt, based on sulfonated pDVB and on fluorinated pDVB respectively, were tested in the direct synthesis of hydrogen peroxide in order to study the effect of the increased metal content on the catalytic performance. In addition, particular attention was paid to the effect of ageing, by following the same approach described in Paragraph 5.9. The features of the investigated catalysts are summarized in Table 32.

Table 32: *3.5 %wt Pd/pDVB catalysts included in the investigation of ageing*

Catalyst	Description of the support	Proton exchange capacity (mmol H^+/g)	% of acylated rings
Pd_3.5%/pDVB	Sulfonated pDVB	3.2	//
Pd_3.5%/pDVB_C4F	Sulfonated pDVB, acylated with C_4F_7OCl	3.0	11 %

As for metal catalysts based on pDVB with a Palladium content of 1 %wt (*Paragraph 5.8*), the trend of catalytic behaviour of the materials is complex (*Figure 94*).

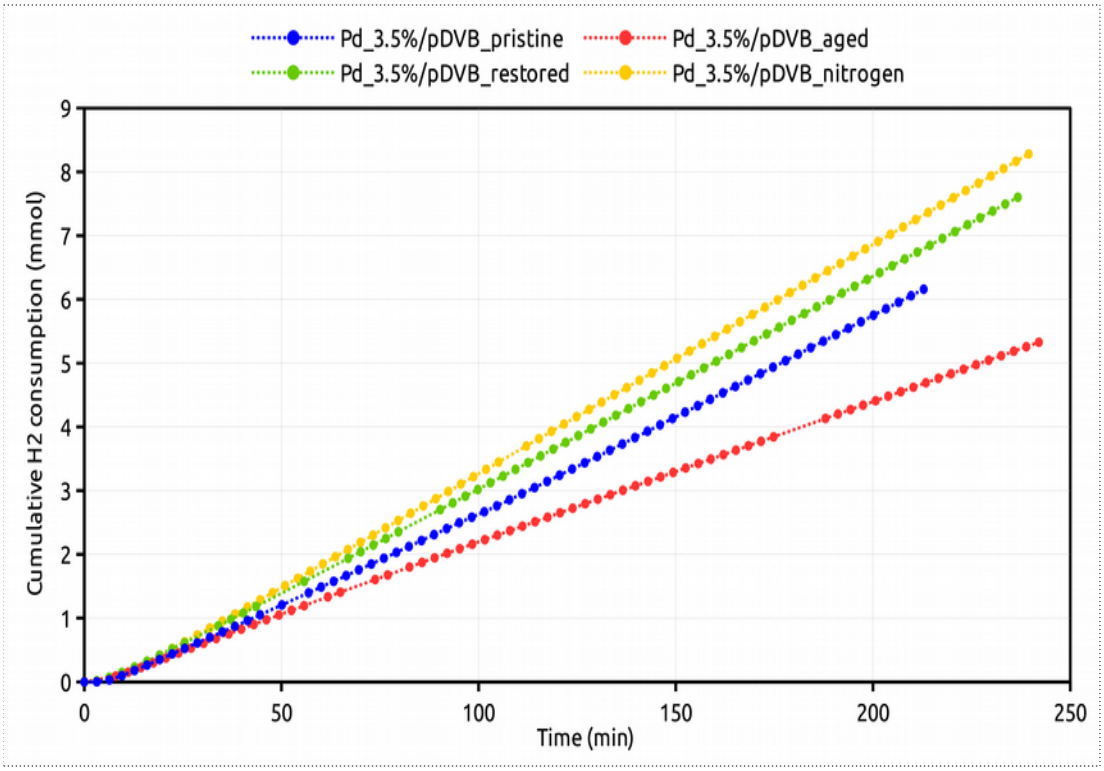

Figure 94 *cumulative consumption of hydrogen for Pd_3.5%/pDVB as prepared, aged in air, aged under nitrogen and restored by reduction. (flow-rates: O_2 = 24 ml/min, H_2 = 1 ml/min; solvent = methanol; volume = 300 ml; T = 25 °C; catalyst: 100 mg, 1% w/w Pd)*

The acylated catalyst stored in the desiccator (*Pd_3.5%/pDVB_C4F_aged*) shows a much lower activity than the pristine catalyst (*Pd_3.5%/pDVB_C4F_pristine*), but it is much more productive because ageing made it much more selective (*Figures 95 and 96*). *Pd_3.5%/pDVB_C4F_aged* is also more selective than *Pd_3.5%/pDVB_C4F_nitrogen* and *Pd_3.5%/pDVB_C4F_restored*, which perform very similarly to *Pd_3.5%/pDVB_C4F_pristine*. This indicates that for the 3.5% wt Pd catalysts, therefore, aggregation phenomena either do not take place or produce negligible effects and the effects of the oxidation of the metal, if any occurs, can be reverted by simply reducing the catalyst again prior the reaction. However, the behaviour of *Pd_3.5%/pDVB_C4F_aged* suggests that some oxidation of Pd could be beneficial, because the formation of some PdO is still possible when the catalyst is stored in the desiccator. Whether it actually takes place or not hence can have a positive effect or not on the selectivity must be confirmed with further investigation.

In any case the different behaviour of the 3.5% wt catalysts with the 1% wt ones shows that ageing has different effects depending on the metal content. This is not surprising because oxidation and aggregation of the nanoparticles can be

expected to occur to different extents when the nanoparticles have different sizes and shapes which can be expected to depend in their turn on the metal content.

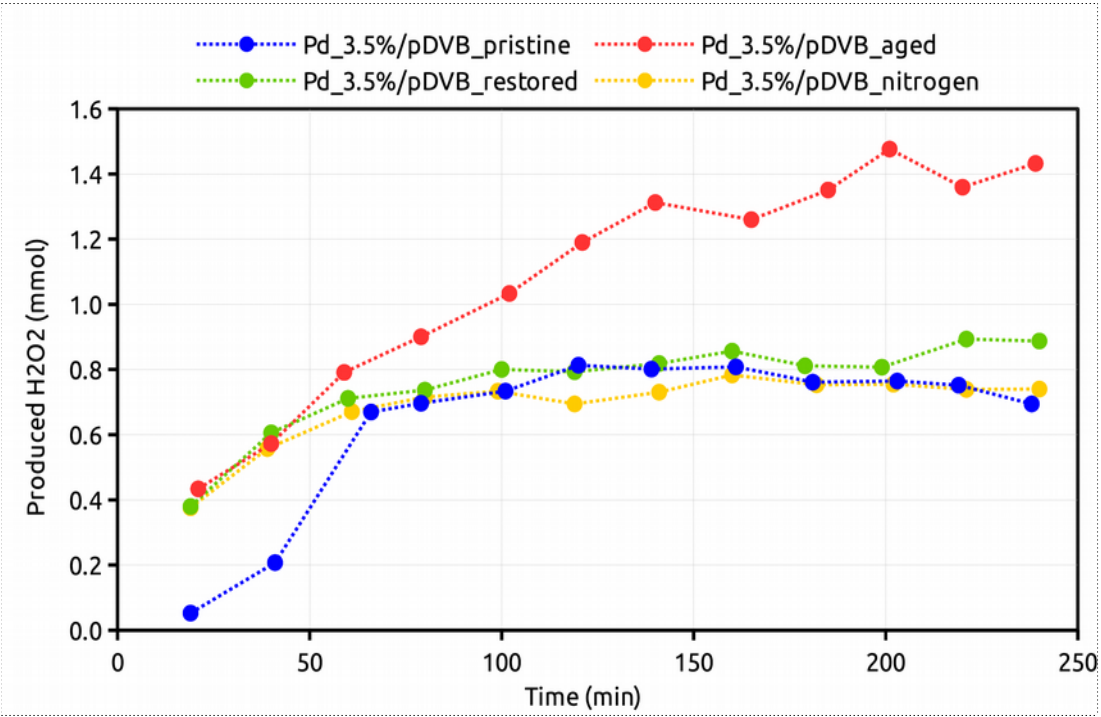

Figure 95: *cumulative production of hydrogen peroxide for Pd_3.5%/pDVB as prepared, aged in air, ged under nitrogen and restored by reduction. (flow-rates: O_2 = 24 ml/min, H_2 = 1 ml/min; solvent = methanol; volume = 300 ml; T = 25 °C; catalyst: 100 mg, 1% w/w Pd)*

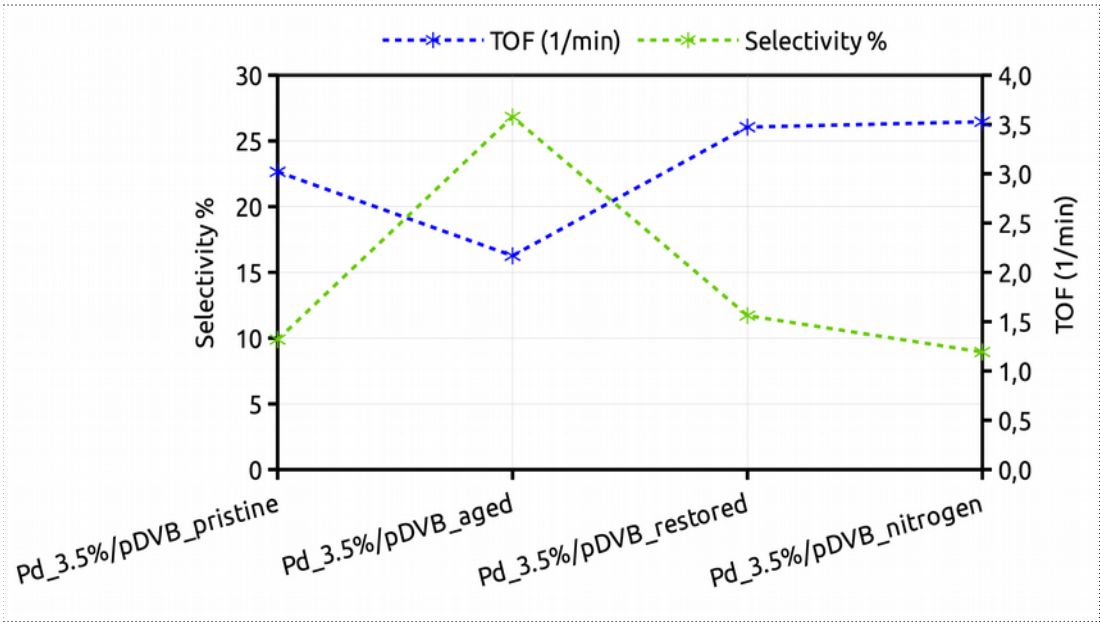

Figure 96: *comparison between TOF and selectivity values for Pd_3.5%/pDVB_C4F as prepared, aged in air, aged under nitrogen and restored by reduction. (flow-rates: O_2 = 24 ml/min, H_2 = 1 ml/min; solvent = methanol; volume = 300 ml; T = 25 °C; catalyst: 100 mg, 1% w/w Pd)*

For the P*d_3.5%/pDVB_C4F* family, the situation is similar: *Pd_3.5%/pDVB_C4F_pristine, Pd_3.5%/pDVB_C4F_nitrogen and Pd_3.5%/pDVB_C4F_restored* have comparable performance, whereas *Pd_3.5%/pDVB_C4F_aged* is less active, but more selective (*Figures 97, 98 and 99*).

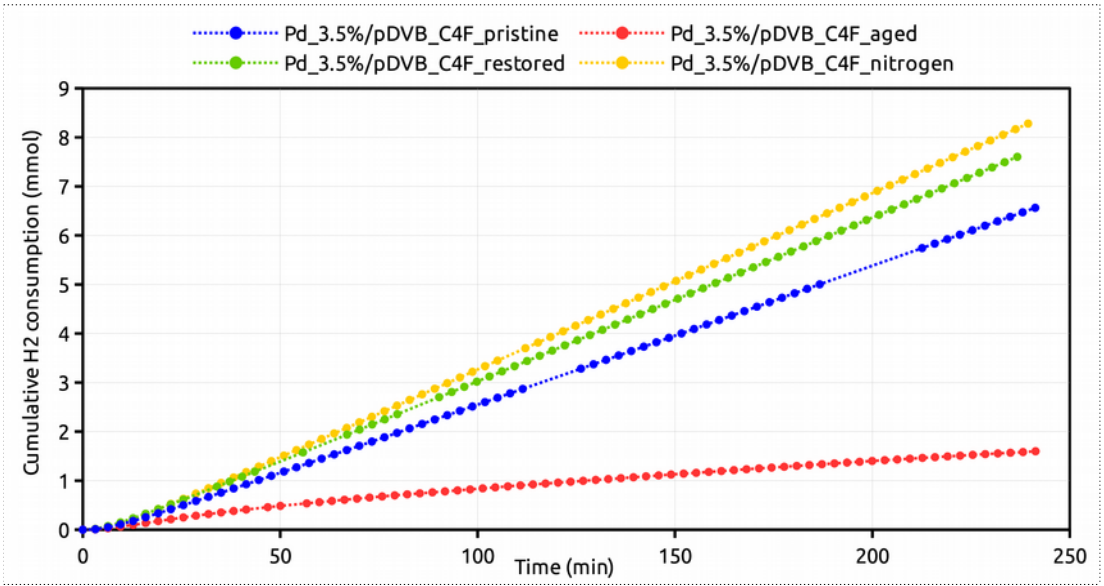

Figure 97 *cumulative consumption of hydrogen for Pd_3.5%/pDVB_C4F as prepared, aged in air or nitrogen and restored by reduction. (flow-rates: O_2 = 24 ml/min, H_2 = 1 ml/min; solvent = methanol; volume = 300 ml; T = 25 °C; catalyst: 100 mg, 1% w/w Pd)*

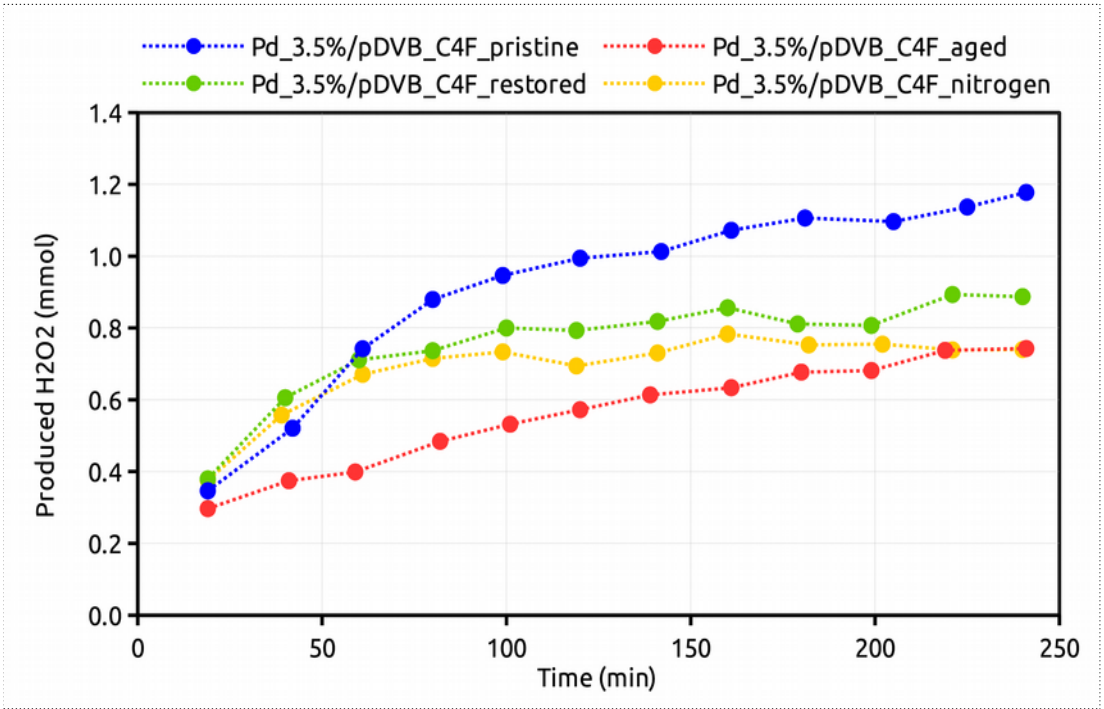

Figure 98: *cumulative production of hydrogen peroxide for Pd_3.5%/pDVB_C4F as prepared, aged in air or nitrogen and restored by reduction. (flow-rates: O_2 = 24 ml/min, H_2 = 1 ml/min; solvent = methanol; volume = 300 ml; T = 25 °C; catalyst = Pd/C, 100 mg, 1% w/w Pd)*

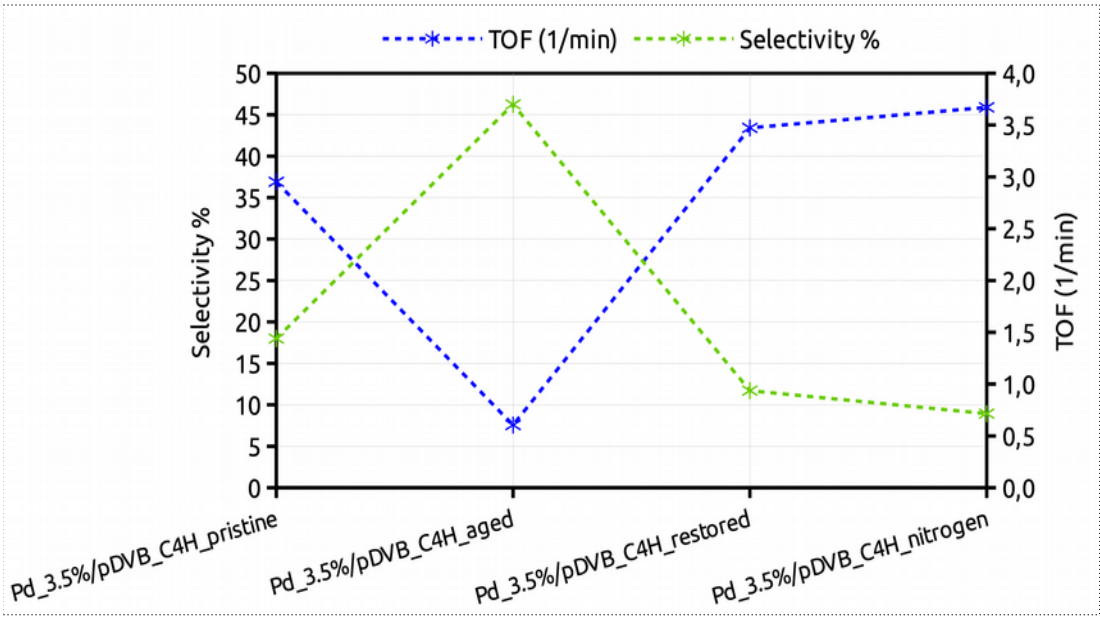

Figure 99: *comparison between TOF and selectivity values for Pd_1%/pDVB_C4F as prepared, aged in air or nitrogen and restored by reduction. (flow-rates: O_2 = 24 ml/min, H_2 = 1 ml/min; solvent = methanol; volume = 300 ml; T = 25 °C; catalyst = Pd/C, 100 mg, 1% w/w Pd)*

However in this case the most productive catalyst is *Pd_3.5%/pDVB_C4F_pristine*. This suggests that it is slightly more sensible to ageing in comparison with *Pd_3.5%/pDVB_pristine*. In particular it could be affected to a larger extent by oxidation possibly because of the affinity of O_2 for the fluorinated phases and the higher content of palladium. In fact, in this case *Pd_3.5%/pDVB_C4F_aged* (where the presence of PdO, if any, should be the relatively highest) is the least productive catalyst, because it undergoes a large decrease of activity which is not compensated by the increase in the selectivity. In any case, it is again confirmed that these 3.5% wt catalysts are affected by ageing in a much different way in comparison with the corresponding 1% wt materials.

5.11: Bromide Ions as selectivity enhancers: the case of Palladium on Carbon

Bromide ions are known to be selectivity enhancers in the direct synthesis of hydrogen peroxide (*Paragraph 5.3*). To evaluate the effect of bromides under the experimental conditions employed in this investigation, a number of catalytic tests were carried out at different concentrations of the enhancer.

A first screening was made with a commercially available 1% wt Palladium catalyst supported on carbon and with hydrobromic acid as the bromide source (*Table 33*).

Table 33: *concentration of HBr in the reactor and molar ratio between palladium and bromide ions for each test. (flow-rates: O_2 = 24 ml/min, H_2 = 1 ml/min; solvent = methanol; volume = 300 ml; T = 25 °C; catalyst = Pd/C, 100 mg, 1% w/w Pd)*

Concentration HBr (mol/L)	Concentration HBr (ppm)	Moles Pd/moles Br	Catalytic Test
$1.21 \cdot 10^{-4}$	12.36	0.26	Pd/C_12ppm
$3.02 \cdot 10^{-5}$	3.09	1.04	Pd/C_3ppm
$6.76 \cdot 10^{-6}$	0.69	4.63	Pd/C_0.7ppm
$1.21 \cdot 10^{-6}$	0.12	25.89	Pd/C_0.12ppm
$9.05 \cdot 10^{-7}$	0.09	34.61	Pd/C_0.09ppm
$6.03 \cdot 10^{-7}$	0.06	51.94	Pd/C_0.06ppm
$3.01 \cdot 10^{-7}$	0.03	104.06	Pd/C_0.03ppm

The H_2 consumption of the catalyst over the time is reported in Figure 100.

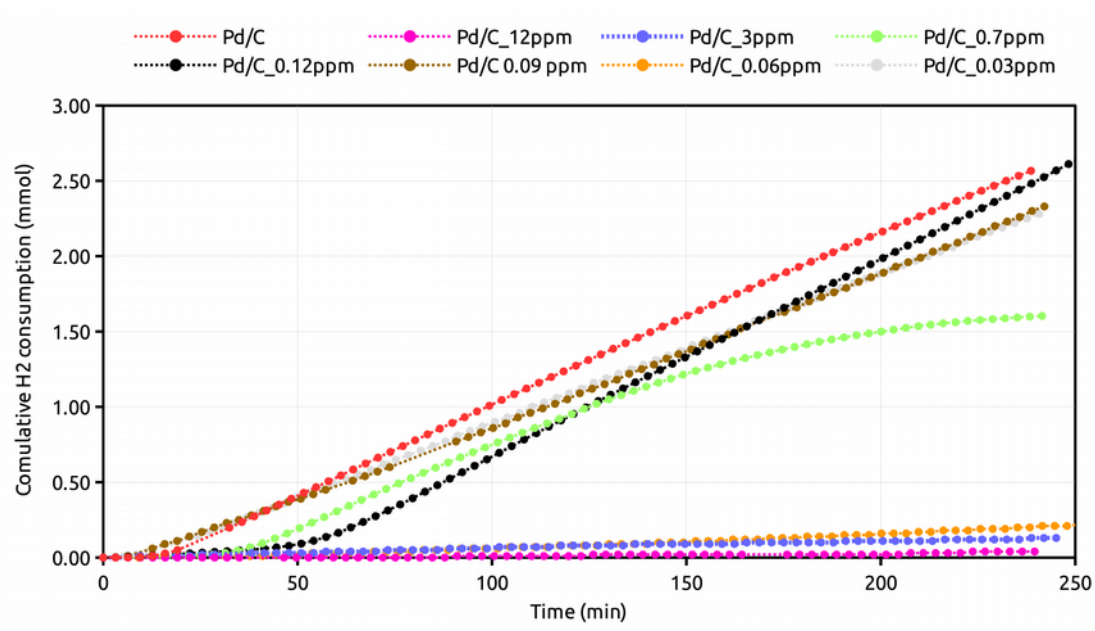

Figure 100: *Cumulative consumption of hydrogen for Pd/C in the presence of different amounts of hydrobromic acid in the reaction mixture. (flow-rates: O_2 = 24 ml/min, H_2 = 1 ml/min; solvent = methanol; volume = 300 ml; T = 25 °C; catalyst = Pd/C, 100 mg, 1% w/w Pd)*

With 12, 0.06 and 3 ppm of HBr the activity of the catalyst is almost completely suppressed, especially at the highest HBr concentration (12 ppm). At 0.7 ppm the catalysts is apparently deactivated about 120 minutes, while at 0.12, 0.09 and 0.03

ppm the catalyst shows an induction time followed by a linear increase of the amount of consumed H_2.

All the curves represented in Figure 100 show a linear portion between about 60 and 120 minutes, with the highest slope relative to each experiment. This indicates that the apparent reaction rate is at its relative maximum value and is constant. Its ratio to the molar amount of palladium employed in each test represents the TOF observed in the relevant experiment (*Table 34* and *Figure 101*).

Table 34: *TOF values (min^{-1}) In presence of different concentrations of HBr. (flow-rates: O_2 = 24 ml/min, H_2 = 1 ml/min; solvent = methanol; volume = 300 ml; T = 25 °C; catalyst = Pd/C ,100 mg, 1% w/w Pd)*

HBr concentration (ppm)	slope (mmol/min)	TOF (min^{-1})
0	$1.20 \cdot 10^{-2}$	1.3
0.03	$9.96 \cdot 10^{-3}$	1.1
0.07	$8.55 \cdot 10^{-4}$	$9.1 \cdot 10^{-2}$
0.09	$9.81 \cdot 10^{-3}$	1.0
0.12	$1.32 \cdot 10^{-2}$	1.4
0.60	$1.07 \cdot 10^{-2}$	1.1
3.00	$6.85 \cdot 10^{-4}$	$7.3 \cdot 10^{-2}$
12.00	$2.36 \cdot 10^{-4}$	$2.5 \cdot 10^{-2}$

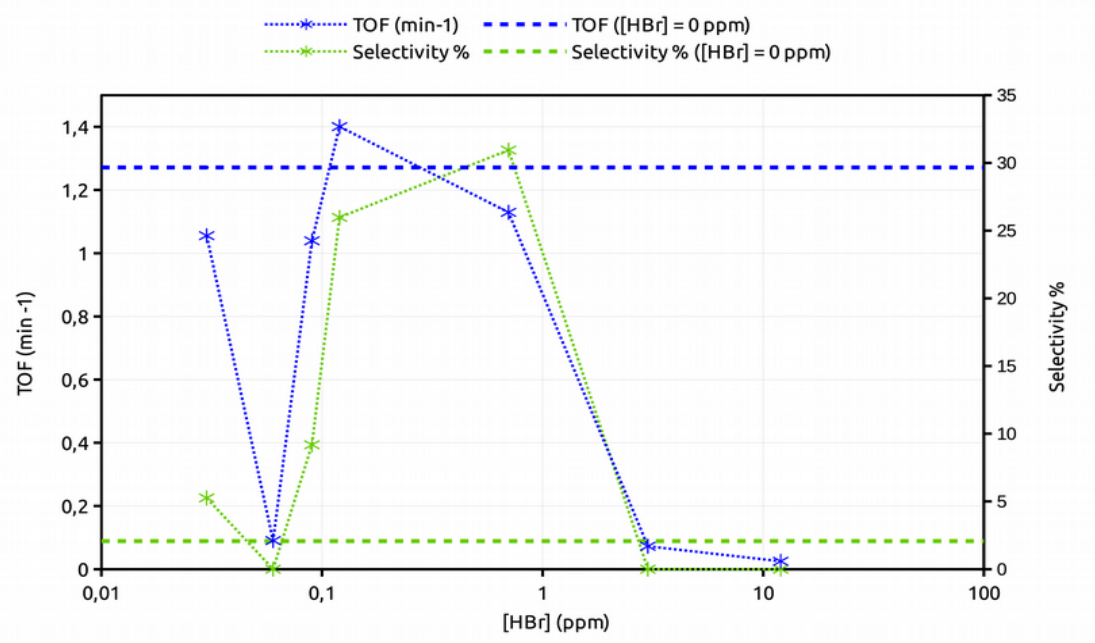

Figure 101: *TOF (min^{-1}) for catalytic tests with different concentration of bromide ions. TOF values are calculated between 60 and 120 minutes. (flow-rates: O_2 = 24 ml/min, H_2 = 1 ml/min; solvent = methanol; volume = 300 ml; T = 25 °C; catalyst = Pd/C, 100 mg, 1% w/w Pd)*

Figures 102 and 103 represent the amount of produced H_2O_2 and the selectivity towards hydrogen peroxide as functions of time.

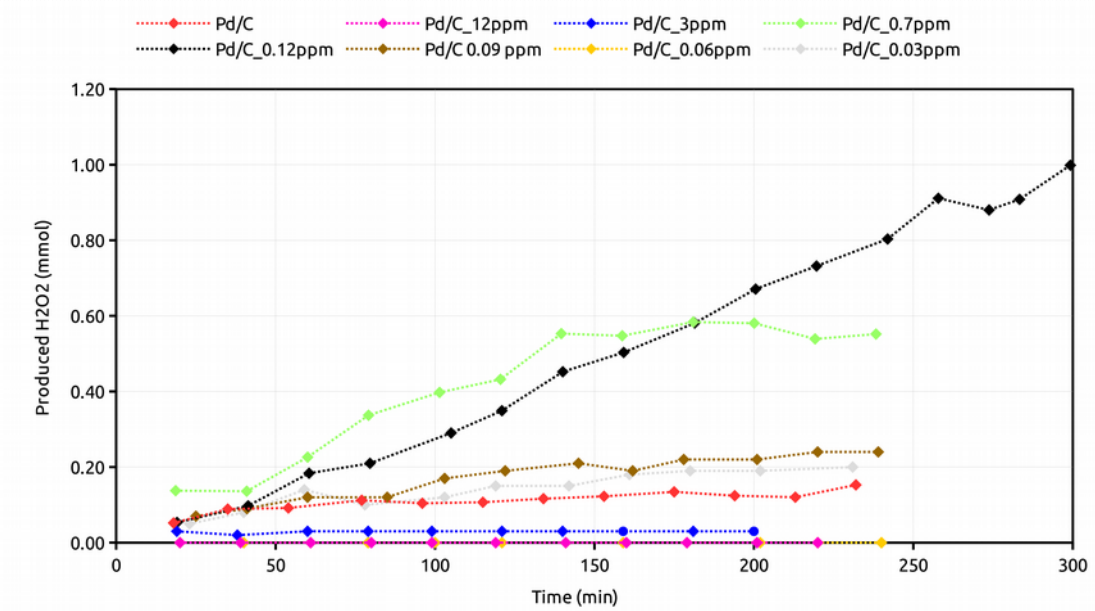

Figure 102: *Production of hydrogen peroxide with a Pd/C catalyst in the presence of different amounts of hydrobromic acid. (flow-rates: O_2 = 24 ml/min, H_2 = 1 ml/min; solvent = methanol; volume = 300 ml; T = 25 °C; catalyst = Pd/C, 100 mg, 1% w/w Pd)*

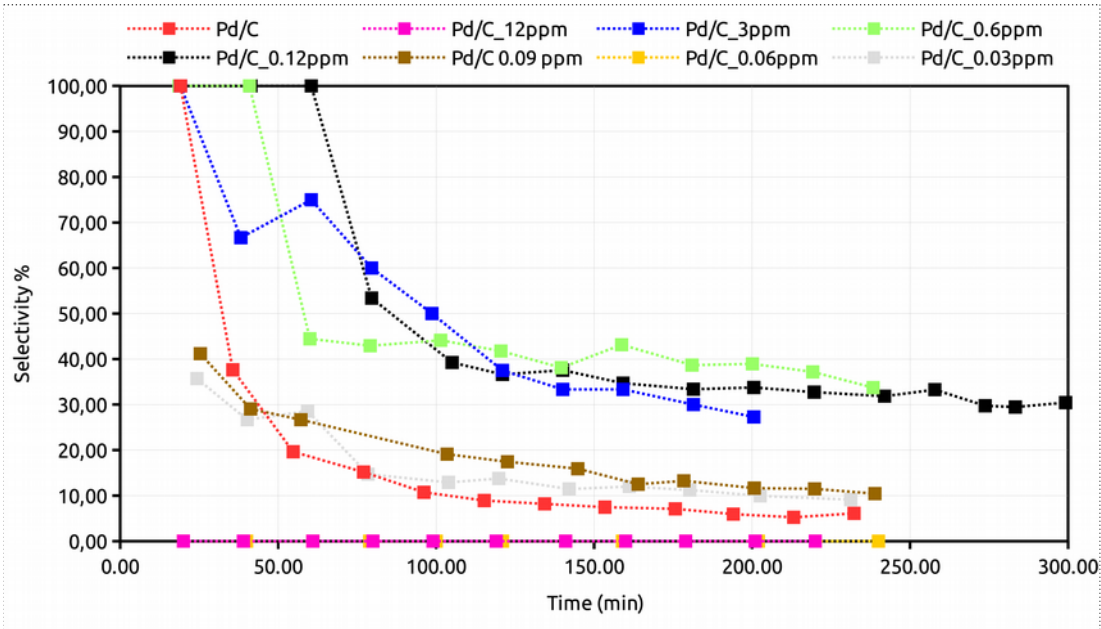

Figure 103: *Selectivity towards hydrogen peroxide for a Pd/C catalyst in the presence of different amounts of hydrobromic acid. (flow-rates: O_2 = 24 ml/min, H_2 = 1 ml/min; solvent = methanol; volume = 300 ml; T = 25 °C; catalyst = Pd/C, 100 mg, 1% w/w Pd)*

The cross-comparison of the TOF values and those of selectivity (*Figure 101*) clearly shows that there exist an optimal range of Br^- concentration. Only with

0.12 and 0.6 ppm of HBr the combination of high activity and selectivity is achieved. Outside this range either the activity or the selectivity (or both) are relatively low. In particular, if the concentration of the enhancer is too high, the catalyst is strongly (3.0 ppm) or even completely (12.0 ppm) deactivated. If it is too low (0.03, 0.06, 0.09 ppm) the catalyst is almost as active as without the enhancer, but the effect on the selectivity, if any, is hardly appreciable.

In summary, the best catalytic performance is obtained with a bromide concentration of 0.12 ppm: after 300 minutes the hydrogen consumption is still increasing (*Figure 100*), with a still linearly increasing hydrogen peroxide amount (*Figure 102*) and a constant selectivity (*Figure 103)*. As a final comment, it should be appreciated that 0.12 ppm is one order of magnitude smaller with respect to the concentration of Br^- usually recommended as optimal (and the most often employed) in the literature. Our results suggest that the behaviour of the enhancer must depend on the features of the catalysts, although we do not know yet how, and that the "one-fits-all" optimal concentration does not exist.

Interestingly, the catalyst is poisoned when the concentration of HBr is increased, but kept *below* the optimal range. On the one hand, this would be pretty obvious if it is assumed, as usual, that Br^- block the most active sites, which are responsible for the dissociative adsorption of O_2 which eventually leads to its complete reduction to water. On the other hand, this explanation cannot account the restoration of activity which we observed for the optimal values of HBr concentration. Therefore our data indicate that the role of Br^- cannot be as simple as generally described in the literature. The formation of selective *and* active sites suggests that they are much different from those present in the unpromoted catalyst. This calls for the reconstruction of the metal surface, possibly associated to a dynamic leaching process promoted by Br^- ions.

In a previous investigation[182] we observed the leaching of palladium oxide (PdO) from the surface of palladium nanoparticles supported on the macroreticular resin Lewatit K2621, which is likely associated to the formation of bromo-complexes of palladium(II) in the liquid phase. Although the experimental set-up and the support were different, the reaction conditions (temperature, pressure and gas ratios) were similar to those employed in this work, hence it can be assumed that leaching affects the Pd/C in a similar way. Accordingly[182], Pd leaching should occur at least at the highest concentrations of bromides, corresponding to the lowest Pd/Br ratio.

The content of Palladium in the reaction mixtures at the and of the tests with 12, 0.7 and 0.12 ppm of bromides was determined by ICP-OES analysis (*Table 35*).

Table 35: *results of ICP-OES analysis and percentage of Palladium, respect to that introduced with the catalyst, remaining in methanol after the test.*

[HBr] (ppm)	Initial m_{Pd} (mg)	m_{Pd} (mg) in the reaction mixture	% leaching
0.12	1.03	0.005	0.5
0.7	1.05	0.012	1.1
12	1.01	0.025	2.5

The fraction of Pd in solution at the end of the reaction is small and, as expected, it increases with HBr concentration. Table 35 also shows that, at concentrations of Br^- higher than the optimal, a more extensive leaching is associated to lower TOF values. If we assume that a higher leaching degree produces a more extensive surface reconstruction, this result suggests that a too extensive reconstruction could be detrimental. As leaching first involves the removal of PdO from the metal phase [23], this could imply that its amount must not be lower than some critical level in order to have a selective and active catalyst. As an alternative or in addition, it could be also possible that a very high concentration of Br^- extensively poisons the catalyst, because its amount is enough to block every kind of active site.

Concluding, from this preliminary study it appears that the choice of the concentration of bromides is not trivial to achieve an effective promotion of the catalyst.

5.12: Bromide Ions as selectivity enhancers: the case of Palladium on pDVB

The effect of HBr as enhancer has been tested also with the most interesting catalyst emerging in this Thesis, *Pd_1%/pDVB* (*Paragraph 5.8*). For this purpose we started from the two concentrations of bromide ions leading to the highest activity and selectivity towards H_2O_2 (0.7 and 0.12 ppm). To minimize possible experimental errors, the same batch of polymer support was used for the synthesis of the metal catalysts included in the investigation.

The consumption of hydrogen of *Pd_1%/pDVB* during the catalytic test, in the presence of different concentration of hydrobromic acid, is reported in Figure 104.

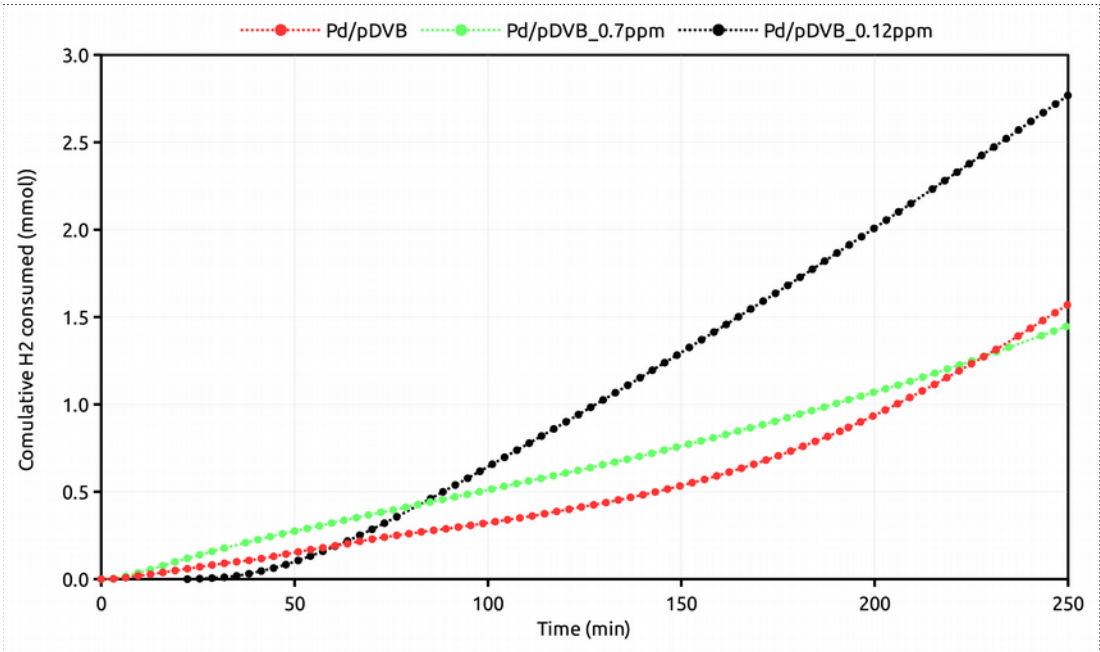

Figure 104: *Cumulative consumption of hydrogen in the presence of different concentrations of hydrobromic acid in the reaction mixture. (flow-rates: O_2 = 24 ml/min, H_2 = 1 ml/min; solvent = methanol; volume = 300 ml; T = 25 °C; catalyst = Pd/pDVB, 100 mg, 1% w/w Pd)*

Similarly to Pd/C, in the presence of 0.12 ppm of bromide ions the catalyst shows a quite long induction (ca 50 min). On the contrary, with a concentration of 0.7 ppm of HBr, the catalyst does not show any induction time just like the catalyst with no enhancer added. In both these cases the activity starts to increase after some time (ca 150 min with no HBr and ca 200 with 0.7 ppm). At 0.7 ppm the presence of Br^- ions delays the achievement of the maximum reaction rate and leads to a less active catalytic system, although a plateau in the amount of consumed H_2 is not reached with *Pd_1%/pDVB*.

As the slope of the curves represented in Figure 104 changed with time, two values of TOF were calculated (*Table 36*) from the slopes between 60 and 120 min and between 200 and 250 minutes (full reaction rate), respectively.

Table 36: *TOF values of Pd/pDVB in the presence of different concentrations of hydrobromic acid (flow-rates: O_2 = 24 ml/min, H_2 = 1 ml/min; solvent = methanol; volume = 300 ml; T = 25 °C; catalyst = Pd/pDVB, 100 mg, 1% w/w Pd).*

[HBr] (ppm)	Slope ($mmol_{H2}$ min^{-1}) between 60 and 120 minutes	Slope ($mmol_{H2}$ min^{-1}) between 200 and 250 minutes	TOF (min^{-1}) between 60 and 120 minutes	TOF (min^{-1}) between 200 and 250 minutes
0	$3.34 \cdot 10^{-3}$	$1.34 \cdot 10^{-2}$	0.34	1.35
0.12	$1.22 \cdot 10^{-2}$	$1.54 \cdot 10^{-2}$	1.29	1.62
0.7	$4.72 \cdot 10^{-3}$	$7.93 \cdot 10^{-3}$	0.50	0.84

In spite of the longer induction time, in the presence of 0.12 ppm of HBr the catalyst reaches its full activity faster than in the other cases and the reaction rate is the highest. However, after the full activation *Pd_1%/pDVB* with no HBr is almost as active as the catalyst promoted with 0.12 ppm of the acid. Moreover, in both these cases very similar selectivities (*Figure 105*) towards hydrogen peroxide are achieved.

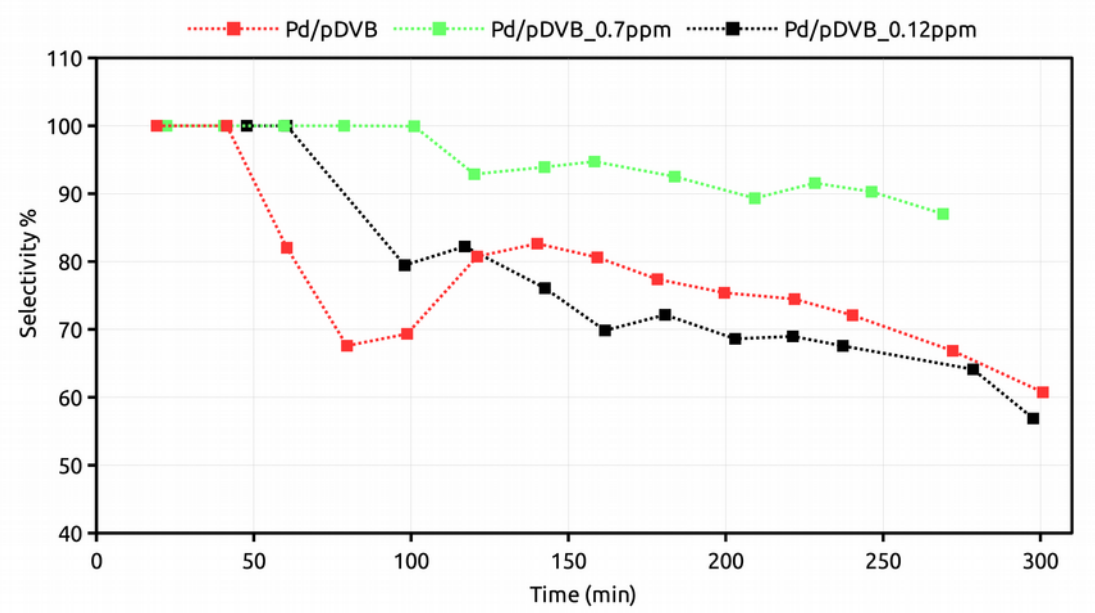

Figure 105: *Selectivity towards hydrogen peroxide in the presence of different amounts of hydrobromidic acid. (flow-rates: O_2 = 24 ml/min, H_2 = 1 ml/min; solvent = methanol; volume = 300 ml; T = 25 °C; catalyst = Pd/pDVB, 100 mg, 1% w/w Pd)*

This is in striking contrast with the behaviour of Pd/C: with no enhancer that is by far less active and selective than in the presence of HBr at the optimized concentration. It should also be appreciated that the selectivities at the end of the reaction are much higher (ca 60 %) than those of the best promoted systems based on Pd/C (ca 30%, *Figure 103*). The increase of the HBr concentration to 0.7

ppm leads to a ca 50% decrease in the full activity of the catalyst, but its selectivity is boosted to more than 90% and it practically never drops below this value during the test. These results show that sulfonated pDVB is a much better support than carbon of the palladium catalysts for the direct synthesis of hydrogen peroxide.

In fact the highest productivity towards hydrogen peroxide over *Pd_1%/pDVB* (*Figure 101*), which is achieved in the presence of 0.12 ppm of HBr (thanks to the relatively high catalytic activity rather than the selectivity), is as high as 2 mmol as compared to 0.6 mmol, the best value obtained with Pd/C in the presence of 0.7 ppm of HBr.

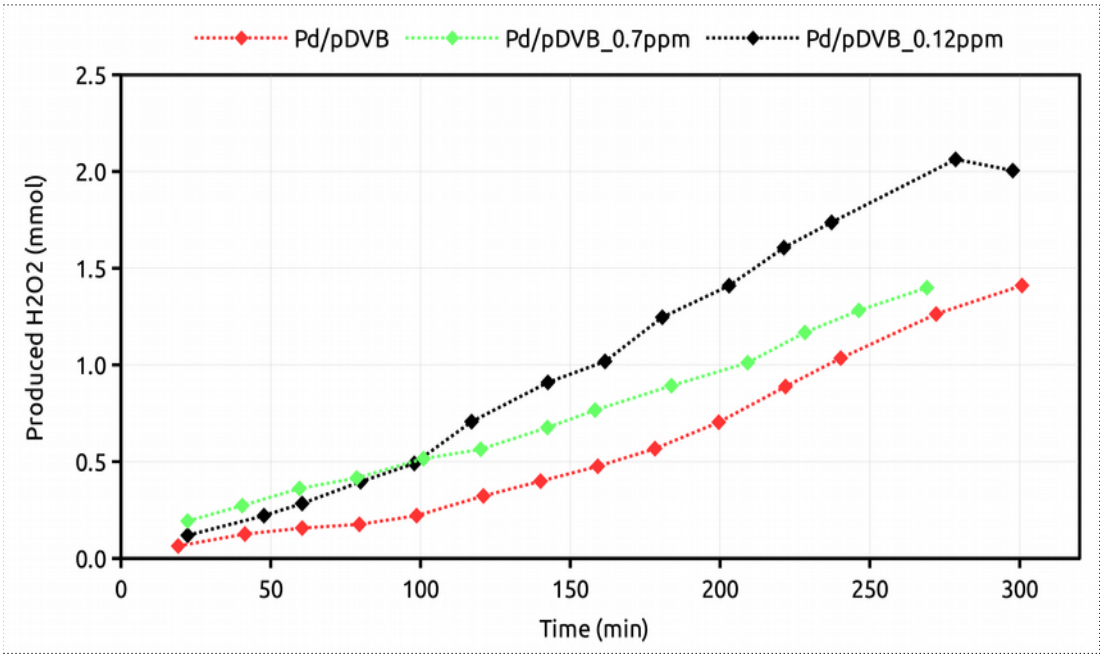

Figure 106: *Cumulative production of hydrogen peroxide in the presence of different amounts of hydrobromic acid in the reaction mixture. (flow-rates: O_2 = 24 ml/min, H_2 = 1 ml/min; solvent = methanol; volume = 300 ml; T = 25 °C; catalyst = Pd/pDVB, 100 mg, 1% w/w Pd)*

In these experiments the effect of increasing HBr concentration is qualitatively comparable to that observe with Pd/C below the optimal value, in that the higher the concentration the lower the activity and the higher the selectivity. This suggests that the optimal concentration of HBr for *Pd_1%/pDVB* could be somewhat higher and that there could be the possibility to achieve an even more selective catalytic system with a relatively high activity. It will be therefore necessary to explore a wider range of concentrations of HBr to find the optimal value and to observe changes in the catalytic performance possibly related to the mechanism of interaction of Br- with the catalyst, as it was done for Pd/C.

5.13: Palladium catalysts based on Mesoporous Carbon

Activated charcoal is a form of synthetic carbon with an extended porosity with usually a high fraction of micropores and surface areas up to 3000 m^2/g. This material is widely used in the fields of catalysis, separation, energy storage and electrodes [183].

It can be obtained from different raw materials, although the most used is coal because of its low cost and abundance [184]. Also waste biomass (for example coconut husk, bagasse, wood,…) can be employed, giving in this way value to unused materials.

The term "activated" indicates that the porosity is generated during the synthetic process. In the physical activation this is achieved after the carbonization by heating the sample at 700-1000 °C with CO_2 or steam to generate the porosity. In the chemical activation, instead, chemical agents, that must be removed after the synthesis, are used to generate the porosity thanks to degradation or dehydration reactions. [185]

The microporosity of activated charcoal represents a limit in a number of applications (catalysis for example) because of mass transport restrictions inside the pores. Therefore, the preparation of mesoporous carbon materials was investigated during the last decades: carbon aerogels (CAs) [183,186] and an ordered mesoporous carbon material [187] (referred as CMK-type carbon) turned out to be the most promising materials. However, the preparation of these materials is time-consuming, complex and expensive. Alternatively, metal salts ($ZnCl_2$, $CaCl_2$ and K_2CO_3) can be used as activating agents, to generate the mesopores during the synthesis.

In this Thesis, a number of selected Palladium catalysts supported on mesoporous carbon materials (*MC*) [188], provided by Prof. U. Simon and Dr. P. Chen (Department of Inorganic Chemistry of Rwth Achen), were tested in the direct synthesis of hydrogen peroxide. The carbon supports were synthesized using fructose as the starting reagent and $ZnCl_2$ as the activation agent. The exploitation of a soluble biomass provides a completely mesoporous material with surface areas greater than 2000 m^2/g, pore volumes larger than 2.5 cm^3/g. The amount of $ZnCl_2$ is a crucial parameter to define the pore sizes of the material: increasing the ratio between metal chloride and fructose from 1 to 4, the average pore diameter increases from 2.2 to 5.2 nm, respectively.

The synthesis consists of the following steps:

1) hydrolysis of fructose to HMF (hydroxymethylfurfural) catalysed by the acidic $ZnCl_2$ (*Figure 107*);
2) polymerization of HFM again catalysed by $ZnCl_2$ (*Figure 107*);
3) solidification of the polymer at controlled temperature;
4) carbonization of the polymer;
5) removal of $ZnCl_2$ by washing with water.

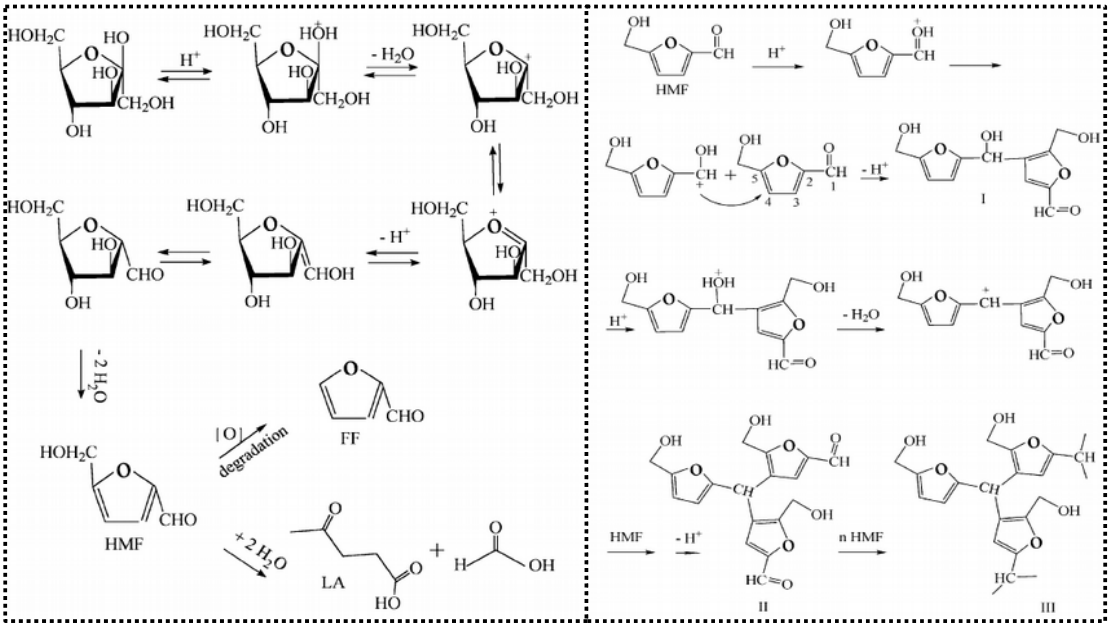

Figure 107: *On the left, schematic mechanism for the conversion of fructose to HFM: Levulinic acid (LA) and Furfural FF) are the main by-products. On the right, schematic mechanism for the polymerization of HFM.*

The introduction of palladium was carried out by impregnation with a solution of its diacetate and the subsequent reduction with H_2 (200 °C, 2 hours, 100 ml/min of 10 %vol H_2 in He), to obtain a catalyst with 1 %wt of metal in the form of nanoparticles.

The same support was also treated with 65% HNO_3 at 120 °C for two hours, to obtain an oxidised form of the mesoporous carbon material (*OMC*). The resulting material was also treated in NH_3 at 400 °C (*NOMC*).

Finally, in the frame of this investigation, a N-rich mesoporous carbon (*NMC*) was also used as catalytic support [189]. This material was obtained using N-containing precursor (melamine), instead of fructose, for the synthesis of the polymer. The main steps of the preparation are the following:

1) an aqueous solution of melamine and formaldehyde (37%) was adjusted to pH 8.5 by addition of Na_2CO_3.
2) The solution was heated at 313 K, to produce a solution of hexamethylomelamine (*Figure 108*).
3) $CaCl_2$ was added to the solution and the pH adjusted to 4.5 by addition of HCl. Then the solution was heated at 333 K for 1 hour to form the resin.
4) The resin was dried at 453 K for 6 hours and subsequently carbonized in at 973-1173 K, under N_2 flow, for 2 hours.
5) $CaCl_2$ was removed by thorough washing the solid with water.

Two samples were prepared, *NMC-1* and *NMC-2*, with, respectively, a weight ratio of $CaCl_2$/resin of one and two. The samples differ in the surface area and average pore diameter, both resulting higher for *NMC-2* material.

These N-rich mesoporous carbon materials are interesting because of their amphipathic properties, making them able to absorb great amount of solvents with different polarity, such as water and benzene.

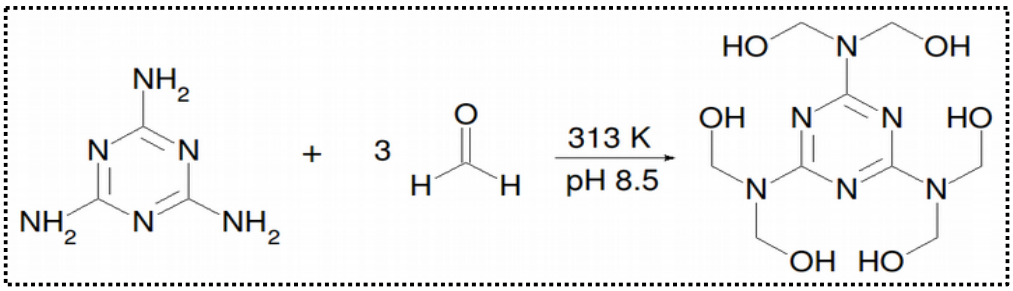

Figure 108: *reaction between melamine and formaldehyde to obtain hexamethylomelamine*

Finally, also a metal catalyst based on oxygen-doped carbon nanotubes (*OCNT*) was tested. This was obtained from commercially available carbon nanotubes (Baytubes C 150 P, supplied by Bayer), by treatment with HNO_3 steam at 200 °C for 48 hours.[190] [191]. The deposition of metal nanoparticles was carried out in a similar way as described before for MC. The 1 %wt carbon-based palladium catalysts are listed in Table 37.

***Table 37**: metal catalyst based on mesoporous carbon and carbon nanotubes. The catalysts, containing 1 %wt of Palladium, were prepared by impregnation with Palladium (II) acetate and reduction with hydrogen (2 hours at 200 °C with a flux of 10 %vol H_2 in He, 100 ml/min).*

Catalyst	Description of the support
Pd_1%/MC	Purified mesoporous carbon [188]
Pd_1%/OMC	*MC* functionalized by treating it in 65% HNO_3 solution at 120 °C for 2 hours
Pd_1%/NOMC	*OMC* functionalized by treating it in 100 ppm NH_3 at 400 °C for 6 hours
Pd_1%/NMC-1	Purified N-rich *MC* using N-containing precursor for the synthesis. *NMC-2* contains a double amount of $CaCl_2$ respect to *NMC-1*. [189]
Pd_1%/NMC-2	
Pd_1%/OCNT [a]	Carbon nanotubes functionalized by treating in 65%wt HNO_3 solution at 120 °C for 2 hours. [191]
Pd_1%/C	Commercially available micro-porous active carbon.

[a]: the Pd loading determined by ICP-OES is 0.89 %wt

The catalytic results are reported in Figures 109, 110 and 111. The results obtained with *Pd_1%/C* are included for comparison.

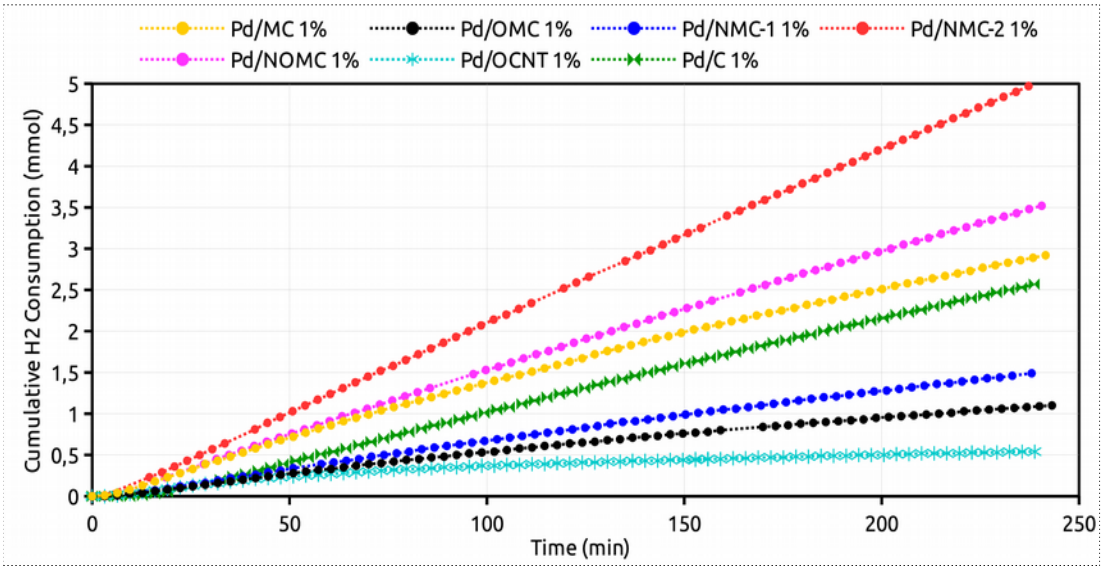

***Figure 109:** Cumulative consumption of hydrogen for the catalysts reported in Table 12 (flow-rates: O_2 = 24 ml/min, H_2 = 1 ml/min; solvent = methanol; volume = 300 ml; T = 25 °C; catalyst: 100 mg, 1% w/w Pd)*

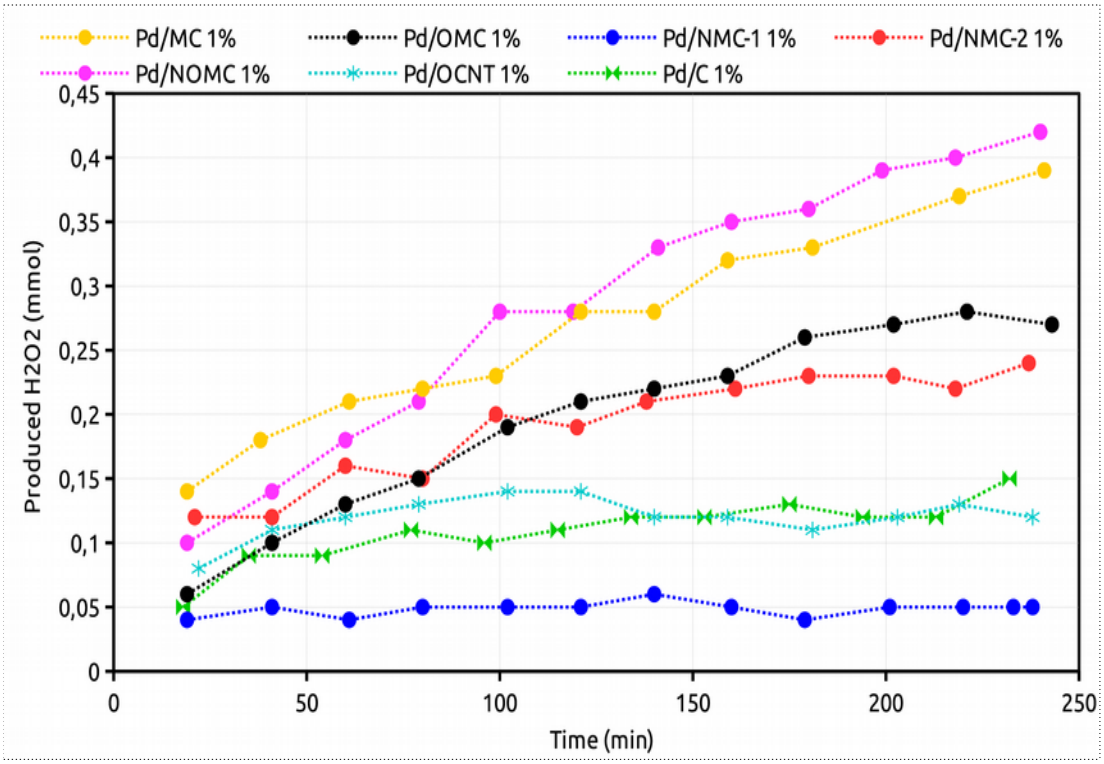

Figure 110: *Cumulative production of hydrogen peroxide for the catalysts reported in Table 12 (flow-rates: O_2 = 24 ml/min, H_2 = 1 ml/min; solvent = methanol; volume = 300 ml; T = 25 °C; catalyst: 100 mg, 1% w/w Pd)*

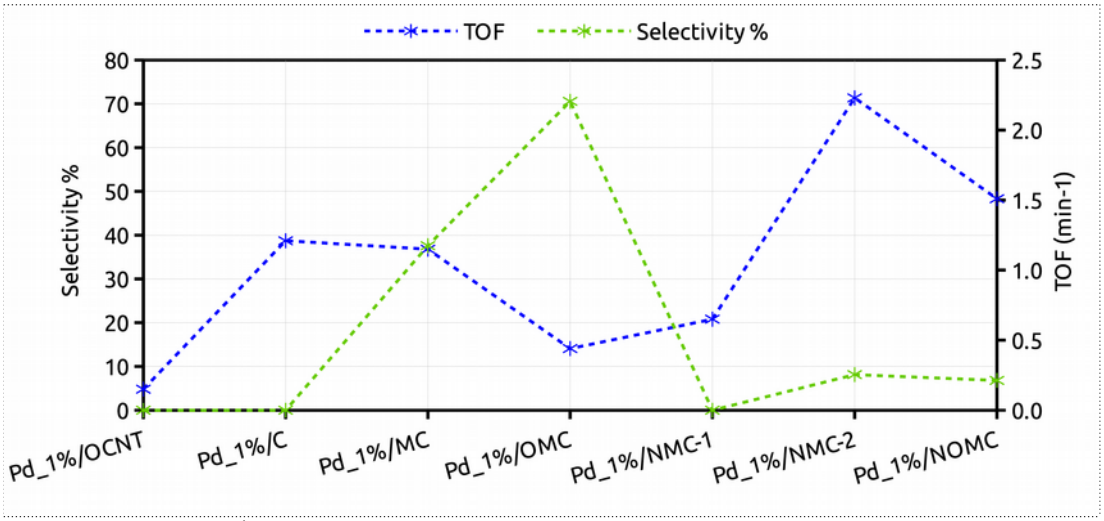

Figure 111 *TOF (min^{-1}) and selectivity for the carbon based catalysts flow-rates: O_2 = 24 ml/min, H_2 = 1 ml/min; solvent = methanol; volume = 300 ml; T = 25 °C; catalyst: 100 mg, 1% w/w Pd). TOF are calculated from the slope of the consumption curves after 100 minutes from the beginning of the test, where the trend is linear.*

In general the productivity of these catalysts (*Figure 110*) is much smaller (0.4 mmol with *Pd_1%/NOMC* as the best value) than that obtained with *Pd_1%/pDVB* (ca. 1.5 mmol, see Figure 82 in Paragraph 5.8). Their activity is not far from that of

Pd/C (*Figure 100*); for instance *Pd_1%/MC,* based on mesoporous carbon, has a TOF comparable with *Pd_1%/C* (1.21 and 1.15 min^{-1}, respectively). In this case the productivity (*Figure 100*), hence the selectivity (*Figure 111*), is remarkably higher for *Pd_1%/MC*. This could depend on the structure and the morphology of the active metal phase, which is not known yet for *Pd_1%/MC*, but it should also appreciated that mesoporous carbon has larger pores than the conventional activated carbon, which is only microporous. It cannot be ruled out yet that the morphology of the support contributes to this remarkable increase of selectivity as it is observed with pDVB based Palladium catalysts (Paragraph 5.8).

The catalysts based on oxidized carbonaceous supports (*Pd_1%/OCNT*, *Pd_1%/OCM*) are generally less active than *Pd_1%/MC*. The catalyst based on oxidized carbon nanotubes (*Pd_1%/OCNT)* is almost inactive, possibly because of the presence of $Pd(OAc)_2$, rather than Pd^0, on the surface of the nanoparticles [191].

On the other hand, *Pd_1%/OMC* is the catalyst with the highest selectivity so that it produces the same amount of hydrogen peroxide as *Pd_1%/OMC*. This suggests that functional groups which contain oxygen could in mesoporous carbon lead to the generation of nanoparticles that are more selective.

The introduction of nitrogen seems to have the opposite effect. *Pd_1%/NMC-1* is also less active than *Pd_1%/MC*, but is also completely non selective. A very poor selectivity, which confirms the detrimental effect of nitrogen in these supports, is achieved with *Pd_1%/NMC-2*. This is however the most active catalyst, probably because of its higher surface area with respect to *Pd_1%/NMC-1*. Nitrogen can be introduced in the support also by treating with ammonia the oxidised OMC (*Pd_1%/NOMC*), but again the selectivity remains low, in spite of an increases in activity. In conclusion the introduction of nitrogen can have a beneficial effect only on the activity, but not on the selectivity, and only under some circumstances. This effect could be partially explained on the basis of the characterization of Palladium catalyst based on OCNT and NCNT [191]. The latter ones are obtained by treating OCNT with flowing ammonia (10 vol% NH_3 in He at 400 °C for 6 hours), but were not included in this investigation. The TEM characterization shows for both materials metal nanoparticles smaller than 5 nm and, in spite of the same average Pd particle size (2.7 nm), a higher standard deviation for Pd/OCNT. Moreover, according to XPS investigation, Pd is in a more reduced state on Pd/NCNT than on Pd/OCNT.

If we assume that the same effect is produced by nitrogen also in mesoporous carbon and taking into account that the metal catalysts are obtained by the very same procedure, we can argue that palladium is formed in a more reduced metal phase. This seems to enhance the activity of palladium and lower its selectivity and shows that the control of the oxidation state of the active metal is a critical issue in the direct synthesis of hydrogen peroxide.

Chapter 6:

EXPERIMENTAL PART

6.1: Reagents and solvents

Reagent	Chemical formula	PM (g/mol)	Density (g/mL)	Supplier
Tetrahydrofuran	C_4H_8O	72.11	0.89	Sigma-Aldrich
Methanol	CH_3OH	32.4	0.79	Sigma-Aldrich
1,4-dioxane	$C_4H_8O_2$	88.11	1.03	Sigma-Aldrich
Carbon Tetrachloride	CCl_4	153.82	1.59	Sigma-Aldrich
1,2-dichloroethane	$C_2H_4Cl_2$	98.97	1.25	Prolabo
Dichloromethane	CH_2Cl_2	84.93	1.33	Sigma-Aldrich
Chloroform	CH_3Cl	119.38	1.49	Carlo Erba
Carbon Disulfide	CS_2	76.14	1.26	Sigma-Aldrich
Acetone	C_3H_6O	58.08	0.79	Prolabo
Ethanol	C_2H_6O	46.07	0.79	Sigma-Aldrich
Diethyl Ether	$C_4H_{10}O$	74.12	0.706	Sigma-Aldrich
Potassium Iodide	KI	166	/	Sigma-Aldrich
Sodium Molybdate	Na_2MoO_4	205.92	/	Carlo Erba
Sulfuric Acid 98%	H_2SO_4	98.09	1.84	Sigma-Aldrich
Hydrochloric Acid 37%	HCl	84.46	1.2	Sigma-Aldrich
Nitric Acid	HNO_3	63.02	1.52	Sigma-Aldrich
Sodium Hydroxide	NaOH	40	/	Prolabo
Phenolphthalein	$C_{20}H_{14}O_4$	318.33	/	Merck
Perfluorobutyryl chloride	C_4F_7OCl	232.48	1.56	Sigma-Aldrich
Copper (I) Bromide	CuBr	143.45	/	Fluk
EDTA	C 10 H 14 N 2 O 8 Na2	336.21	/	Prolabo
Sodium Chloride	NaCl	58.44	/	Prolabo
Aluminium Chloride	$AlCl_3$	133.34	/	Sigma-Aldrich
N,N,N',N''; N'' - pentamethyldiethylentriamine	$C_9H_{23}N_3$	173,3	0.83	Sigma-Aldrich
1H, 1H, 2H, 2H - perfluorodecylacrylate	$C_{13}H_7O_2F_{17}$	518.17	1.64	Sigma-Aldrich
Butyryl Chloride		106.55	1.03	Sigma-Aldrich

Sodium Thiosulfate	$Na_2S_2O_3$	158.11	/	J.T. Baker
Potassium Dichromate (Normex, 0.1 N)	$K_2Cr_2O_7$	294.19	/	Cecchinato
Hydrobromic Acid 48%	HBr	80.92	1.49	Fluka
Tetrammine Palladium (II) Sulphate	$Pd(NH_3)_4]SO_4$	270.4	/	Alfa Aesar
Palladium on Carbon, activated, eggshell, (1 %wt)	Pd/C	/	/	Alfa Aesar
Divinylbenzene 80%	$C_{10}H_{10}$	130.18	0.91	Sigma-Aldrich
2,2' - Azobis(2-methylpropionitrile)	$C_8H_{12}N_4$	164.21	/	Janssen
Oxygen				Air Liquid
Hydrogen				Air Liquid
Stearic Acid	$C18H_{36}O_2$	284.48	/	Sigma-Aldrich
Acetic Anhydride	$C_4H_6O_3$	102.09	1.08	Sigma-Aldrich
p-toluenesulfonic acid	$C_7H_8SO_3 \cdot H_2O$	190.22	/	Sigma-Aldrich

6.2: Synthesis of mesoporous pDVB

Poly-divinylbenzene materials were synthesized according to ref. [22].

In a typical preparation of the pDVB1 material, 6.0 g of divinylbenzene (technical grade 80%), 60 mL of tetrahydrofurane (THF), 165 mg of 2,2' azobis(2-methylpropionitrile) (AIBN), the initiator, and 6 mL of distilled water were introduced, under magnetic stirring, in a teflon vessel with a capacity of 85 ml. The stirring was maintained for three hours.

The vessel, containing the pale yellow polymerization mixture, was transferred in a closed autoclave and let to react at 110 °C for 48 hours under autogenic pressure (2.1 bar).

After cooling to room temperature, a white gelatinous monolith was removed from the autoclave and left to dried at room temperature for ten days. The polymer turned out to be stiffer and more brittle.

6.3: Acylation with butyryl chloride

In a typical experiment ca. 2 g of resin was left to fully swell in a round-bottomed flask with 20 mL of CS_2. Under mild magnetic stirring were added ca. 4 g of aluminium chloride, 3.0 mL of lauroyl chloride (29 mmol) and 20 ml of CS_2. The reaction mixture was gently stirred at room temperature for 48 hours. After the addition of 150 mL of HCl 1.2 M, the mixture was left under moderate stirring at room temperature for 24 hours. The CS_2 was removed with a rotary evaporator and 100 mL of HCl 1.2 M was added to the reaction mixture. The product was recovered by vacuum filtration on a gooch and washed with 300 mL of distilled water, 300 mL of a water:THF mixture (1:1 v/v), 300 ml of THF and with 300 mL of dichloromethane.

6.4: Acylation with perfluorobutyryl chloride

In a typical experiment ca. 2 g of resin was left to fully swell in a round-bottomed flask with 20 mL of $CHCl_3$. Under mild magnetic stirring were added ca. 4 g of aluminium chloride, ca. 8 g of perfluorobutyryl chloride (35 mmol) and 20 ml of $CHCl_3$. The reaction mixture was gently stirred at room temperature for 48 hours. After the addition of 150 mL of HCl 1.2 M, the mixture was left under moderate stirring at room temperature for 24 hours. The $CHCl_3$ was removed with a rotary evaporator and 100 mL of HCl 1.2 M was added to the reaction mixture. The product was recovered by vacuum filtration on a gooch and washed with 300 mL of distilled water, 300 mL of a water: THF mixture (1:1 v/v), 300 ml of THF, 300 ml of $CHCl_3$ and with 300 mL of dichloromethane.

6.5: Sulfonation with concentrated sulfuric acid

ca. 2 g of polymer were let to swell overnight in an suitable volume of 1,2-dichloroethane in a jacket glass reactor equipped with a back condenser. 50-100 ml of 98% H_2SO_4 (acid:solvent, 5:1 v/v) was slowly added to the swollen polymer.

The mixture was heated up to 80°C for 3 hours, under moderate stirring and cooled to room temperature. The reaction mixture was diluted with five portions of ca. 30 mL of sulfuric acid with lower and lower concentration (10 M; 5 M; 2,5 M; 1 M; 0,1 M), maintaining a low temperature by flowing cold water through the jacket of the reactor. Finally the resin was recovered by filtration, washed with distilled water up to neutral pH and dried at 110 °C.

6.6: Sulfonation with oleum

The procedure is the same used for the sulfonation with sulfuric acid, except for the use of oleum as sulfonating agent.

6.7: Sulfonation with chlorosulfonic acid acid

The resin (ca. 2 g) was pre-swollen overnight with 1,2-dichloroethane in a glass jacket reactor. 24 ml of 1,2-dichloroethane and 16 ml of $HClSO_3$ were added under magnetic stirring and the mixture was let to react for three hours at 42 °C. 50 ml of cold distilled water were added dropwise to the reaction mixture, maintained at low temperature with an ice bath. the chlorosulfonated resin was recovered by vacuum filtration (G3 gooch) and washed with distilled water until neutral pH. The resin was transferred into 40 ml of a 2%wt NaOH solution in dioxane:water 1:1 vol, at 40 °C for two hours. The solid product was recovered by vacuum filtration (gooch G3) and washed with a 10% HCl solution in dioxane:water 1:1 vol with a dioxane:water 1:1 vol solution, until disappearance of chloride ions from the filtrate ($AgNO_3$ test) and finally with methanol. The product was dried at 110°C overnight.

6.8: Functionalization with ATRP

6.8.1: Bromination of pDVB

In a jacketed glass vessel, ca. 1 g of pDVB was swelled in 40 ml of CCl_4 for two hours. Then 350 mg of N – bromosuccinimide and 50 mg of AIBN were introduced. The reaction was carried out under magnetic stirring and under reflux (Teb = 77 °C) for three hours. The resin was then recover by filtration and washed with 60 ml of acetone, 60 ml of warm (ca. 50 °C) distilled water, 60 ml of HCl 1.2 M in water:1,4-dioxane 1:1 v/v, water:1,4-dioxane 1:1 v/v up to neutral pH and 30 ml of 1,4-dioxane.

6.8.2: Sulfonation of the brominated pDVB and its neutralization

The sulfonation of the brominated resin was performed according to the procedure described in the paragraph 6.5. The resin was not dried before sulfonation, but simply washed with 1,2-dichloroethane.
For the neutralization, the resin was placed in a Erlenmeyer flask with 250 ml of $NaOH_{(aq)}$ 0.5 M and left under mechanical stirring overnight. The neutralized resin was recovered by filtration and washed with distilled water up to neutral pH and then with methanol.

6.8.3: ATRP

ATRP was performed under inert atmosphere and magnetic stirring. 650 mg of sulfonated and brominated resin, without being dried, are placed in a three-necks round-bottomed flask with 15 ml of methanol and left to swell for two hours. Then 55 mg of CuBr are added and the solvent was degassed by freeze – pump using liquid N_2 as refrigerant. After the adding of 3.8 ml of 1H, 1H, 2H, 2H – perfluorodecyl acrylate and 6 ml of PMDETA, the reaction mixture was heated at 80 °C. Spent four hours, the resin was filtered and washed with 50 ml of methanol, 150 ml of EDTA 0.1 M, 250 ml of NaCl 0.1 M and 300 ml of distilled water. Finally, the solid was dried at 110 °C for a night. Before performing the reaction, the inhibitors were removed from the monomer by using a chromatographic column with a small amount of neutral alumina inside.

6.9: Synthesis of Palladium catalysts

6.9.1: Metallation of the sulfonated resin

First the sulfonated resin was grounded and sieved to isolate the fraction with particle diameters between 180 and 400 μm. and then dried in oven at 110 °C for a night.
The desired amount of resin (typically 1 g) was swelled in the smallest possible amount of distilled water (about 5 ml for 1 g of sulfonated macroreticular resin and 10 ml for 1 g of sulfonated pDVB). Then a solution of $[Pd(NH_3)_4]Cl_2$ with a proper concentration, depending on the final Palladium loading, was added to the swelled resin that was stirred under mechanical stirring overnight.

6.9.2: Reduction of the metal precursor

The resin was recovered by filtration and washed with distilled water (about 30 ml for each gram of resin) and THF (about 25 ml for each gram of resin). Then it was swelled in THF (ca. 30 ml for 1 g of resin) in a glass vessel that was put in a steel autoclave. After three purges with H_2, the autoclave was filled with H_2 up to 4.5 bar and warmed at 60 °C (at this temperature the pressure inside the vessel increases up to 5 bar). The reaction was performed under magnetic stirring for five hours. After this time, the resin is recovered by filtration and dried in oven at 70 °C for a night.
Nb: before the use, THF is purified on neutral alumina to prevent the presence of peroxide species according the reference [192]. Purified THF is kept under inert atmosphere.

6.10: Characterization Methods

6.10.1: Determination of the proton-exchange capacity of sulfonated resins

Proton exchange capacity is determined by acid-base back titration. About 100 mg of resin was exactly weighted after drying overnight at 110 8C in an oven. Each

sample was treated with 10.0 cm^3 of a standard aqueous solution (ca. 0.1 M) of NaOH in a 50 cm^3 stoppered Erlenmeyer flask. The suspension was mechanically swirled (orbiting plate) overnight. To allow for possible reaction with atmospheric CO_2, a blank with 10.0 cm of the NaOH solution was prepared as well. The solutions (sample and blank) were eventually titrated with standard 0.1 M HCl and phenolphthalein as the indicator. The apparent specific content of sulfonic groups was calculated as the difference of the initial and final millimoles of NaOH (corrected for overconsumption due to CO_2, if any) divided by the resin mass.
Alternatively, the proton-exchange capacity can be calculated from the results of the elemental analysis about sulphur and carbon.

6.10.2: ICP analysis

After the metallation of the resin, the filtered and the washing water was collected and analysed by ICP-OES to determine the not reacted metal.
For the analysis of the reaction mixture, first it is transferred in a round-bottom flask to remove methanol with a rotary evaporator. Then ca. 10 ml of aqua regia are added and the flask is carefully heated with a heat gun to solubilize the metal. The solution is quantitatively transferred in a volumetric flask and dilute with distilled water.

6.10.3: ISEC investigation

The swollen state morphology of the sulfonated resins was characterized by ISEC (Inverse Steric Exclusion Chromatography) measurements. The resin was used as the stationary phase in a chromatographic column and the elution volumes of standard solutes with known molecular size are measured. The measurements were performed using a 0.2 M sodium sulfate solution as the mobile phase and D_2O, sugars and dextrans as standard solutes.

6.10.4: Solid state MAS NMR

^{1}H-^{13}C CP-MAS, ^{19}F MAS, ^{19}F-^{13}C CP-MAS spectra were run at 25°C on a Varian 400 spectrometer equipped with a 4 mm MAS probe. In order to homogenise the

samples, resin beads were grounded to obtain a fine powder prior to insertion into the rotor.

6.10.5: ^1H NMR

NMR spectra were recorded on a Bruker Avance 300 Mhz spectrometer. All the spectra have been recorded at 298 K. The chemical shift values (δ) are reported in units of ppm relative to the residual deuterated solvent.

6.10.6: TEM and STEM characterization

Samples for TEM and STEM analysis were prepared by grinding of the material to be examined up to obtain particles smaller than 140 μm. Then the powder was ultrasonically dispersed in isopropanol and transferred as a suspension to a copper grid covered with a lacey carbon film.

6.10.7: Elemental Analysis of Chlorine

The content of chlorine was determined by burning the sample in oxygen.

6.11: Catalytic Tests of direct synthesis of hydrogen peroxide

First 100 mg of catalyst (carefully weighted) are swelled in methanol for two hour. Meanwhile, the reactor is filled with methanol and gases are fluxed (1 ml/min of H_2 and 24 ml/min of O_2) to expel air, the condenser is cooled at -9 °C and the reactor is thermostated at 25 °C.
At this point, the catalyst and the swelling solvent are added to the reactor (zero-point of the test). The total amount of methanol inside the reactor, included the portion used for the swelling of the catalyst, is 300 ml.
In the case of catalytic tests performed in presence of HBr, 1 ml of a solution of HBr in methanol is added. The solution, whose concentration is properly chosen depending on the desired amount of HBr in the reaction mixture, is prepared by

dilution of a solution of HBr 36.2 mM in methanol (0.3049 g of HBr 48% in 50 ml of methanol).

During the test the gaseous mixture is continuously analysed every 3 minutes by a μ-GC to determine the consumption of H_2. The produced H_2O_2, instead, is determined by titration of samples of the reaction (ca. 1 ml) mixtures collected every approximately 20 minutes.

The test is stopped after 4 hours of reaction.

6.11.1: Determination of H_2 consumption

Once calibrated the instrument (*Table 38* and *Figure 112*), the value of the exit flow of H_2 at a certain time can be determined from the area of its chromatographic peak (*Equation 9*).

Table 38: *Flows and molar fraction of H_2 and O_2 used for the registration of the calibration curve for H_2. The value of the corresponding R^2 is 0.999.*

Flow H_2 (ml/min)	Flow O_2 (ml/min)	Molar Fraction H_2 (mol%)	Molar Fraction O_2 (mol%)
0.5	49.5	1	99
1	49	2	98
1	24	4	96
1.5	23.5	6	94

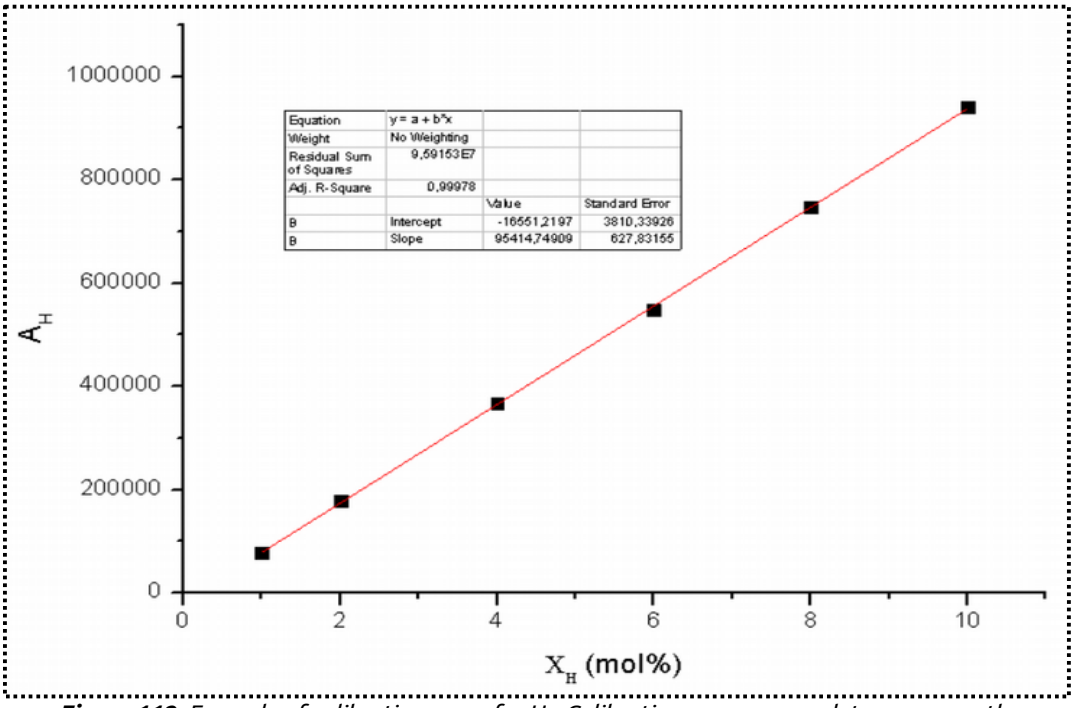

Figure 112: *Example of calibration curve for H_2. Calibration curve was update every month.*

$$\Phi_{ex} = \frac{(A_{H_2} - a)}{b} \frac{\Phi_{fed}}{X_{H_2}}$$

Equation 9: *determination of exit flow of H_2 (Φ_{ex}) from the fed flow of H_2 (Φ_{fed}). A_{H2} = area of the chromatographic peak; a = intercept of calibration curve; b = slope of calibration curve; X_{H2} = molar fraction of H_2.*

From the value of the flow of H_2 fed into the reactor (1 ml/min), the amount of consumed H_2 in ml/min is determined. This is converted in mmol/min thanks to the value of molar volume of H_2 at 25 °C and 1 atm. Knowing the interval of time passed, the cumulative consume of H_2 is calculated (*Equation 10*).

$$\left(Cumulative\, consumption_{H_2}\right)_{t_n} = ¿$$
$$Consumption\left(mmol/min\right)_{t_n} * \left(t_n - t_{(n-1)}\right) + \sum_{i=0}^{i=t_{n-1}} Consumption_{t_i} * \left(t_i - t_{i-1}\right)$$

Equation 10: *determination of the cumulative consumption of H_2 at a certain time t_n*

6.11.2: Determination of H_2O_2 production

The titration of the collected samples is made by iodometric method (*Equations 11-13*), using starch as indicator.

$$H_2O_2 + 2\,I^- + 2\,H^+ \rightarrow I_2 + 2\,H_2O$$

Equation 11: *iodide anions reduce hydrogen peroxide to water producing iodine.*

$$I^- + I_2 \rightarrow I_3^-$$

Equation 12: *formation of triiodine anions from iodine*

$$I_3^- + 2\,S_2O_3^- \rightarrow 3\,I^- + S_4O_6^{2-}$$

Equation 13: *titration of triiodine anion with tiosulfate.*

For each sample 2 ml of an aqueous solution containing 0.13 g/ml of Na_2MoO_4 and H_2SO_4 10^{-3} M and 3 ml of an aqueous solution of KI 10 g/L were added before the titration. The exact concentration of the $Na_2S_2O_3$ solution (9.947 mM) was determined by using dichromate - iodide method. 40 mg of KI and 1 ml of HCl 2 M are added to 10.0 ml of a a standard potassium dichromate (0.8 mM) (*Equation 14*). The solution is then titrated with the solution of $Na_2S_2O_3$ (*Equation 13*).

$$Cr_2O_7^{2-} + 6I^- + 14H^+ \rightarrow 2Cr^{3+} + 3I_2 + 7H_2O$$

Equation 14: *formation of iodine by oxidation of iodide anions with dichromate.*

6.12: Catalytic tests of esterification of stearic acid

The day before the test, in a Schott-Duran glass bottle 72 g of sunflower oil and 8 g of stearic acid were added and magnetically mixed under mild heating up to dissolution of stearic acid.

The next day, 500 mg of catalyst were swelled in ca. 5 ml of methanol for two hours. Then methanol was removed and re-added with a Pasteur pipette up neutral pH of the solvent. The resin is then dried in a vacuum oven at 40 °C just to remove the excess of the solvent.

The catalyst and 20 g of methanol are introduced in the bottle, prepared the day before, that was closed with the teflon cap and introduced in a oil batch pre-heated to 150 °C. The zero-point of the reaction coincides with the moment in which the temperature of the reaction mixture is 65 °C.

During the test at certain times some samples of the reaction mixture (ca. 1 g) were collected with a syringe. The test was stopped after 8 hours.

6.12.1: Determination of stearic acid consumption

Each collected sample of reaction mixture was titrated to determine the not consumed stearic acid from which the amount of consumed acid is easily deducible.

Each samples was first dissolved (in some case using a ultrasounds bath) in ca. 50 ml of a mixture of ethanol and diethyl ether 1:1 v/v. The solution was titrated with a solution of NaOH 20 mM, using phenolphthalein as indicator. The exact concentration of the basic solution was determined by titration of 50.0 ml with a standard solution of HCl 0.1 M, prepared using a Normex.

During the titration of the sample the sample could became turbid. In these cases, solvent was added up to the recovery of the transparency.

Regarding the test performed using p-toluenesulfonic acid as catalyst, each collected sample was immediately cooled in ice and titrated as quickly as possible.

6.12.2: Calculation of TOF values

TOF values were determined from the first derivative of the curves of TON values in function of time calculated at t = 0.

Each curve was first interpolated with the equation of a branch of hyperbola , where the parameter *a,* representing the intercept with the x axis, is imposed to be zero (*Equation 15*).

$$TON = \frac{k(t+a)}{t+b} \rightarrow y = \frac{kt}{t+b}$$

Equation 15: *equation of a branch of hyperbola used for the interpolation of the catalytic data.*

For the interpolation, the value of k is imposed to be smaller than the ratio between the moles of introduced stearic acid and the moles of acid groups of the catalyst.

TOF (t^{-1}) is therefore the value of the derivative calculated for t = 0 (*Equation 16*).

$$TOF = \left(\frac{d(TON)}{dt} \right)_{t=0} = \frac{k}{b}$$

Equation 16: *determination of TOF (t^{-1}) from the parameters of the interpolation.*

Chapter 7:
CONCLUSIONS

The results of the research activity clearly point out the remarkable performance of mesoporous polydivinylbenzene (pDVB) for catalytic purpose, directly connected to his peculiar morphology. In fact, differently from conventional cross-linked polymers showing a negligible porosity at the dry state, this material is featured by remarkably high surface area and pore volume, mainly generated by mesopores. Moreover, according to the general behaviour of functional resins, pDVB also swells in suitable liquid medium, due to the polymer chains solvation, further increasing surface area, pore size and pore volume. Accordingly, this material is affected by considerably lower diffusion limitations, respect to conventional materials with comparable chemical structure (i. e. polystyrene-divinylbenzene resins). As the consequence, among the catalytic systems considered in the frame of this investigation (including gel-type and macroreticular resins, micro- and mesoporous carbon materials), those based on pDVB showed the best performance.

In particular, two technologically relevant reactions, such as the esterification of a stearic acid solution in sunflower oil with methanol and the direct synthesis of hydrogen peroxide, were selected as target processes for acid and metal catalysis, respectively.

As to the esterification of a stearic acid, sulfonated pDVB provided the best performance (reagent conversion and TOF) among the resin based acid catalysts included in the investigation, due to the highly accessible morphology enhancing the diffusion of the hindering substrate towards the catalytic sites.

The role of the mesoporous polymer matrix is even more evident, when the material is used as the support for Palladium nanoparticles in the frame of the reaction of formation of H_2O_2. In this case, the catalyst based on pDVB not only provides the highest activity (i. e. the rate of hydrogen consumption), due to the highest accessibility of the gaseous reactants to the metal nanoparticles ensured by mesopores, but also the highest H_2O_2 productivity. In fact, the mesoporous morphology also makes easier the back-diffusion of hydrogen peroxide towards the bulk solution, minimizing the probability of its further hydrogenation on the Palladium nanoparticles. As the consequence, the selectivity of the Pd/pDVB

catalyst is remarkably high, even in the absence of enhancers. Noticeably, in the presence of HBr, the selectivity is exceptionally high and is maintained over the whole catalytic test. Interestingly, the HBr concentration providing the best catalytic performance is significantly lower for Pd/pDVB than for the reference catalyst, Pd/C: this makes the catalytic system potentially more suitable for technological purposes, according to the limited corrosion properties and the lower reactivity towards organic substrates.

As the result of this investigation, pDVB appears, due to the remarkable mesoporous morphology minimizing the diffusion limitations, a versatile and promising material with potential application both as acid catalyst (after proper functionalization) and support for metal nanoparticles, in the preparation of redox catalysts.

REFERENCES

(1) de Gruyter, W. *Ion Exchangers*; K. Dorfner (Ed.), 1991.
(2) Staudinger, H.; Huseman, E. *Berichte* **1935**, *68*, 1618.
(3) Topp, N. E.; Pepper, K. W. *J. Chem. Soc.* **1949**, No. 0, 3299–3303.
(4) Hale, D. K.; Reichenberg, D. *Discuss. Faraday Soc.* **1949**, *7* (0), 79–90.
(5) Pepper, K. W. *J. Appl. Chem.* **1951**, *1* (3), 124–132.
(6) Merrifield, R. B. *J. Am. Chem. Soc.* **1963**, *85* (14), 2149–2154.
(7) Ancillotti, F.; Mauri, M. M.; Pescarollo, E. *J. Catal.* **1977**, *46* (1), 49–57.
(8) Ancillotti, F.; Pescarollo, E.; Massi Mauro, M. PROCESS FOR THE SYNTHESIS OF METHYL-TERT-BUTYL ETHER FROM METHANOL AND ISOBUTYLENE IN THE PRESENCE OF BUTADIENE. US 4039590, 1977.
(9) Haag, W. O.; Whitehurst, D. D. 1969.
(10) Lange, P. M.; Martinola, F.; Oeckl, S. *Hydrocarb. Process.* **1985**, *64* (12), 51–52.
(11) Wagner, R.; Lange, P. M. In *Erdöl, Erdgas, Kohle*; Urban, 1989; Vol. 105, pp 414–419.
(12) Okay, O. *Prog. Polym. Sci.* **2000**, *25* (6), 711–779.
(13) Gokmen, M. T.; Du Prez, F. E. *Prog. Polym. Sci.* **2012**, *37* (3), 365–405.
(14) Dusek, K. In *olymer networks: structure and mechanical properties*; Plenum Press: New York, 1971; pp 245–260.
(15) Biffis, A.; Corain, B.; Zecca, M.; Corvaja, C.; Jerabek, K. *J. Am. Chem. Soc.* **1995**, *117* (5), 1603–1606.
(16) M. Zecca; A. Biffis; G. Palma; C. Corvaja; S. Lora; K. Jerabek; B. Corain. *Macromolecules* **1996**, *29*, 4655–4661.
(17) Jerabek, K. *Anal. Chem.* **1985**, *57* (8), 1598–1602.
(18) Jerabek, K. *Anal. Chem.* **1985**, *57* (8), 1595–1597.
(19) Zhang, Y.; Wei, S.; Liu, F.; Du, Y.; Liu, S.; Ji, Y.; Yokoi, T.; Tatsumi, T.; Xiao, F.-S. *Nano Today* **2009**, *4* (2), 135–142.
(20) Liu, F.; Meng, X.; Zhang, Y.; Ren, L.; Nawaz, F.; Xiao, F.-S. *J. Catal.* **2010**, *271* (1), 52–58.
(21) Huglin, M. B.; Yip, D. C. F. *Macromolecules* **1992**, *25* (4), 1333–1337.
(22) Sterchele, S.; Centomo, P.; Zecca, M.; Hanková, L.; Jeřábek, K. *Microporous Mesoporous Mater.* **2014**, *185*, 26–29.
(23) Hanková, L.; Holub, L.; Jeřábek, K. *J. Polym. Sci. Part B Polym. Phys.* **2015**, *53* (11), 774–781.
(24) Goldstein, S.; Schmuckler, G. *Ion Exch. Membr.* **1972**, *1*, 63–66.
(25) Law, R. V.; Sherrington, D. C.; Snape, C. E.; Ando, I.; Korosu, H. *Ind. Eng. Chem. Res.* **1995**, *34* (8), 2740–2749.
(26) Hanková, L.; Holub, L.; Jeřábek, K. *React. Funct. Polym.* **2006**, *66* (6), 592–598.
(27) Theodoropoulos, A. G.; Tsakalos, V. T.; Valkanas, G. N. *Polymer* **1993**, *34* (18), 3905–3910.
(28) Rabia, I.; Zerouk, J. E.; Mekhalif, S. *Polym. Adv. Technol.* **1998**, *9* (2), 107–112.
(29) Freeman, D. H.; Goldstein, S.; Schmuckler, G. *Isr. J. Chem.* **1969**, *7* (6), 741–749.
(30) Jeřábek, K.; Hanková, L.; Prokop, Z.; Lundquist, E. G. *Appl. Catal. Gen.* **2002**, *232* (1–2), 181–188.
(31) Cerfontain, H. *Mechanistic Aspects in aromatic sulfonation and desulfonation*; Interscience: New York, 1968.
(32) Hart, M.; Fuller, G.; Brown, D. R.; Park, C.; Keane, M. A.; Dale, J. A.; Fougret, C. M.; Cockman, R. W. *Catal. Lett.* **2001**, *72* (3–4), 135–139.
(33) Jeřábek, K. In *Strategies in Size Exclusion Chromatography*; ACS Symposium Series; American Chemical Society, 1996; Vol. 635, pp 211–224.

(34) Zundel, G. *Hydration and Intermolecular Interaction: Infrared Investigations with Polyelectrolyte Membranes*; Elsevier, 2012.
(35) Barnard, D.; Fabian, J. M.; Koch, H. P. *J. Chem. Soc. Resumed* **1949**, 2442–2454.
(36) Feairheller, W. R.; Katon, J. E. *Spectrochim. Acta* **1964**, *20* (7), 1099–1108.
(37) Errede, L. A.; Newmark, R. A.; Hill, J. R. *Macromolecules* **1986**, *19* (3), 651–654.
(38) Cánovas, M. J.; Sobrados, I.; Sanz, J.; Acosta, J. L.; Linares, A. *J. Membr. Sci.* **2006**, *280* (1–2), 461–469.
(39) Law, R. V.; Sherrington, D. C.; Snape, C. E.; Ando, I.; Kurosu, H. *Macromolecules* **1996**, *29* (19), 6284–6293.
(40) Yang, J. C.; Jablonsky, M. J.; Mays, J. W. *Polymer* **2002**, *43* (19), 5125–5132.
(41) Su, Z.; Hsu, S. L.; Li, X. *Macromolecules* **1994**, *27* (1), 287–291.
(42) Sherrington, D. C.; Hodge, P. *Syntheses and separations using functional polymers*; Wiley, 1988.
(43) Corain, B.; Zecca, M.; Canton, P.; Centomo, P. *Philos. Trans. R. Soc. Lond. Math. Phys. Eng. Sci.* **2010**, *368* (1915), 1495–1507.
(44) Corain, B.; Schmid, G.; Toshima, N. *Metal Nanoclusters in Catalysis and Materials Science: The Issue of Size Control*; Elsevier, 2011.
(45) Corain, B.; Centomo, P.; Lora, S.; Kralik, M. *J. Mol. Catal. Chem.* **2003**, *204–205*, 755–762.
(46) Mbaraka, I. K.; Shanks, B. H. *J. Catal.* **2005**, *229* (2), 365–373.
(47) Harmer, M. A.; Sun, Q. *Appl. Catal. Gen.* **2001**, *221* (1–2), 45–62.
(48) Centomo, P.; Bonato, I.; Hanková, L.; Holub, L.; Jeřábek, K.; Zecca, M. *Top. Catal.* **2013**, *56* (9–10), 611–617.
(49) Riess, J. G.; Le Blanc, M. *Pure Appl. Chem.* **1982**, *54* (12), 2383–2406.
(50) Law, R. V.; Sherrington, D. C.; Snape, C. E.; Ando, I.; Korosu, H. *Ind. Eng. Chem. Res.* **1995**, *34* (8), 2740–2749.
(51) Ford, W. T.; Periyasamy, M.; Mohanraj, S.; McEnroe, F. J. *J. Polym. Sci. Part Polym. Chem.* **1989**, *27* (7), 2345–2355.
(52) Law, R. V.; Sherrington, D. C.; Snape, C. E. *Macromolecules* **1997**, *30* (10), 2868–2875.
(53) Liu, F.; Meng, X.; Zhang, Y.; Ren, L.; Nawaz, F.; Xiao, F.-S. *J. Catal.* **2010**, *271* (1), 52–58.
(54) Zhao, C.; Zhou, R.; Pan, H.; Jin, X.; Qu, Y.; Wu, C.; Jiang, X. *J. Org. Chem.* **1982**, *47* (11), 2009–2013.
(55) Tanaka, S.; Matsumoto, M.; Goseki, R.; Ishizone, T.; Hirao, A. *Macromolecules* **2013**, *46* (1), 146–154.
(56) Matyjaszewski, K.; Xia, J. *Chem. Rev.* **2001**, *101* (9), 2921–2990.
(57) Zhang, L.-Y.; Fan, G.-Q.; Guo, C.-Y.; Dong, J.-Y.; Hu, Y.-L.; Huang, M.-B. *Eur. Polym. J.* **2006**, *42* (5), 1043–1050.
(58) Tsarevsky, N. V.; Pintauer, T.; Matyjaszewski, K. *Macromolecules* **2004**, *37* (26), 9768–9778.
(59) Mendonça, P. V.; Serra, A. C.; Coelho, J. F. J.; Popov, A. V.; Guliashvili, T. *Eur. Polym. J.* **2011**, *47* (7), 1460–1466.
(60) Wang, Y.; Matyjaszewski, K. *Macromolecules* **2010**, *43* (9), 4003–4005.
(61) Wolfram, C.; Shelef, O.; Gertler, P. *J. Econ. Perspect.* **2012**, *26* (1), 119–137.
(62) BP. June 2016.
(63) Crowley, T. J. *Science* **2000**, *289* (5477), 270–277.
(64) Böhringer, C. *Oxf. Rev. Econ. Policy* **2003**, *19* (3), 451–466.
(65) COMMISSION OF THE E; UROPEAN COMMUNITIES. 2007.
(66) Kennel, C. F.; Briggs, S.; Victor, D. G. *Science* **2016**, *354* (6311), 421–422.
(67) Rajamani, L. *Int. Amp Comp. Law Q.* **2016**, *65* (2), 493–514.

(68) Rogelj, J.; den Elzen, M.; Höhne, N.; Fransen, T.; Fekete, H.; Winkler, H.; Schaeffer, R.; Sha, F.; Riahi, K.; Meinshausen, M. *Nature* **2016**, *534* (7609), 631–639.
(69) Viñuales, J. E.; Depledge, J.; Reiner, D. M.; Lees, E. *Clim. Policy* **2017**, *17* (1), 1–8.
(70) Intergovernmental Panel on Climate Change. 2014.
(71) Lashof, D. A.; Ahuja, D. R. *Nature* **1990**, *344* (6266), 529–531.
(72) Green, M. M.; Wittcoff, H. A. *Organic Chemistry Principles and Industrial Practice*; Wiley, 2003.
(73) Weissermel, K.; Arpe, H.-J. *Industrial Organic Chemistry*, fourth edition.; Wiley, 2003.
(74) Witze, A. *Nature* **2007**, *445* (7123), 14–17.
(75) Klass, D. L. *Biomass for Renewable Energy, Fuels, and Chemicals*; Academic Press, 1998.
(76) Gallezot, P. *Chem. Soc. Rev.* **2012**, *41* (4), 1538–1558.
(77) Huber, G. W.; Iborra, S.; Corma, A. *Chem. Rev.* **2006**, *106* (9), 4044–4098.
(78) Nabi, M. N.; Akhter, M. S.; Zaglul Shahadat, M. M. *Bioresour. Technol.* **2006**, *97* (3), 372–378.
(79) Refaat, A. A. *Int. J. Environ. Sci. Technol.* **2009**, *6* (4), 677–694.
(80) Agarwal, A. K. *Prog. Energy Combust. Sci.* **2007**, *33* (3), 233–271.
(81) Knothe, G.; Krahl, J.; Van Gerpen, J. *The biodiesel handbook*; Elsevier, 2015.
(82) Demirbas, A. *Appl. Energy* **2009**, *86*, *Supplement 1*, S108–S117.
(83) Wyman, C. E. *Appl. Biochem. Biotechnol.* **1994**, *45–46* (1), 897–915.
(84) Aditiya, H. B.; Mahlia, T. M. I.; Chong, W. T.; Nur, H.; Sebayang, A. H. *Renew. Sustain. Energy Rev.* **2016**, *66*, 631–653.
(85) Naik, S. N.; Goud, V. V.; Rout, P. K.; Dalai, A. K. *Renew. Sustain. Energy Rev.* **2010**, *14* (2), 578–597.
(86) Nigam, P. S.; Singh, A. *Prog. Energy Combust. Sci.* **2011**, *37* (1), 52–68.
(87) Chisti, Y. *Biotechnol. Adv.* **2007**, *25* (3), 294–306.
(88) Demirbas, A.; Fatih Demirbas, M. *Energy Convers. Manag.* **2011**, *52* (1), 163–170.
(89) Demirbas, M. F. *Appl. Energy* **2011**, *88* (10), 3473–3480.
(90) John, R. P.; Anisha, G. S.; Nampoothiri, K. M.; Pandey, A. *Bioresour. Technol.* **2011**, *102* (1), 186–193.
(91) Singh, A.; Nigam, P. S.; Murphy, J. D. *Bioresour. Technol.* **2011**, *102* (1), 10–16.
(92) Lotero, E.; Liu, Y.; Lopez, D. E.; Suwannakarn, K.; Bruce, D. A.; Goodwin, J. G. *Ind. Eng. Chem. Res.* **2005**, *44* (14), 5353–5363.
(93) Shay, E. G. *Biomass Bioenergy* **1993**, *4* (4), 227–242.
(94) Singh, S. P.; Singh, D. *Renew. Sustain. Energy Rev.* **2010**, *14* (1), 200–216.
(95) Gerpen, J. V. *Fuel Process. Technol.* **2005**, *86* (10), 1097–1107.
(96) Freedamn, B. B.; Butterfield, R. O. *J. Am. Oil Chem. Soc.* **1986**, *63* (10), 1375–1380.
(97) Meher, L. C.; Vidya Sagar, D.; Naik, S. N. *Renew. Sustain. Energy Rev.* **2006**, *10* (3), 248–268.
(98) Pagliaro, M.; Rossi, M. *The Future of Glycerol*; Royal Society of Chemistry, 2010.
(99) M. Canakci; J. Van Gerpen. *Trans. ASAE* **2001**, *44* (6).
(100) Russbueldt, B. M. E.; Hoelderich, W. F. *Appl. Catal. Gen.* **2009**, *362* (1–2), 47–57.
(101) Smith, M. B.; March, J. *March's Advanced Organic Chemistry: Reactions, Mechanisms, and Structure*; John Wiley & Sons, 2007.
(102) King, E. L. *Int. J. Chem. Kinet.* **1982**, *14* (11), 1285–1286.

(103) Pladziewicz, J. R.; Lesniak, J. S.; Abrahamson, A. J. *J. Chem. Educ.* **1986**, *63* (10), 850.
(104) Burato, C.; Centomo, P.; Pace, G.; Favaro, M.; Prati, L.; Corain, B. *J. Mol. Catal. Chem.* **2005**, *238* (1–2), 26–34.
(105) Kralik, M.; Hronec, M.; Jorik, V.; Lora, S.; Palma, G.; Zecca, M.; Biffis, A.; Corain, B. *J. Mol. Catal. Chem.* **1995**, *101* (2), 143–152.
(106) Park, J.-Y.; Kim, D.-K.; Lee, J.-S. *Bioresour. Technol.* **2010**, *101* (1, Supplement), S62–S65.
(107) Park, J.-Y.; Wang, Z.-M.; Kim, D.-K.; Lee, J.-S. *Renew. Energy* **2010**, *35* (3), 614–618.
(108) Reichenberg, D.; McCauley, D. J. *J. Chem. Soc.* **1955**, No. 0, 2741–2749.
(109) Anastas, P. T.; Warner, J. C. *Green chemistry : theory and practice*; Oxford university press: Oxford, 2000.
(110) Campos-Martin, J. M.; Blanco-Brieva, G.; Fierro, J. L. G. *Angew. Chem. Int. Ed.* **2006**, *45* (42), 6962–6984.
(111) Samanta, C. *Appl. Catal. Gen.* **2008**, *350* (2), 133–149.
(112) Henkel, H.; Weber, W. Manufacture of hydrogen peroxid. US1108752 A, 1914.
(113) Landon, P.; Collier, P. J.; Carley, A. F.; Chadwick, D.; Papworth, A. J.; Burrows, A.; Kiely, C. J.; Hutchings, G. J. *Phys. Chem. Chem. Phys.* **2003**, *5* (9), 1917–1923.
(114) Edwards, J. K.; Thomas, A.; Carley, A. F.; Herzing, A. A.; Kiely, C. J.; Hutchings, G. J. *Green Chem.* **2008**, *10* (4), 388–394.
(115) Li, G.; Edwards, J.; Carley, A. F.; Hutchings, G. J. *Catal. Today* **2007**, *122* (3–4), 361–364.
(116) Liu, Q.; Bauer, J. C.; Schaak, R. E.; Lunsford, J. H. *Appl. Catal. Gen.* **2008**, *339* (2), 130–136.
(117) Burch, R.; Ellis, P. R. *Appl. Catal. B Environ.* **2003**, *42* (2), 203–211.
(118) Edwards, J. K.; Solsona, B. E.; Landon, P.; Carley, A. F.; Herzing, A.; Kiely, C. J.; Hutchings, G. J. *J. Catal.* **2005**, *236* (1), 69–79.
(119) Solsona, B. E.; Edwards, J. K.; Landon, P.; Carley, A. F.; Herzing, A.; Kiely, C. J.; Hutchings, G. J. *Chem. Mater.* **2006**, *18* (11), 2689–2695.
(120) Ishihara, T.; Ohura, Y.; Yoshida, S.; Hata, Y.; Nishiguchi, H.; Takita, Y. *Appl. Catal. Gen.* **2005**, *291* (1–2), 215–221.
(121) Edwards, J. K.; Solsona, B.; Landon, P.; Carley, A. F.; Herzing, A.; Watanabe, M.; Kiely, C. J.; Hutchings, G. J. *J. Mater. Chem.* **2005**, *15* (43), 4595–4600.
(122) Edwards, J. K.; Solsona, B.; N, E. N.; Carley, A. F.; Herzing, A. A.; Kiely, C. J.; Hutchings, G. J. *Science* **2009**, *323* (5917), 1037–1041.
(123) Dalton, A. I. D.; Skinner, R. W. Synthesis of hydrogen peroxide. US4336239 A, June 22, 1982.
(124) Gosser, L. W.; Schwartz, J.-A. T. Catalytic process for making hydrogen peroxide from hydrogen and oxygen employing a bromide promoter. US4772458 A, September 20, 1988.
(125) Maraschino, M. J. Process for producing hydrogen peroxide. US5169618 A, December 8, 1992.
(126) Paparatto, G.; Rivetti, F.; Andrigo, P.; De Alberti, G. Process for the continuous production of hydrogen peroxide. US6649140.
(127) Liu, Q.; Lunsford, J. H. *J. Catal.* **2006**, *239* (1), 237–243.
(128) Gosser, L. W. Catalytic process for making H2 O2 from hydrogen and oxygen, July 1987.
(129) Gosser, L. W.; Schwartz, J.-A. T. Catalytic process for making hydrogen peroxide from hydrogen and oxygen employing a bromide promoter, 1989.

(130) Luckoff, U.; Paucksch, H.; Luft, G. PROCESS FOR THE PRODUCTION OF H2O2, FROM THE ELEMENTS. US Patent 5, 505, 921, 1996.
(131) Chuang, K. T.; Zhou, B. Production of hydrogen peroxide, August 1994.
(132) Landon, P.; Collier, P. J.; Carley, A. F.; Chadwick, D.; Papworth, A. J.; Burrows, A.; Kiely, C. J.; Hutchings, G. J. *Phys. Chem. Chem. Phys.* **2003**, *5* (9), 1917–1923.
(133) Choudhary, V. R.; Sansare, S. D.; Gaikwad, A. G. *Catal. Lett. 84* (1–2), 81–87.
(134) Krishnan, V. V.; Dokoutchaev, A. G.; Thompson, M. E. *J. Catal.* **2000**, *196* (2), 366–374.
(135) Chinta, S. *J. Catal.* **2004**, *225* (1), 249–255.
(136) Choudary, V. R.; Sansare, S. D.; Gaikwad, A. G. Hydrophobic multicomponent catalyst useful for direct oxidation of hydrogen to hydrogen peroxide. US 6346228, 2002.
(137) Sander, R. *Atmospheric Chem. Phys.* **2015**, *15* (8), 4399–4981.
(138) Luehring, P.; Schumpe, A. *J. Chem. Eng. Data* **1989**, *34* (2), 250–252.
(139) Hâncu, D.; Green, J.; Beckman, E. J. *Acc. Chem. Res.* **2002**, *35* (9), 757–764.
(140) Landon, P.; Collier, P. J.; Papworth, A. J.; Kiely, C. J.; Hutchings, G. J. *Chem. Commun.* **2002**, No. 18, 2058–2059.
(141) Melada, S.; Rioda, R.; Menegazzo, F.; Pinna, F.; Strukul, G. *J. Catal.* **2006**, *239* (2), 422–430.
(142) Burato, C.; Centomo, P.; Rizzoli, M.; Biffis, A.; Campestrini, S.; Corain, B. *Adv. Synth. Catal.* **2006**, *348* (1–2), 255–259.
(143) Burch, R.; Ellis, P. R. *Appl. Catal. B Environ.* **2003**, *42* (2), 203–211.
(144) Liu, Q.; Gath, K. K.; Bauer, J. C.; Schaak, R. E.; Lunsford, J. H. *Catal. Lett.* **2009**, *132* (3–4), 342.
(145) Pospelova, T. A.; Kobozev, N. I.; Eremin, E. N. *Russ. J. Phys. Chem.* **1961**, *35*, 143–147.
(146) Han, Y.; Lunsford, J. *J. Catal.* **2005**, *230* (2), 313–316.
(147) Abate, S.; Centi, G.; Melada, S.; Perathoner, S.; Pinna, F.; Strukul, G. *Catal. Today* **2005**, *104* (2–4), 323–328.
(148) Choudhary, V. R.; Samanta, C. *J. Catal.* **2006**, *238* (1), 28–38.
(149) Pospelova, T. A.; Kobozev, N. I.; Eremin, E. N. *Russ J Phys Chem Trans* **1961**, *35*, 584.
(150) Dissanayake, D. P.; Lunsford, J. H. *J. Catal.* **2003**, *214* (1), 113–120.
(151) Ntainjua N., E.; Piccinini, M.; Pritchard, J. C.; He, Q.; Edwards, J. K.; Carley, A. F.; Moulijn, J. A.; Kiely, C. J.; Hutchings, G. J. *ChemCatChem* **2009**, *1* (4), 479–484.
(152) Choudhary, V. R.; Samanta, C.; Jana, P. *Ind. Eng. Chem. Res.* **2007**, *46* (10), 3237–3242.
(153) Corain, B.; Jerabek, K.; Centomo, P.; Canton, P. *Angew. Chem.* **2004**, *116* (8), 977–980.
(154) Grubbs, R. H.; Kroll, L. C. *J. Am. Chem. Soc.* **1971**, *93* (12), 3062–3063.
(155) Hodge, P. *Chem. Soc. Rev.* **1997**, *26* (6), 417–424.
(156) Biffis, A.; Ricoveri, R.; Campestrini, S.; Kralik, M.; Jeřàbek, K.; Corain, B. *Chem. – Eur. J.* **2002**, *8* (13), 2962–2967.
(157) Ohtaki, M.; Komiyama, M.; Hirai, H.; Toshima, N. *Macromolecules* **1991**, *24* (20), 5567–5572.
(158) Barrault, J.; Bouchoule, C.; Duprez, D.; Montassier, C.; Guisnet, M.; Pérot, G. *Heterogeneous Catalysis and Fine Chemicals*; Elsevier, 1988.
(159) Corain, B.; Zecca, M.; Biffis, A.; Lora, S.; Palma, G. *J. Organomet. Chem.* **1994**, *475* (1), 283–288.
(160) Corain, B.; Zecca, M.; Sam, F. O.; Palma, G.; Lora, S. *Angew. Chem. Int. Ed. Engl.* **1990**, *29* (4), 384–385.

(161) Gautron, E.; Garron, A.; Bost, E.; Epron, F. *Catal. Commun.* **2003**, *4* (8), 435–439.
(162) Ramarao, C.; Ley, S. V.; Smith, S. C.; Shirley, I. M.; DeAlmeida, N. *Chem. Commun.* **2002**, No. 10, 1132–1133.
(163) Zhang, K.; Neckers, D. C. *J. Polym. Sci. Polym. Chem. Ed.* **1983**, *21* (11), 3115–3127.
(164) Pathak, S.; Greci, M. T.; Kwong, R. C.; Mercado, K.; Prakash, G. K. S.; Olah, G. A.; Thompson, M. E. *Chem. Mater.* **2000**, *12* (7), 1985–1989.
(165) Yu, W.; Liu, H.; An, X. *J. Mol. Catal. Chem.* **1998**, *129* (1), L9–L13.
(166) Centomo, P.; Canton, P.; Ferroni, M.; Zecca, M. *New J. Chem.* **2010**, *34* (12), 2956–2961.
(167) Schröder, V.; Emonts, B.; Janßen, H.; Schulze, H.-P. *Chem. Eng. Technol.* **2004**, *27* (8), 847–851.
(168) García-Serna, J.; Moreno, T.; Biasi, P.; Cocero, M. J.; Mikkola, J.-P.; Salmi, T. O. *Green Chem.* **2014**, *16* (5), 2320.
(169) Luehring, P.; Schumpe, A. *J. Chem. Eng. Data* **1989**, *34* (2), 250–252.
(170) Huang, X.; Zhang, H.; Guo, C.; Zhou, Z.; Zheng, N. *Angew. Chem.* **2009**, *121* (26), 4902–4906.
(171) Rossi, L. M.; Silva, F. P.; Vono, L. L. R.; Kiyohara, P. K.; Duarte, E. L.; Itri, R.; Landers, R.; Machado, G. *Green Chem.* **2007**, *9* (4), 379.
(172) Venkatesan, R.; Prechtl, M. H. G.; Scholten, J. D.; Pezzi, R. P.; Machado, G.; Dupont, J. *J. Mater. Chem.* **2011**, *21* (9), 3030.
(173) Gates, B. C. *Catalytic Chemistry*; Wiley, 1992.
(174) Sterchele, S.; Biasi, P.; Centomo, P.; Campestrini, S.; Shchukarev, A.; Rautio, A.-R.; Mikkola, J.-P.; Salmi, T.; Zecca, M. *Catal. Today* **2015**, *248*, 40–47.
(175) Gemo, N.; Sterchele, S.; Biasi, P.; Centomo, P.; Canu, P.; Zecca, M.; Shchukarev, A.; Kordás, K.; Salmi, T. O.; Mikkola, J.-P. *Catal. Sci. Technol.* **2015**, *5* (7), 3545–3555.
(176) Sterchele, S.; Biasi, P.; Centomo, P.; Canton, P.; Campestrini, S.; Salmi, T.; Zecca, M. *Appl. Catal. Gen.* **2013**, *468*, 160–174.
(177) Gaikwad, A. G.; Sansare, S. D.; Choudhary, V. R. *J. Mol. Catal. Chem.* **2002**, *181* (1–2), 143–149.
(178) Choudhary, V. R.; Samanta, C. *J. Catal.* **2006**, *238* (1), 28–38.
(179) Choudhary, V. R.; Samanta, C.; Jana, P. *Ind. Eng. Chem. Res.* **2007**, *46* (10), 3237–3242.
(180) Krishnan, V. V.; Dokoutchaev, A. G.; Thompson, M. E. *J. Catal.* **2000**, *196* (2), 366–374.
(181) Liu, Q.; Gath, K. K.; Bauer, J. C.; Schaak, R. E.; Lunsford, J. H. *Catal. Lett.* **2009**, *132* (3–4), 342.
(182) Centomo, P.; Meneghini, C.; Sterchele, S.; Trapananti, A.; Aquilanti, G.; Zecca, M. *ChemCatChem* **2015**, *7* (22), 3712–3718.
(183) Marsh, H.; Reinoso, F. R. *Activated Carbon*; Elsevier, 2006.
(184) Ahmadpour, A.; Do, D. D. *Carbon* **1996**, *34* (4), 471–479.
(185) Dias, J. M.; Alvim-Ferraz, M. C. M.; Almeida, M. F.; Rivera-Utrilla, J.; Sánchez-Polo, M. *J. Environ. Manage.* **2007**, *85* (4), 833–846.
(186) Yamamoto, T.; Nishimura, T.; Suzuki, T.; Tamon, H. *J. Non-Cryst. Solids* **2001**, *288* (1–3), 46–55.
(187) Ryoo, R.; Joo, S. H.; Jun, S. *J. Phys. Chem. B* **1999**, *103* (37), 7743–7746.
(188) Huang, Y. 'an; Hu, S.; Zuo, S.; Xu, Z.; Han, C.; Shen, J. *J. Mater. Chem.* **2009**, *19* (41), 7759–7764.
(189) Huang, Y.; Yang, F.; Xu, Z.; Shen, J. *J. Colloid Interface Sci.* **2011**, *363* (1), 193–198.
(190) Xia, W.; Jin, C.; Kundu, S.; Muhler, M. *Carbon* **2009**, *47* (3), 919–922.

(191) Chen, P.; Chew, L. M.; Kostka, A.; Muhler, M.; Xia, W. *Catal. Sci. Technol.* **2013**, *3* (8), 1964–1971.
(192) Jackson, H. L.; McCormack, W. B.; Rondestvedt, C. S.; Smeltz, K. C.; Viele, I. E. *J. Chem. Educ.* **1970**, *47* (3), A175.